Electronic Supplementary Material (ESI) for ChemComm.

Redshifted and Thermally Bistable One-Way Quantitative Hemithioindigo-derived Photoswitches Enabled by Isomer-Specific Excited State Intramolecular Proton Transfer

Mikkel Krell-Jørgensen[1], Habiburrahman Zulfikri[2,3], Magnus Grage Bonnevie[1], Frederik Simonsen Bro[1], Asmus Ougaard Dohn[2,4] and Luca Laraia[1]*

[1]*Department of Chemistry, Technical University of Denmark, Kemitorvet 2800 Kongens Lyngby, Denmark; *luclar@kemi.dtu.dk*

[2]*Science Institute and Faculty of Physical Sciences, University of Iceland, Reykjavík, Iceland*

[3]*Department of Chemical Engineering, Faculty of Engineering, Universitas Indonesia, Depok 16424, Indonesia*

[4]*Department of Physics, Technical University of Denmark, Fysikvej 2800 Kongens Lyngby, Denmark*

Supplementary Information

Table of Contents

Supporting experimental figures and schemes

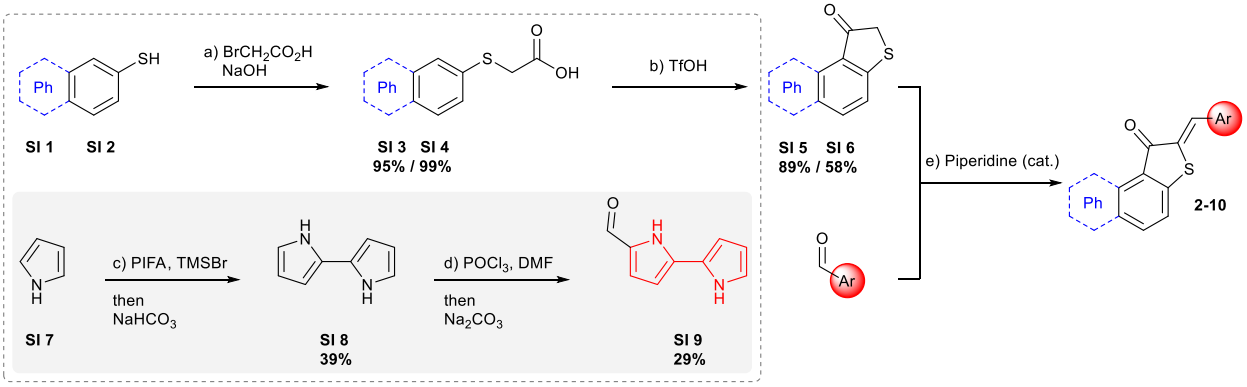

Scheme S1. Synthesis of hemithioindigo derived photoswitches. Substitution of arylthiols **SI 1-2** with 2-bromoacetic acid afforded the corresponding arylthioacetic acids **SI 3-4**. Subsequently, intramolecular Friedel-Crafts type acylation catalysed by triflic acid to initiate ring-closure, allowed access to thioindigo building blocks **SI 5-6** in good yields. Coupling with various aldehydes via aldol condensations catalysed by piperidine resulted in the corresponding HTI photoswitches **1-9** in varying yields. Bipyrrole aldehyde **SI 9** was the only non-commercially available aldehyde that had to be prepared. This was accomplished in two synthetic steps via PIFA-mediated oxidative homo coupling of pyrrole **SI 7** to give bipyrrole **SI 8** following a Vilsmeier-Haack formylation under stoichiometric control to afford aldehyde **SI 9**.

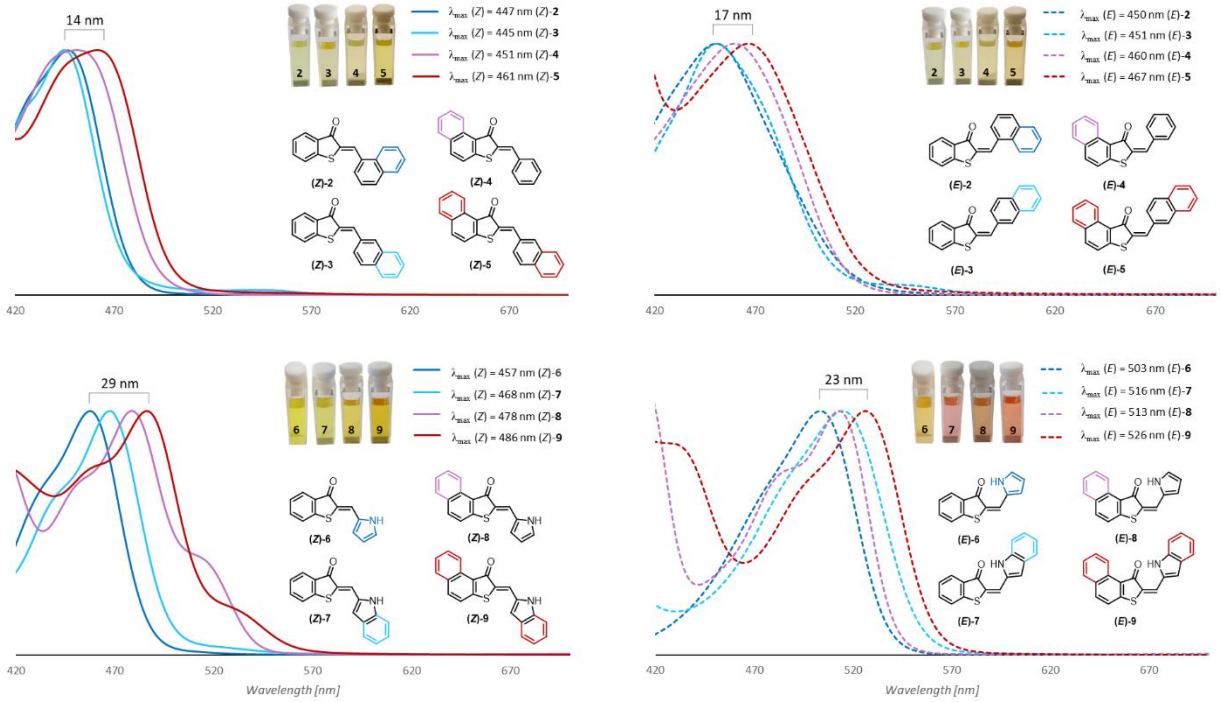

Figure S1. Normalized UV-Vis spectra (33 µM in CH_2Cl_2) displaying the redshifted trend in π-extended hemithioindigo photoswitches visible to the naked eye. Solid lines (Z-isomers). Dashed lines (E-isomers).

1 Supplementary computational details and figures

1.1 Computational details of DFT and TDDFT calculations

The B3LYP hybrid DFT functional[1–3] has previously been successfully employed in a computational study of hemiindigo, a class of photoswitches closely related to the hemithioindigo photoswitch in the present work.[4] Before performing TDDFT vertical excitation energy calculations, we optimized the ground-state geometries of the first and second series of HTI using B3LYP. For the third series, the DLPNO-MP2 method is chosen as the computation benefits from the local correlation scheme especially when more pyrrole rings are connected covalently to the photoswitch. The Dunning's cc-pVTZ basis set[5] is employed for both DFT and DLPNO-MP2 geometry optimizations which are performed until the root mean square of the force is less than 10^{-5} a.u. We then conduct frequency calculations to determine the nature of the resulting stationary points and ensure that optimized geometries without imaginary vibrational frequencies are obtained. The solvation model based on density (SMD) scheme[6] was first tested (see next section) and subsequently used to model the solvent implicitly. The considered solvents of increasing polarity are toluene, DCM, and DMSO.

DFT and TDDFT calculations are performed using Gaussian16. For the TDDFT calculations, we used the maug-cc-pVTZ basis set.[7] DLPNO-MP2 calculations are performed using ORCA version 4.2.1.[8,9] Unless otherwise stated, the default settings of the software are used.

The oscillator strength for excited state i (f_i), is computed as

$$f_i = \frac{8\,\pi^2 \tilde{\nu}_i\, m_e c}{3he^2} D_i\,,$$

where $\tilde{\nu}_i$ is the excitation energy corresponding to the electronic excitation of interest i, m_e is the electron mass, c is the speed of light, h is the Planck's constant, e is the electronic charge, and D_i or sometimes refer to as μ_{fi} is the dipole strength. The employed formulation allows the value of f_i to be greater than unity. Moreover, f_i is proportional to the dipole strength D_i, which means that larger values of f_i indicate bright excited states whereas lower values of f_i point to dark excited states.

1.2 Effect of the choice of implicit solvent models

Implicit solvent models can affect the relative energy of the ground state isomers of a photoswitch. For example, a previous study on the DASA photoswitch showed that the reactant isomer in one solvent model was the most stable, whereas for another solvent model, the product was the most stable.[10] Therefore, we examined two of the most commonly used solvent models: SMD and IEFPCM.[11]

We have examined the effect of two implicit solvent models (SMD and IEFPCM) on the geometry, relative energy, and vertical excitation energy of four isomers of HTI pyrrole (see Figure below) at the level of B3LYP/cc-pVTZ. The four isomers are the stereoisomers of the two carbon-carbon bonds connecting the hemithioindigo and pyrrole moieties. They are labeled as A_A: the first letter indicates the stereoisomer of the formal double bond (C_3=C_4), and the second letter in subscript designated the stereoisomers of the formal single bond (C_4–C_5). The "E" isomer in the main text is the "E_Z" while the main text "Z" isomer refers

either Z_Z or Z_E as they are experimentally indiscernible. Six atoms are numbered in red to indicate bonds, the lengths of which are compared.

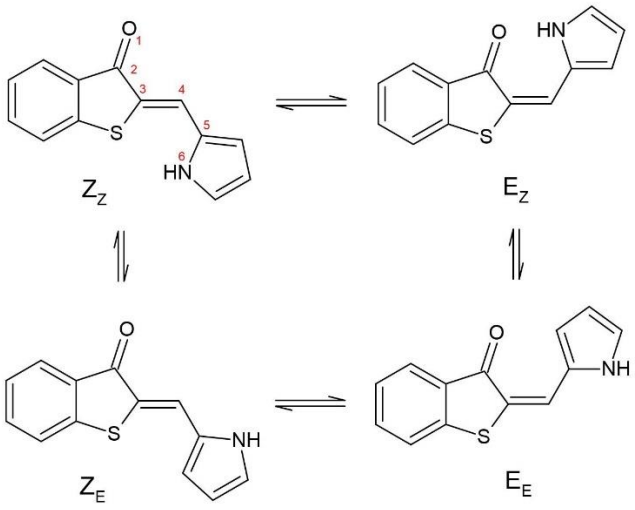

Table S1 shows the relative ground-state electronic energy of four stereoisomers of HTI pyrrole in different implicit solvent models against isomer Z_Z. The application of the SMD solvent model results in the same trend of the relative energies (within the chemical accuracy of 1 kcal/mol) as that of the IEFPCM method across three studied solvents of increasing polarity: toluene (nonpolar), DCM (semipolar), and DMSO (polar). The SMD- and IEFPCM-optimized bond-length patterns for an individual isomer on a particular solvent are similar, as shown in Table S2 for five bond lengths connecting atoms O and N. Furthermore, using the same B3LYP/cc-pVTZ/SMD geometry, computation of the wavelength of maximum absorbance (λ_{max}) of the first bright excited state using the SMD and IEFPCM methods separately yielded similar results within 1 nm (see Table S3). Altogether, our findings reveal that the quantities of interest are independent of the choice of the two investigated solvent model. Thus, we chose to continue with the SMD method.

Table S1. B3LYP/cc-pVTZ relative ground-state electronic energy of HTI pyrrole (**6**) in kcal/mol

Solvent model	Solvent	Z_Z	Z_E	E_Z	E_E
SMD	toluene	0.0	−0.1	−3.5	4.0
	DCM	0.0	−0.8	−2.4	3.1
	DMSO	0.0	−1.0	−1.9	2.9
IEFPCM	toluene	0.0	−0.0	−3.6	4.0
	DCM	0.0	−0.4	−2.6	3.6
	DMSO	0.0	−0.5	−2.3	3.5

Table S2. B3LYP/cc-pVTZ ground-state bond lengths of isomers Z_Z and E_Z of HTI pyrrole (**6**) in Å

Isomer	Solvent model	Solvent	O_1=C_2	C_2–C_3	C_3=C_4	C_4–C_5	C_5-N_6
Z_Z	SMD	toluene	1.222	1.487	1.353	1.421	1.383
		DCM	1.225	1.484	1.355	1.419	1.384
		DMSO	1.225	1.484	1.355	1.419	1.384
	IEFPCM	toluene	1.222	1.486	1.354	1.420	1.384
		DCM	1.226	1.483	1.355	1.419	1.384
		DMSO	1.227	1.482	1.356	1.418	1.384
E_Z	SMD	toluene	1.239	1.469	1.367	1.414	1.379
		DCM	1.241	1.468	1.368	1.414	1.379
		DMSO	1.240	1.468	1.368	1.414	1.380
	IEFPCM	toluene	1.240	1.469	1.367	1.414	1.379
		DCM	1.241	1.468	1.368	1.413	1.380
		DMSO	1.242	1.467	1.369	1.413	1.380

Table S3. TDDFT/B3LYP/maug-cc-pVTZ wavelength of maximum absorbance (λ_{max}) in nm and the corresponding oscillator strength in parenthesis of four isomers of HTI pyrrole (**6**).

Solvent model	Solvent	Z_Z	Z_E	E_Z	E_E
SMD	toluene	443 (0.50)	449 (0.48)	479 (0.34)	465 (0.36)
	DCM	446 (0.49)	449 (0.48)	476 (0.32)	464 (0.35)
	DMSO	446 (0.49)	448 (0.49)	474 (0.33)	463 (0.35)
IEFPCM	toluene	443 (0.48)	449 (0.45)	478 (0.31)	465 (0.34)
	DCM	446 (0.46)	450 (0.45)	477 (0.30)	466 (0.33)
	DMSO	448 (0.46)	450 (0.46)	476 (0.30)	466 (0.33)

1.3 Comparison of MP2 and B3LYP ground-state calculations

Having established the choice of the implicit solvent model, we then investigated the performance of the B3LYP functional and MP2 method in computing the relative energy of four isomers of compounds **6-9** at the corresponding optimized geometries in vacuum and in toluene, DCM and DMSO solutions. As shown in Tables S4 and S5, both B3LYP and MP2 produced similar trend of relative electronic energy, ΔE_{el}. It is interesting to note that the ($Z_E - E_Z$) decreases as the solvent polarity increases. To directly compare computational and experimental results with respect to the most stable isomer, we computed the Gibbs free energy of each isomer and put a comparison of their relative Gibbs free energies, ΔG, in Table S6. The numbers in Table S6 and S5 are very similar to each other, indicating that comparing the electronic energy of the isomers is already representative of a full Gibbs free energy comparison. The calculations predict that the most stable configuration is isomer E_Z, whereas in experiments, we observed that the most stable is either isomer Z_Z or Z_E. It appears the chosen computational method in this work overstabilizes the E_Z isomer, which has an intramolecular hydrogen bond. However, this discrepancy will not affect vertical excitation energies on the Franck-Condon (FC) geometries of each individual isomer. Thus, we proceed with the B3LYP geometry for the computation of TDDFT vertical excitation energy using the B3LYP functional, as this procedure has been demonstrated to obtain a very good agreement of the computed vertical excitation energy to the measured maximum absorption for a closely related hemiindigo photoswitches.[4]

Table S4. MP2/cc-pVTZ relative ground-state electronic energy in kcal/mol of four isomers of four HTI photoswitches in different media. The last column indicates the ($Z_E - E_Z$) energy difference.

Compound	Environment	Z_Z	Z_E	E_Z	E_E	($Z_E - E_Z$)
6	vacuum	0.0	0.2	−4.2	5.0	4.4
	toluene	0.0	−0.6	−3.0	4.1	2.4
	DCM	0.0	−1.3	−2.2	3.1	0.9
	DMSO	0.0	−1.6	−1.8	3.0	0.2
7	vacuum	0.0	0.4	−2.9	5.4	3.3
	toluene	0.0	−0.4	−1.9	4.6	1.5
	DCM	0.0	−1.0	−1.2	3.7	0.2
	DMSO	0.0	−1.2	−0.8	3.7	0.4
8	vacuum	0.0	0.3	−4.4	4.9	4.7
	toluene	0.0	−0.6	−3.2	4.0	2.6
	DCM	0.0	−1.2	−2.4	3.1	1.2
	DMSO	0.0	−1.5	−2.0	3.0	0.5
9	vacuum	0.0	0.3	−3.2	5.2	3.5
	toluene	0.0	−0.4	−2.1	4.5	1.7
	DCM	0.0	−1.1	−1.5	3.6	0.4
	DMSO	0.0	−1.3	−1.1	3.5	0.2

Table S5. B3LYP/cc-pVTZ relative ground-state electronic energy in kcal/mol of four isomers of four HTI photoswitches in different media. The last column indicates the ($Z_E - E_Z$) energy difference.

Compound	Environment	Z_Z	Z_E	E_Z	E_E	($Z_E - E_Z$)
6	vacuum	0.0	0.4	−4.7	4.3	5.1
	toluene	0.0	−0.1	−3.5	4.0	3.4
	DCM	0.0	−0.8	−2.4	3.1	1.6
	DMSO	0.0	−1.0	−1.9	2.9	0.9
7	vacuum	0.0	0.5	−3.5	4.6	4.0
	toluene	0.0	0.0	−2.4	4.3	2.4
	DCM	0.0	−0.5	−1.6	3.5	1.1
	DMSO	0.0	−0.8	−1.2	3.4	0.4
8	vacuum	0.0	0.4	−4.7	4.4	5.1
	toluene	0.0	−0.2	−3.7	3.9	3.5
	DCM	0.0	−0.8	−2.6	3.1	1.8
	DMSO	0.0	−1.0	−2.0	2.8	1.0
9	vacuum	0.0	0.5	−3.4	4.7	3.9
	toluene	0.0	0.0	−2.7	4.4	2.7
	DCM	0.0	−0.5	−1.8	3.6	1.3
	DMSO	0.0	−0.7	−1.3	3.4	0.6

Table S6. B3LYP/cc-pVTZ relative ground-state Gibbs free energy in kcal/mol of four isomers of four HTI photoswitches in different media. The last column indicates the ($Z_E - E_Z$) energy difference.

Compound	Environment	Z_Z	Z_E	E_Z	E_E	($Z_E - E_Z$)
6	vacuum	0.0	0.9	−3.4	4.9	4.3
	toluene	0.0	−0.3	−3.1	3.8	2.8
	DCM	0.0	−0.9	−2.2	3.0	1.3
	DMSO	0.0	−0.8	−1.3	3.0	0.5
7	vacuum	0.0	0.8	−2.3	5.0	3.1
	toluene	0.0	−0.4	−2.3	4.4	1.9
	DCM	0.0	−1.0	−1.6	3.8	0.6
	DMSO	0.0	−1.0	−0.7	2.9	0.3
8	vacuum	0.0	0.8	−3.5	4.9	4.3
	toluene	0.0	−0.2	−2.5	4.1	2.3
	DCM	0.0	−1.0	−1.7	3.0	0.7
	DMSO	0.0	−1.2	−1.6	2.8	0.4
9	vacuum	0.0	0.8	−2.3	5.1	3.1
	toluene	0.0	0.1	−1.7	4.2	1.8
	DCM	0.0	−0.6	−1.1	3.4	0.5
	DMSO	0.0	−1.0	−1.0	3.1	0.0

1.4 Vertical excitation energy of the second series of HTI photoswitches

In Table S7, we list the computed vertical excitation energy of four HTI photoswitches belonging to the second series in different media to complement data in Table 1 of the manuscript. Note (i) the redshifting of the λ_{max} and the increasing of oscillator strength when the molecule is embedded in a solution phase and (ii) that the solvent polarity only slightly alters the absorption profile.

Table S7. TDDFT/B3LYP/maug-cc-pVTZ wavelength of maximum absorbance (λ_{max}) in nm and the corresponding oscillator strength in parenthesis of four HTI photoswitches different in the location and the number of fused aromatic rings.

Compound	Environment	Z_Z	Z_E	E_Z	E_E
6	vacuum	422 (0.33)	431 (0.30)	464 (0.20)	450 (0.22)
	toluene	443 (0.50)	449 (0.48)	479 (0.34)	465 (0.36)
	DCM	446 (0.49)	449 (0.48)	476 (0.32)	464 (0.35)
	DMSO	446 (0.49)	448 (0.49)	474 (0.33)	463 (0.35)
7	vacuum	447 (0.51)	450 (0.49)	490 (0.34)	476 (0.37)
	toluene	471 (0.71)	471 (0.70)	509 (0.51)	495 (0.53)
	DCM	473 (0.68)	471 (0.68)	506 (0.48)	494 (0.50)
	DMSO	473 (0.67)	469 (0.68)	504 (0.48)	492 (0.50)
8	vacuum	443 (0.27)	452 (0.23)	472 (0.18)	464 (0.17)
	toluene	459 (0.52)	465 (0.48)	483 (0.37)	474 (0.35)
	DCM	460 (0.52)	464 (0.51)	479 (0.37)	471 (0.36)
	DMSO	460 (0.53)	462 (0.53)	478 (0.37)	470 (0.37)
9	vacuum	465 (0.45)	468 (0.40)	499 (0.31)	487 (0.30)
	toluene	484 (0.74)	486 (0.72)	515 (0.54)	501 (0.52)
	DCM	485 (0.72)	487 (0.72)	510 (0.51)	499 (0.51)
	DMSO	484 (0.72)	482 (0.73)	508 (0.51)	497 (0.50)

1.5 Computational details of multireference wavefunction calculations

Multireference wavefunction calculations are performed mainly to investigate the possibility of ESIPT on isomer E_Z. We employ state-averaged complete active-space self-consistent-field (SAn-CASSCF)[12] wave function involving n singlet states with equal weights over the states. For HTI indole (**7**), three (n=3) states are considered (S_0, S_1, and S_2), and the active space consists of four electrons in three orbitals (see Figure S3), i.e. CAS(4,3). This active space is adequate to model the three states because, from a comparison with SA3-CASSCF calculations using larger active space, i.e. CAS(12,12), the main configuration state function of the three states involves three orbitals (Figure S4) that resemble the CAS(4,3) orbitals. The most important determinant in S_0 is the doubly occupied RHF configuration, i.e., orbitals A_{X-H} and B_{X-H} are doubly occupied, whereas orbital C_{X-H} is empty (X=O,N). S1 is dominated by an excitation from orbital B_{X-H} to C_{X-H}. The main excitation in S_2 is an excitation from orbital A_{X-H} to C_{X-H}. Note that, the proton-transfer geometry used to compute the SA3-CASSCF wavefunction and plot the active orbitals (depicted in Figures S3b and S4b) is the optimized excited-state (S_1) geometry.

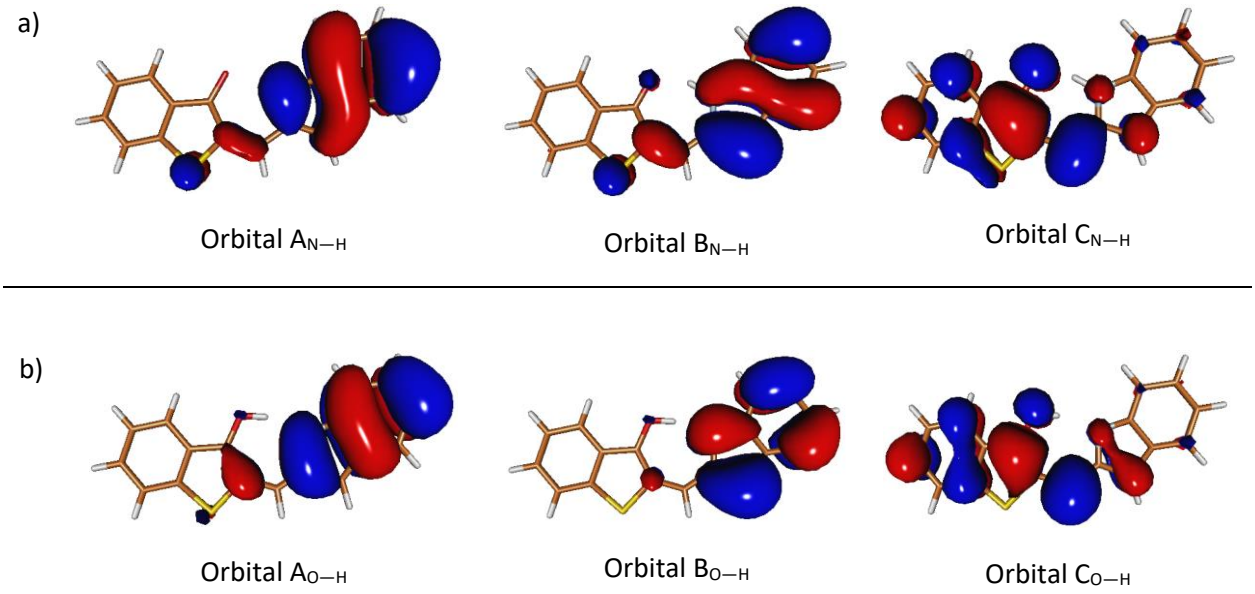

Figure S2. Three active orbitals in a CAS(4,3) active space utilized in SA3-CASSCF and MS3-CASPT2 calculations on the ground-state geometry (a) and proton-transfer S1 geometry (b) of **7**.

a)

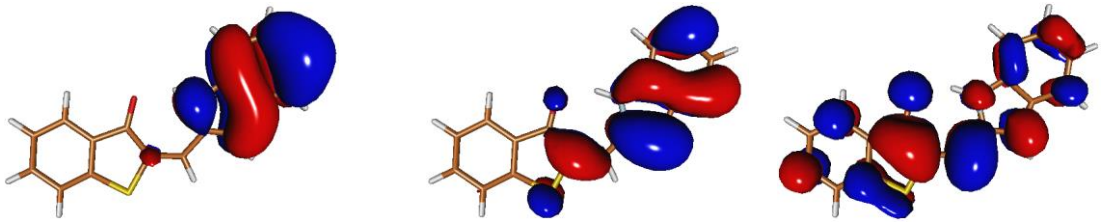

Orbital A_{N-H} Orbital B_{N-H} Orbital C_{N-H}

b)

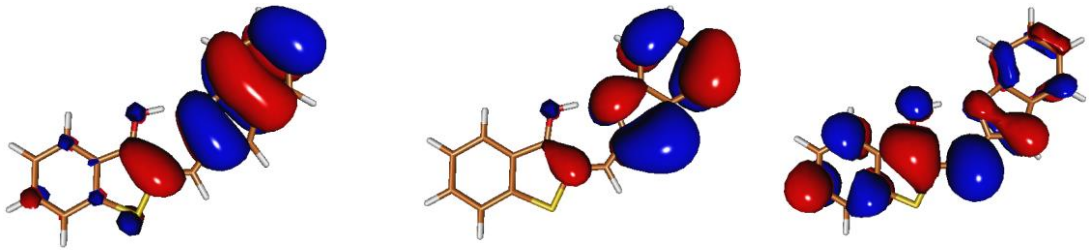

Orbital A_{O-H} Orbital B_{O-H} Orbital C_{O-H}

Figure S3. Three most important SA3-CASSCF and MS3-CASPT2 active orbitals in a CAS(12,12) active space on the ground-state geometry (a) and proton-transfer S1 geometry (b) of **7**.

For HTI pyrrole (**6**), the active space (Figure S5) is slightly larger than that of HTI indole in order to cover all $\pi\pi^*$ state involved in the ESIPT process. As shown in Table S10, the order of the $\pi\pi^*$ state is different in both geometries. For instance, the $A_{N-H} \rightarrow D_{N-H}$ excitation characterizes S_3 in the ground-state geometry whereas it is the dominant excitation for S1 in the proton-transfer geometry.

a)

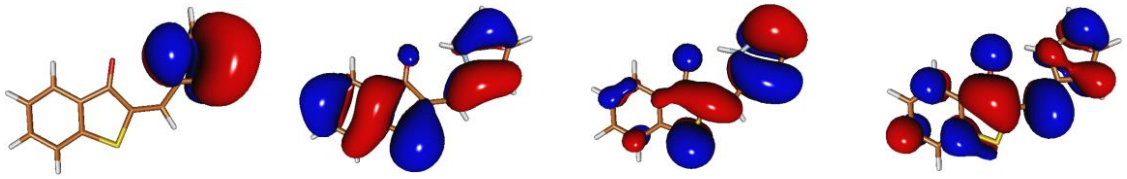

Orbital A_{N-H} Orbital B_{N-H} Orbital C_{N-H} Orbital D_{N-H}

b)

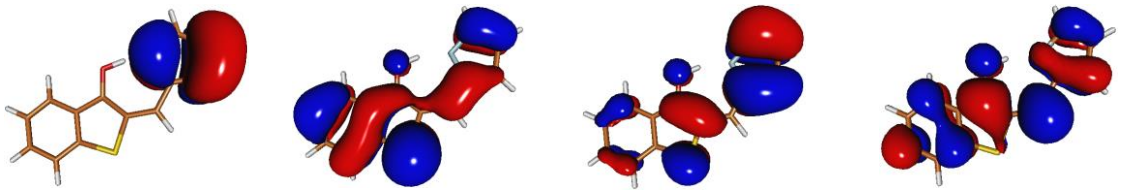

Orbital A_{O-H} Orbital B_{O-H} Orbital C_{O-H} Orbital D_{O-H}

Figure S4. Four active orbitals in a CAS(6,4) active space utilized in SA4-CASSCF and MS4-CASPT2 calculations on the ground-state geometry (a) and proton-transfer S1 geometry (b) of **6**.

Table S8. The most important excitation of three singlet excited states of two E_Z tautomers of HTI pyrrole (**6**) different in the relative position of the polar hydrogen atom

State	Ground-state geometry	Proton-transfer geometry
S_1	$C_{N-H} \rightarrow D_{N-H}$	$A_{O-H} \rightarrow D_{O-H}$
S_2	$B_{N-H} \rightarrow D_{N-H}$	$C_{O-H} \rightarrow D_{O-H}$
S_3	$A_{N-H} \rightarrow D_{N-H}$	$B_{O-H} \rightarrow D_{O-H}$

To account for the missing dynamical electron correlation, the energy is refined using multi-state complete-active-space second-order perturbation theory (MS-CASPT2) method[13–15] using the same active space, basis set, and the same number of states. The gradients of the electronic energy with respect to nuclear coordinates are computed analytically for the CASSCF wave functions[16] and numerically for the CASPT2 method. In the CASPT2 calculations, we employ the default zero-order Hamiltonian[17] with an IPEA shift of 0.25 a.u. and, to eliminate intruder-state problems, an imaginary level shift[18] of 0.2 a.u. is employed. Furthermore, to speed up the CASPT2 calculations, the Cholesky decomposition of the two-electron integrals[19] with a default threshold of 10^{-4} is used. All multireference excited-state calculations use ANO-S-VDZP basis set without polarization functions on hydrogen atoms (denoted as ANO-S-VDZP') and are performed with OpenMolcas package.[20]

1.6 CASSCF and CASPT2 results on compound 6

Exploration of the potential energy surface of S_1 begins with geometry optimization starting from the ground-state MP2 geometry at the level of SA3-CASSCF(4,3). Our computation found an in-plane minimum (min_1) where the hydrogen is covalently bonded to the nitrogen atom as in the FC geometry case. For the investigation of the possibility of ESIPT, we moved the hydrogen atom covalently bonded to the nitrogen atom in the ground-state optimized geometry closer to the oxygen atom by 1.0 Å, and started the S_1 geometry optimization. The computation yields another in-plane stationary point in which the proton is covalently bonded to the oxygen atom. Interestingly, this proton-transfer S_1 geometry (min_2) is more stable by 12.3 kcal/mol (SA3-CASSCF) or 11.1 kcal/mol (MS3-CASPT2) than the previously located S_1 minimum (min_1).

Table S9. Optimized bond lengths in Å of tautomers of the E_Z isomer of HTI indole (**7**) in different states.

Geometry	O_1=C_2	C_2–C_3	C_3=C_4	C_4–C_5	C_5-N_6
S0 MP2	1.250	1.489	1.387	1.430	1.385
S1 SA3-CASSCF(4,3), min_1	1.246	1.472	1.361	1.474	1.313
S1 SA3-CASSCF(4,3), min_2	1.321	1.409	1.372	1.473	1.362

The fact that there are two in-plane minima indicates the presence of a barrier connecting them. We therefore scan the S_1 potential energy surface along the O—H bond coordinate at the level of SA3-CASSCF(4,3) and show the energy profiles of S_0, S_1 and S_2 in Figure S6. There is a small barrier of 1.4 kcal/mol to overcome from min_1 to min_2 and this barrier is unrelated to the crossing with higher S2 state. However, the refined MS3-CASPT2(4,3)/SA3-CASSCF(4,3) excited-state (S1) potential energy profile (Figure 1 in main text) reveals that the ESIPT pathway is barrier-less, and has no well-defined crossing points to either the upper (S2) and lower (S0) states. We thus note the significant contribution of dynamic correlation to the pathways.

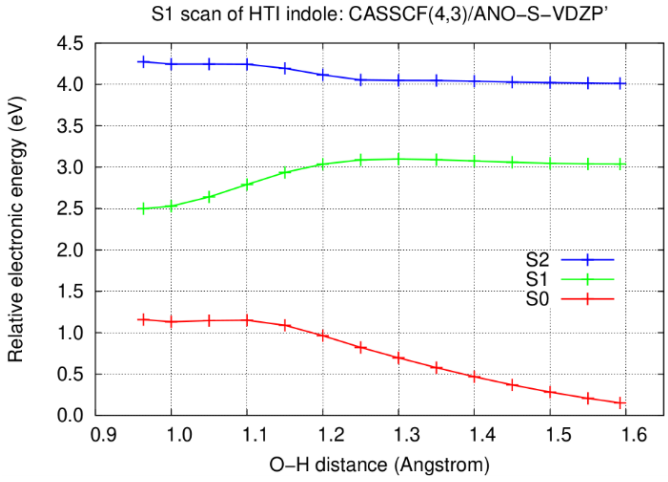

Figure S5. SA3-CASSCF(4,3) relative electronic energy of S_0, S_1 and S_2 on the geometries obtained by scanning the S_1 potential energy surface along the O—H bond.

1.7 CASSCF and CASPT2 results on compound 6

In **Table S10**, we show the relative energy of two in-plane excited-state (S_1) E_Z tautomers of HTI pyrrole (**6**) obtained from three different calculations. The effect of the missing electron correlation in SA4-CASSCF(6,4) energy is very apparent in this case: MS4-CASPT2(6,4)/SA4-CASSCF(6,4) calculation reverses the order of the SA4-CASSCF(6,4) relative energy such that the min_1 geometry is more stable than the min_2 (proton-transfer) geometry. As the size of the HTI pyrrole (**5**) is smaller than that of HTI indole (**6**), excited-state (S_1) CASPT2 geometry optimization is computationally affordable for **5**. In Table S12, we show that the MS4-CASPT2(6,4) energy ordering of the two minima is the same as that of MS4-CASPT2(6,4)/SA4-CASSCF(6,4).

Table S10. Relative energy of two excited-state (S1) E_Z tautomers of HTI pyrrole (**6**) in kcal/mol

Method	$E(min_2) - E(min_1)$
SA4-CASSCF(6,4)	−6.6
MS4-CASPT2(6,4)/SA4-CASSCF(6,4)	6.2
MS4-CASPT2(6,4)	7.5

In **Table S11**, we list the bond lengths of tautomers of the E_Z isomer of HTI indole (**6**) in different states. It is interesting to note that the CASSCF and CASPT2 bond-length pattern of the min_1 geometry is different considerably, while those of the min_2 are in quite good agreement with each other. As the E/Z photoisomerization occur experimentally, the elongation of the formal C_3=C_4 double bond from the FC geometry to the MS4-CASPT2(6,4) S_1 min_1 geometry indicates the weakening of such bond easing the rotation around it. Therefore, the MS4-CASPT2(6,4) method yield more representative picture in the excited states. It is important to note that, while the SA4-CASSCF(6,4) and MS4-CASPT2(6,4) excited-state geometries are quite different especially for the min_1 geometry, performing MS4-CASPT2(6,4) single-point calculations on top the SA4-CASSCF(6,4) geometries still results in the correct energy ordering of min_1 and min_2 as benchmarked against the full MS4-CASPT2(6,4) method (**Table S11**).

Table S11. Optimized bond lengths in Å of tautomers of the E_Z isomer of HTI indole (**7**) in different states using different methods.

Geometry	O_1=C_2	C_2−C_3	C_3=C_4	C_4−C_5	C_5-N_6
S_0 MP2	1.253	1.481	1.388	1.426	1.384
S_1 SA4-CASSCF(6,4), min_1	1.239	1.523	1.340	1.477	1.337
S_1 SA4-CASSCF(6,4), min_2	1.326	1.398	1.384	1.479	1.349
S_1 MS4-CASPT2(6,4), min_1	1.294	1.474	1.429	1.403	1.417
S_1 MS4-CASPT2(6,4), min_2	1.348	1.440	1.394	1.465	1.384

1.8 Ground-state relative energies and vertical excitation energies of the extended third series of HTI photoswitches

In **Table S12**, we show the DLPNO-MP2/cc-pVTZ relative ground-state electronic energy of four isomers in different environment. The findings and analysis are similar to those of the second series of HTI photoswitches (**Table S4**).

Table S12. DLPNO-MP2/cc-pVTZ relative ground-state electronic energy in kcal/mol of four isomers of four HTI oligopyrrole in different media. The last column indicates the ($Z_E - E_Z$) energy difference.

Compound	Environment	Z_Z	Z_E	E_Z	E_E	($Z_E - E_Z$)
HTI pyrrole (**6**)	vacuum	0.0	0.2	−4.2	5.0	4.4
	toluene	0.0	−0.6	−3.0	4.1	2.4
	DCM	0.0	−1.3	−2.2	3.1	0.9
	DMSO	0.0	−1.6	−1.8	3.0	0.2
HTI bipyrrole (**10**)	vacuum	0.0	0.9	−4.4	5.2	5.3
	toluene	0.0	−0.2	−3.6	4.2	3.4
	DCM	0.0	−1.0	−3.2	3.3	2.2
	DMSO	0.0	−1.2	−2.9	3.2	1.7
HTI tripyrrole	vacuum	0.0	0.9	−4.7	5.3	5.6
	toluene	0.0	−0.1	−3.7	4.2	3.6
	DCM	0.0	−0.9	−3.2	3.2	2.3
	DMSO	0.0	−1.2	−2.9	3.2	1.7

In **Table S13**, we show the computed vertical excitation energy of three HTI photoswitches belonging to the third series of HTI photoswitches in different media, extended to include compounds which have not yet been synthesized. Adding more pyrrole rings covalently seem to increase both the maximum absorbance and the oscillator strength. We note that extending the conjugation of the molecule any further, would likely separate the location of HOMO and LUMO orbitals further (as illustrated in Figure S2), increasing the charge-transfer character of the S_1. Therefore, TDDFT results using B3LYP functional, which is known to perform poorly for charge-transfer excited state,[21–23] will become inaccurate for larger molecules.

Table S13. TDDFT/B3LYP/cc-pVTZ//DLPNO/cc-pVTZ wavelength of maximum absorbance (λ_{max}) in nm and the corresponding oscillator strength in parenthesis of four HTI photoswitches different in the number of pyrrole moieties.

Compound	Environment	Z_Z	Z_E	E_Z	E_E
HTI pyrrole (**6**)	vacuum	419 (0.34)	427 (0.30)	463 (0.21)	449 (0.23)
	toluene	440 (0.52)	445 (0.49)	478 (0.34)	464 (0.37)
	DCM	442 (0.50)	444 (0.49)	475 (0.33)	463 (0.36)
	DMSO	441 (0.50)	442 (0.50)	474 (0.33)	461 (0.36)
HTI bipyrrole (**10**)	vacuum	466 (0.65)	464 (0.75)	511 (0.47)	482 (0.65)
	toluene	503 (0.85)	502 (1.00)	543 (0.65)	516 (0.92)
	DCM	509 (0.86)	509 (1.02)	541 (0.64)	519 (0.94)
	DMSO	510 (0.86)	510 (1.02)	539 (0.64)	520 (0.95)
HTI tripyrrole	vacuum	515 (0.78)	512 (0.87)	559 (0.67)	520 (0.91)
	toluene	564 (0.98)	561 (1.10)	604 (0.85)	568 (1.14)
	DCM	578 (0.98)	578 (1.09)	609 (0.85)	581 (1.14)
	DMSO	582 (0.98)	581 (1.08)	610 (0.85)	584 (1.14)

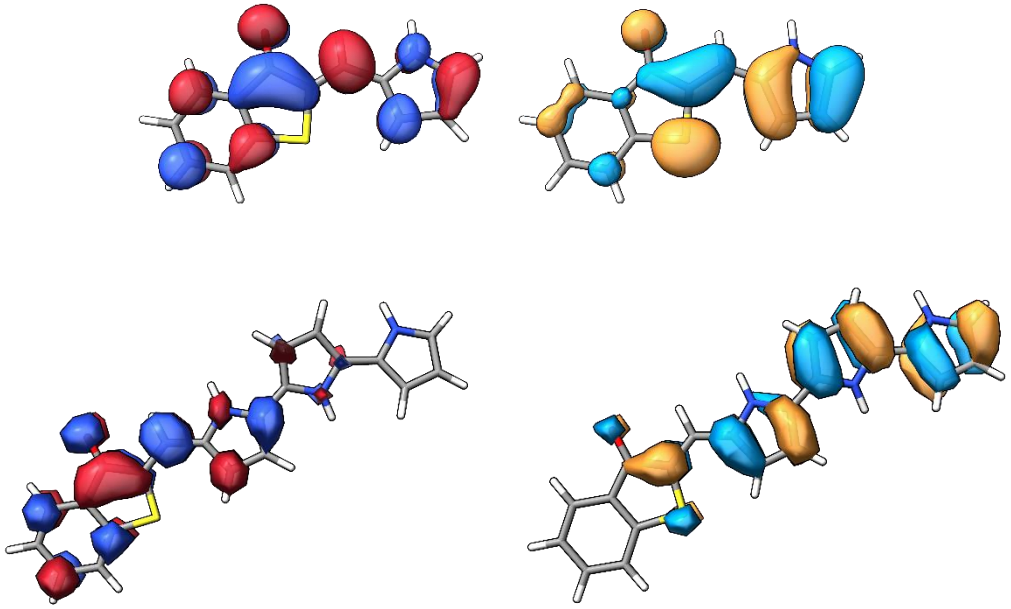

Figure S6. B3LYP/cc-pVTZ HOMO(left) and LUMO (right) of HTI pyrrole (top) and tripyrrole (bottom) Z-isomers.

2 General directions

Chemical reactions were carried out under an inert atmosphere of nitrogen or argon using solvents of HPLC grade or anhydrous solvents (MeCN, DCM, DMF, DMSO, Et_2O, THF and PhMe) obtained from a PureSolv system (Innovative Technology, Tronyx). Synthesis was performed in the dark or reaction equipment was wrapped with aluminium foil to shield it from light. Commercially available reagents were used as received from Sigma Aldrich, Combi-Blocks, Fisher Scientific, Strem or Merck without further purification. Reactions were monitored by thin layer chromatography (TLC) and/or reversed-phase ultra-performance liquid chromatography mass spectrometry (RP-UPLC-MS).

Analytical TLC was performed on Merck aluminum sheets covered with silica gel (60 F_{256}). The plates were visualized using UV-light or stained by dipping in a developing agent followed by gentle heating. $KMnO_4$ stain was used as developing agent [3 g in H_2O (300 mL), K_2CO_3 (20 g) and 5% aqueous NaOH (5 mL)].

Column chromatography was performed using Merck Si 60A (40-63 µm) silica gel for flash column chromatography (FCC) and Merck Si 60A (15-40 µm) silica gel for dry column vacuum chromatography (DCVC).

Characterization of new compounds were done by TLC, NMR, MS (ESI), HRMS (ESI), melting point, UV-Vis spectroscopy, fluorescence spectroscopy and/or HPLC retention time (byproducts were not fully characterized).

Structural assignments were made for new compounds using a combination of 2D NMR techniques when relevant (gCOSY, DQF-COSY, HSQC, HMBC, H2BC, 2D NOESY). For the recording of ^{1}H NMR and ^{13}C NMR either a 400 MHz Bruker Ascend with a Prodigy CryoProbe and Avance IIIHD NanoBay console, 400 MHz Bruker UltraShield Plus with a Room Temperature Broadband ^{19}F Observe (RT BBFO) SmartProbe and Avance III console, 800 MHz Bruker Ascend refitted with a TCI (Triple Resonance NMR 'Inverse') CryoProbe and Avance IIIHD console, or 800 MHz Oxford instruments refitted with a TCI CryoProbe and Avance III console was used. Measurements were performed with a sample temperature of 25°C unless otherwise stated. The chemical shifts (δ) are reported in parts per million (ppm) and the coupling constants (*J*) in Hz. Spectra were referenced using the residual solvent peaks of the respective solvents; DMSO (δ 2.50 ppm for ^{1}H NMR DMSO-d_5 and δ 39.52 ppm for ^{13}C NMR DMSO-d_6), $CDCl_3$ (δ 7.26 ppm for ^{1}H NMR $CHCl_3$ and δ 77.16 ppm for ^{13}C NMR $CDCl_3$), MeOD (δ 3.31 ppm for ^{1}H NMR CHD_2OD and δ 49.00 ppm for ^{13}C NMR CD_3OD), DCM (δ 5.32 ppm for ^{1}H NMR $CHDCl_2$ and δ 54.00 ppm for ^{13}C NMR CD_2Cl_2). When THF-H_8 was used as NMR solvent, a double solvent suppression of the proton signals was performed. The following abbreviations were used to report peak multiplicities: s = singlet, bs = broad singlet, d = doublet, dd = doublet of doublets, ddd = doublet of doublets of doublets, dt = doublet of triplets, t = triplet, td = triplet of doublets, tt = triplet of triplets, q = quartet, dq = doublet of quartets, m = multiplet. $CDCl_3$ was treated with K_2CO_3 and filtered before use.

Analytical RP-UPLC-MS (ESI) was performed on an S2 Waters AQUITY RP-UPLC system equipped with a diode array detector using a Thermo Accucore C18 column (d 2.6 µm, 2.1 x 50 mm; column temp: 50°C; flow: 1.0 mL/min). Eluents A (0.1% HCO_2H in H_2O) and B (0.1% HCO_2H in MeCN) were used with a linear gradient (5% B to 100% B) in 2.4 min or 4.8 min and then held for 0.1 min at 100% B (total run time: 2.6 min or 5.0 min). Injection volume was 2 µL. The LC system was coupled to a Single Quadrupole Detector (SQD) 1 or SQD2 mass spectrometer.

UHPLC-HRMS analyses were measured on an Agilent Infinity 1290 UHPLC system (Agilent Technologies, Santa Clara, CA, USA) equipped with a diode array detector. Separation was obtained on an Agilent Poroshell 120 phenyl-hexyl column (d 2.7 µm, 2.1 × 250 mm; column temp: 60°C; flow: 0.35 mL/min).

Eluents A (20 mM HCO_2H in H_2O) and B (20 mM HCO_2H in MeCN) were used with a linear gradient (40% B to 100% B) in 3 min and then held for 5 min at 100% B, returned to 40% B in 0.1 min and held for the remaining 2 min. An injection volume of 0.1 µL was used. MS detection was performed in positive detection on an Agilent 6545 Quadrupole Time-Of-Flight (QTOF) MS equipped with Agilent Dual Jet Stream electrospray ion source with a drying gas temperature of 250°C, gas flow of 8 L/min, sheath gas temperature of 300°C and flow of 12 L/min. Capillary voltage was set to 4000 V and nozzle voltage to 500 V. Mass spectra were recorded as centroid data for *m*/*z* 50–1000, with an acquisition rate of 10 spectra/s. Lock mass solution in 70:30 MeOH:H_2O was infused in the second sprayer using an extra LC pump at a flow of 15 µL/min using a 1:100 splitter. The solution contained 1 µM tributylamine (Sigma-Aldrich) and 10 µM Hexakis(2,2,3,3-tetrafluoropropoxy)phosphazene (Apollo Scientific Ltd., Cheshire, UK) as lock masses. The $[M + H]^+$ ions (*m*/*z* 186.2216 and 922.0098 respectively) of both compounds were used.

Melting points were obtained using a Stuart SMP30 melting point apparatus.

UV-Vis spectroscopy was measured on an Analytik Jena Specord® 210 PLUS double beam spectrophotometer using precision cells 108B-QS made of quartz Suprasil with a 10 mm light path from Hellma® Analytics. Measurements were calibrated against air and pure dry solvent used to dissolve the respective samples to give a final concentration of 33 µM. Absorption wavelengths (λ) are reported in nm and the extinction coefficients (ε) in $L \cdot mol^{-1} \cdot cm^{-1}$. Unless otherwise stated, all included spectra were obtained after irradiation with the respective wavelength and photostationary state at 25°C. Spectra of (*Z*)-isomers are generally reported for non-irradiated samples (dark state) as these mostly gave exclusively the (*Z*)-isomer.

UV-Vis thermal relaxation spectroscopy was obtained similarly to UV-Vis spectroscopy. The relaxation of the metastable (*E*)-isomer to its stable (*Z*)-isomer was determined by measuring the absorption every 5 minutes for 10 hours at 28°C in the respective dry solvent unless otherwise stated. The sample was kept dark inside in the instrument. Lambda max (λ_{max}) or representative wavelengths (λ) with a significant change between isomers were used to calculate thermal relaxation. Half-life was calculated similar to the literature[24–26] by plotting the absorbance at a specific wavelength relevant for one isomer over time and fitting the data to an exponential using Graphpad Prism.

Kinetic analysis of thermal *E*-to-*Z* isomerisation was performed by looking at the initial rate of the thermal relaxation from the *E*-isomer to the *Z*-isomer assuming first order kinetics as described in V. Josef *et al*.[24]

Fluorescence spectroscopy were recorded on a Perkin Elmer LS-55 fluorescence spectrophotometer using precision cells 101-QS made of quartz Suprasil with a 10 mm light path from Hellma® Analytics. Measurements were calibrated against air and pure dry solvent used to dissolve the respective samples to give a final concentration of 33 µM. Emission wavelengths (λ) are reported in nm. Unless otherwise stated, all included spectra were obtained after irradiation with the respective wavelength and photostationary state at 25°C.

Photoirradiation was carried out with LEDs purchased from Thorlabs (M340L4 (340 nm), M365L2 (365 nm), M415L4 (415 nm), M470L4 (470 nm), M530L3 (530 nm), M590L4 (590 nm), M625L4 (625 nm) and M660L4 (660 nm)) with collimator (SM2F32-A) and power supply/driver (LEDD1B) to focus the light beam and control the current, respectively.

HPLC quantification of photostationary state (PSS) composition was performed with samples prepared in DCM (2 mg/mL) and irradiated (1 Amp) with respective LEDs in borosilicate glass HPLC vials purchased from Fischer Scientific (fischerbrand 11525884), unless otherwise stated. An Aliquot (0.25 mL) of the

sample was transferred to a new HPLC vial and the DCM removed with a flow of nitrogen while the sample was kept dark. A solvent mixture of *n*-hexane/iPrOH (1:1) was added to give the final concentration (0.5 mg/mL). The samples were measured using a Waters 2695 Alliance Separations module HPLC with a ChiralPak AD-H column (5 μm, 250 x 4.6 mm) and a Waters 2996 PhotoDiode Array (PDA) detector. For details regarding the eluent system (*n*-hexane/iPrOH), see the results for each measured photoswitch. The same eluent system used for HPLC quantification of the respective photoswitch was also used in determining the isosbestic point of that photoswitch by UV-Vis spectroscopy. The composition was determined as area under the curve. Chromatograms are representatives.

NMR photoisomerization was achieved by irradiating an NMR sample of the respective compound in the respective deuterated solvent (unless otherwise stated) for 30 min in a 3 mm NMR standard tube using LEDs with wavelengths as described for the UV-Vis spectroscopy data of that compound. The *Z*/*E* ratio was determined by ^{1}H NMR integration of the singlet enone β-proton or the pyrrole/indole-NH.

^{1}H NMR thermal relaxation spectroscopy was obtained similarly to the NMR photoisomerization. The relaxation of the metastable (*E*)-isomer to its stable (*Z*)-isomer was monitored by ^{1}H NMR with spectra recorded every one hour for 24 hours (y-axes) and the integral of the pyrrole/indole-NH of the (*E*)-isomer plotted vs. time. The sample was kept dark inside the instrument at a constant temperature of 24°C. Occasionally, a low change in observed relaxation resulted in weak exponential fit. For these instances, half-lives $T_{1/2}$ were reported as worst case (lowest value) and not necessarily for the total 24 hours as indicated by the respective graphs.

3 General procedures

General procedure A: Coupling of HTI (or derivatives) with mono-aldehydes

To a heat gun-dried reaction vessel evacuated with inert atmosphere was added hemithioindigo (or derivative) (1 eq.) dissolved in benzene (0.10-0.30 M). Aldehyde (0.9-1 eq.) and piperidine (1-2 drops) were added and the reaction vessel transferred to a pre-warmed oil bath (40 or 100°C) and stirred for the indicated time before cooling to room temperature. A saturated aqueous NH_4Cl solution (10 mL) was added and the aqueous phase extracted with EtOAc (3 x 10 mL). The combined organic extracts were washed with brine, dried over anhydrous Na_2SO_4, filtered and concentrated under reduced pressure by rotary evaporation. Purification by flash column or dry column vacuum chromatography on silica gel afforded the corresponding mono-substituted photoswitch.

General procedure B: Coupling of HTI (or derivatives) with mono-aldehydes

To a heat gun-dried reaction vessel evacuated with inert atmosphere was added hemithioindigo (or derivative) (1 eq.) dissolved in PhMe (0.14-0.25 M). Aldehyde (0.8-1 eq.) and piperidine (1-2 drops) were added and the reaction vessel transferred to a pre-warmed oil bath (40 or 100°C) and stirred for the indicated time before cooling to room temperature. *n*-Hexane (5 mL) was added and the reaction vessel transferred to an ice bath (0°C) for 30-45 min. The precipitate was filtered, washed with cold *n*-hexane until the filtrate ran clear and dried under high vacuum to afford the corresponding mono-substituted photoswitch.

4 Specific reaction procedures for intermediates and building blocks

Thiophenoxy acetic acid (SI 4)

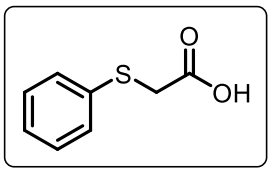

To a 100 mL round-bottomed flask were added deionized H_2O (30 mL), 2-bromoacetic acid (1.99 g, 14.3 mmol, 1.0 eq.) and thiophenol (1.47 mL, 14.3 mmol, 1.0 eq.). 6 M aqueous NaOH (5.0 mL, 30.0 mmol, 2.1 eq.) was added at room temperature and the solution stirred for 22 h. The solution was acidified with dilute 1 M aqueous HCl and extracted with EtOAc (3 x 30 mL). The combined organic extracts were dried over anhydrous Na_2SO_4, filtered and concentrated under reduced pressure by rotary evaporation to afford the title compound **SI 4** (2.39 g, 4.21 mmol, 99%) as a white solid.

The data is in accordance with previously reported work.[27]

TLC: R_f = 0.50 (1:1 EtOAc/*n*-heptane + 1% AcOH)

LCMS (ESI) $[M]^-$ *m/z* calcd for $C_8H_7O_2S^-$: 167.0172 , *m/*z found: 166.83 $[M]^-$

R_t: 1.04 min (total run time: 2.6 min), purity >99%

^{1}H NMR (400 MHz, $CDCl_3$): δ 10.22 (s, 1H), 7.49 – 7.41 (m, 2H), 7.38 – 7.31 (m, 2H), 7.31 – 7.27 (m, 1H), 3.70 (s, 2H)

^{13}C NMR (101 MHz, $CDCl_3$): δ 175.9, 134.6, 130.2, 129.3, 127.4, 36.7

Hemithioindigo (SI 6)

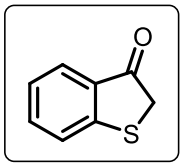

To an oven-dried reaction tube were added thiophenoxy acetic acid **SI 1** (1.92 g, 11.4 mmol, 1.0 eq.) and DCM (20 mL, 0.570 M). The solution was purged with nitrogen for 5 min. Triflic acid (5.0 mL, 56.6 mmol, 5.0 eq.) was carefully added and the reaction tube transferred to a pre-warmed oil bath set to 40°C and stirred for 44 h. The reaction mixture was allowed to cool to room temperature before carefully poured into icy H_2O (200 mL). The aqueous phase was extracted with EtOAc (2 x 100 mL) and the combined organic extracts were washed with a saturated aqueous $NaHCO_3$ (100 mL) and brine (50 mL), dried over anhydrous Na_2SO_4, filtered and concentrated under reduced pressure by rotary evaporation to afford the title compound **SI 6** (1.09 g, 6.66 mmol, 58%) as an orange solid.

Important note: Store in a freezer under inert atmosphere to prevent oxidation and prolong shelf life.

The data is in accordance with previously reported work.[28]

TLC: R_f = 0.80 (1:1 EtOAc/*n*-heptane + 1% AcOH)

LCMS (ESI) $[M+H]^+$ *m/z* calcd for $C_8H_7OS^+$: 151.0212 , *m/*z found: 150.86 $[M+H]^+$

R_t: 1.11-1.21 min (total run time: 2.6 min), purity >90%

^{1}H NMR (400 MHz, $CDCl_3$): δ 7.78 (d, *J* = 6.7 Hz, 1H), 7.55 (t, *J* = 7.6 Hz, 1H), 7.43 (d, *J* = 8.0 Hz, 1H), 7.22 (t, *J* = 7.4 Hz, 1H), 3.80 (s, 2H)

^{13}C NMR (101 MHz, $CDCl_3$): δ 200.2, 154.4, 135.8, 131.1, 126.8, 124.9, 124.8, 39.4

(2-Naphthylthio)acetic acid (SI 3)

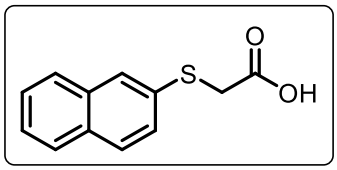

To a 100 mL round-bottomed flask were added deionized H_2O (30 mL), EtOH (20 mL), 2-bromoacetic acid (2.00 g, 14.4 mmol, 1.0 eq.) and 2-naphthalenethiol (2.00 mL, 14.5 mmol, 1.0 eq.). 6 M aqueous NaOH (5.0 mL, 30.0 mmol, 2.1 eq.) was added at room temperature and the solution stirred for 4.5 h. The reaction mixture was filtered and the filtrate acidified with dilute 2 M aqueous HCl. Another filtration was performed and the residues combined, washed with *n*-heptane (3 x 20 mL) and concentrated under reduced pressure by rotary evaporation to afford the (naphthylthio)acetic acid **SI 3** (2.99 g, 13.7 mmol, 95%) as a white solid.

TLC: R_f = 0.45 (1:1 EtOAc/*n*-heptane + 1% AcOH)

LCMS (ESI) $[M+H]^+$ *m/z* calcd for $C_{12}H_{11}O_2S^+$: 219.0474 , *m/*z found: 218.91 $[M+H]^+$

R_t: 1.41 min (total run time: 2.6 min), purity >90%

^{1}H NMR (400 MHz, CD_3OD): δ 7.81 – 7.71 (m, 4H), 7.48 – 7.35 (m, 3H), 3.73 (s, 2H)

^{13}C NMR (101 MHz, CD_3OD): δ 175.7, 136.4, 135.4, 133.0, 129.2, 128.6, 128.0, 127.6, 127.5, 126.4, 39.0

^{1}H NMR (400 MHz, DMSO-d_6): δ 7.82 (d, *J* = 8.1 Hz, 1H), 7.78 (d, *J* = 3.6 Hz, 1H), 7.76 (d, *J* = 3.1 Hz, 1H), 7.72 (bs, 1H), 7.46 (ddd, *J* = 8.2, 6.8, 1.4 Hz, 1H), 7.43 – 7.36 (m, 2H), 3.67 (s, 2H)

^{13}C NMR (101 MHz, DMSO-d_6): δ 170.2, 136.4, 133.5, 130.6, 127.8, 127.5, 126.7, 126.5, 125.9, 125.0, 123.4, 38.1

Naphtho[2,1-b]thiophen-1(2H)-one (SI 5)

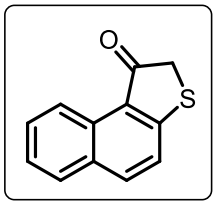

To an oven-dried reaction tube were added (2-naphthylthio)acetic acid **3** (1.00 g, 4.58 mmol, 1.0 eq.) and DCM (7.0 mL, 0.654 M). Triflic acid (2.0 mL, 22.9 mmol, 5.0 eq.) was carefully added, the solution purged with Ar for 5 min and the reaction tube transferred to a pre-warmed oil bath set to 40°C and stirred for 22 h. The reaction mixture was allowed to cool to room temperature before carefully poured onto icy H_2O (100 mL). The aqueous phase was extracted with DCM (3 x 30 mL) and the combined organic extracts were washed with a saturated aqueous $NaHCO_3$ (30 mL) and brine (30 mL), dried over anhydrous Na_2SO_4, filtered and concentrated under reduced pressure by rotary evaporation to afford the title compound **SI 5** (0.816 g, 4.08 mmol, 89%) as a dark orange solid.

Important note: Store in a freezer under inert atmosphere to prevent oxidation and prolong shelf life.

TLC: R_f = 0.38 (1:6 EtOAc/*n*-heptane)

LCMS (ESI) $[M+H]^+$ *m/z* calcd for $C_{12}H_9OS^+$: 201.0369 , *m/*z found: 200.93 $[M+H]^+$

R_t: 1.59 min (total run time: 2.6 min), purity >98%

^{1}H NMR (400 MHz, DMSO-d_6): δ 10.65 (s, 1H, enol-OH), 9.10 (d, *J* = 8.3 Hz, 1H), 7.99 (dd, *J* = 8.0, 1.4 Hz, 1H), 7.88 (d, *J* = 8.7 Hz, 1H), 7.78 (d, *J* = 8.7, 1H), 7.63 – 7.57 (m, 1H), 7.57-7.51 (m, 1H), 6.67 (s, 1H)

^{13}C NMR (101 MHz, DMSO-d_6): δ 151.9, 135.6, 130.9, 129.2, 128.0, 126.0, 125.4, 125.1, 125.1, 123.6, 121.6, 98.5

Note: NMR spectroscopy in DMSO-d_6 resulted in the enol tautomer.

1H,1'H-2,2'-Bipyrrole (SI 8)

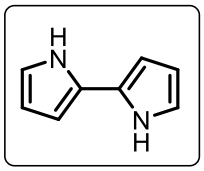

To an oven-dried round-bottomed flask were added pyrrole (0.52 mL, 7.49 mmol, 1.0 eq.) in DCM (100 mL, 0.0745 M), PIFA (1.07 g, 2.48 mmol, 0.33 eq.) and TMSBr (0.65 mL, 4.97 mmol, 0.66 eq.) at -78°C. The reaction mixture was stirred for 80 min, allowed to slowly heat to room temperature and saturated aqueous $NaHCO_3$ (120 mL) was added. This was stirred vigorously for 30 min. The aqueous phase was extracted with DCM (5 x 30 mL) and the combined organic extracts were dried over anhydrous Na_2SO_4, filtered and concentrated under reduced pressure by rotary evaporation. Purified by DCVC (5% to 25% EtOAc in *n*-hexane with 1% increments) to afford the title compound **SI 8** (192 mg, 3.73 mmol, 39%).

The data is in accordance with previously reported work.[29]

LCMS (ESI) $[M+H]^+$ *m/z* calcd for $C_8H_9N_2^+$: 133.0760 , *m/*z found: 132.95 $[M+H]^+$

R_t: 1.08 min (total run time: 2.6 min), purity >99%

^{1}H NMR (400 MHz, $CDCl_3$): δ 8.31 (bs, 2H,), 6.81 – 6.71 (m, 2H), 6.29 – 6.19 (m, 4H)

^{13}C NMR (101 MHz, $CDCl_3$): δ 126.1, 117.7, 109.6, 103.7

1H,1'H-[2,2'-Bipyrrole]-5-carbaldehyde (SI 9)

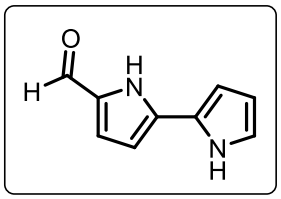

To an oven-dried round-bottomed flask was added bipyrrole **5** (151 mg, 1.14 mmol, 1.0 eq.) and DMF (7.5 mL, 0.152 M). The solution was cooled to 0°C, and $POCl_3$ (0.10 mL, 1.07 mmol, 1.0 eq.) was added using a Hamilton syringe. The reaction mixture was stirred at 0°C for 2 h and saturated aqueous Na_2CO_3 (40 mL) was added. The mixture was heated to 70°C for 30 min, cooled to room temperature and filtered. The residue was washed with H_2O, cold MeOH, cold Et_2O and cold *n*-pentane to afford the title compound **SI 9** (52.6 mg, 0.328 mmol, 29%) as a crystalline green-yellow solid.

Data is in accordance with previously reported work.[30]

TLC: R_f = 0.52 (1:1 EtOAc/*n*-heptane)

LCMS (ESI) $[M+H]^+$ *m/z* calcd for $C_9H_9N_2O^+$: 161.0709 , *m/*z found: 160.94 $[M+H]^+$

R_t: 1.00 min (total run time: 2.6 min), purity >99%

^{1}H NMR (400 MHz, DMSO-d_6): δ 11.97 (s, 1H), 11.23 (s, 1H), 9.34 (s, 1H), 7.00 (d, *J* = 3.9 Hz, 1H), 6.88 (q, *J* = 2.1 Hz, 1H), 6.75 – 6.70 (m, 1H), 6.53 (d, *J* = 3.9 Hz, 1H), 6.11 (q, *J* = 3.1, 2.5 Hz, 1H)

^{13}C NMR (101 MHz, DMSO-d_6): δ 177.4, 134.6, 132.0, 123.5, 119.9, 109.2, 107.5, 106.2

Note: There is one quaternary carbon signal missing from the ^{13}C NMR spectrum.

5 Specific reaction procedures and analyses of photoswitches

(*Z*)-2-(Naphthalen-1-ylmethylene)benzo[b]thiophen-3(2H)-one (2)

Prepared according to general procedure A.

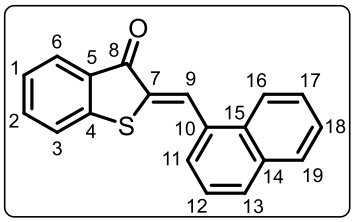

Hemithioindigo **SI 6** (109 mg, 0.727 mmol, 1.0 eq.), benzene (4.0 mL, 0.182 M), 1-naphthaldehyde (1.04 mL, 0.726 mmol, 1.0 eq.). The aldehyde was added in two portions with stirring for 45 min under N_2 at 100°C in between. Stirring continued for 2 h at 100°C and 17 h at room temperature. Purified by flash column chromatography (0% to 15% EtOAc in *n*-heptane) to afford the title compound (*Z*/*E*)-**1** (64.3 mg, 0.223 mmol, 31%) as an orange solid.

TLC: R_f = 0.38 (1:6 EtOAc/*n*-heptane)

LCMS (ESI) $[M+H]^+$ *m/z* calcd for $C_{19}H_{13}OS^+$: 289.0682 , *m/*z found: N/A $[M+H]^+$

R_t: 3.39 min (total run time: 5.2 min), purity >99%

^{1}H NMR (800 MHz, CD_2Cl_2): δ 8.71 (s, 1H, **H-9**), 8.27 (d, *J* = 8.4 Hz, 1H), 7.98 (d, *J* = 7.1 Hz, 1H), 7.97 – 7.96 (m, 1H), 7.96 – 7.95 (m, 1H), 7.94 (d, *J* = 8.0 Hz, 1H), 7.65 – 7.57 (m, 4H), 7.54 (dd, *J* = 7.9, 1.8 Hz, 1H), 7.34 (td, *J* = 7.4, 1.6 Hz, 1H)

^{13}C NMR (101 MHz, CD_2Cl_2): δ 188.5, 147.0, 135.9, 134.3, 133.7, 132.8, 132.0, 131.4, 131.2, 130.1, 129.4, 128.2, 127.6, 127.4, 127.1, 126.2, 126.0, 124.6, 124.1

HRMS-ESI $[M+H]^+$ *m/z* calcd for $C_{19}H_{13}OS^+$: 289.0682 , *m/*z found: 289.0678 $[M+H]^+$ (ppm error: -1.34)

(*E*)-**1**:

^{1}H NMR (400 MHz, CD_2Cl_2): δ 7.98 (m, 1H), 7.96 – 7.90 (m, 3H), 7.88 (s, 1H, **H-9**), 7.74 (ddd, *J* = 7.7, 1.4, 0.7 Hz, 1H), 7.63 – 7.56 (m, 2H), 7.56 – 7.52 (m, 2H), 7.51 – 7.48 (m, 1H), 7.26 (ddd, *J* = 8.1, 7.2, 1.0 Hz, 1H)

Note: A 1:5 (*Z*/*E*)-ratio was observed for (*E*)-**10** by ^{1}H NMR.

UV-Vis spectroscopy

HTI 1-naphthalene (**2**) (33 µM in DCM)

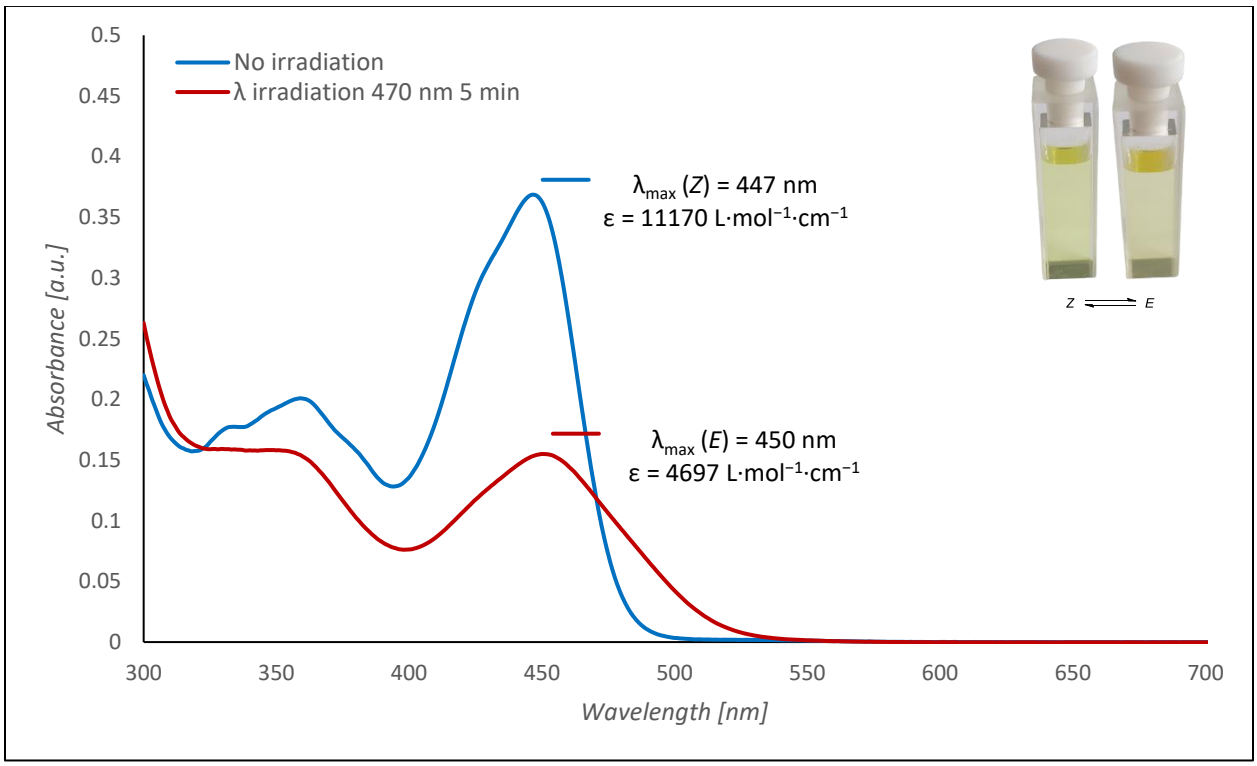

HTI 1-naphthalene (**2**) (33 µM in *n*-hexane/iPrOH 9:1)

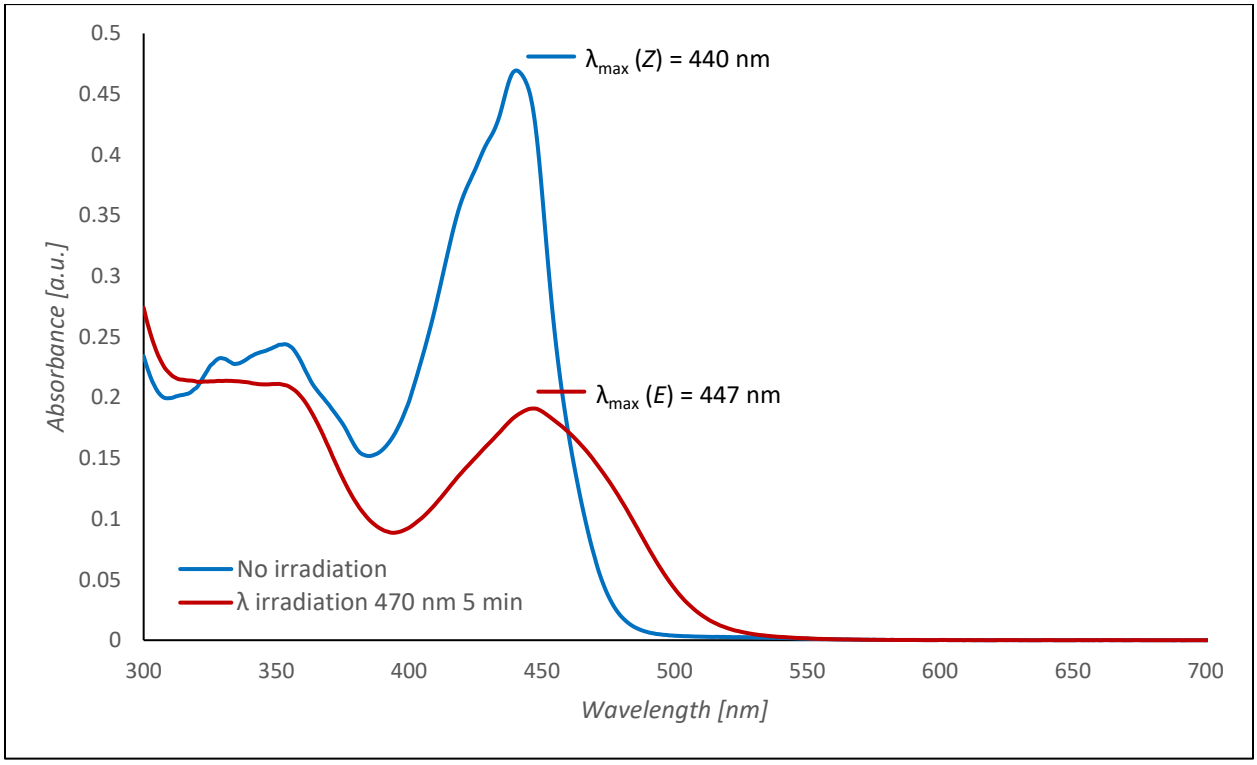

HTI 1-naphthalene (**2**) (33 μM in PhMe)

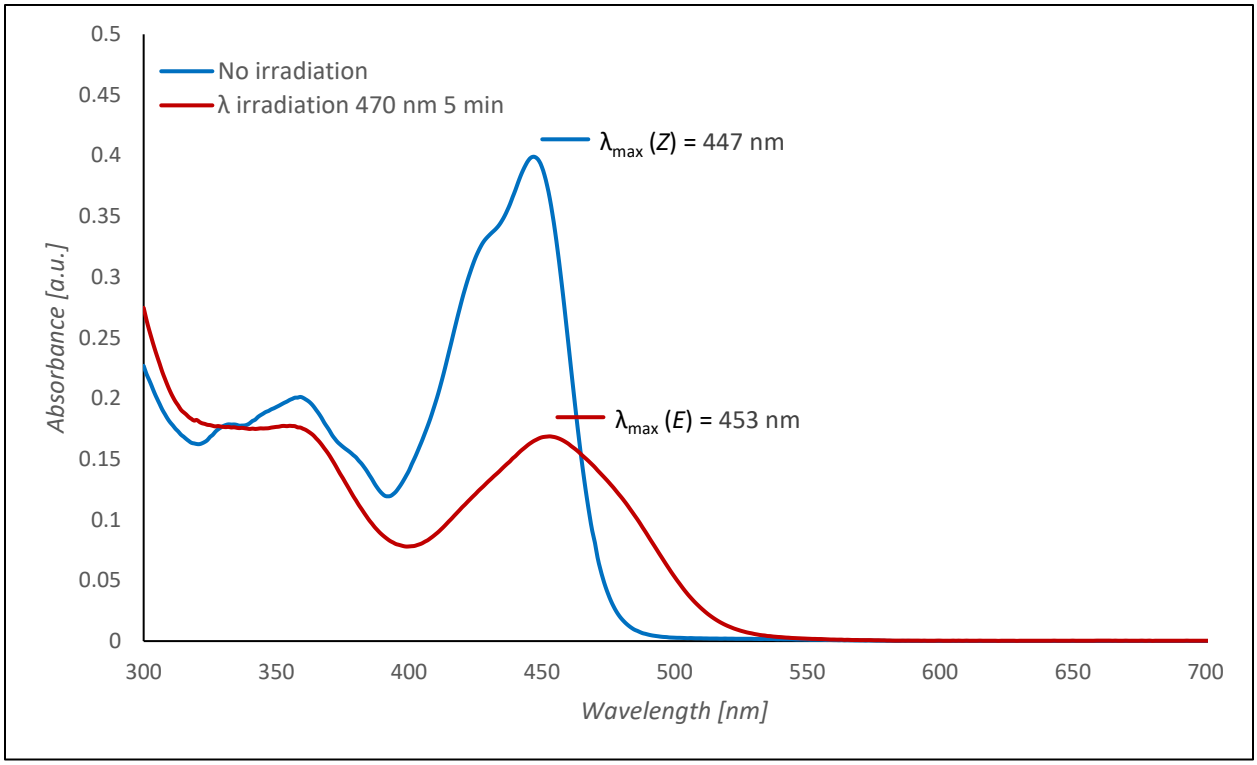

UV-Vis thermal relaxation spectroscopy

HTI 1-naphthalene (**2**) (33 μM in PhMe)

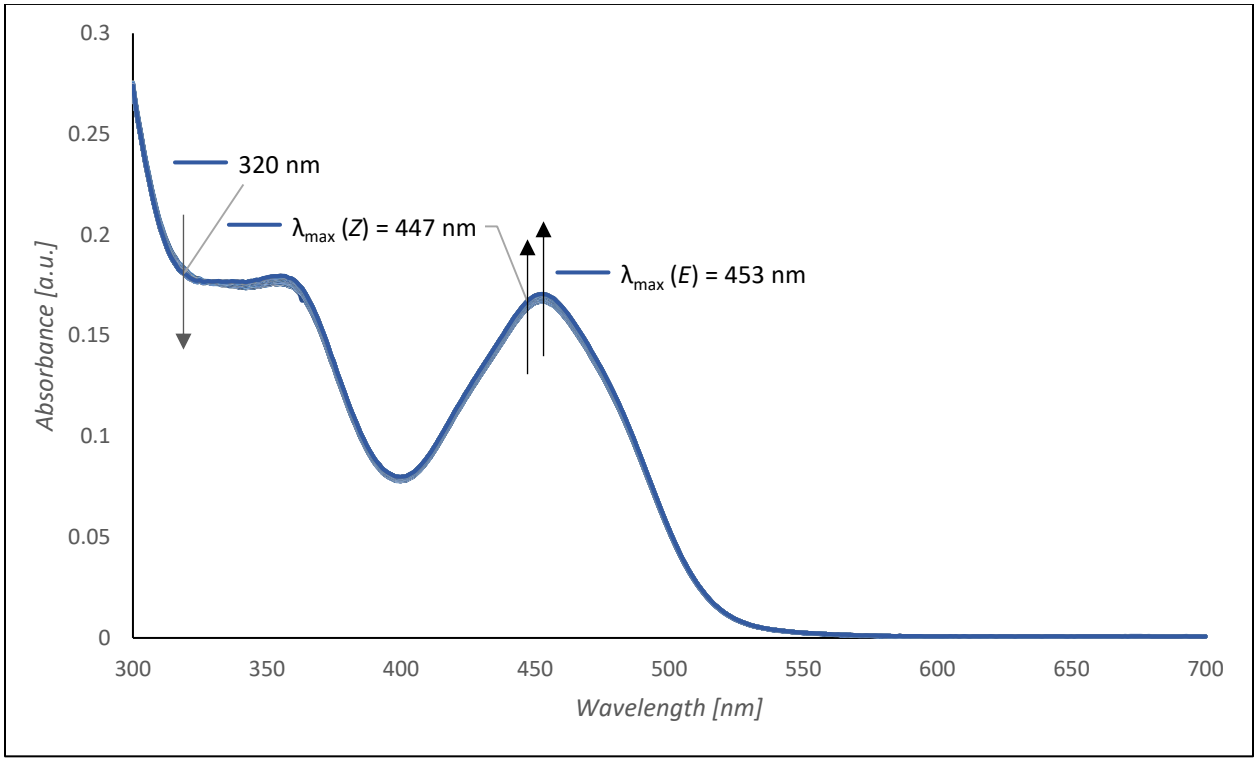

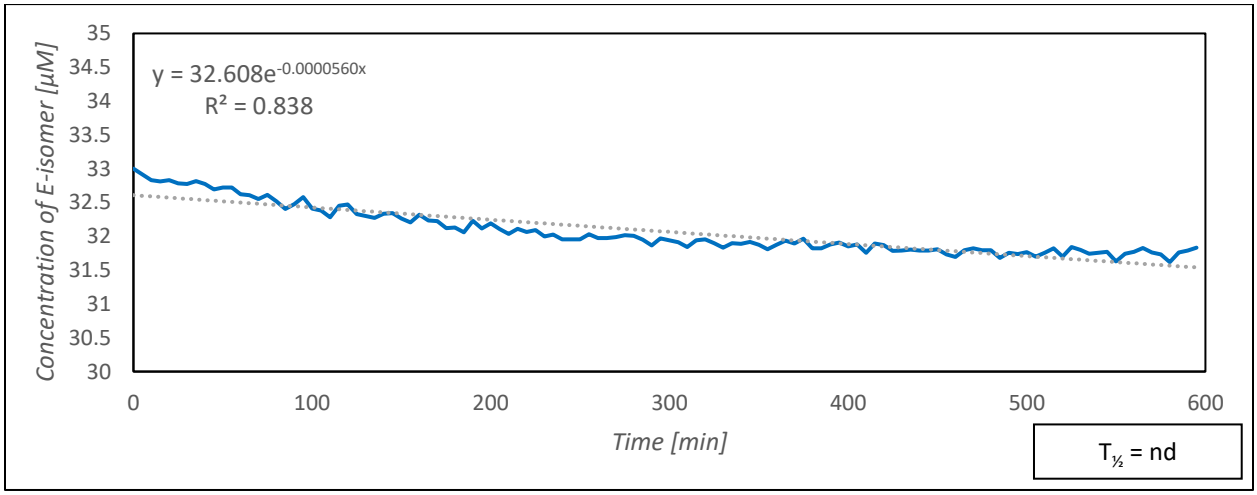

Note: Concentrations of isomers were calculated using λ_{max} (*Z*) = 447 nm and 320 nm as representative for λ_{max} (*E*) = 453 nm.

HPLC conditions

Column:	ChiralPak AD-H column (5 µm, 250 x 4.6 mm)
Mobile Phase	90:10 *n*-hexane/iPrOH (isocratic, 1 mL/min)
Isosbestic Point	460 nm (in HPLC mobile Phase)
t_R(E)	11.88 min
t_R(Z)	9.95 min

Solution composition (%*E*-isomer)

Initial solution composition before irradiation: *E*-isomer (0.00%) / *Z*-isomer (100.00%)

Time	**470 nm**	**Time**	**530 nm**
5 min	85.60%	**10 min**	15.14%
10 min	86.14%	**20 min**	14.17%

Representative HPLC traces

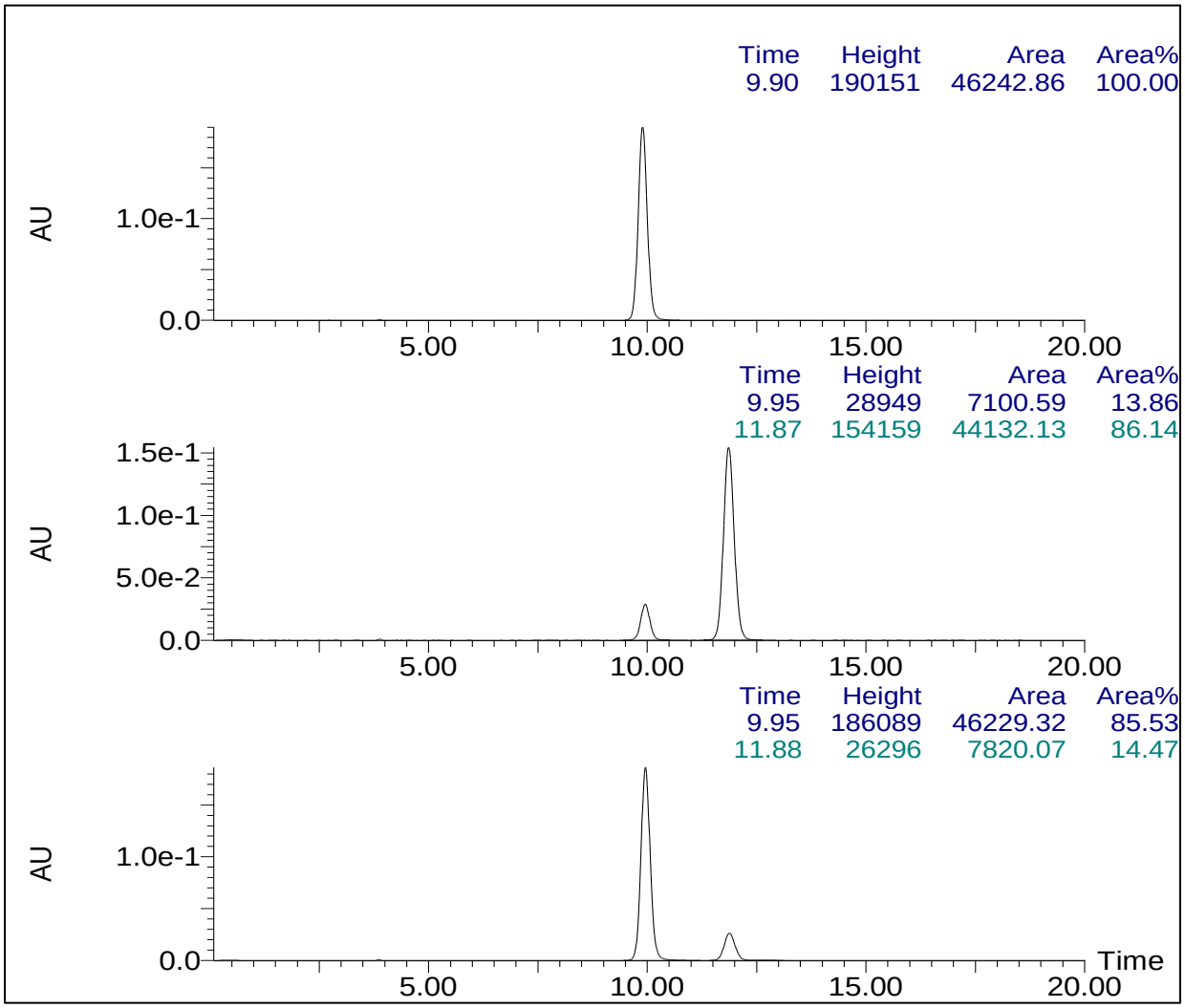

(*Z*)-2-(Naphthalen-2-ylmethylene)benzo[b]thiophen-3(2H)-one (3)

Prepared according to general procedure A.

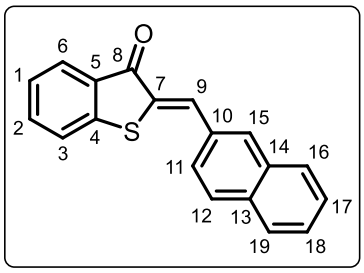

Hemithioindigo **SI 6** (95.0 mg, 0.633 mmol, 1.0 eq.), benzene (4.0 mL, 0.158 M), 2-naphthaldehyde (88.9 mg, 0.569 mmol, 0.90 eq.). Stirred for 14 h under N_2 at 100°C. Upon cooling to room temperature precipitation occurred. Purified by DCVC (0% to 10% EtOAc in *n*-heptane with 1% increments) to afford the title compound (*Z*)-**3** (145 mg, 0.503 mmol, 88%) as an orange solid.

The data is in accordance with previously reported work.[31] No photophysical properties reported.

TLC: R_f = 0.70 (1:1 EtOAc/*n*-heptane)

LCMS (ESI) $[M+H]^+$ *m/z* calcd for $C_{19}H_{13}OS^+$: 289.0682 , *m/*z found: 288.97 $[M+H]^+$

R_t: 2.28 min (total run time: 2.6 min), purity >97%

^{1}H NMR (400 MHz, $CDCl_3$): δ 8.21 (s, 1H, **H-15**), 8.14 (s, 1H, **H-9**), 7.98 (d, *J* = 6.6 Hz, 1H, **H-6**), 7.96 – 7.91 (m, 2H), 7.89 – 7.84 (m, 1H), 7.81 (dd, *J* = 8.6, 1.8 Hz, 1H), 7.63 – 7.52 (m, 4H, **H-1**, **H-3**), 7.33 (td, *J* = 7.3, 1.0 Hz, 1H, **H-2**)

^{13}C NMR (101 MHz, $CDCl_3$): δ 188.8 (**C-8**), 146.3 (**C-5**), 135.4 (**C-1**), 134.0 (**C-10**/**C-14**), 133.9 (**C-9**), 133.4, 132.1 (**C-15**), 132.0, 130.7, 130.6, 129.0, 128.9, 127.9, 127.9, 127.3, 127.3, 127.0, 125.8 (**C-2**), 124.1

HRMS-ESI $[M+H]^+$ *m/z* calcd for $C_{19}H_{13}OS^+$: 289.0682 , *m/*z found: 289.0684 $[M+H]^+$ (ppm error: 0.726)

UV-Vis spectroscopy

HTI 2-naphthalene (**3**) (33 µM in DCM)

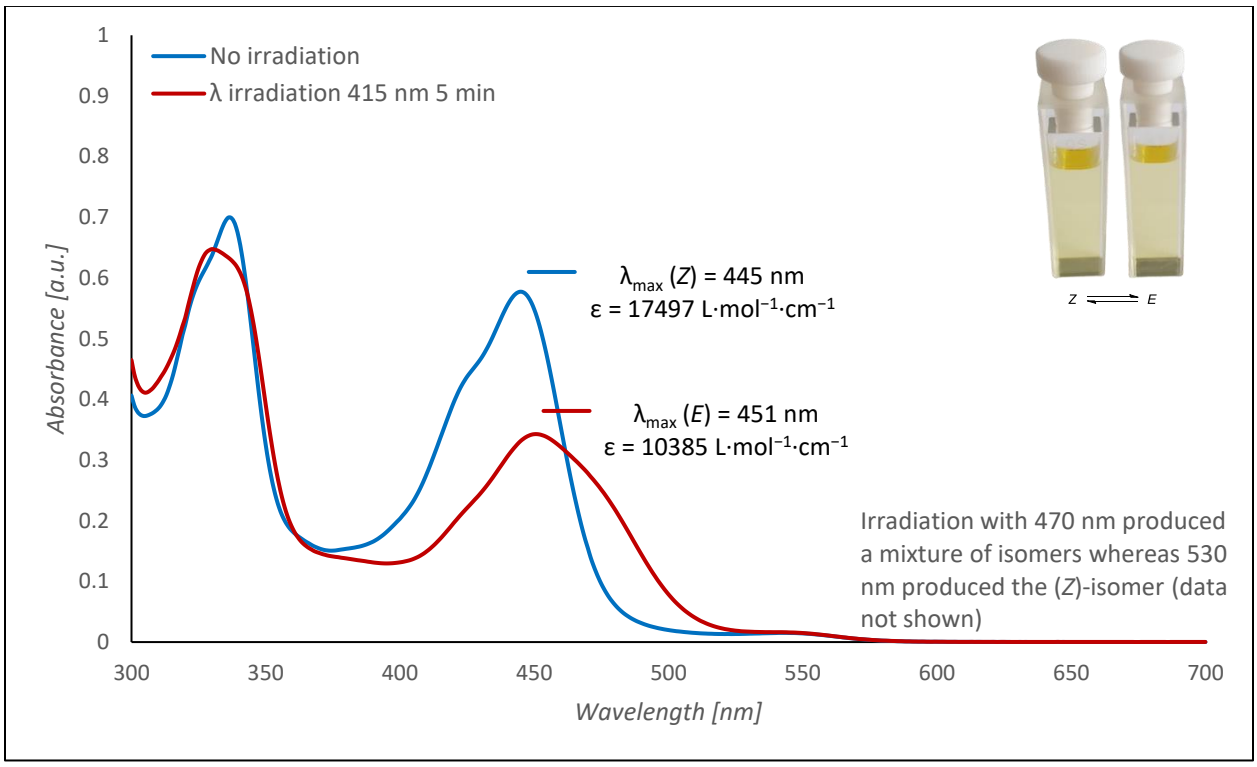

HTI 2-naphthalene (**3**) (33 µM in *n*-hexane/iPrOH 9:1)

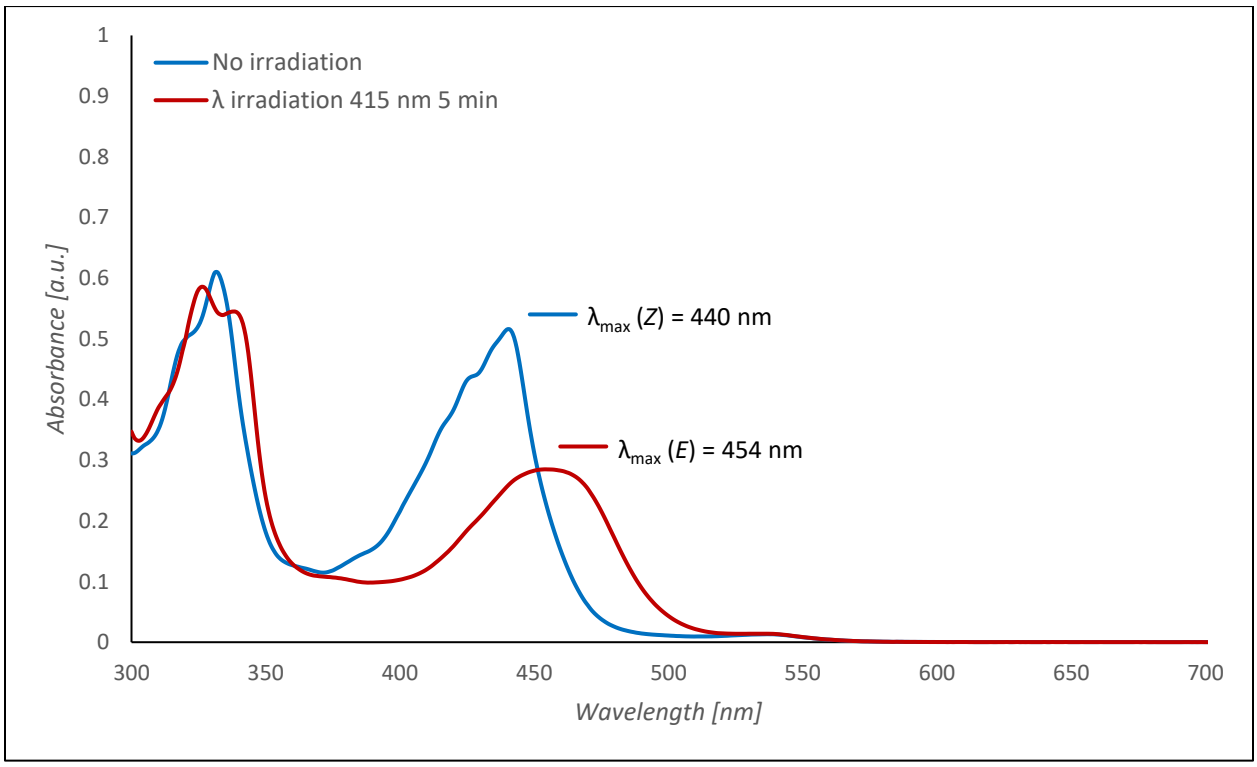

HTI 2-naphthalene (**3**) (33 μM in PhMe)

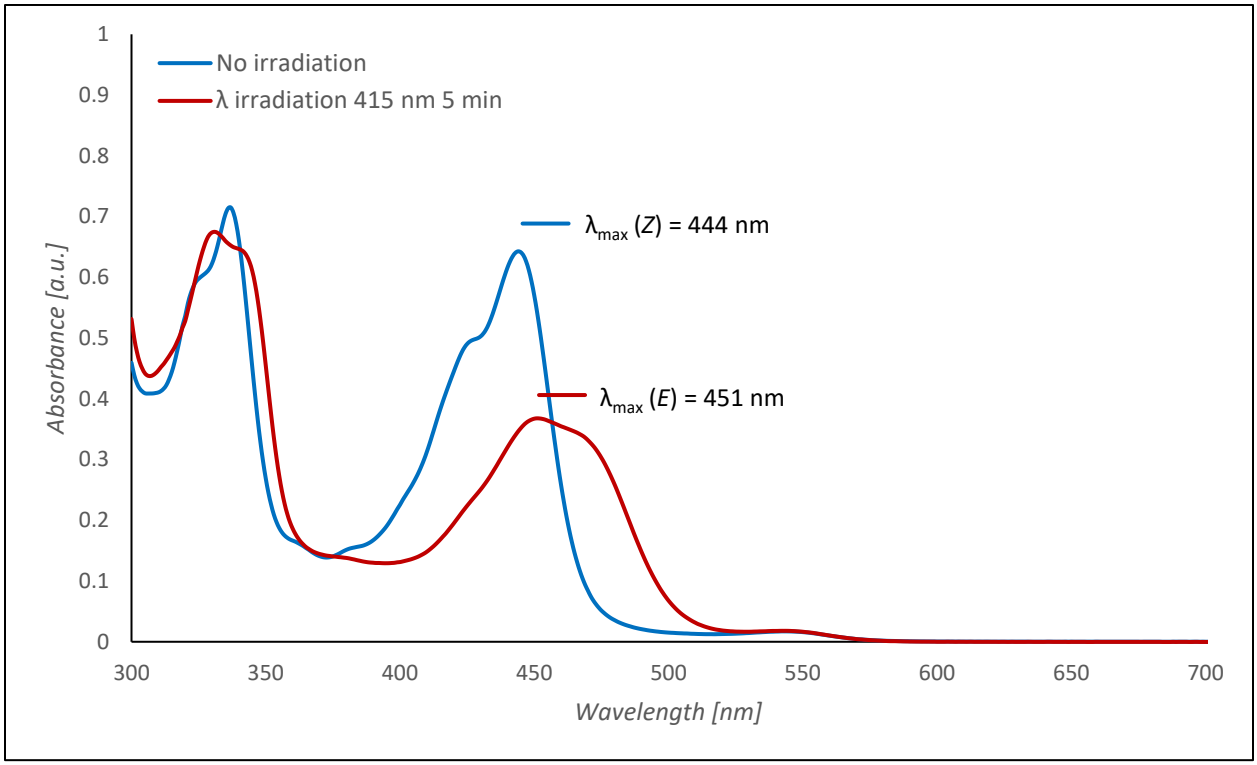

UV-Vis thermal relaxation spectroscopy

HTI 2-naphthalene (**3**) (33 μM in PhMe)

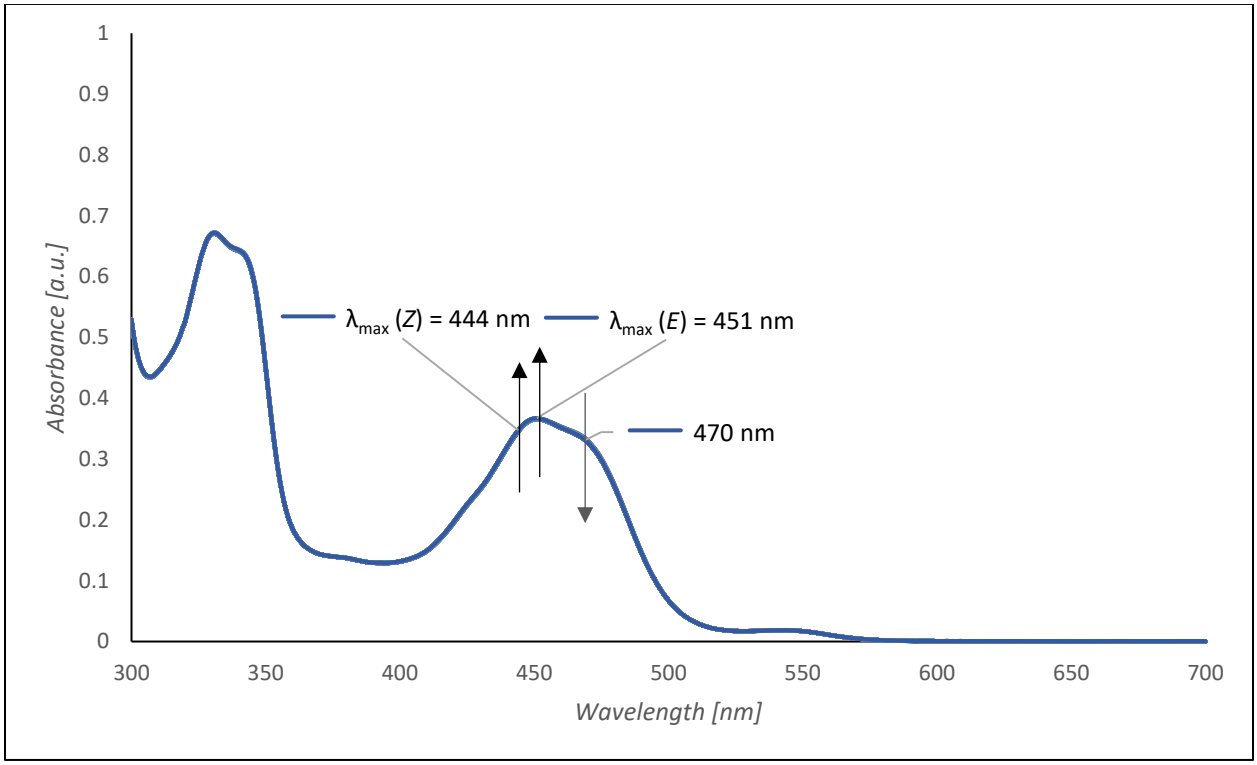

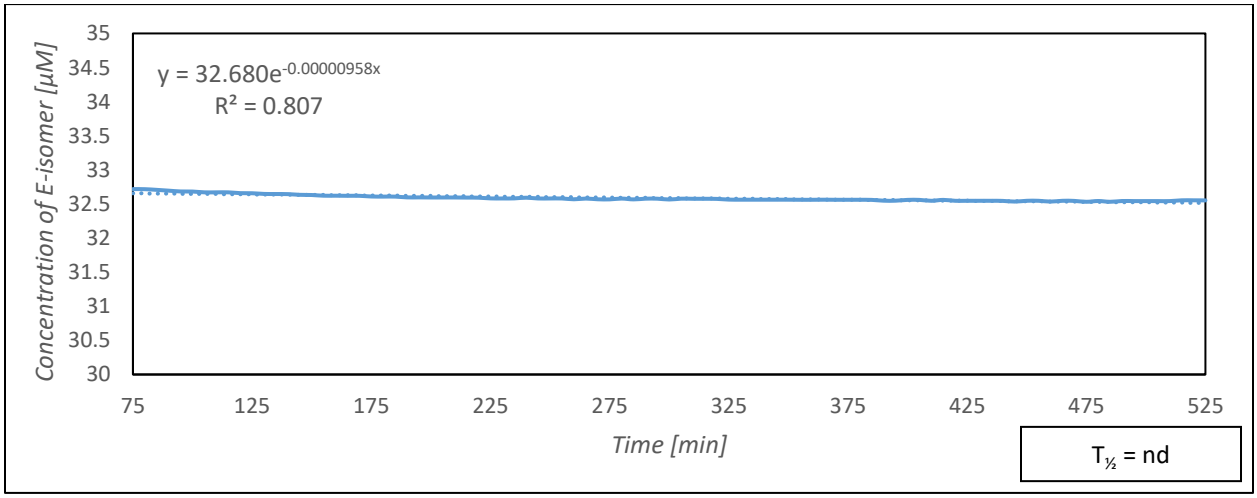

Note: Concentrations of isomers were calculated using λ_{max} (*Z*) = 444 nm and 470 nm as representative for λ_{max} (*E*) = 451 nm.

HPLC conditions

Column:	ChiralPak AD-H column (5 µm, 250 x 4.6 mm)
Mobile Phase	90:10 *n*-hexane/iPrOH (isocratic, 1 mL/min)
Isosbestic Point	451 nm (in HPLC mobile Phase)
t_R(E)	12.42 min
t_R(Z)	11.38 min

Solution composition (%*E*-isomer)

Initial solution composition before irradiation: *E*-isomer (5.80%) / *Z*-isomer (94.20%)

Time	**415 nm**	**530 nm**
5 min	81.93	3.87
10 min	82.25	4.03

Representative HPLC traces

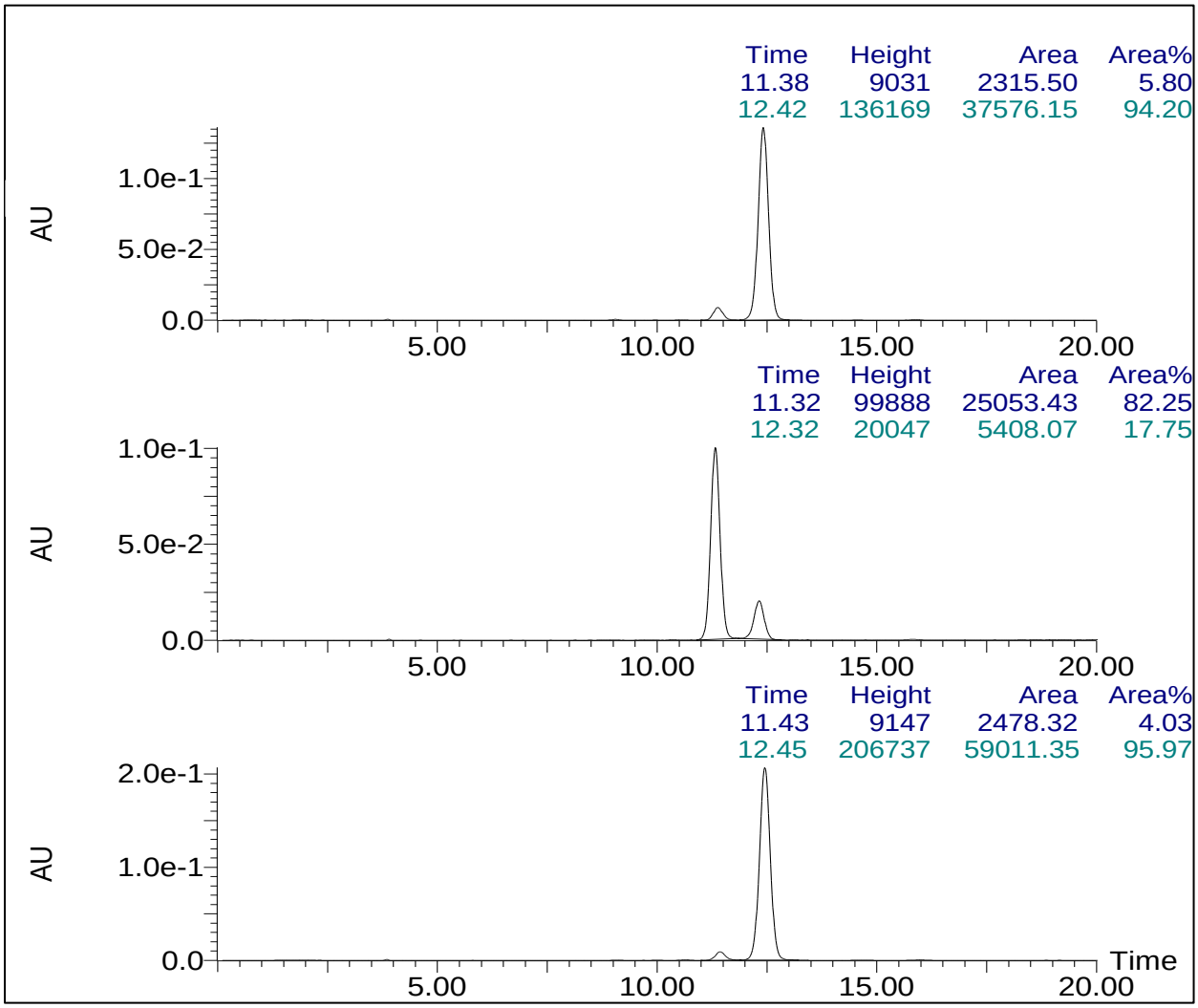

(*Z*)-2-Benzylidenenaphtho[2,1-b]thiophen-1(2H)-one (4)

Prepared according to general procedure A.

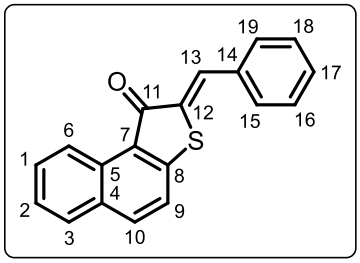

Hemithioindigo derivative **SI 5** (81.2 mg, 0.405 mmol, 1.0 eq.), benzene (4.0 mL, 0.101 M), benzaldehyde (0.36 mL, 0.354 mmol, 0.9 eq.). Stirred for 3 h under N_2 at 100°C. Purified by DCVC (0% to 5% EtOAc in *n*-heptane with 0.5% increments) to afford the title compound (*Z*)-**4** (27 mg, 0.354 mmol, 26%) as a yellow orange solid.

TLC: R_f = 0.40 (1:1 EtOAc/*n*-heptane)

LCMS (ESI) $[M+H]^+$ *m/z* calcd for $C_{19}H_{13}OS^+$: 289.0682 , *m/*z found: 289.01 $[M+H]^+$

R_t: 3.55 min (total run time: 5.2 min), purity >99%

^{1}H NMR (400 MHz, DMSO-d_6): δ 9.25 (d, *J* = 8.4 Hz, 1H), 8.33 (d, *J* = 8.6 Hz, 1H), 8.10 (d, *J* = 8.1 Hz, 1H), 8.05 (s, 1H, **H-13**), 7.93 (d, *J* = 8.6 Hz, 1H), 7.88 (m, 1H, **H-15**/**19**), 7.86 (m, 1H, **H-15**/**19**), 7.83 – 7.77 (m, 1H), 7.69 – 7.50 (m, 4H)

^{13}C NMR (101 MHz, DMSO-d_6): δ 188.0 (**C-11**), 149.7, 136.9, 133.8 (**C-13**), 133.8, 131.5, 130.9 (**C-15**/**19**), 130.9 (**C-15**/**19**), 130.7, 130.4, 130.2, 129.9, 129.4 (**C-16**/**18**), 129.4 (**C-16**/**18**), 129.1, 126.6, 122.3, 122.2, 122.1

HRMS-ESI $[M+H]^+$ *m/z* calcd for $C_{19}H_{13}OS^+$: 289.0682 , *m/*z found: 289.0684 $[M+H]^+$ (ppm error: 0.726)

Note: The ^{13}C NMR peaks at 130.9 ppm and 129.4 ppm both correspond to 2 carbon signals each disclosed by 2D NMR.

UV-Vis spectroscopy

Phenyl HTI derivative (**4**) (33 µM in DCM)

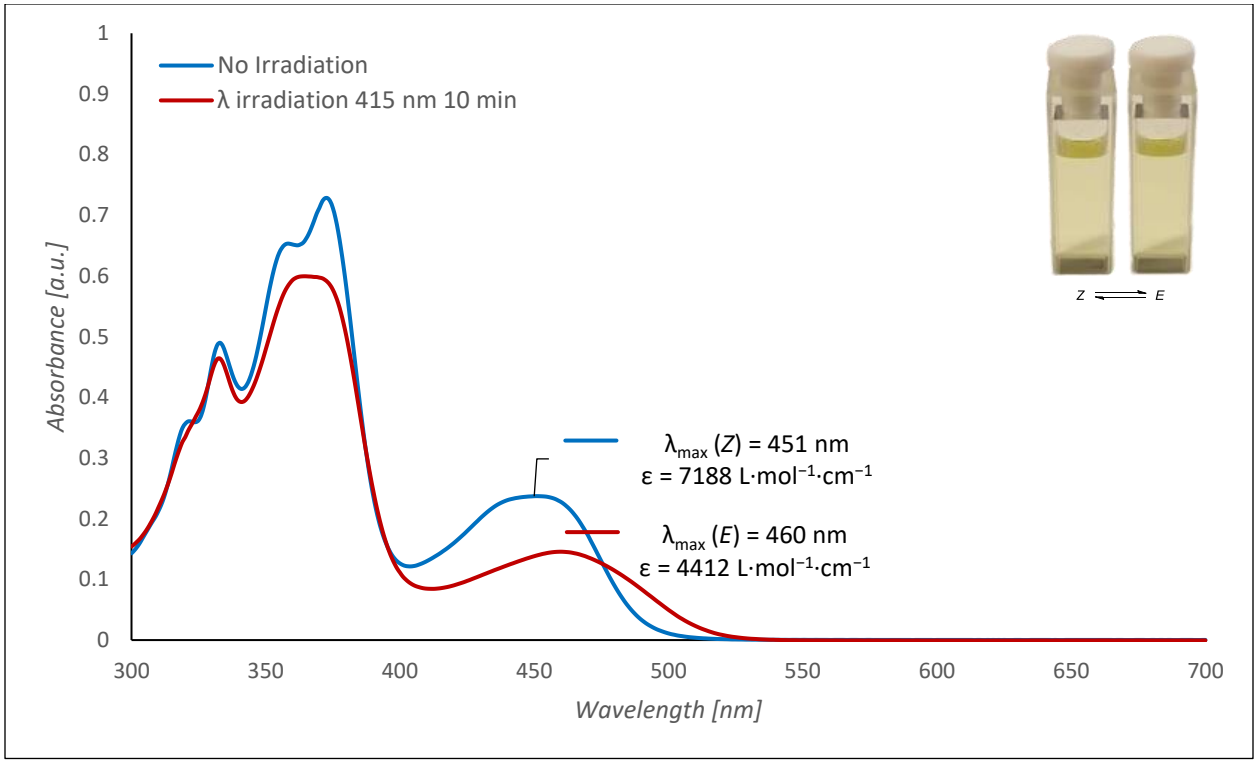

Phenyl HTI derivative (**4**) (33 µM in *n*-hexane/iPrOH 9:1)

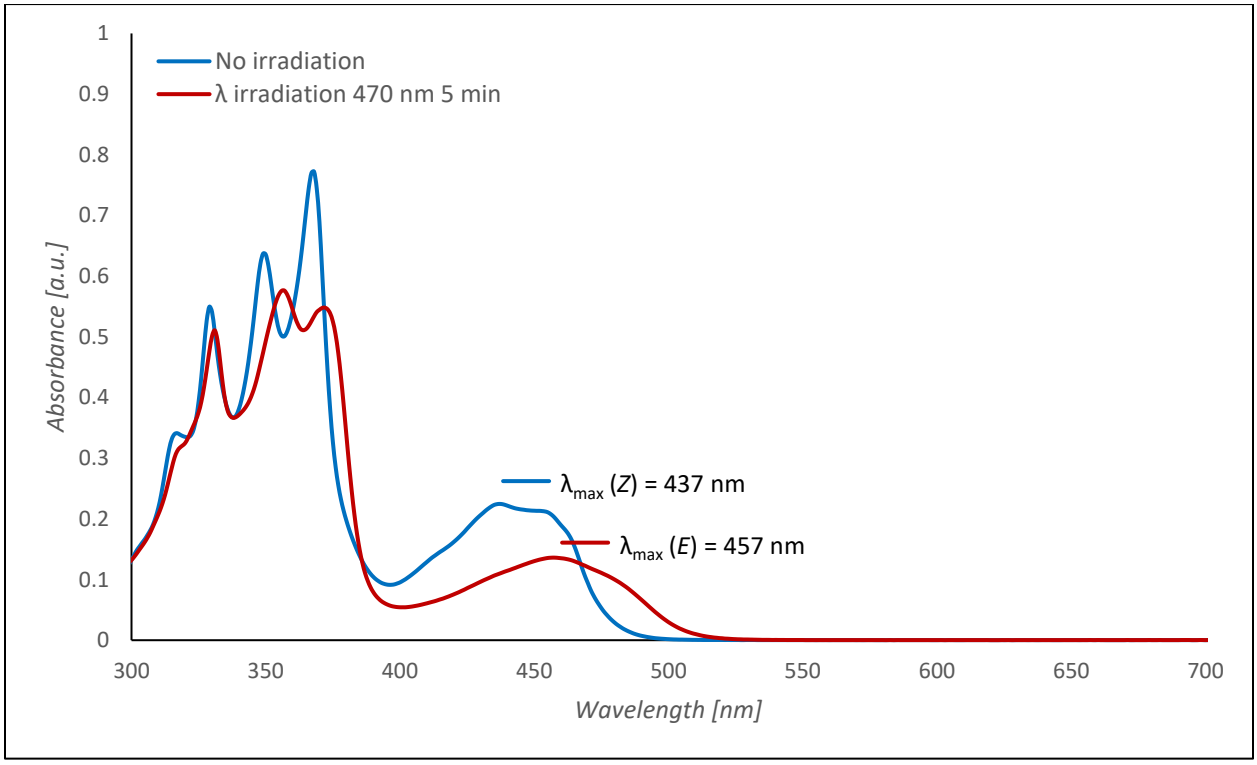

Phenyl HTI derivative (**4**) (33 µM in PhMe)

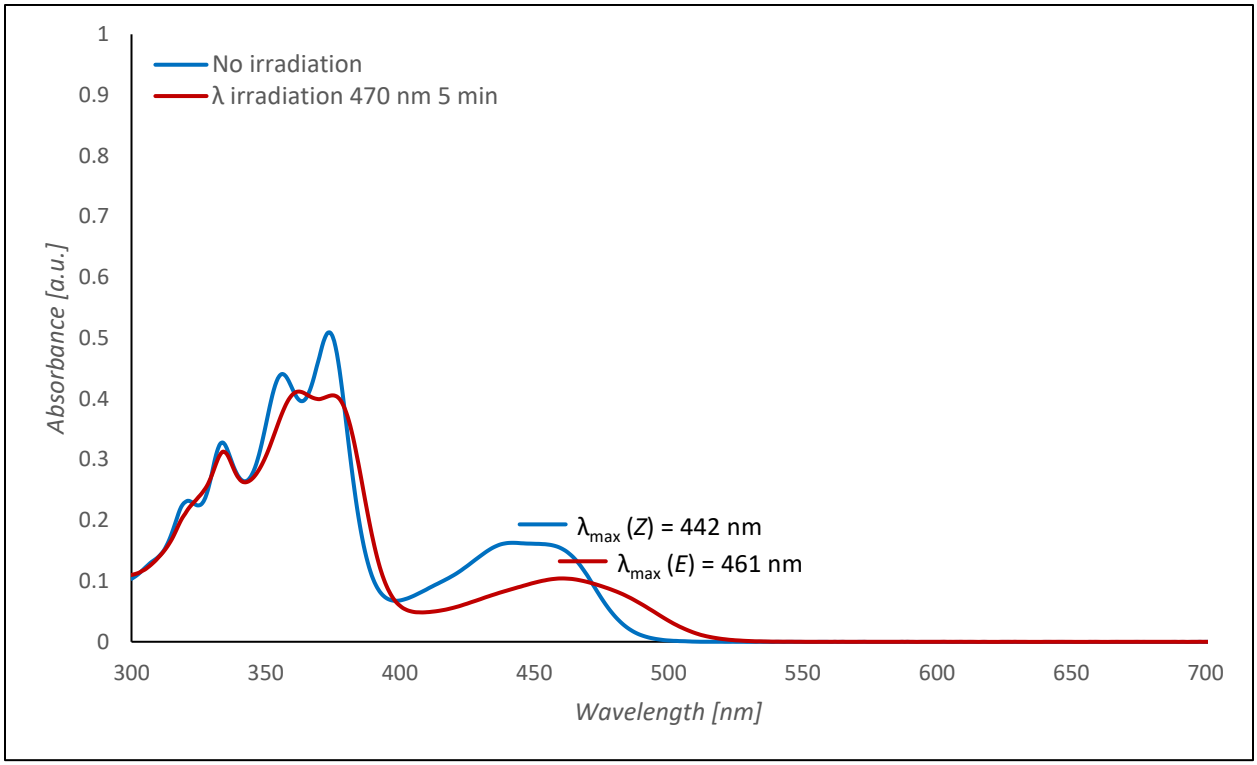

UV-Vis thermal relaxation spectroscopy

Phenyl HTI derivative (**4**) (33 µM in PhMe)

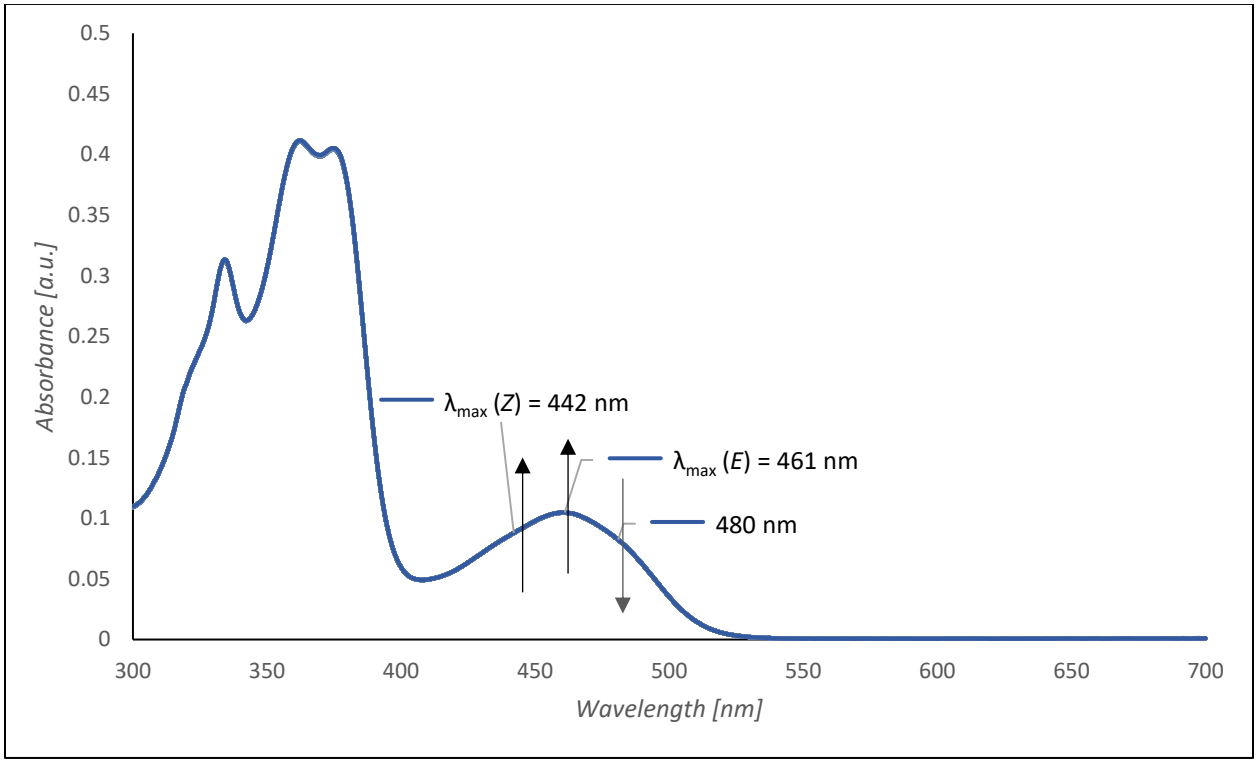

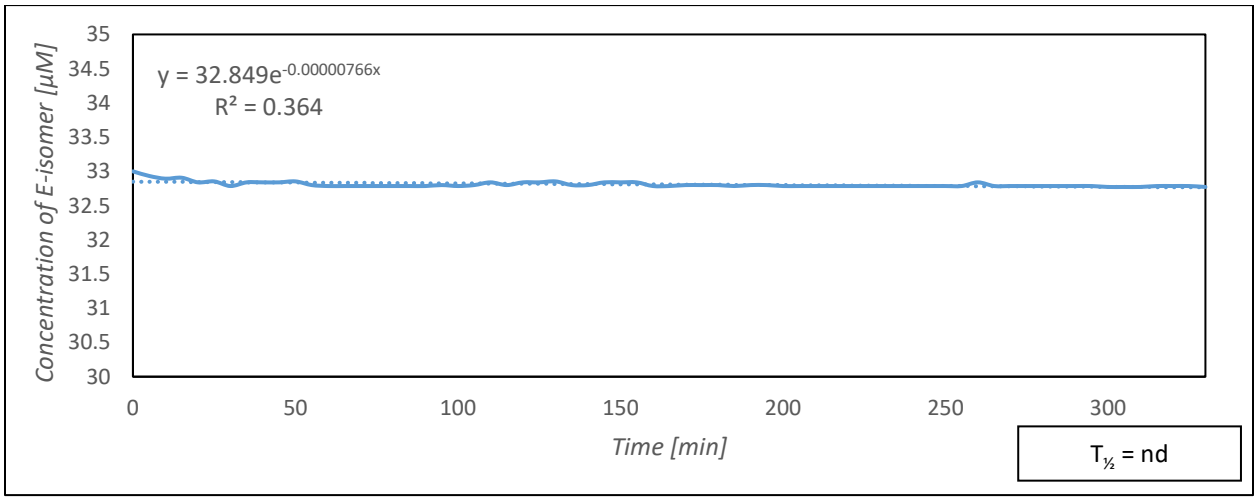

Note: Concentrations of isomers were calculated using λ_{max} (*Z*) = 442 nm and 480 nm as representative for λ_{max} (*E*) = 461 nm.

HPLC conditions

Column:	ChiralPak AD-H column (5 µm, 250 x 4.6 mm)
Mobile Phase	90:10 *n*-hexane/iPrOH (isocratic, 1 mL/min)
Isosbestic Point	467 nm (in HPLC mobile Phase)
t_R(E)	8.05 min
t_R(Z)	9.37 min

Solution composition (%*E*-isomer)

Initial solution composition before irradiation: *E*-isomer (0.00%) / *Z*-isomer (100.00%)

Time	**470 nm**	**530 nm**
10 min	59.77	12.17
20 min	75.00	11.28
30 min	77.13	11.31

Note: The sample was irradiated in DCM following a direct injection.

Representative HPLC traces

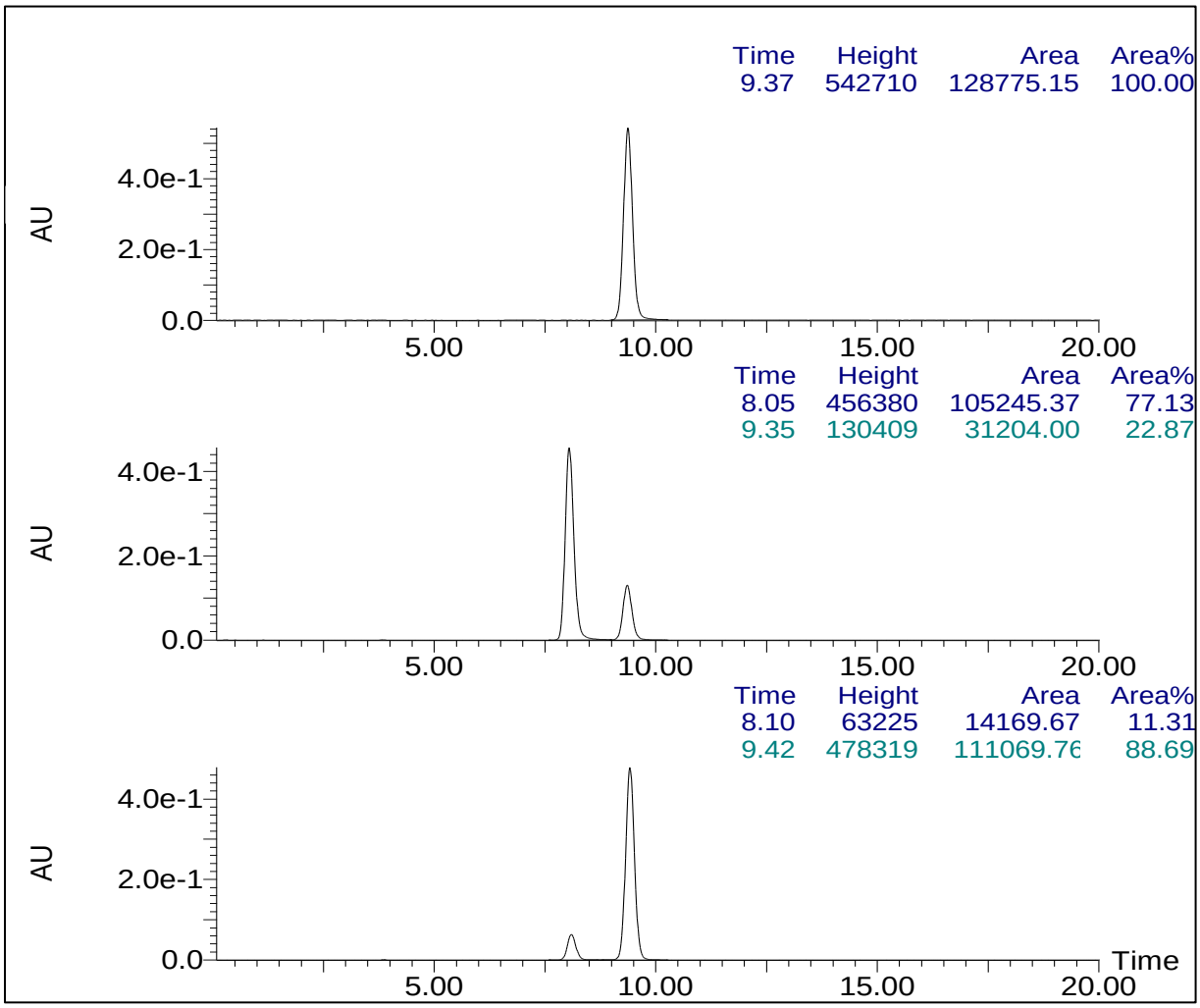

(*Z*)-2-(Naphthalen-2-ylmethylene)naphtho[2,1-b]thiophen-1(2H)-one (5)

Prepared according to general procedure **A.**

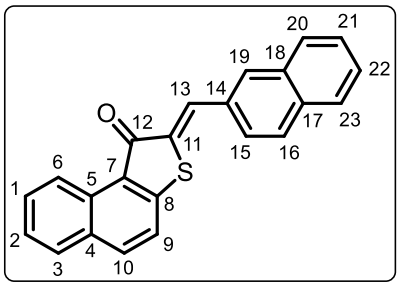

Hemithioindigo derivative **SI 5** (83.1 mg, 0.415 mmol, 1.0 eq.), benzene (4.0 mL, 0.104 M), 2-naphthaldehyde (63.8 mg, 0.408 mmol, 1.0 eq.). Stirred for 2.5 h under N_2 at 100°C. Compound was judged sufficiently pure after work-up. Afforded the title compound (*Z*)-**5** (70 mg, 0.207 mmol, 51%) as an orange-brown solid.

TLC: R_f = 0.57 (1:1 EtOAc/*n*-heptane)

R_t: 1.62 min (84%) + 2.17 min (16%) (total run time: 2.6 min)

^{1}H NMR (400 MHz, DMSO-d_6): δ 9.26 (dd, *J* = 8.1, 0.9 Hz, 1H), 8.44 (m, 1H), 8.32 (d, *J* = 8.6 Hz, 1H), 8.18 (s, 1H, **H**-**13**), 8.09 (m, 3H), 8.02 – 7.99 (m, 1H), 7.95 (m, 1H), 7.93 (m, 1H), 7.80 (ddd, *J* = 8.4, 6.9, 1.3 Hz, 1H), 7.68 – 7.61 (m, 3H)

^{13}C NMR (101 MHz, DMSO-d_6): δ 188.0 (**C**-**12**), 149.7, 137.0, 133.9 (**C**-**13**), 133.5, 132.9, 132.0, 131.6, 131.4, 130.5, 130.0, 129.1, 129.0, 128.8, 128.2, 127.8, 127.2, 126.7, 126.6, 122.4, 122.3, 122.1

HRMS-ESI $[M+H]^+$ *m/z* calcd for $C_{23}H_{15}OS^+$: 339.0838 , *m/z* found: 339.0837 $[M+H]^+$ (ppm error: -0.295)

Note: There is one quaternary carbon signal missing from the ^{13}C NMR spectrum. Performing 2D NMR did not disclose the missing peak.

UV-Vis spectroscopy

2-Naphthyl HTI derivative (**5**) (33 µM in DCM)

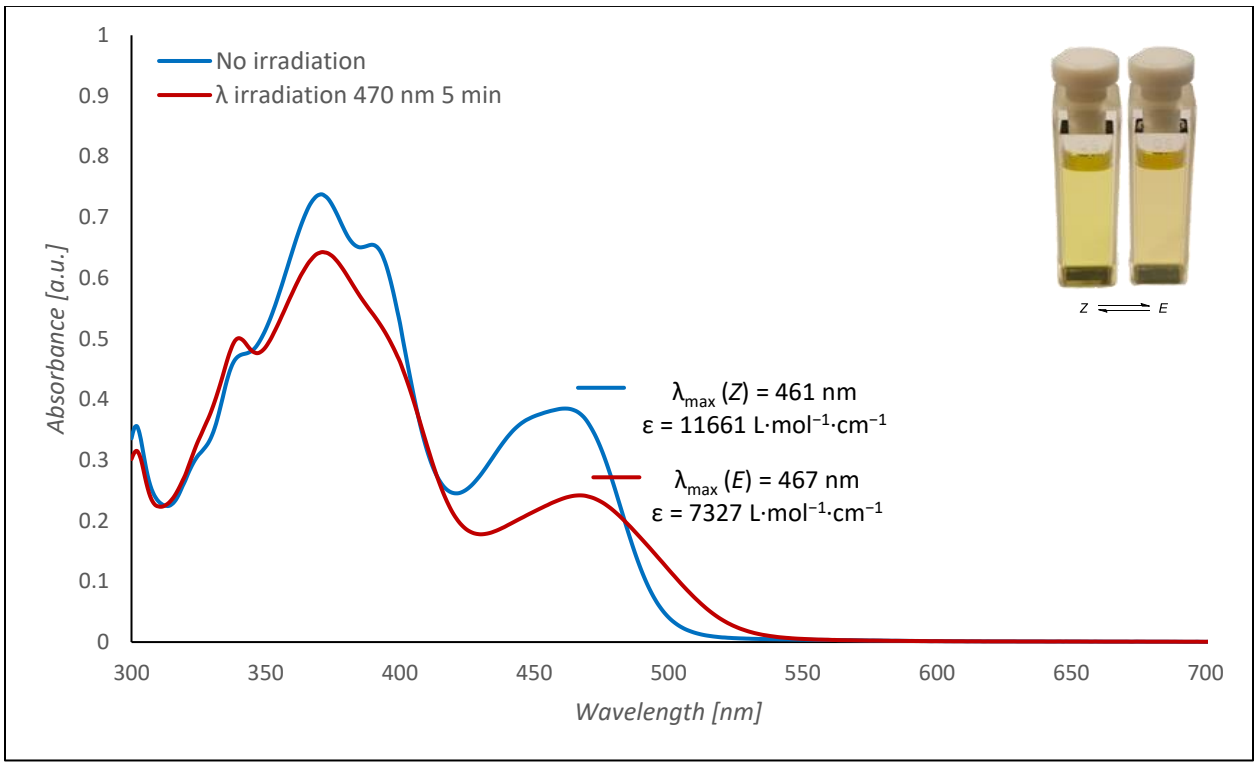

2-Naphthyl HTI derivative (**5**) (33 µM in *n*-hexane/iPrOH 9:1)

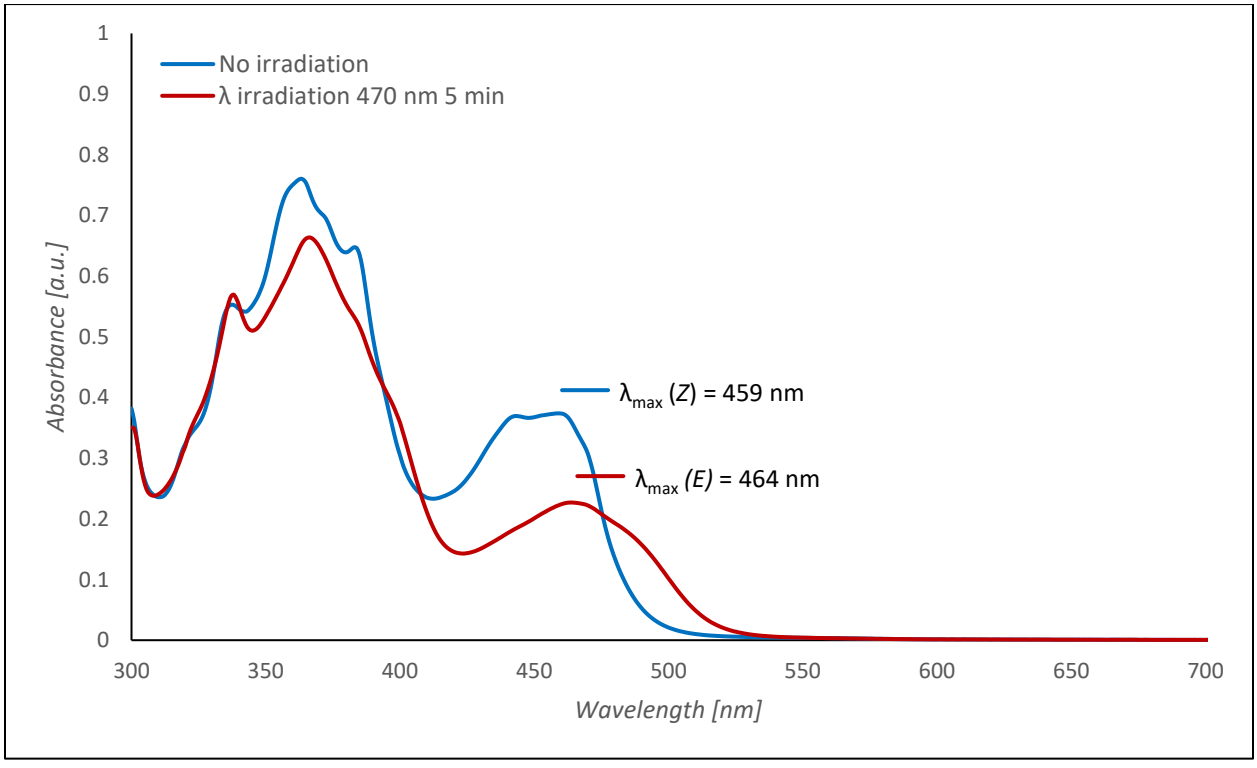

2-Naphthyl HTI derivative (**5**) (33 μM in PhMe)

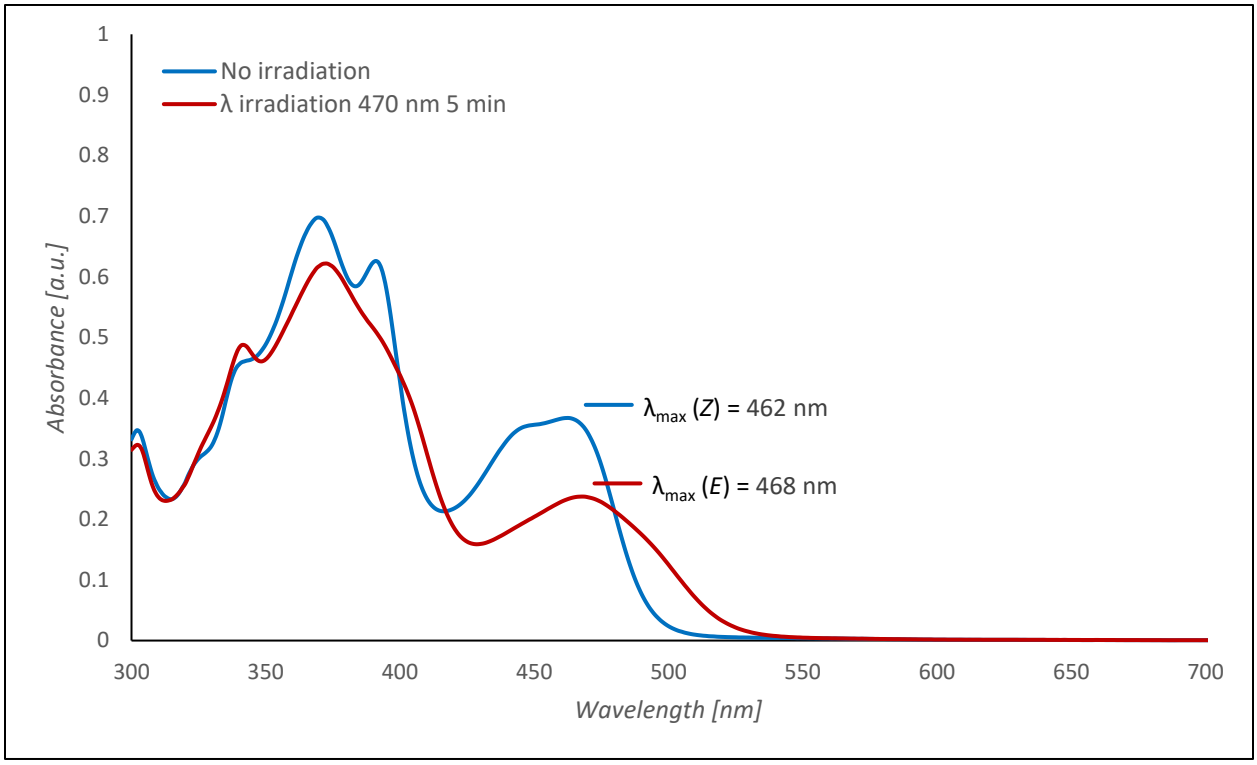

UV-Vis thermal relaxation spectroscopy

2-Naphthyl HTI derivative (**5**) (33 μM in PhMe)

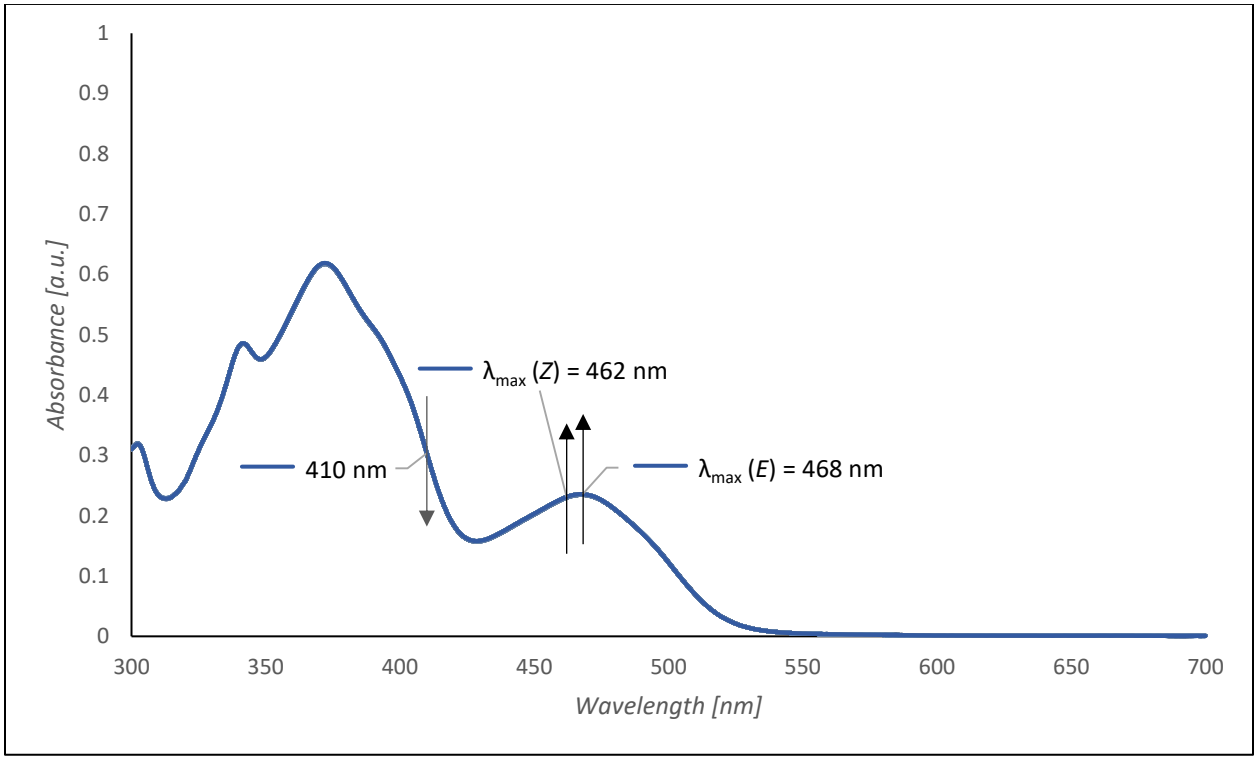

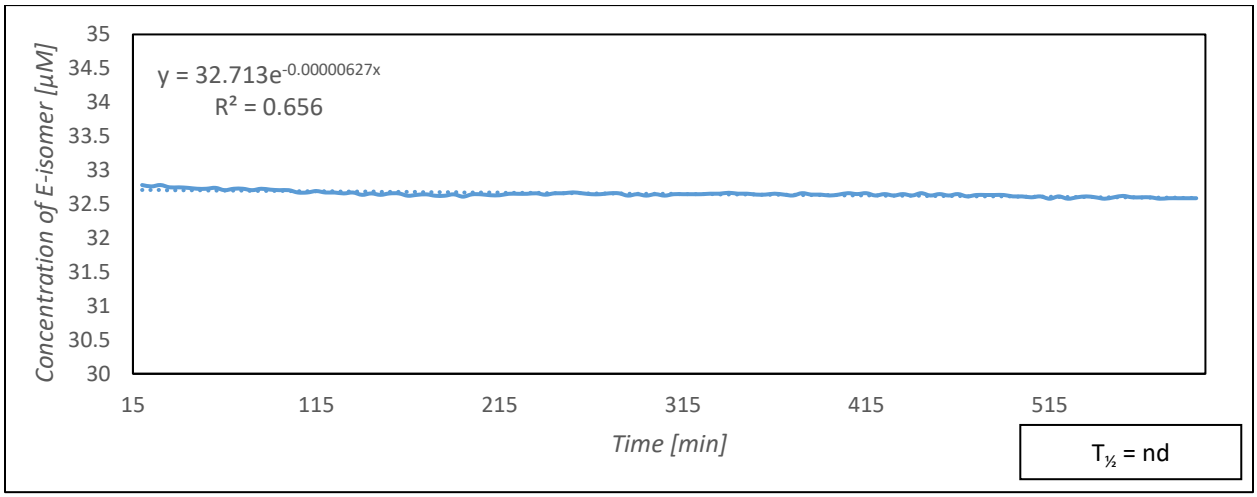

Note: Concentrations of isomers were calculated using λ_{max} (*Z*) = 462 nm and 410 nm as representative for λ_{max} (*E*) = 468 nm.

HPLC conditions

Column:	ChiralPak AD-H column (5 µm, 250 x 4.6 mm)
Mobile Phase	90:10 *n*-hexane/iPrOH (isocratic, 1 mL/min)
Isosbestic Point	475 nm (in HPLC mobile Phase)
t_R(E)	15.32 min
t_R(Z)	12.90 min

Solution composition (%*E*-isomer)

Initial solution composition before irradiation: *E*-isomer (0.78%) / *Z*-isomer (99.22%)

Time	**470 nm**	**530 nm**
5 min	74.17	14.58
10 min	75.09	13.41

Note: The sample (1 mg/mL) was irradiated in DCM following a direct injection.

Representative HPLC traces

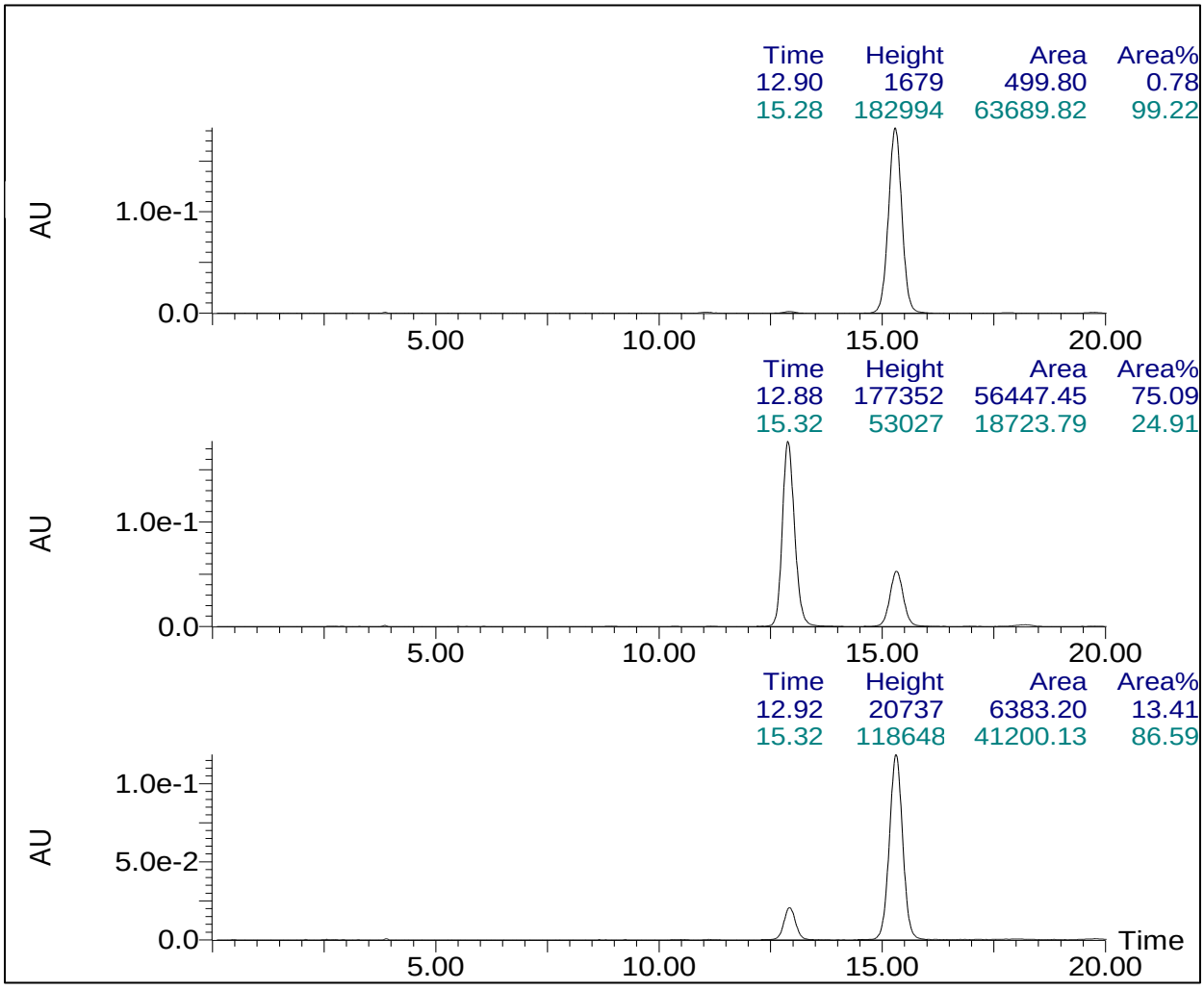

(*Z*)-2-((1H-Pyrrol-2-yl)methylene)benzo[b]thiophen-3(2H)-one (6)

Prepared according to general procedure A.

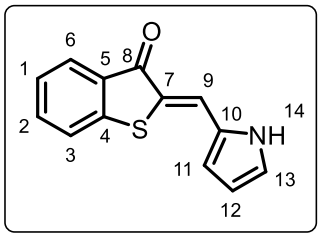

Hemithioindigo **SI 6** (87.0 mg, 0.582 mmol, 1.0 eq.), EtOH (2.0 mL, 0.291 M), 1H-pyrrole-2-carbaldehyde (56.0 mg, 0.593 mmol, 1.0 eq.). The solution was purged with N_2 for 10 min before piperidine was added. Stirred for 22 h under Ar at 40°C. Purified by DCVC (0% to 50% EtOAc in *n*-heptane with 5% increments) to afford the title compound (*Z*)-**6** (70.0 mg, 0.308 mmol, 53%) as an orange solid.

The data is in accordance with previously reported work.[28]

TLC: R_f = 0.41 (2:3 EtOAc/*n*-heptane)

LCMS (ESI) $[M+H]^+$ *m/z* calcd for $C_{13}H_{10}NOS^+$: 228.0478, *m/*z found: 228.45 $[M+H]^+$

R_t: 1.69 min (total run time: 2.6 min), purity >98%

^{1}H NMR (800 MHz, DMSO-d_6): δ 11.84 (s, 1H, **H-14**), 7.87 (s, 1H, **H-9**), 7.82 – 7.80 (m, 1H, **H-6**), 7.77 – 7.74 (m, 1H, **H-3**), 7.68 (ddd, *J* = 8.2, 7.1, 1.4 Hz, 1H, **H-1**), 7.37 (m, 1H, **H-2**), 7.28 (td, *J* = 2.6, 1.2 Hz, 1H, **H-13**), 6.79 – 6.76 (m, 1H, **H-11**), 6.42 (dt, *J* = 4.2, 2.3 Hz, 1H, **H-12**)

^{13}C NMR (201 MHz, DMSO-d_6): δ 186.8 (**C-8**), 144.4 (**C-5**), 135.2 (**C-1**), 131.0 (**C-4**), 128.2 (**C-10**), 126.1 (**C-6**), 125.9 (**C-2**), 125.7 (**C-13**), 124.6 (**C-3**), 123.6 (**C-9**), 122.9 (**C-7**), 115.3 (**C-11**), 112.6 (**C-12**)

HRMS-ESI $[M+H]^+$ *m/z* calcd for $C_{13}H_{10}NOS^+$: 228.0478 , *m/*z found: 228.0483 $[M+H]^+$ (ppm error: 2.19)

(*E*)-**14**:

^{1}H NMR (800 MHz, DMSO-d_6): δ 13.31 (s, 1H, **H-14**), 7.90 (ddd, *J* = 7.8, 1.3, 0.7 Hz, 1H, **H-6**), 7.76 (tt, *J* = 3.6, 0.8 Hz, 1H, **H-3**), 7.68 (ddd, *J* = 8.1, 7.0, 1.3 Hz, 2H, **H-1**), 7.64 (s, 1H, **H-9**), 7.45 – 7.43 (m, 1H, **H-13**), 7.39 (ddd, *J* = 8.0, 7.0, 1.0 Hz, 1H, **H-2**), 6.93 (dt, *J* = 3.6, 1.7 Hz, 1H, **H-11**), 6.45 (dt, *J* = 3.7, 2.3 Hz, 1H, **H-12**)

^{13}C NMR (201 MHz, DMSO-d_6): δ 184.7 (**C-8**), 145.1 (**C-5**), 134.4 (**C-1**), 132.6 (**C-4**), 130.5 (**C-10**), 130.0 (**C-9**), 127.0 (**C-13**), 126.2 (**C-6**), 125.0 (**C-2**), 124.1 (**C-3**), 122.0 (**C-11**), 121.4 (**C-7**), 112.8 (**C-12**)

Note: A 1:2 (*Z*/*E*)-ratio was observed for (*E*)-**14** by ^{1}H NMR.

UV-Vis spectroscopy

HTI pyrrole (**6**) (33 µM in DCM)

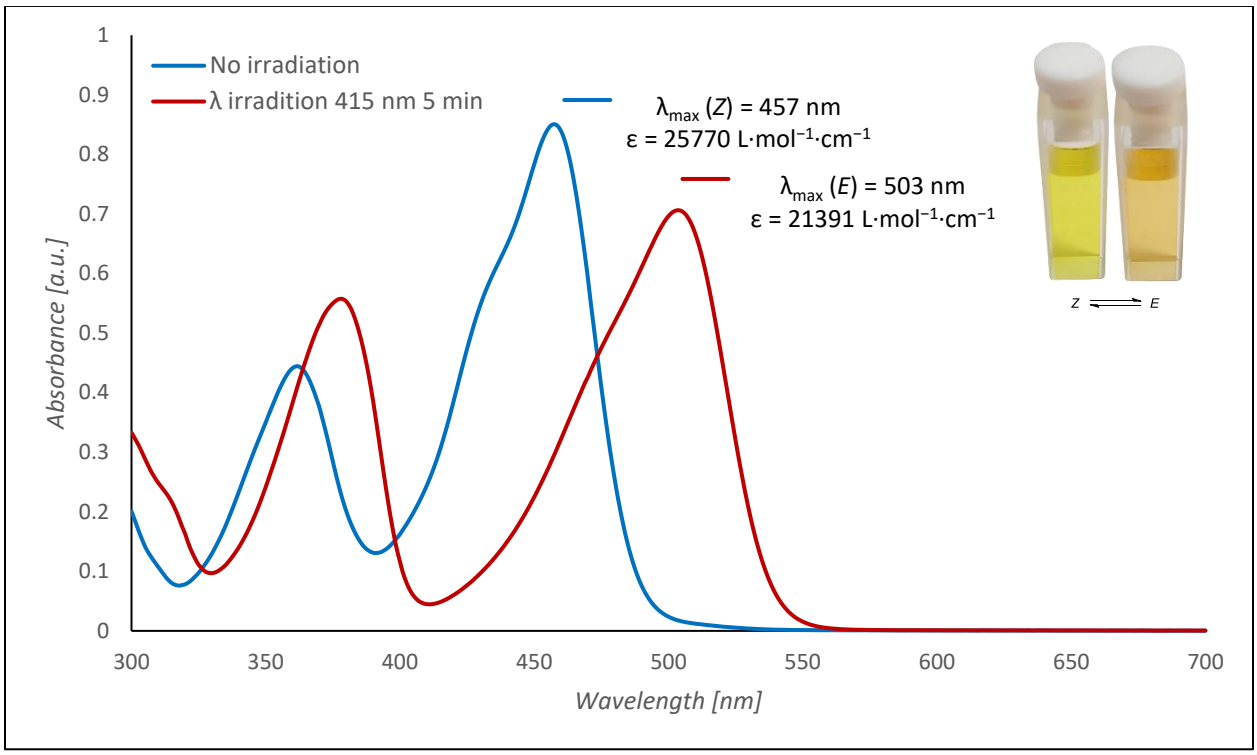

HTI pyrrole (**6**) (33 µM in *n*-hexane/iPrOH 1:1)

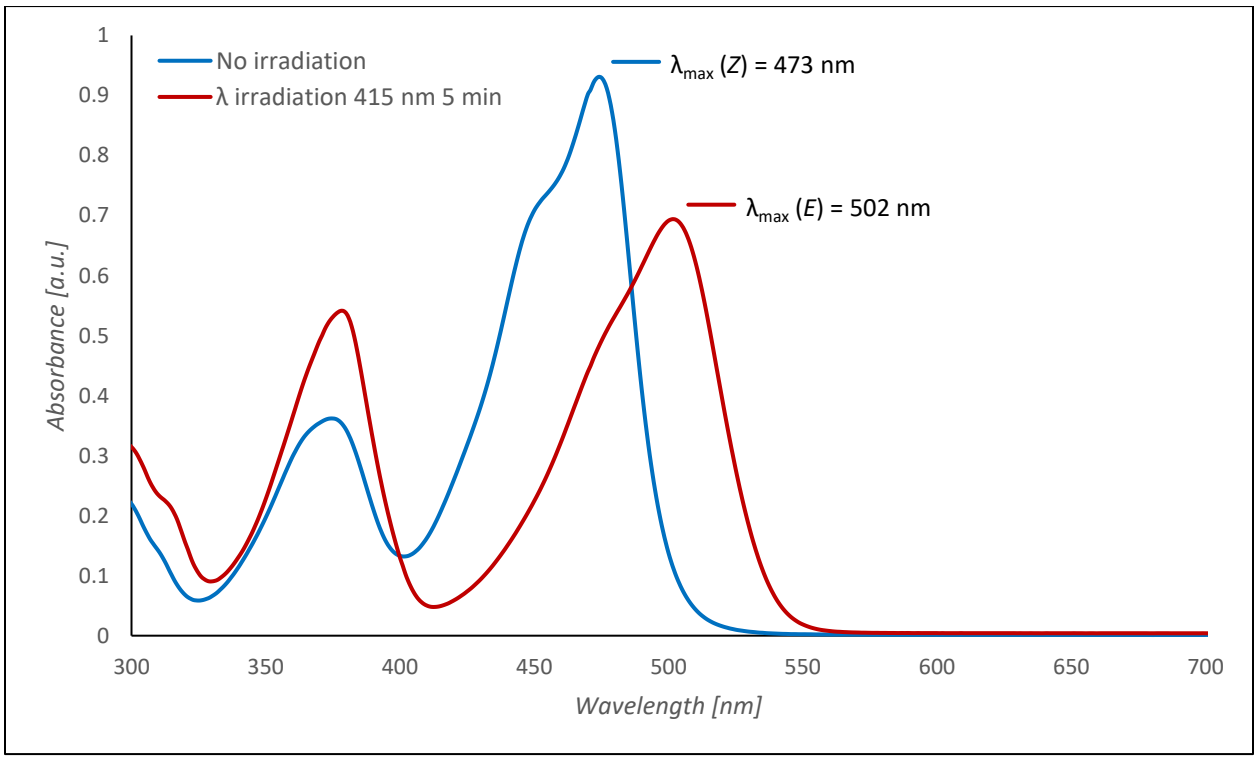

HTI pyrrole (**6**) (33 μM in *n*-hexane/iPrOH 9:1)

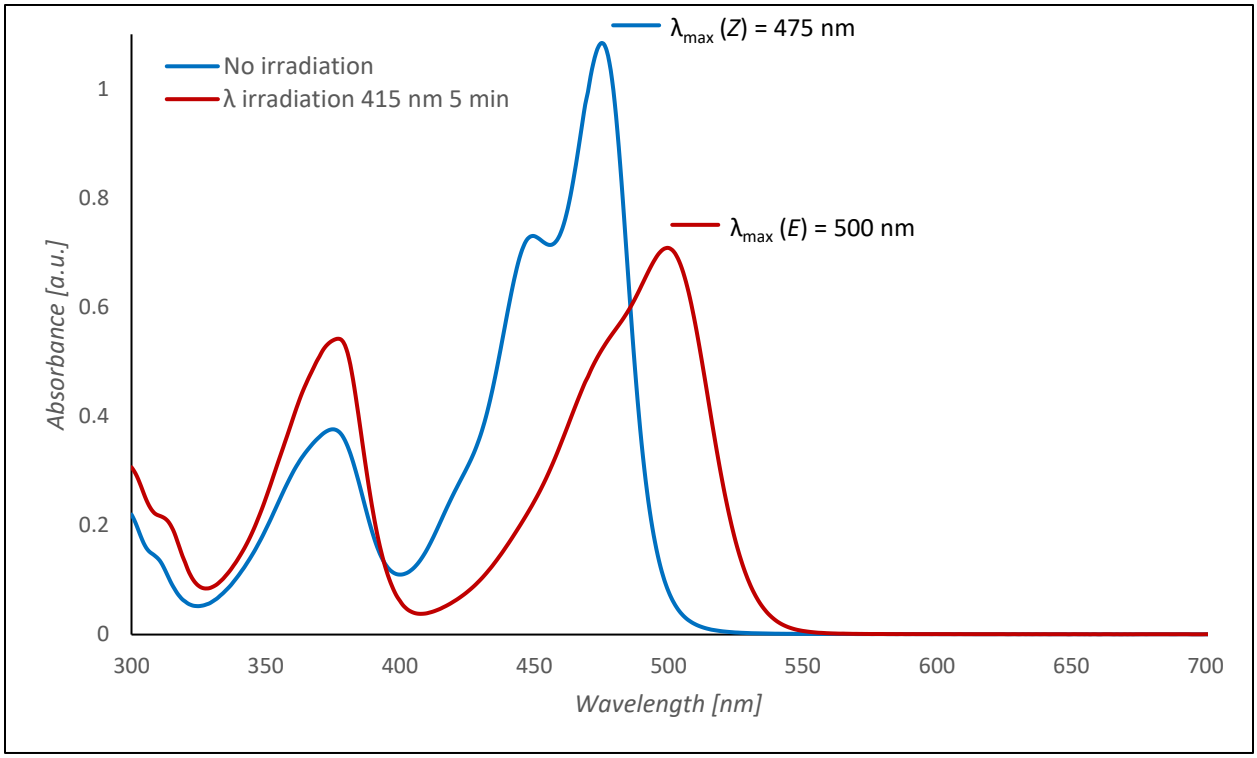

HTI pyrrole (**6**) (33 μM in PhMe)

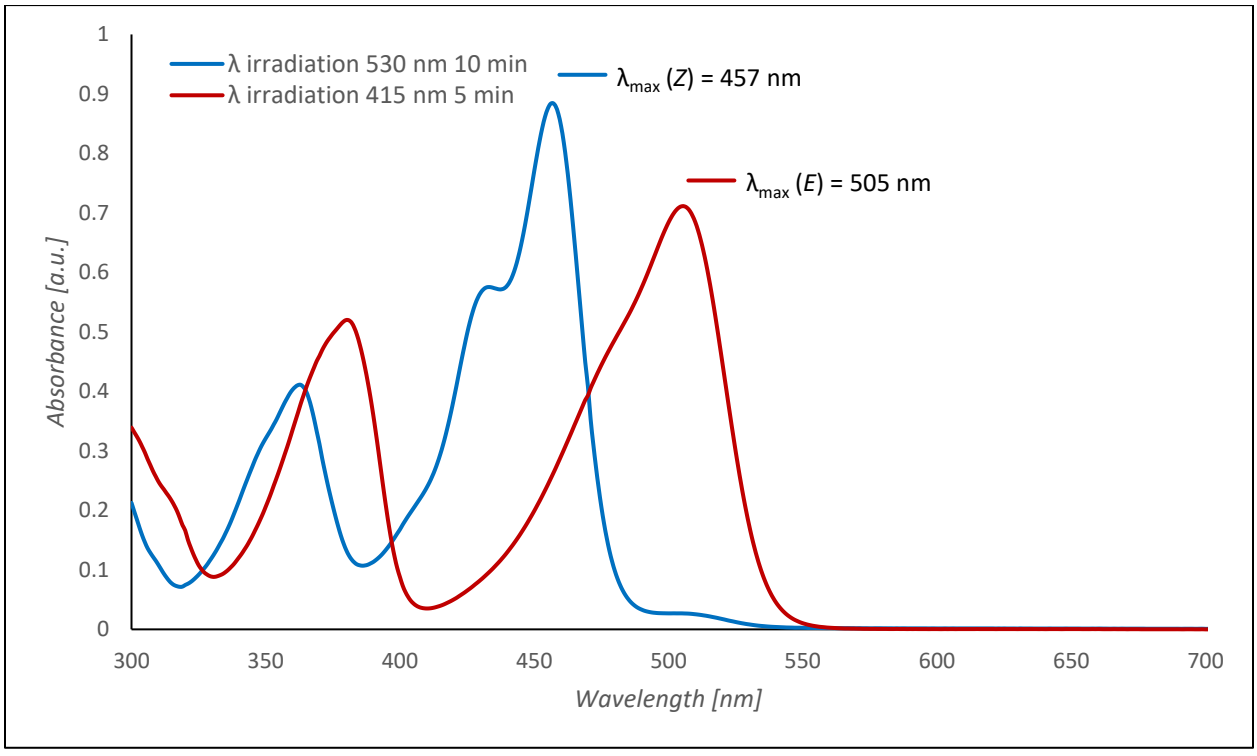

Fluorescence spectroscopy

HTI pyrrole (**6**) (33 µM in DCM)

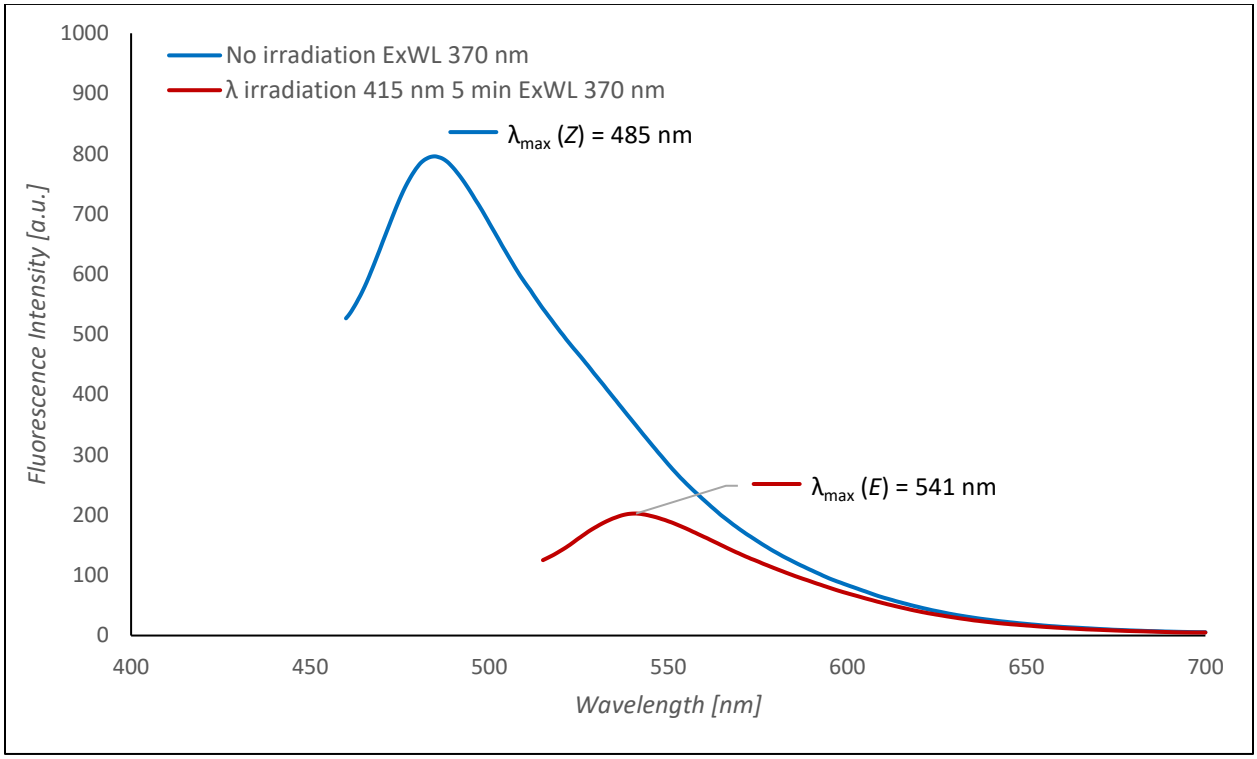

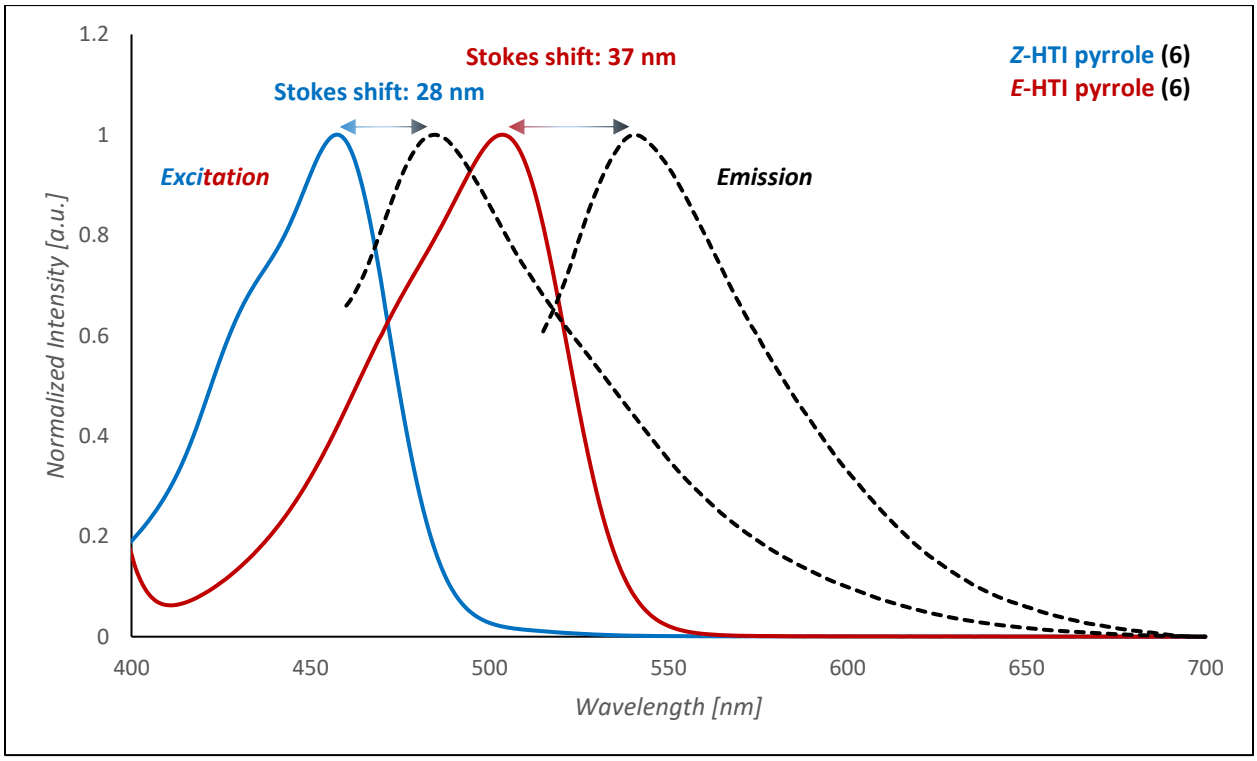

UV-Vis thermal relaxation spectroscopy

HTI pyrrole (**6**) (33 μM in PhMe)

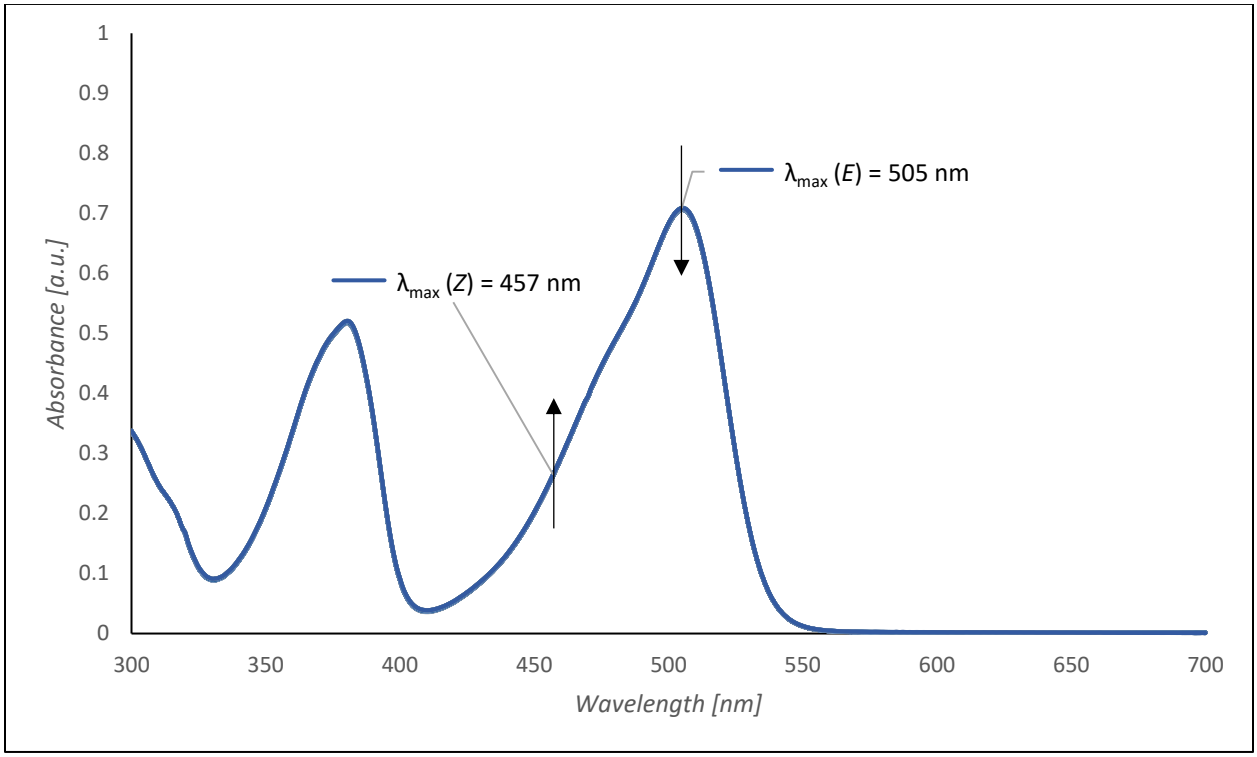

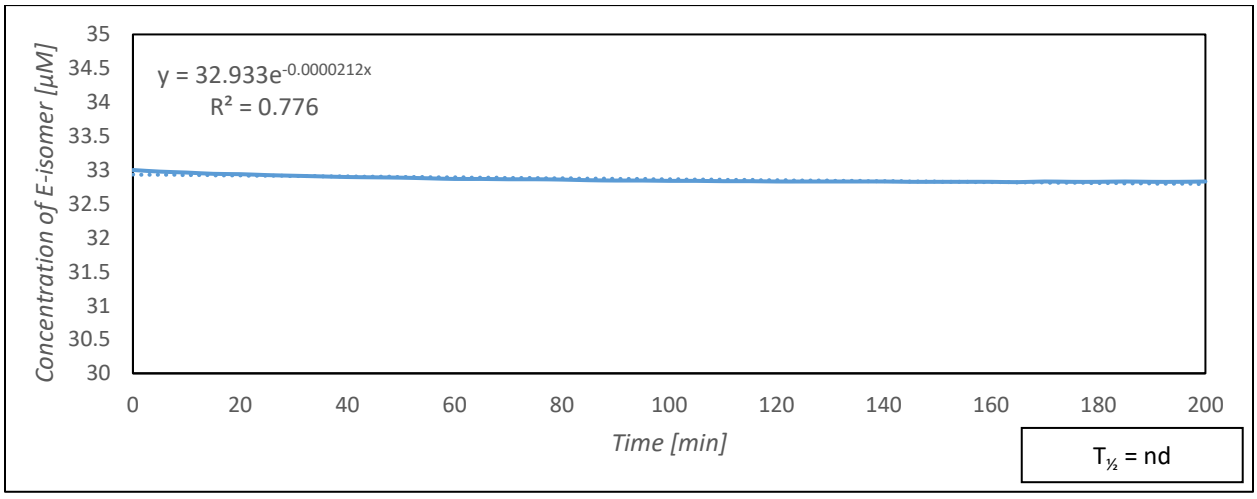

HPLC conditions

Column:	ChiralPak AD-H column (5 µm, 250 x 4.6 mm)
Mobile Phase	90:10 *n*-hexane/iPrOH (isocratic, 1 mL/min)
Isosbestic Point	486 nm (in HPLC mobile Phase)
t_R(E)	7.37 min
t_R(Z)	12.38 min

Solution composition (%*E*-isomer)

Initial solution composition before irradiation: *E*-isomer (0.86%) / *Z*-isomer (99.14%)

Time	**415 nm**	**530 nm**
10 min	88.04	2.54
20 min	95.93	3.75

Representative HPLC traces

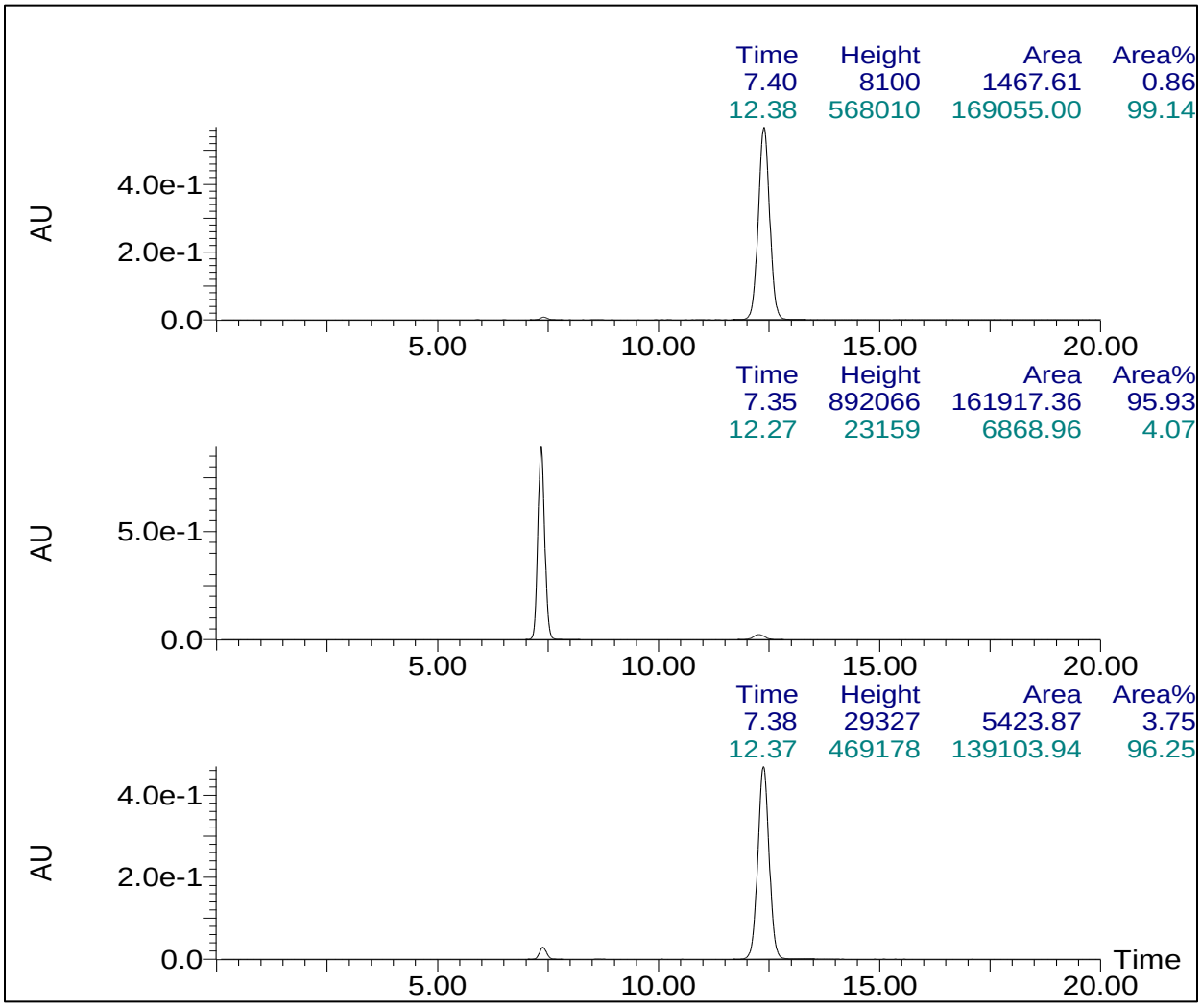

(*Z*)-2-((1H-Indol-2-yl)methylene)benzo[b]thiophen-3(2H)-one (7)

Prepared according to general procedure A.

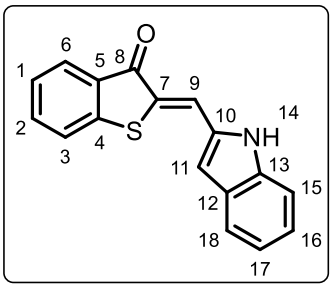

Hemithioindigo **SI 6** (89.0 mg, 0.594 mmol, 1.0 eq.), benzene (2.0 mL, 0.297 M), indole-2-carbaldehyde (73.0 mg, 0.504 mmol, 0.85 eq.). The solution was purged with N_2 for 10 min before piperidine was added. Stirred for 17 h under Ar at 40°C. Purified by DCVC (0% to 100% EtOAc in *n*-heptane with 5% increments) to afford the title compound (*Z*)-**7** (116 mg, 0.419 mmol, 83%) as a bordeaux red solid.

TLC: R_f = 0.24 (1:3 EtOAc/*n*-heptane)

LCMS (ESI) $[M+H]^+$ *m/z* calcd for $C_{17}H_{12}NOS^+$: 278.0634, *m/*z found: 278.50 $[M+H]^+$

R_t: 2.09 min (total run time: 2.6 min), purity >98%

^{1}H NMR (800 MHz, DMSO-d_6): δ 11.75 (s, 1H, **H-14**), 7.95 (m, 1H, **H-9**), 7.87 (ddd, *J* = 7.6, 1.3, 0.6 Hz, 1H, **H-6**), 7.82 (d, *J* = 7.8 Hz, 1H, **H-3**), 7.74 (ddd, *J* = 8.0, 7.2, 1.3 Hz, 1H, **H-1**), 7.71 (dd, *J* = 8.0, 1.0 Hz, 1H, **H-18**), 7.46 (dd, *J* = 8.2, 1.0 Hz, 1H, **H-15**), 7.42 (td, *J* = 7.4, 0.9 Hz, 1H, **H-2**), 7.25 (ddd, *J* = 8.1, 6.9, 1.1 Hz, 1H, **H-17**), 7.09 (ddd, *J* = 7.9, 6.9, 1.0 Hz, 1H, **H-16**), 7.07 (m, 1H, **H-11**)

^{13}C NMR (201 MHz, DMSO-d_6): δ 187.0 (**C-8**), 144.5 (**C-5**), 137.9 (**C-12**), 135.9 (**C-1**), 133.1 (**C-10**), 130.3 (**C-4**), 128.7 (**C-7**), 128.6 (**C-13**), 126.5 (**C-6**), 126.3 (**C-2**), 124.7 (**C-3**), 124.7 (**C-17**), 122.9 (**C-9**), 121.6 (**C-18**), 120.5 (**C-16**), 112.0 (**C-15**), 107.4 (**C-11**)

HRMS-ESI $[M+H]^+$ *m/z* calcd for $C_{17}H_{12}NOS^+$: 278.0634 , *m/*z found: 278.0636 $[M+H]^+$ (ppm error: 0.719)

(*E*)-**15**:

^{1}H NMR (400 MHz, DMSO-d_6): δ 12.56 (s, 1H, **H-14**), 7.93 (m, 1H), 7.81 (m, 1H), 7.77 (m, 1H), 7.73 (ddd, *J* = 8.1, 6.2, 1.3 Hz, 1H), 7.70 – 7.67 (m, 2H), 7.42 (m, 1H), 7.32 (ddd, *J* = 8.2, 6.9, 1.1 Hz, 1H), 7.20 (m, 1H), 7.11 (ddd, *J* = 8.1, 7.0, 0.9 Hz, 1H)

Note: A sample of (*Z*)-**7** was irradiated in an LCMS vial in DCM followed by a solvent exchange to DMSO-d_6. A 1:4 (*Z*/*E*)-ratio was observed for (*E*)-**7** by ^{1}H NMR. Photoisomerization of an NMR sample performed directly in DMSO-d_6 did not produce the desired (*E*)-isomer in greater than *Z*/*E* 9:1. Switching directly in CD_2Cl_2 afforded the (*E*)-isomer cleanly, however with a loss in ^{1}H NMR spectrum quality.

UV-Vis spectroscopy

HTI indole (**7**) (33 µM in DCM)

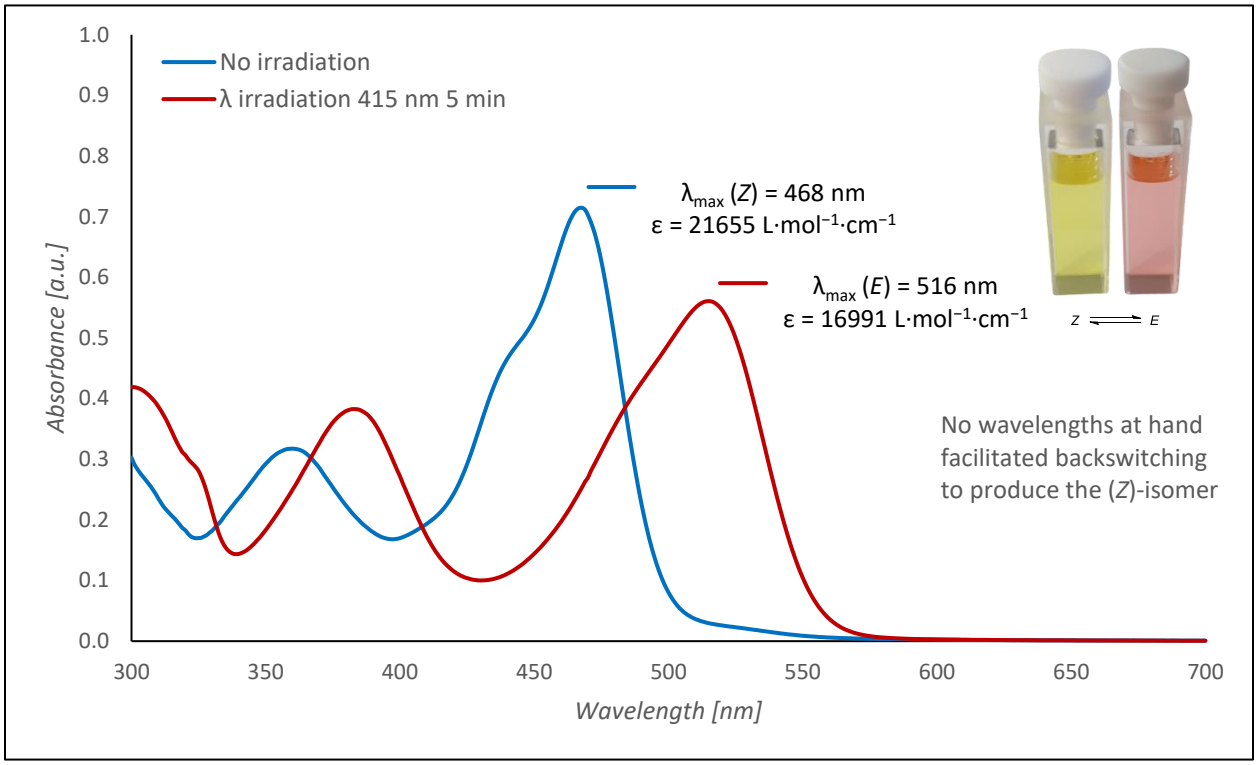

HTI indole (**7**) (33 µM in *n*-hexane/iPrOH 9:1)

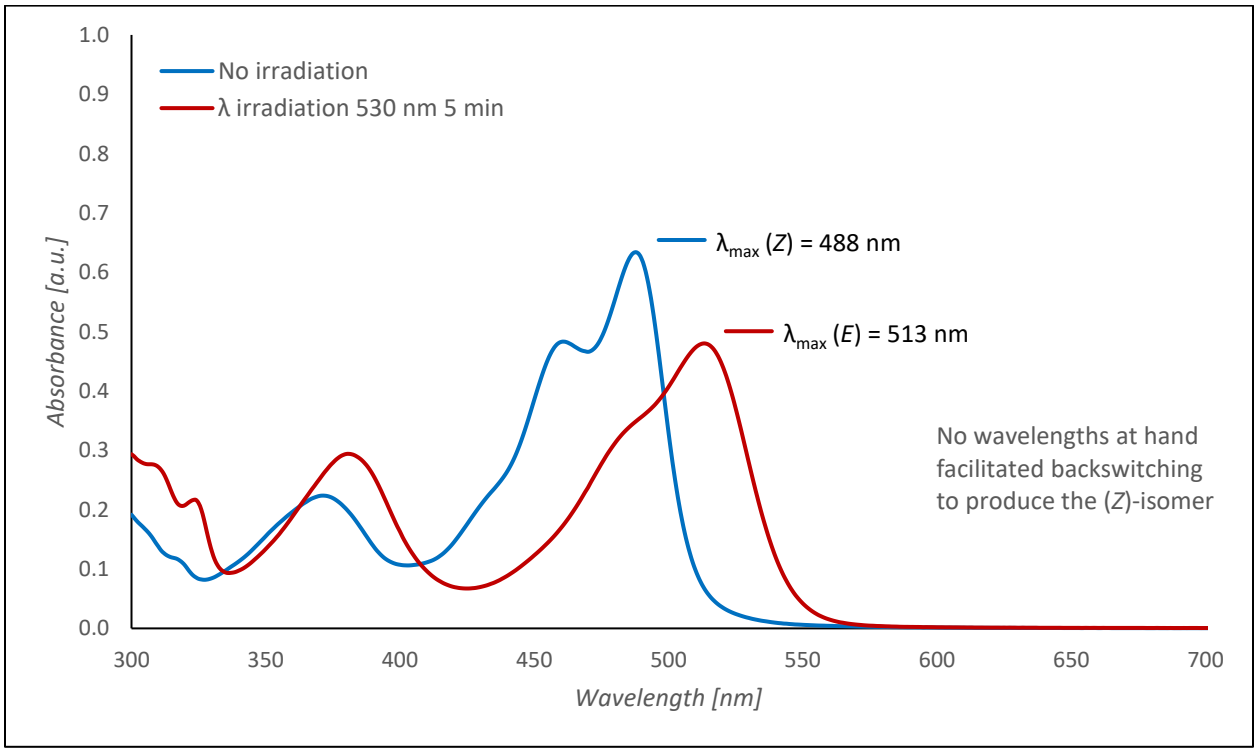

HTI indole (**7**) (33 μM in iPrOH). The apparent lack of an isosbestic point is likely due to photodegradation with prolonged irradiation times.

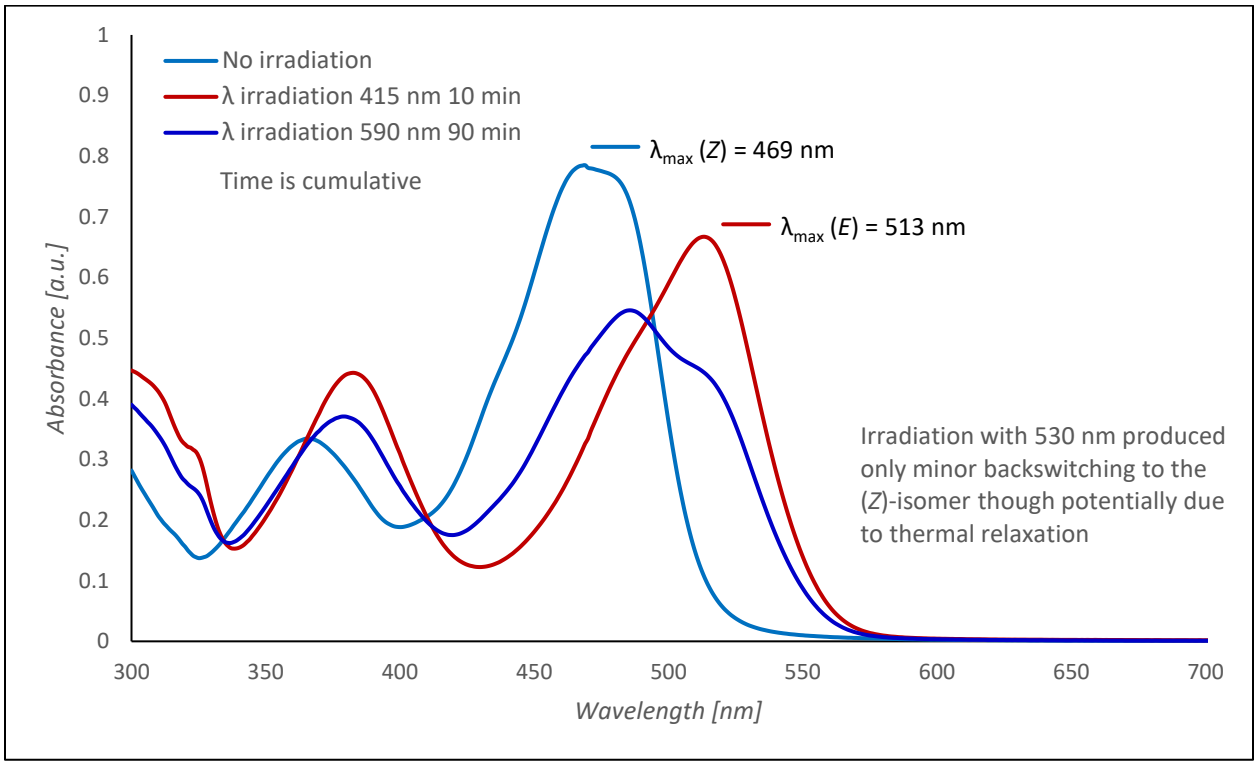

HTI indole (**7**) (33 μM in THF)

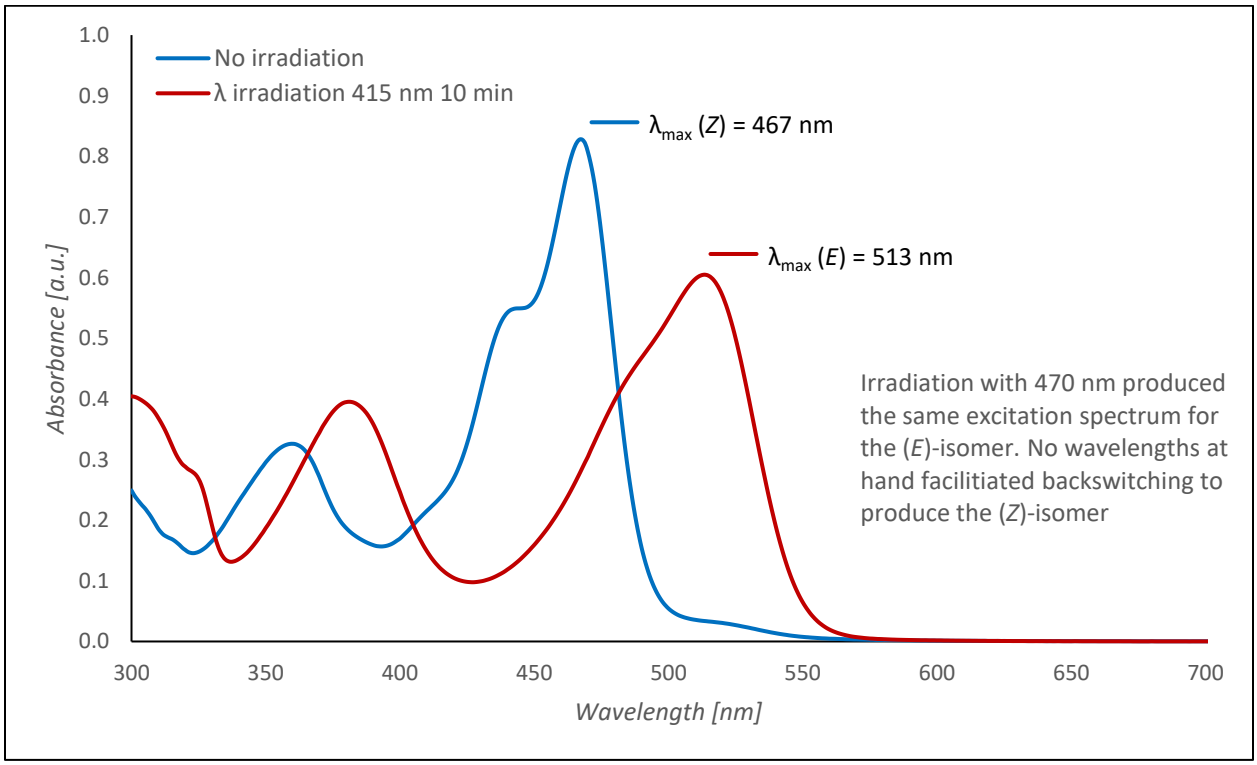

HTI indole (**7**) (33 µM in PhMe)

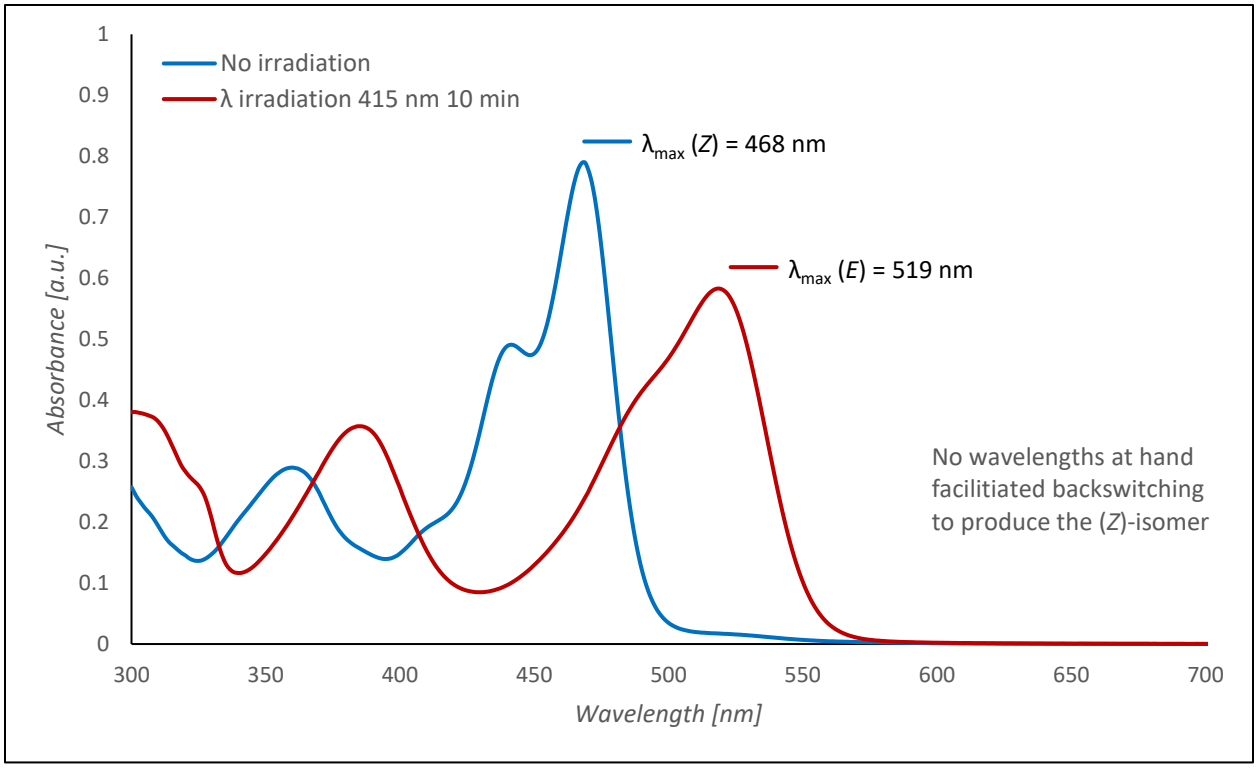

HTI indole (**7**) (33 µM in DMSO)

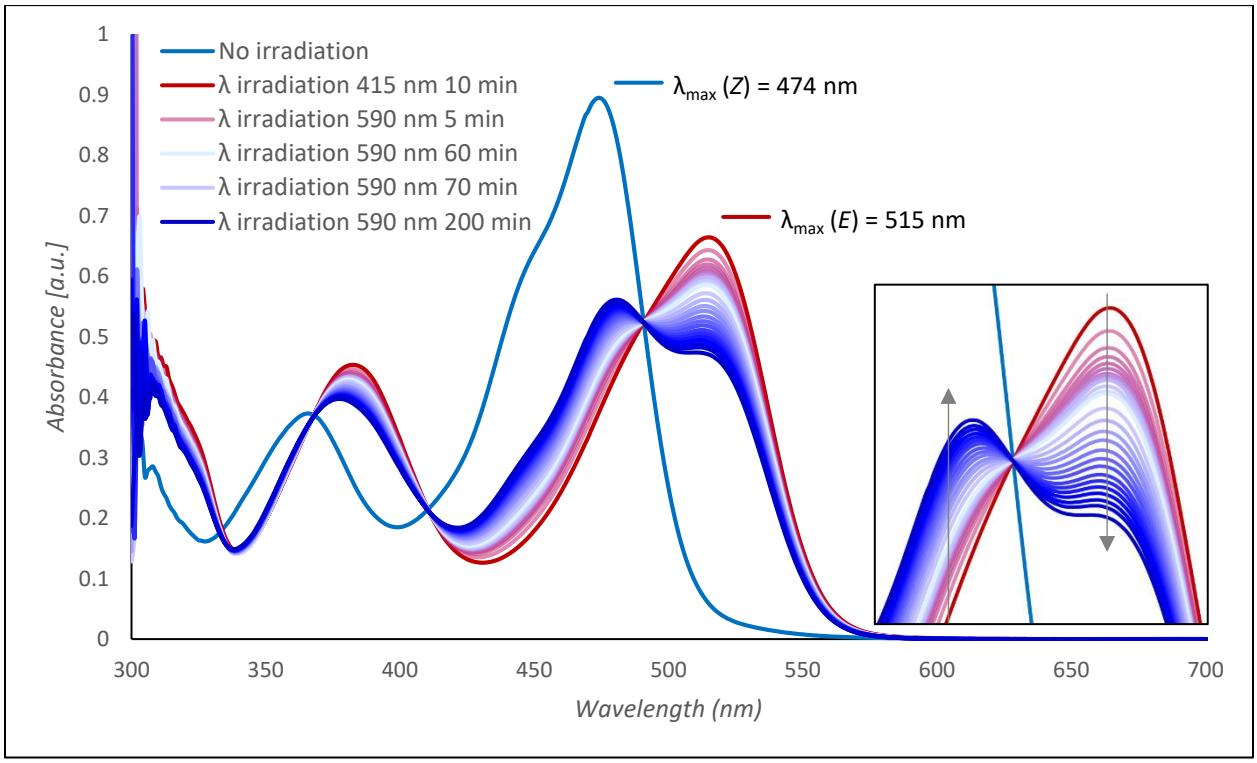

HTI indole (**7**) (33 µM in DMSO/H_2O 1:1, T = 20 °C)

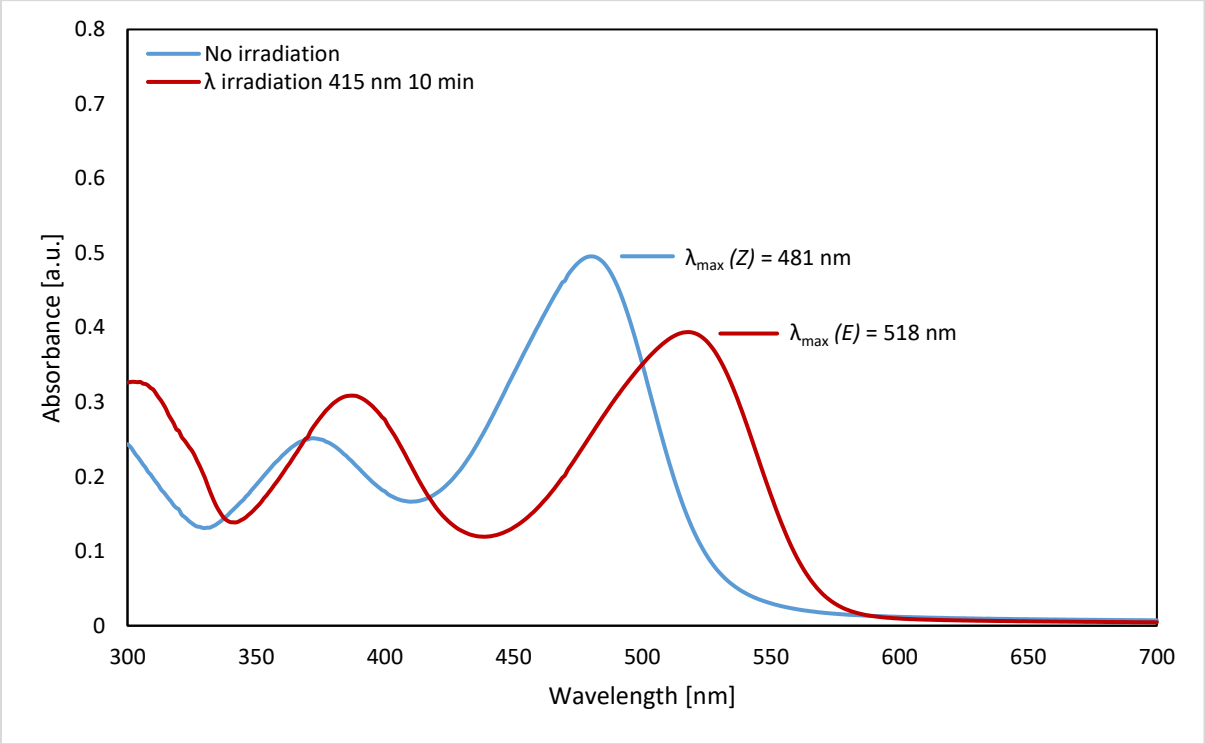

Fluorescence spectroscopy

HTI indole (**7**) (33 μM in DCM)

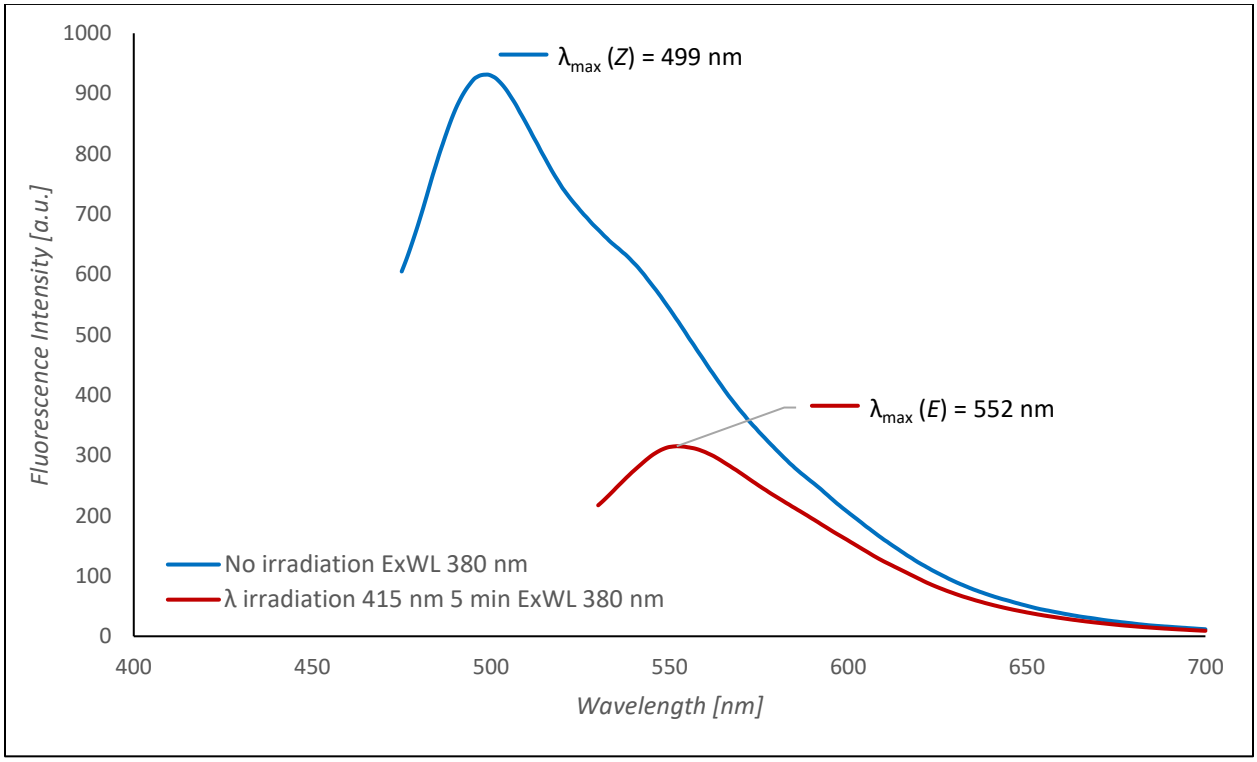

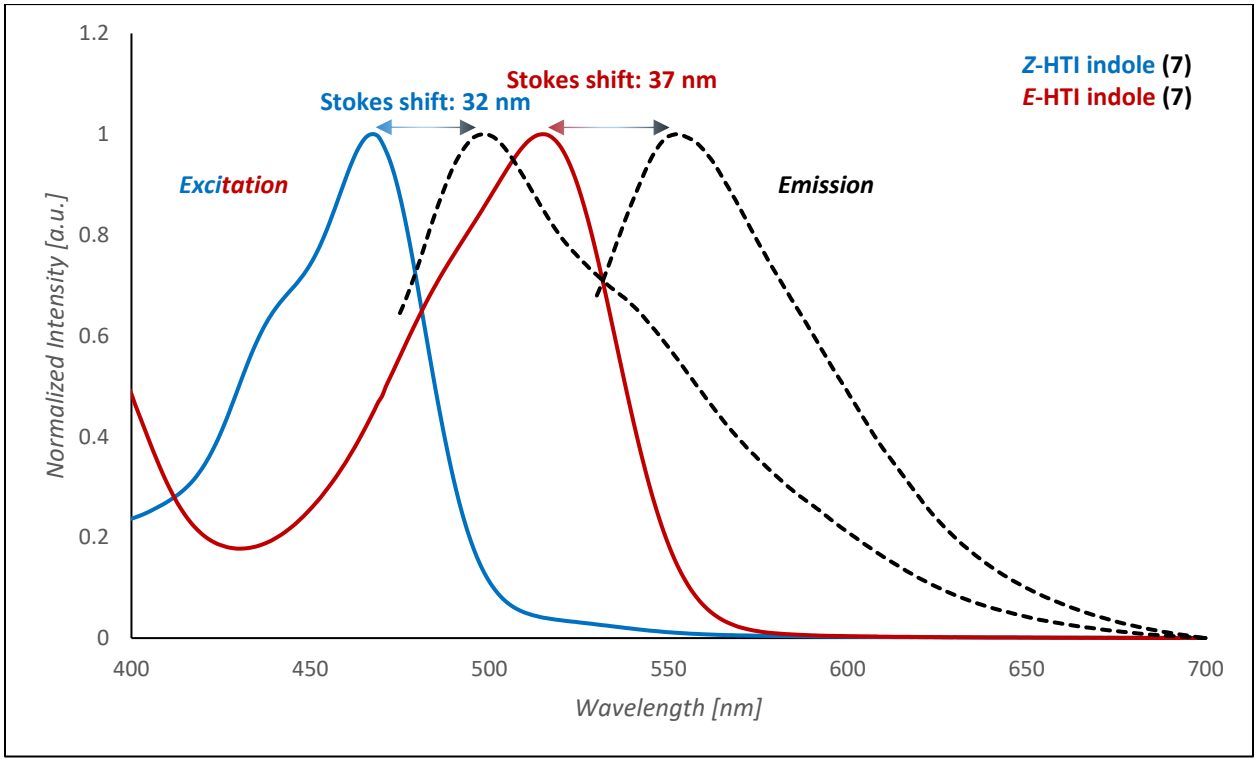

UV-Vis thermal relaxation spectroscopy

HTI indole (**7**) (33 μM in DMSO)

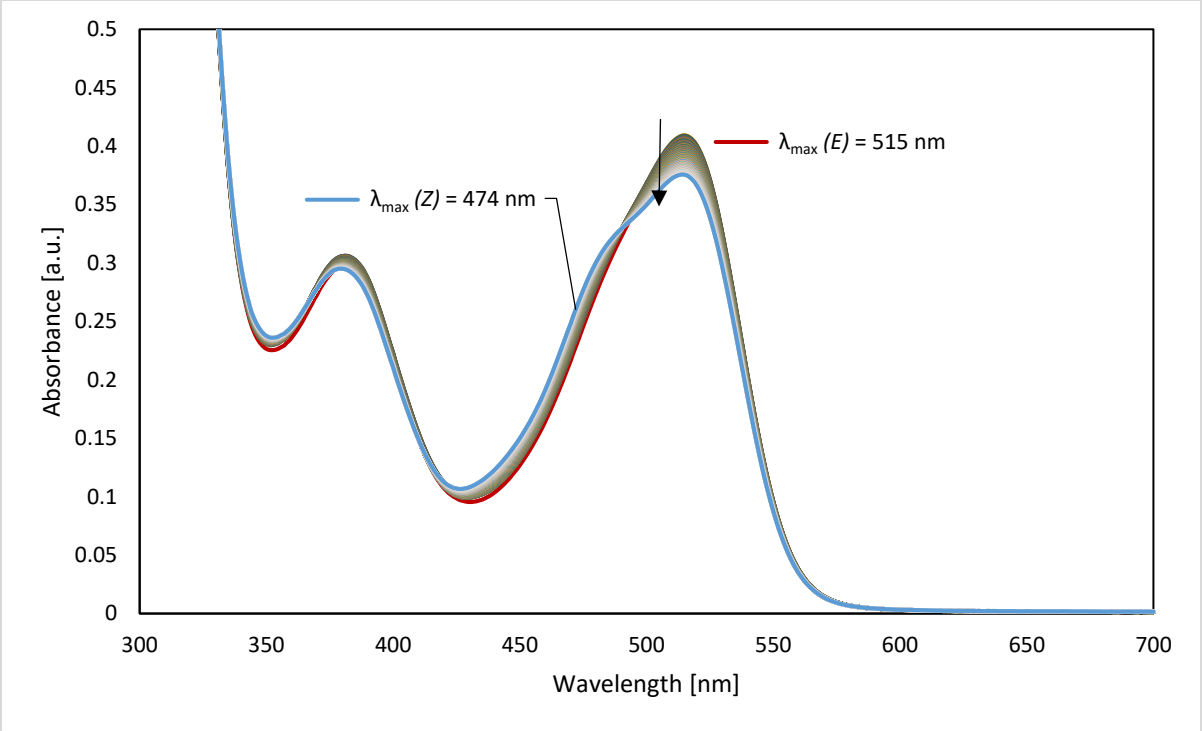

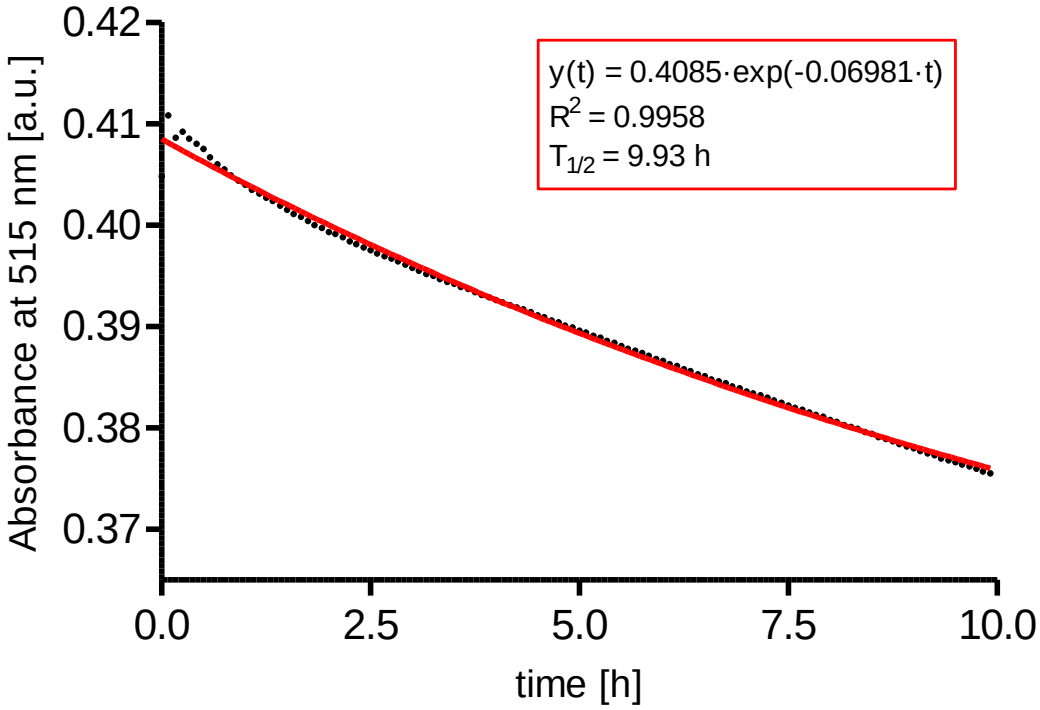

HTI indole (**7**) (33 µM in DMSO, T = 28 °C, first 75 minutes)

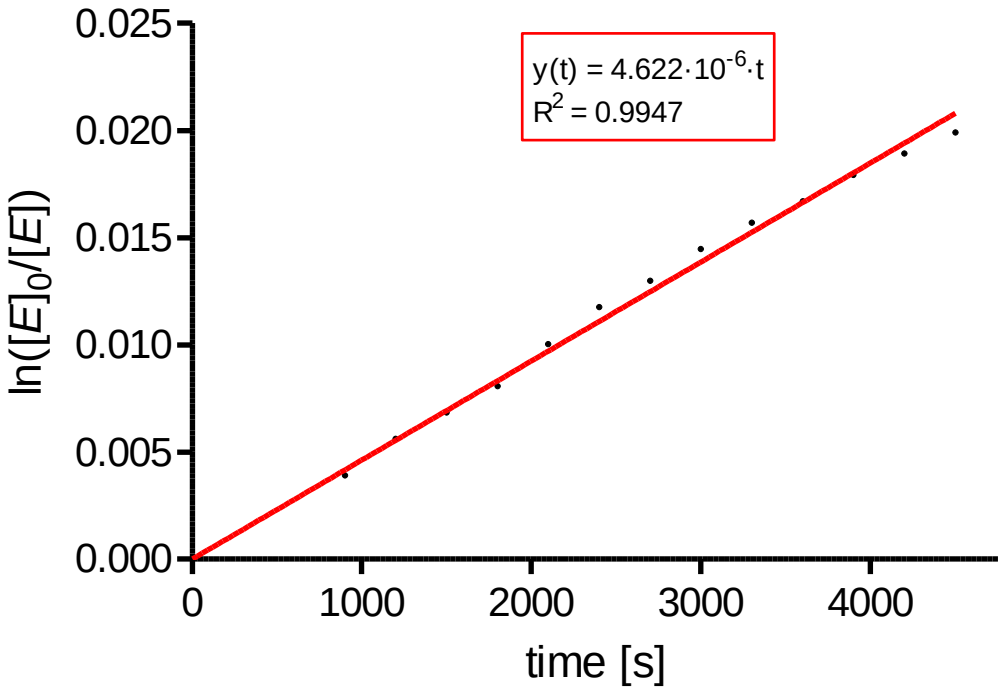

The linear fit gives the first order rate constant k = 4.62·10^{-6} s^{-1}. This corresponds to a Gibbs energy of activation of **$\Delta G^{\ddagger}$ = 105 kJ·mol^{-1} = 25.0 kcal·mol^{-1}**.

HTI indole (**7**) (33 μM in PhMe)

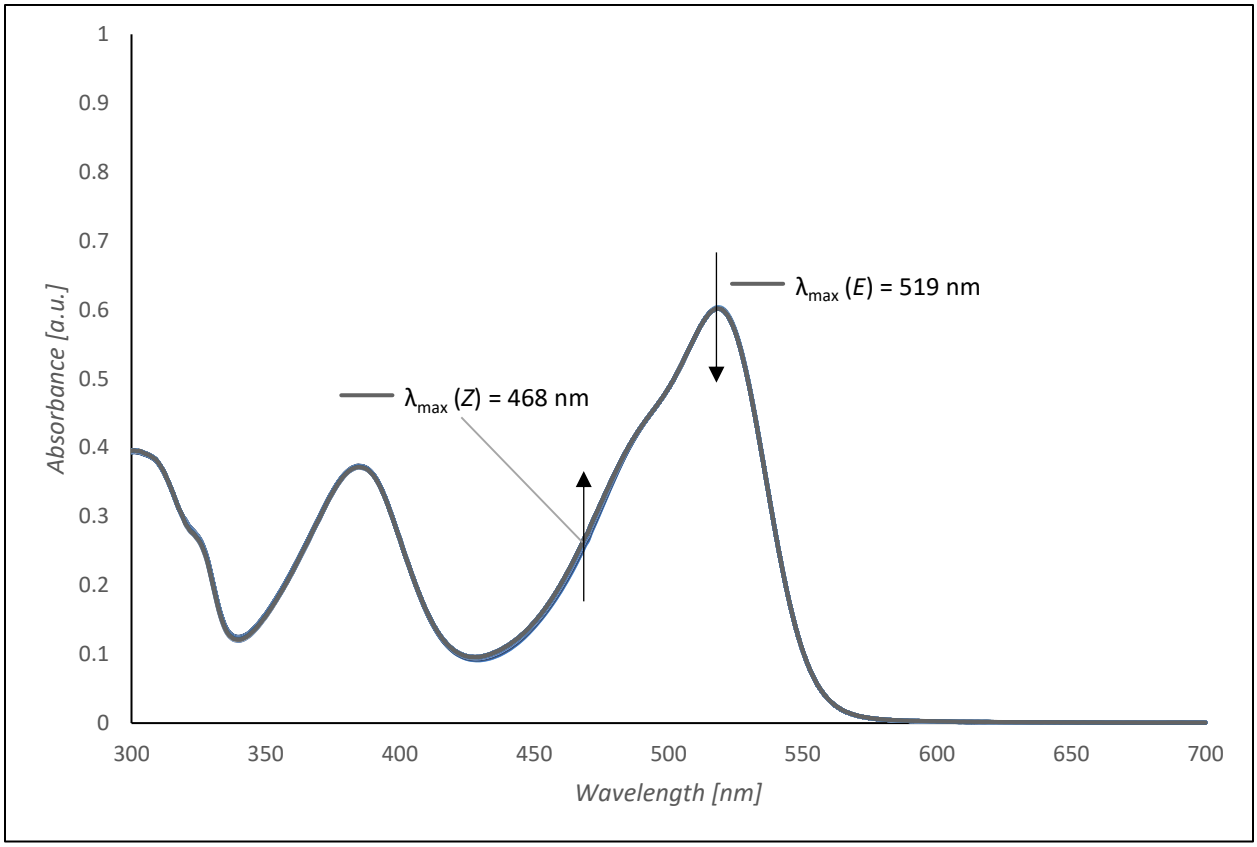

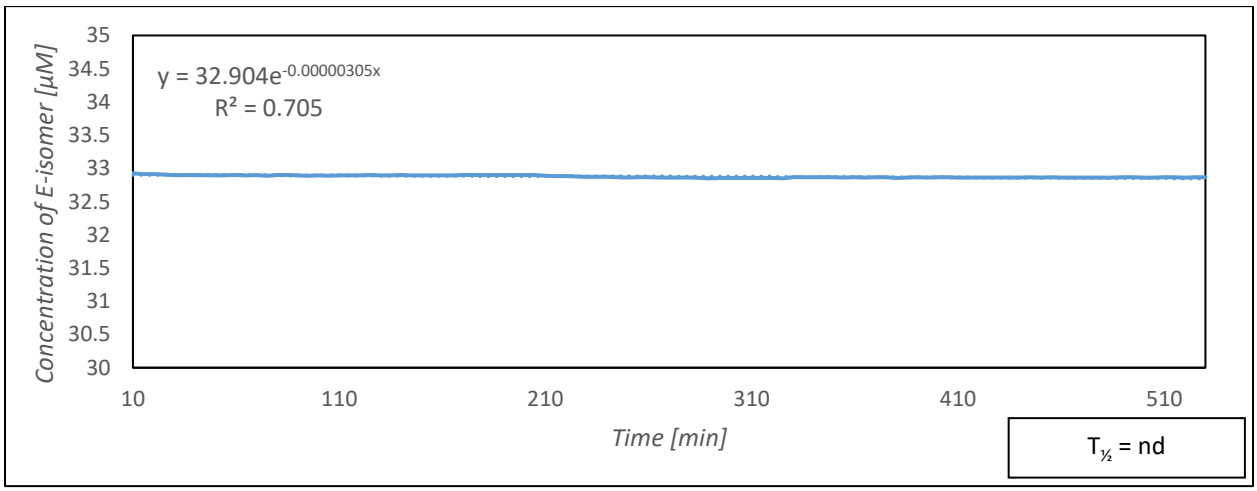

HTI indole (**7**) (33 µM in DMSO/H_2O 1:1, T = 20 °C, measurement every 20 minutes for 24 hours)

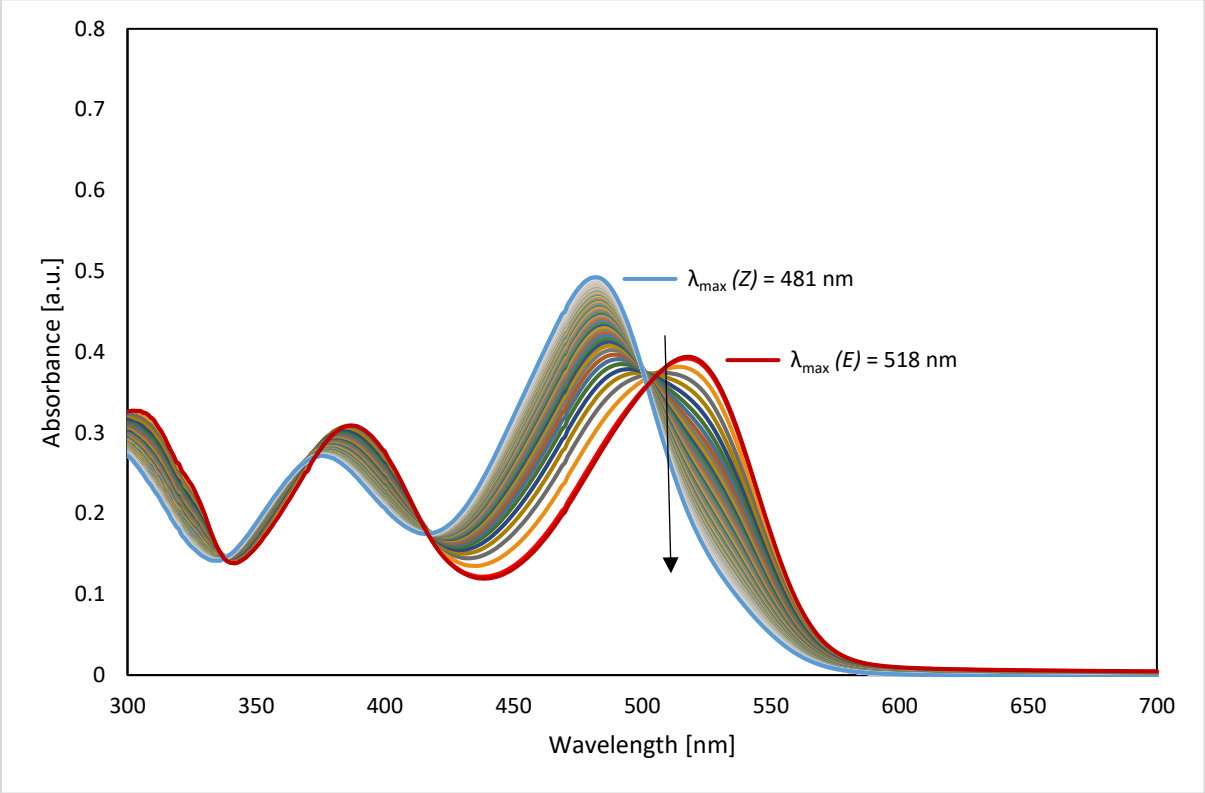

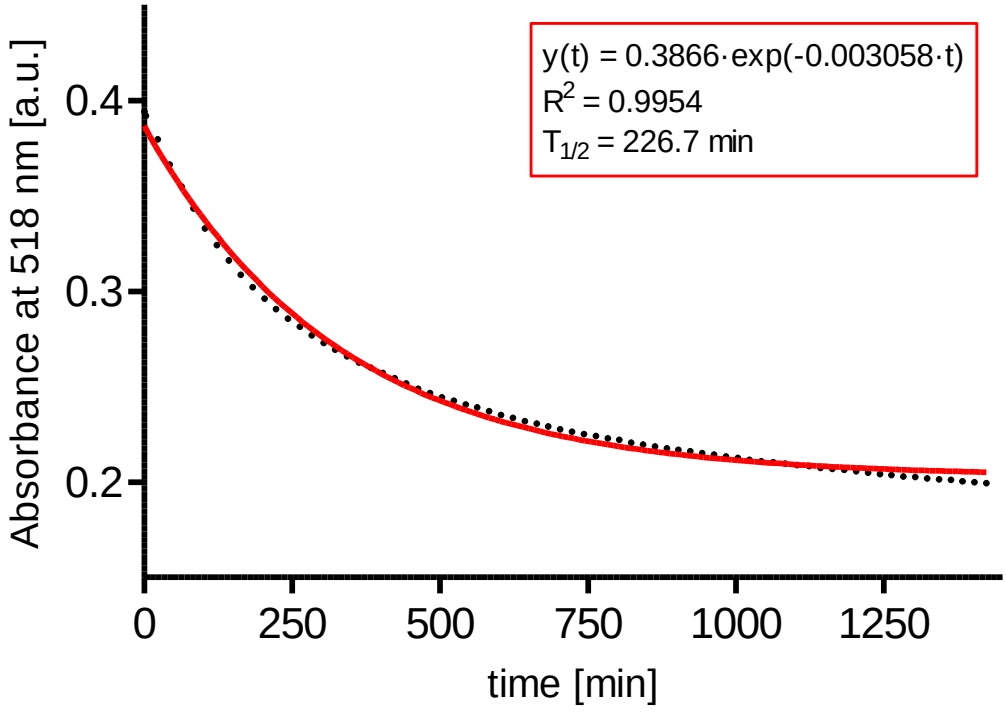

Kinetic analysis of thermal *E*-to-*Z* isomerisation

HTI indole (**7**) (33 µM in DMSO/H_2O 1:1, T = 20 °C, first 183 minutes)

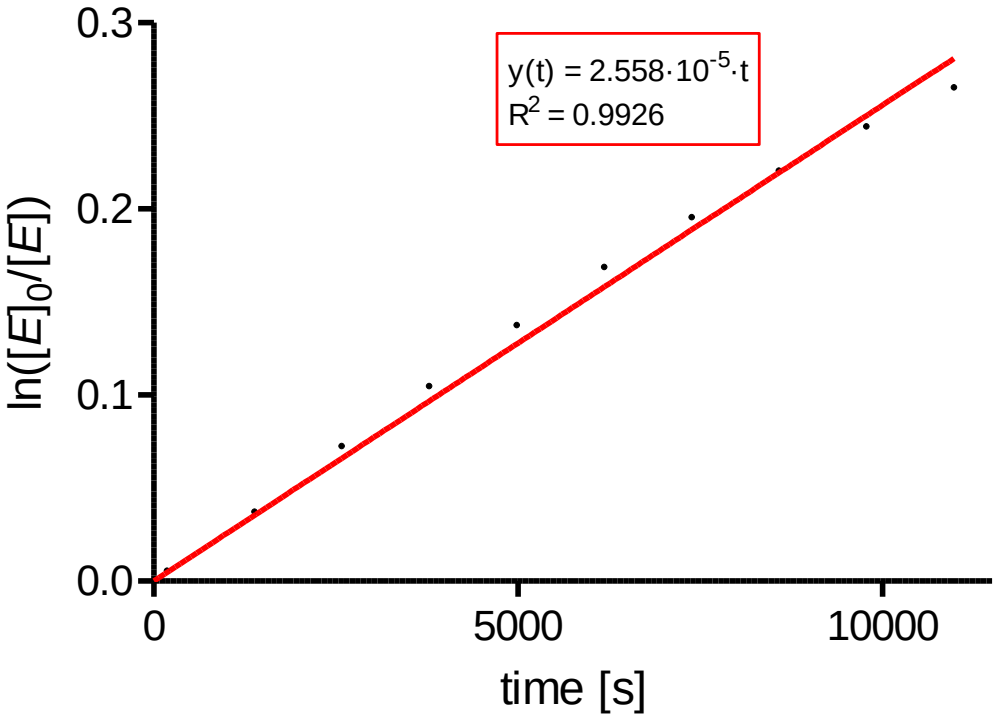

The linear fit gives the first order rate constant $k = 2.56 \cdot 10^{-5}$ s^{-1}. This corresponds to a Gibbs energy of activation of $\boldsymbol{\Delta G^{\ddagger} = 97.5\ kJ \cdot mol^{-1} = 23.3\ kcal \cdot mol^{-1}}$.

HPLC conditions

Column:	ChiralPak AD-H column (5 µm, 250 x 4.6 mm)
Mobile Phase	90:10 *n*-hexane/iPrOH (isocratic, 1 mL/min)
Isosbestic Point	498 nm (in HPLC mobile Phase)
t_R(E)	8.82 min
t_R(Z)	17.05 min

Solution composition (%*E*-isomer)

Initial solution composition before irradiation: *E*-isomer (2.60%) / *Z*-isomer (97.40%)

Time	**415 nm**	**530 nm**
10 min	98.43	94.79
20 min	99.21	96.16

Representative HPLC traces

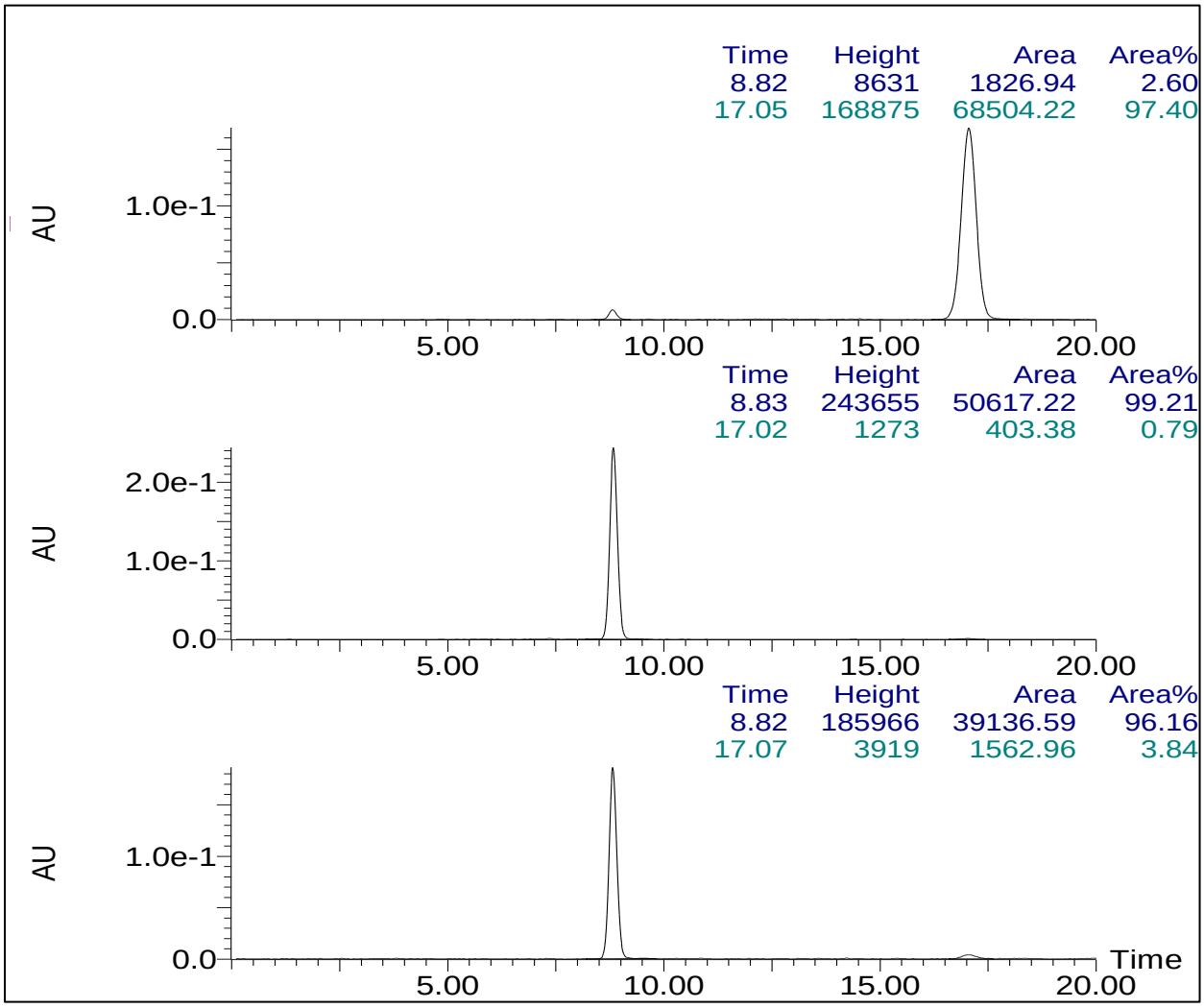

HPLC conditions

Column:	ChiralPak AD-H column (5 µm, 250 x 4.6 mm)
Mobile Phase	90:10 *n*-hexane/iPrOH (isocratic, 1 mL/min)
Isosbestic Point	498 nm (in HPLC mobile Phase)
t_R(E)	8.37-8.65 min
t_R(Z)	14.6-15.75 min

Solution composition (%*E*-isomer)

Initial solution composition before irradiation: *E*-isomer (1.64%) / *Z*-isomer (98.36%)

Time	**415 nm**	**590 nm**
10 min	97.88	86.74
20 min	-	80.82
30 min	-	70.83
40 min	-	63.14

Note: Sample prepared (0.66 mg/mL), filtered, irradiated in and measured directly from **iPrOH**.

Representative HPLC traces

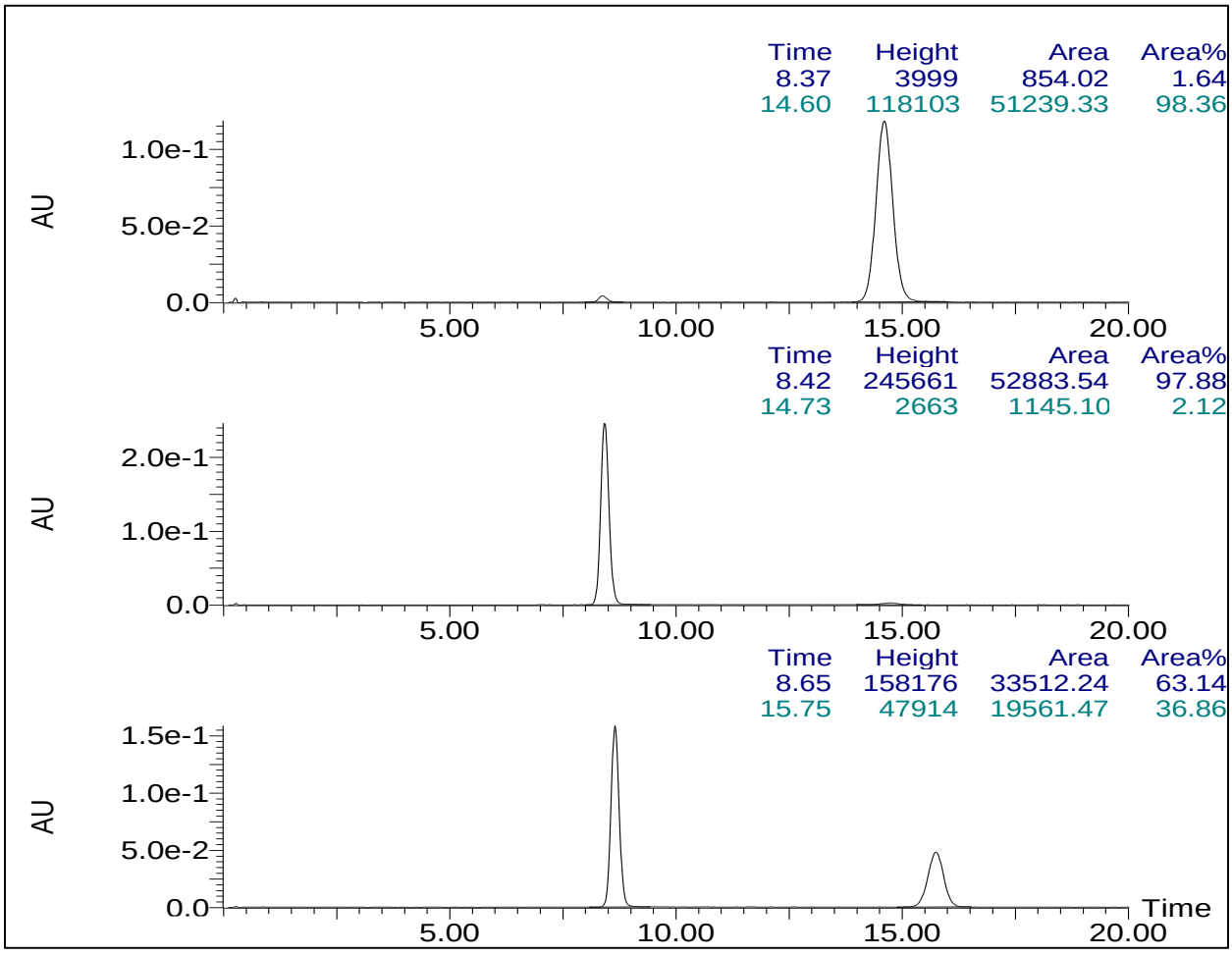

^{1}H NMR thermal relaxation spectroscopy

HTI indole (**7**) (CD_2Cl_2)

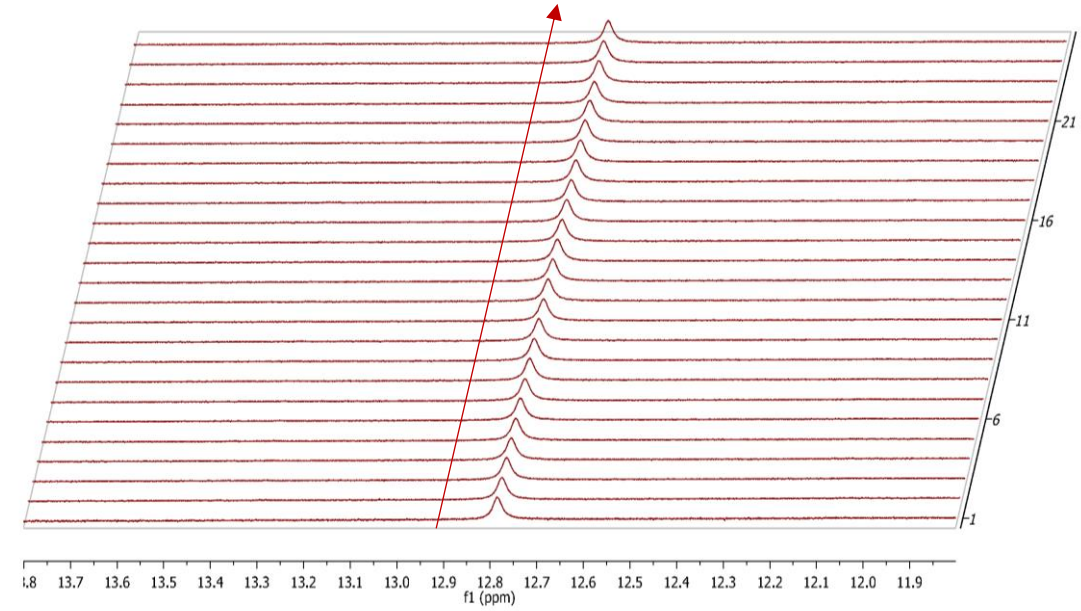

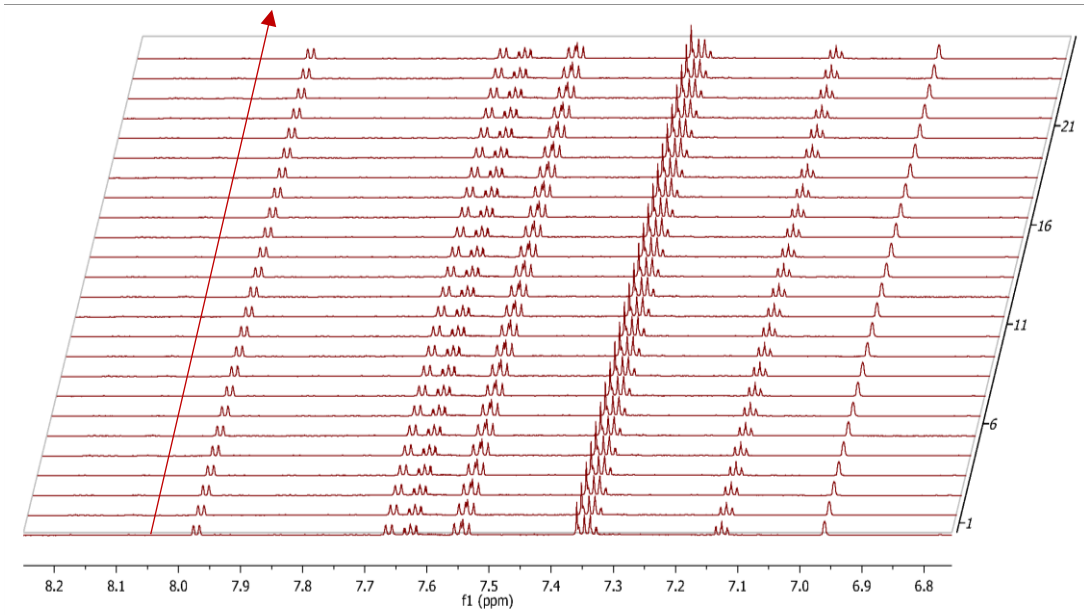

Note: Indole-NH of the (*E*)-**7** at 12.78 ppm plotted vs. time (relaxation).

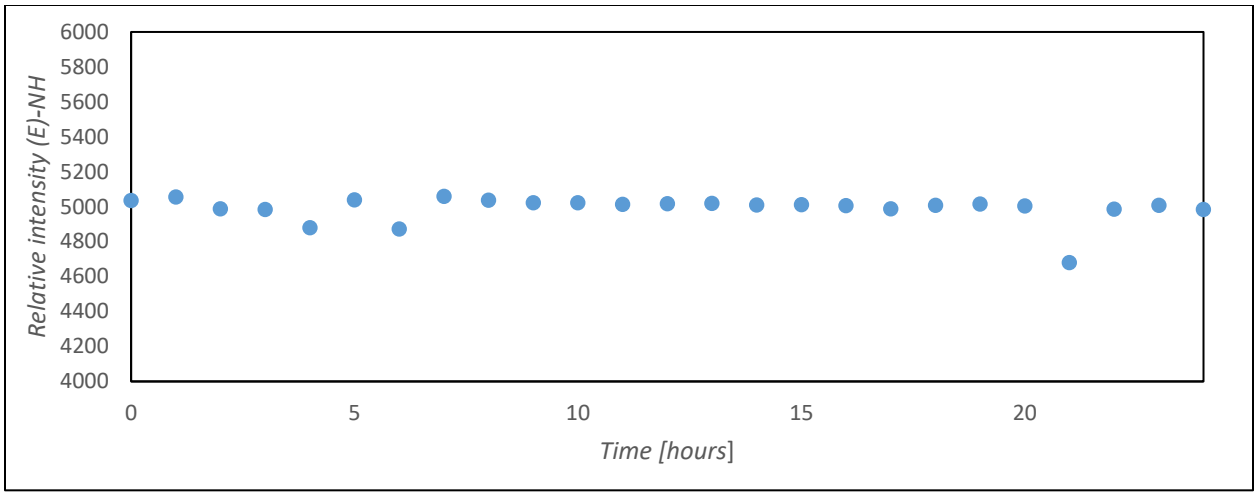

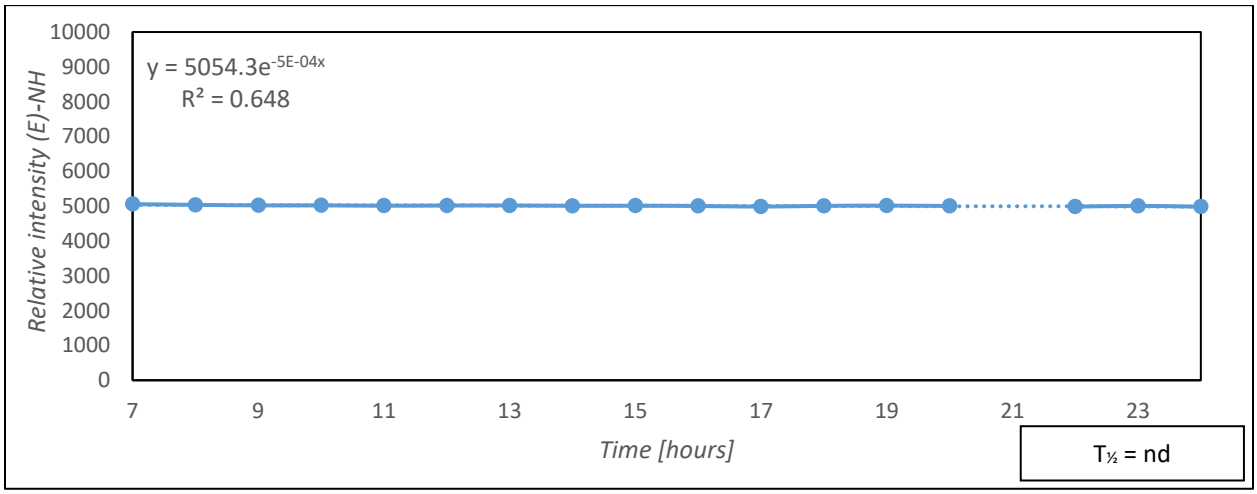

(*Z*)-**7**:

^{1}H NMR (800 MHz, CD_2Cl_2): δ 8.61 (s, 1H), 7.93 (s, 1H), 7.91 (m, 1H), 7.70 (dq, *J* = 8.0, 1.0 Hz, 1H), 7.63 (m, 1H), 7.59 (dt, *J* = 7.8, 0.9 Hz, 1H), 7.46 (dq, *J* = 8.2, 0.9 Hz, 1H), 7.35 (ddd, *J* = 7.9, 7.1, 1.0 Hz, 1H), 7.31 (ddd, *J* = 8.1, 6.9, 1.1 Hz, 1H), 7.16 (ddd, *J* = 7.9, 7.0, 1.0 Hz, 1H), 7.12 (m, 1H)

(*E*)-**7**:

^{1}H NMR (800 MHz, CD_2Cl_2): δ 12.78 (s, 1H), 7.97 (ddd, *J* = 7.8, 1.3, 0.7 Hz, 1H), 7.66 (dq, *J* = 8.1, 1.0 Hz, 1H), 7.63 (ddd, *J* = 8.3, 7.1, 1.3 Hz, 1H), 7.55 (m, 1H), 7.54 (dt, *J* = 7.9, 0.9 Hz, 1H), 7.36 (s, 1H), 7.35 (m, 1H), 7.33 (m, 1H), 7.13 (ddd, *J* = 7.9, 6.8, 0.9 Hz, 1H), 7.96 (m, 1H)

(*Z*)-2-((1H-Pyrrol-2-yl)methylene)naphtho[2,1-b]thiophen-1(2H)-one (8)

Prepared according to general procedure B.

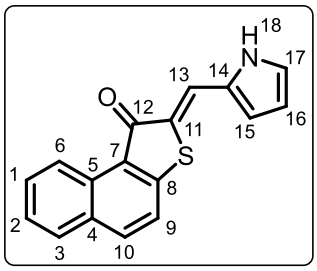

Hemithioindigo derivative **SI 5** (93.5 mg, 0.467 mmol, 1.0 eq.), PhMe (2.0 mL, 0.234 M) and pyrrole-2-carbaldehyde (44.4 mg, 0.467 mmol, 1.0 eq.). Stirred for 3 h under Ar at 40°C. Afforded the title compound (*Z*)-**8** (107 mg, 0.385 mmol, 82%) as an orange solid.

TLC: R_f = 0.61 (1:1 EtOAc/*n*-heptane)

LCMS (ESI) $[M+H]^+$ *m/z* calcd for $C_{17}H_{12}NOS^+$: 278.0634, *m/z* found: 278.27 $[M+H]^+$

R_t: 2.10 min (total run time: 2.6 min), purity >99%

^{1}H NMR (800 MHz, DMSO-d_6): δ 11.90 (s, 1H, **H-18**), 9.29 (d, *J* = 8.3 Hz, 1H, **H-6**), 8.23 (d, *J* = 8.6 Hz, 1H, **H-10**), 8.05 (d, *J* = 8.1 Hz, 1H, **H-3**), 7.95 (s, 1H, **H-13**), 7.87 (d, *J* = 8.6 Hz, 1H, **H-9**), 7.74 (t, *J* = 7.6 Hz, 1H, **H-1**), 7.60 (t, *J* = 7.4 Hz, 1H, **H-2**), 7.31 (s, 1H, **H-15**), 6.84 (s, 1H, **H-17**), 6.45 (s, 1H, **H-16**)

^{13}C NMR (201 MHz, DMSO-d_6): δ 187.3 (**C-12**), 148.0 (**C-8**), 135.7 (**C-10**), 131.4 (**C-4**/**5**), 130.5 (**C-4**/**5**), 129.4 (**C-1**), 128.8 (**C-3**), 128.1 (**C-14**), 126.2 (**C-2**), 125.7 (**C-15**), 124.2 (**C-13**), 123.4 (**C-7**/**11**), 123.4 (**C-7**/**11**), 122.3 (**C-9**), 122.1 (**C-6**), 115.1 (**C-17**), 112.6 (**C-16**)

HRMS-ESI $[M+H]^+$ *m/z* calcd for $C_{17}H_{12}NOS^+$: 278.0634, *m/z* found: 278.0635 $[M+H]^+$ (ppm error: 0.360)

Melting point: 245-250°C (decomposes)

UV-Vis spectroscopy

2-Pyrrole HTI derivative (**8**) (33 µM in DCM)

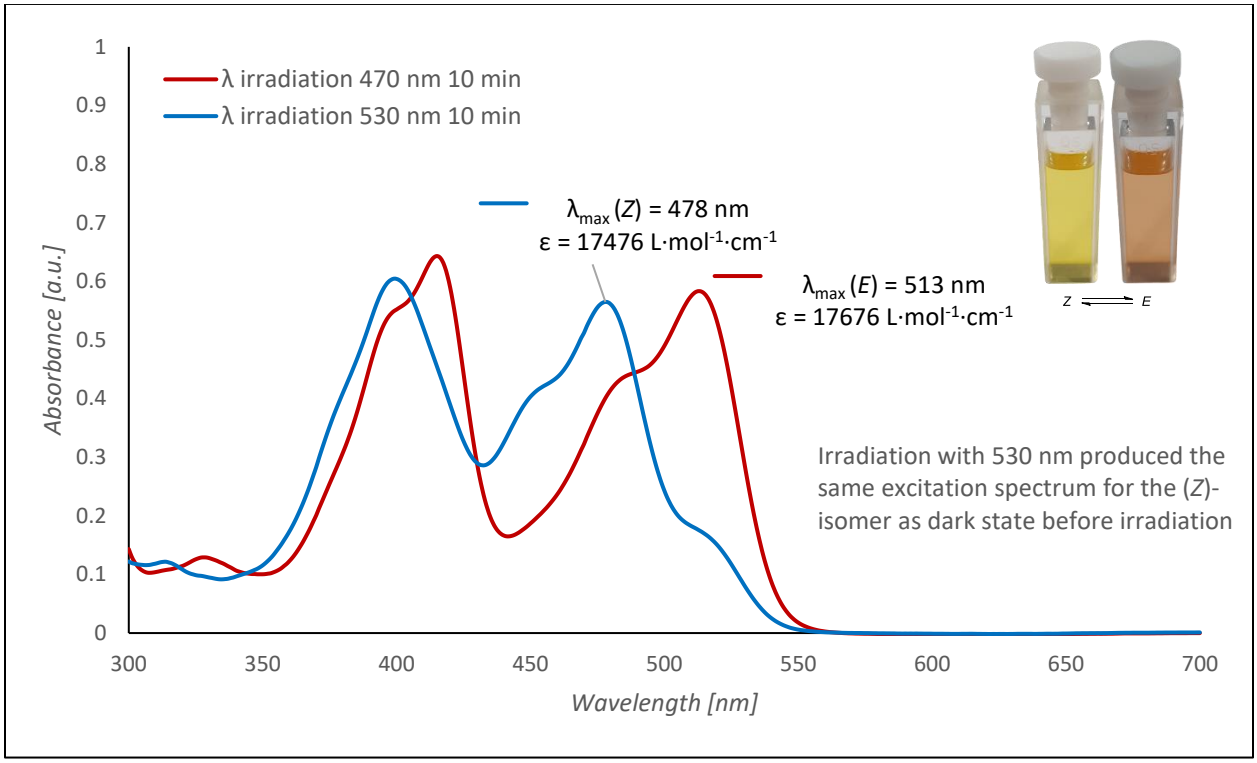

2-Pyrrole HTI derivative (**8**) (33 µM in *n*-hexane/iPrOH 9:1)

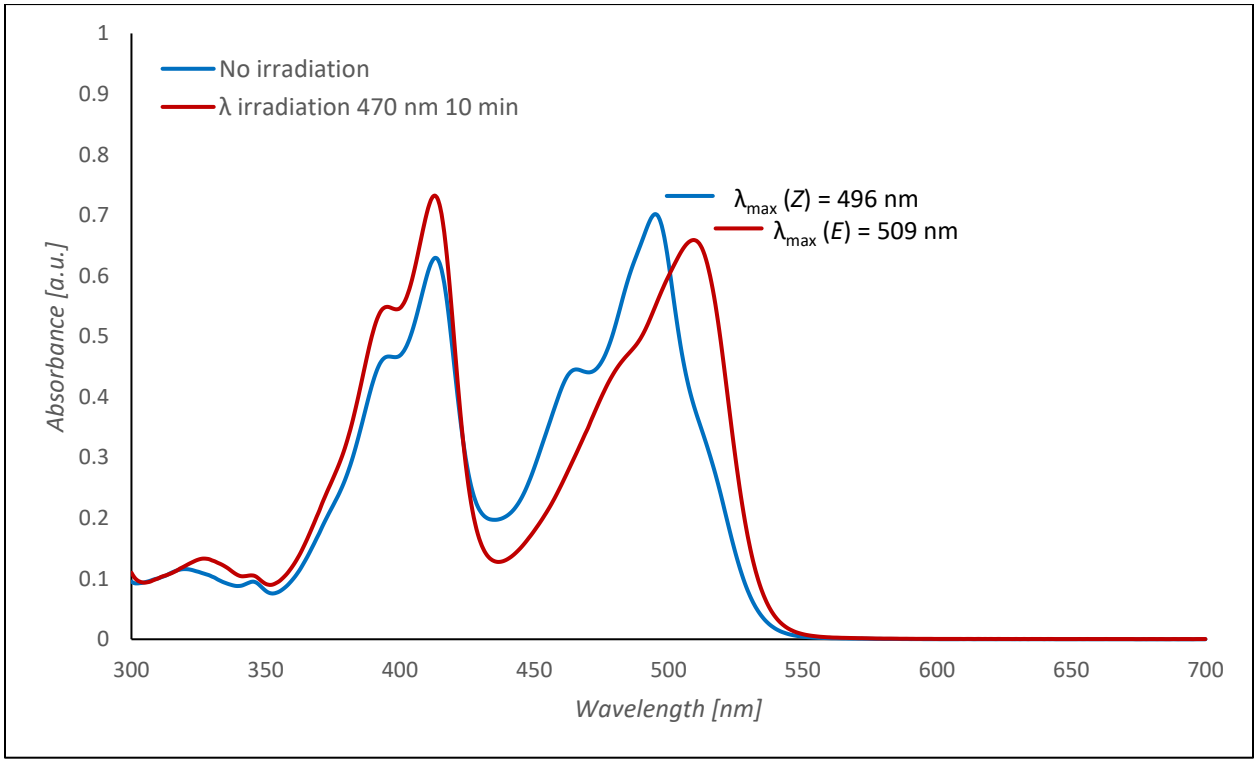

2-Pyrrole HTI derivative (**8**) (33 µM in PhMe)

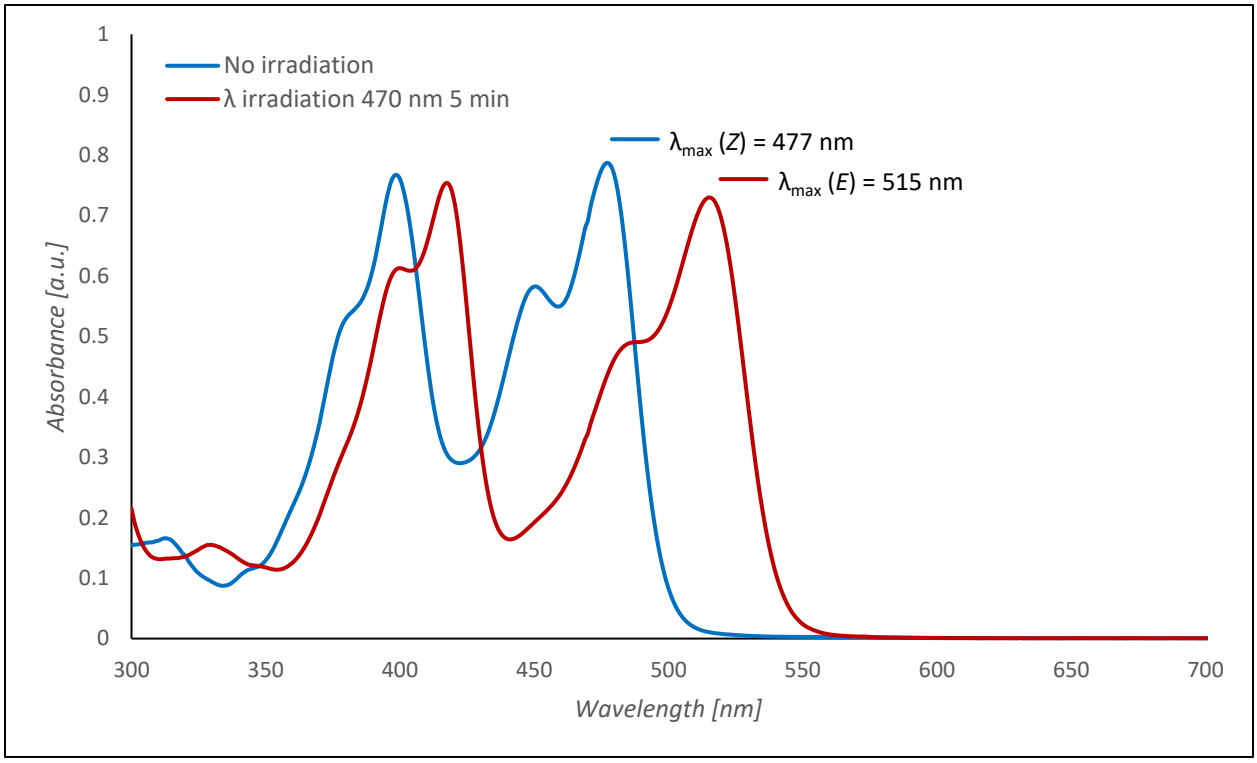

2-Pyrrole HTI derivative (**8**) (33 µM in DMSO, T = 18 °C)

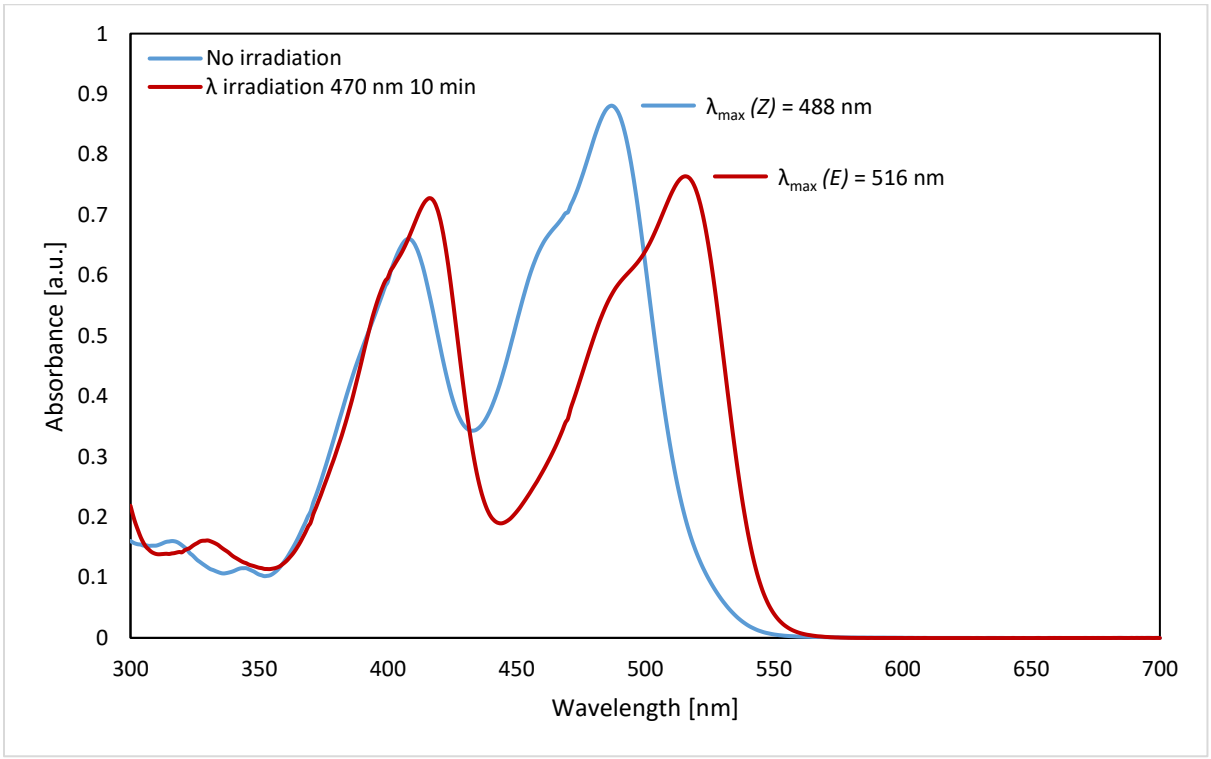

Fluorescence spectroscopy

2-Pyrrole HTI derivative (**8**) (33 µM in DCM)

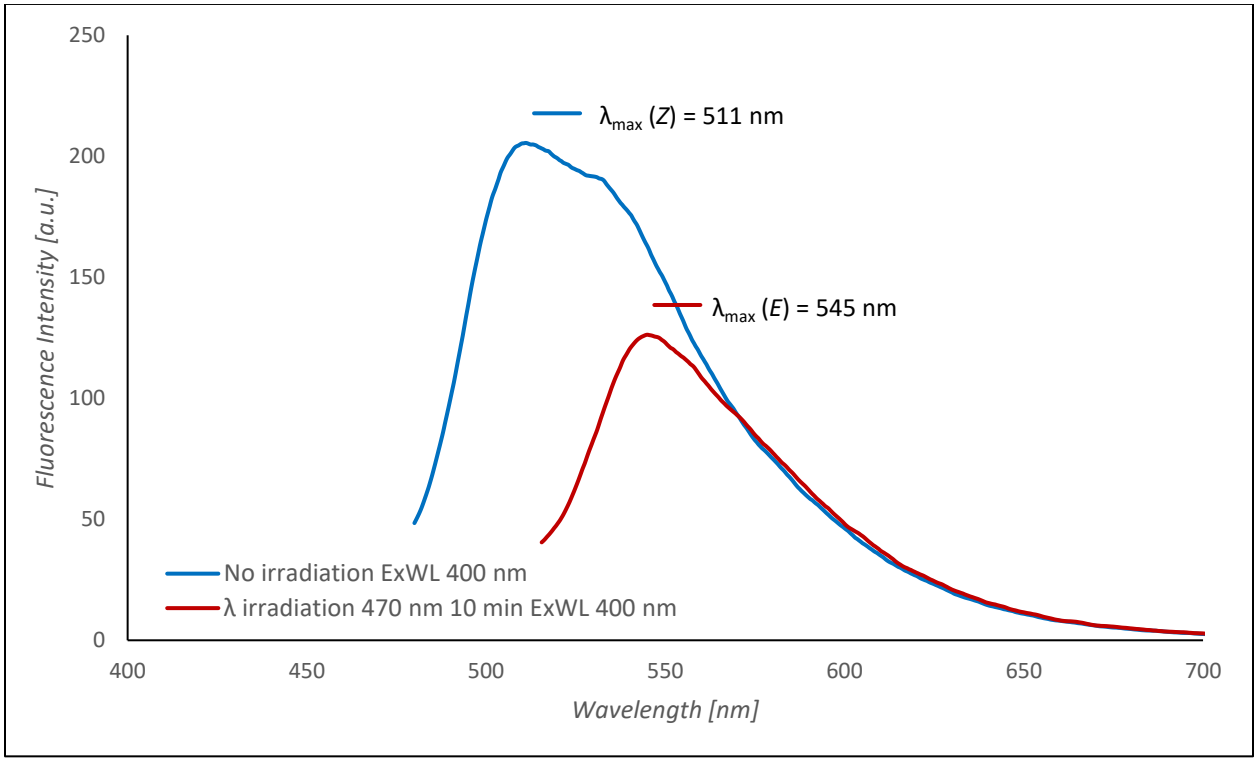

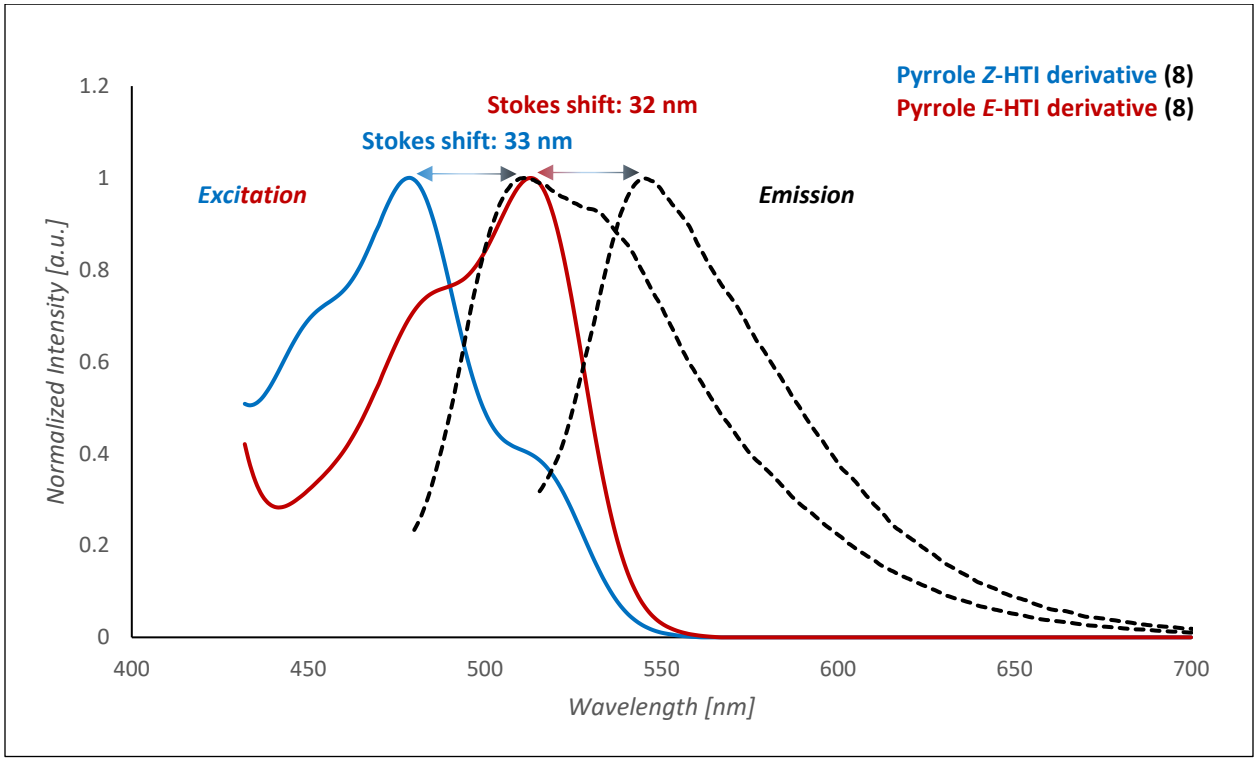

UV-Vis thermal relaxation spectroscopy

2-Pyrrole HTI derivative (**8**) (33 µM in DCM)

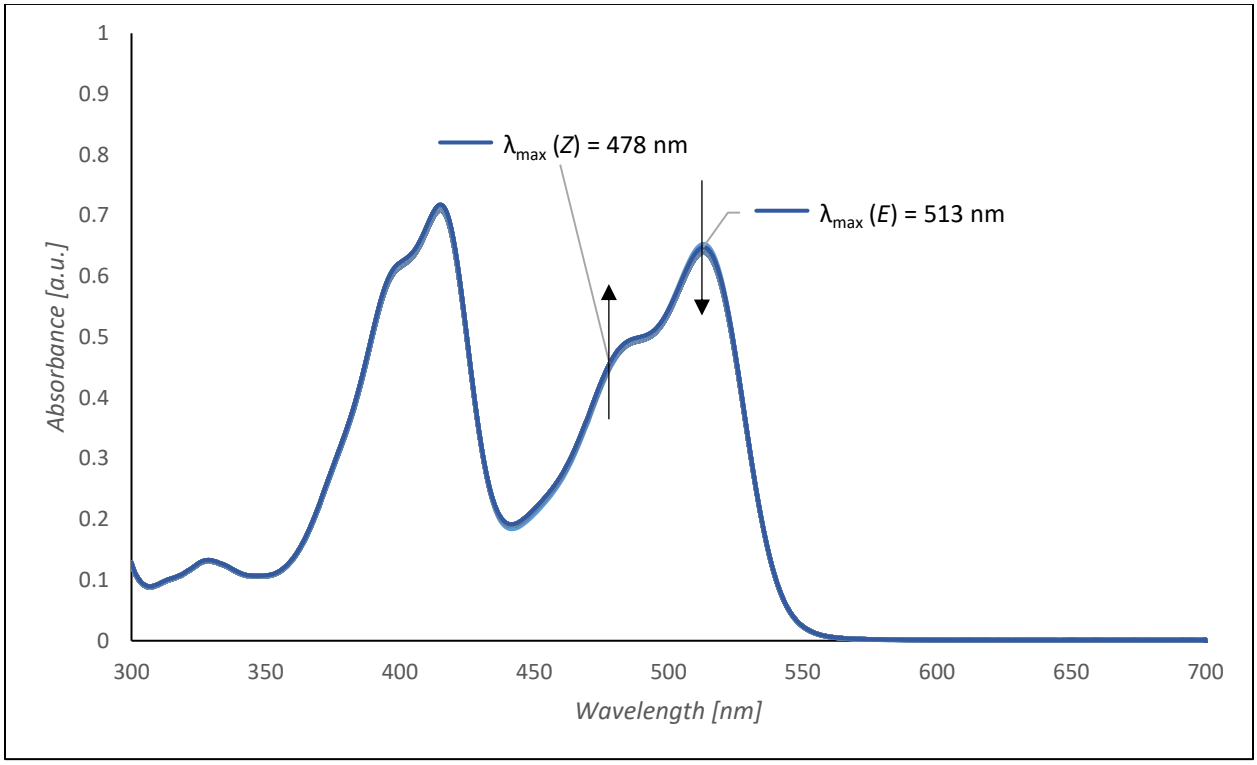

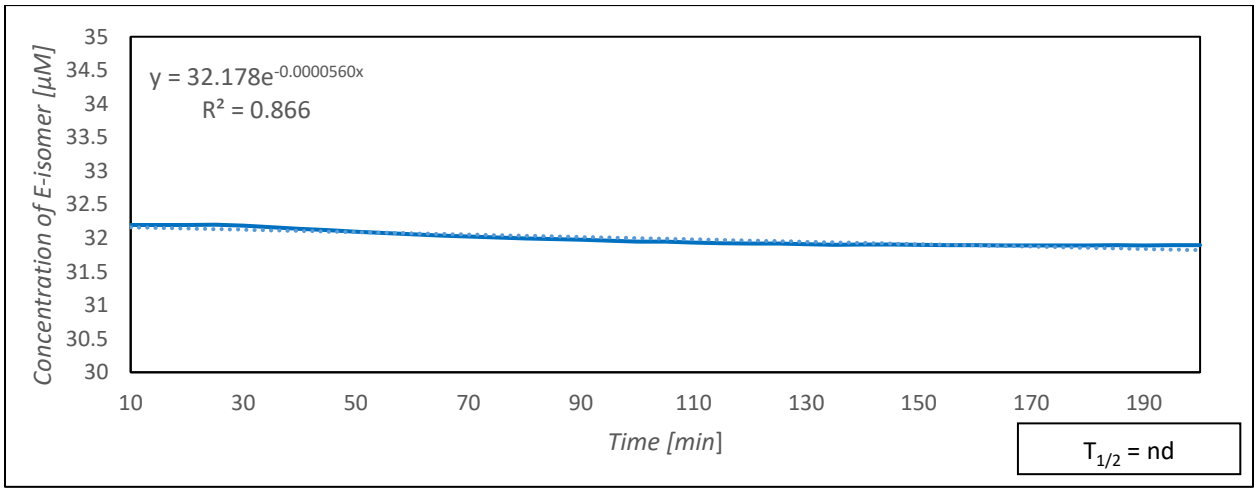

2-Pyrrole HTI derivative (**8**) (33 µM in PhMe)

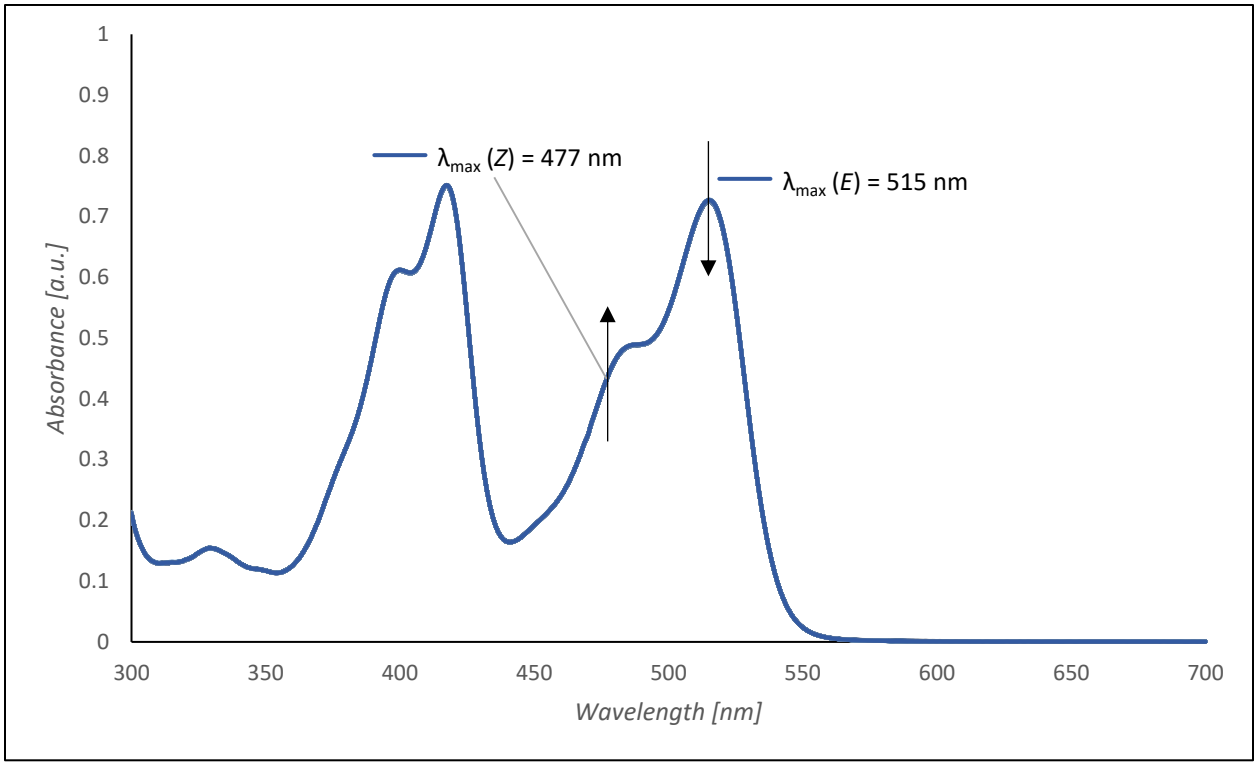

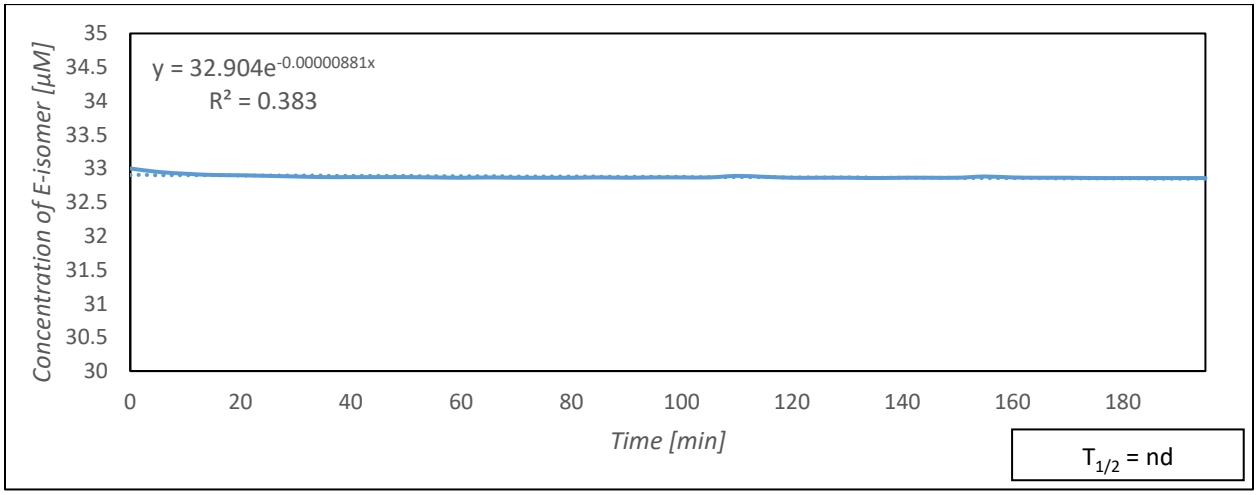

2-Pyrrole HTI derivative (**8**) (33 µM in DMSO, T = 18 °C, measurement every 10 minutes for 18 hours)

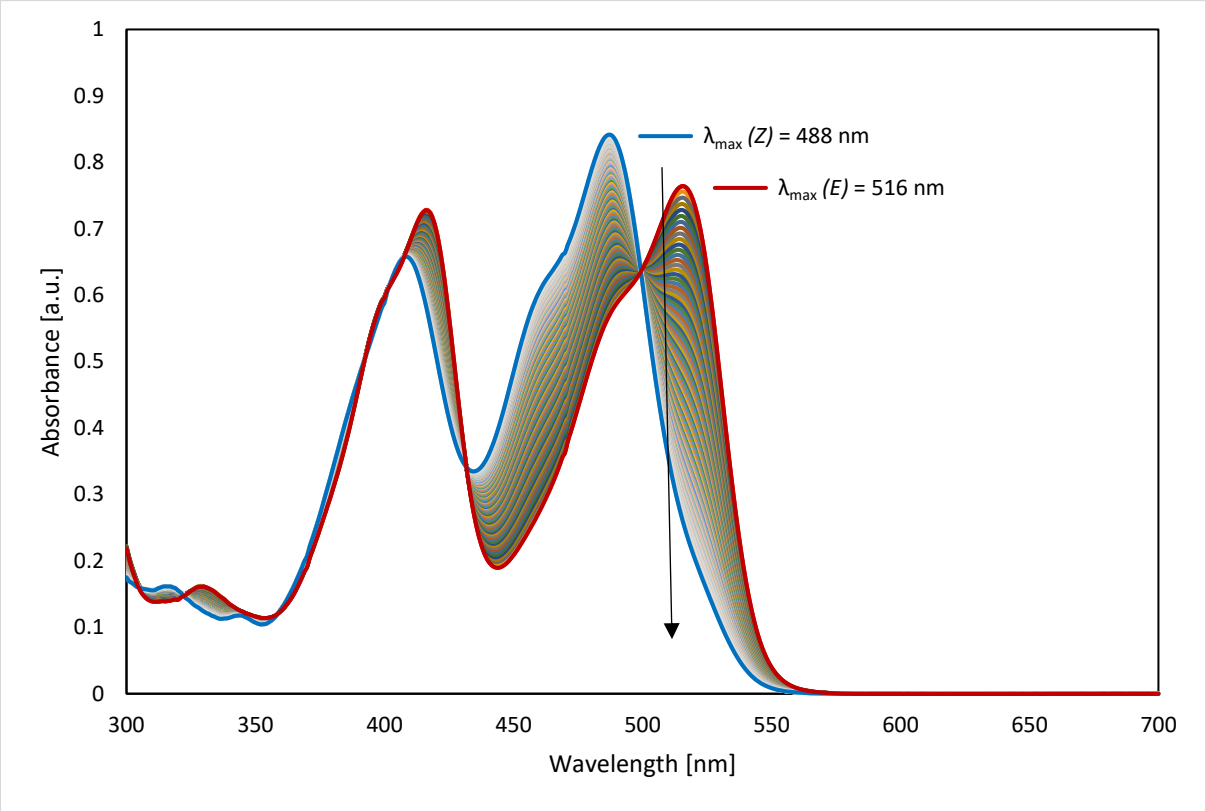

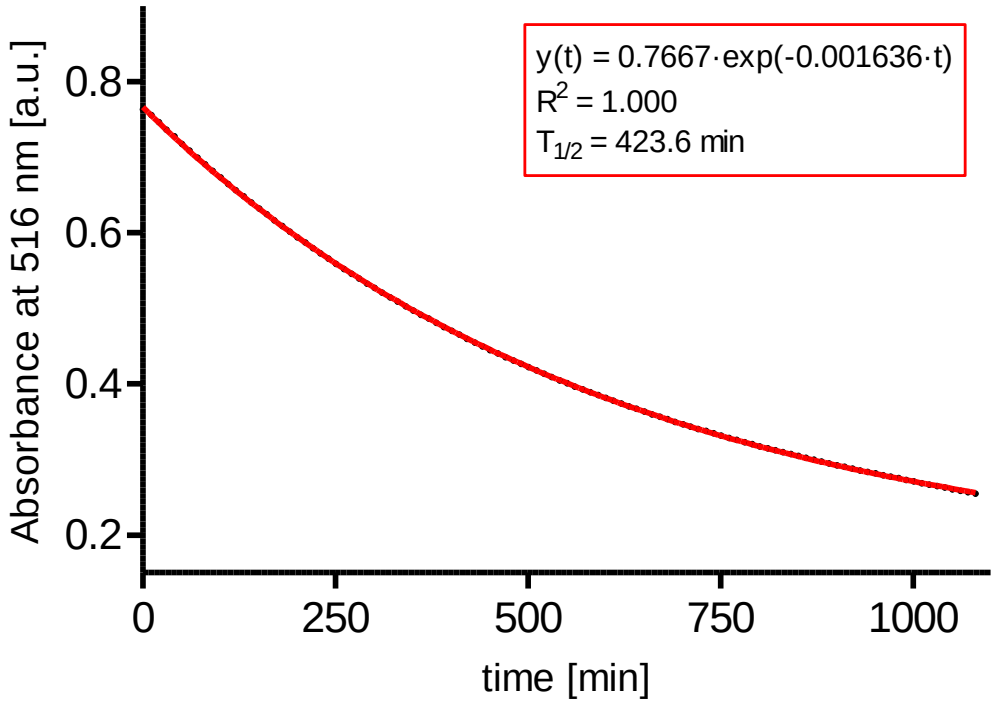

Kinetic analysis of thermal *E*-to-*Z* isomerisation

2-Pyrrole HTI derivative (**8**) (33 µM in DMSO, T = 18 °C, first 331 minutes)

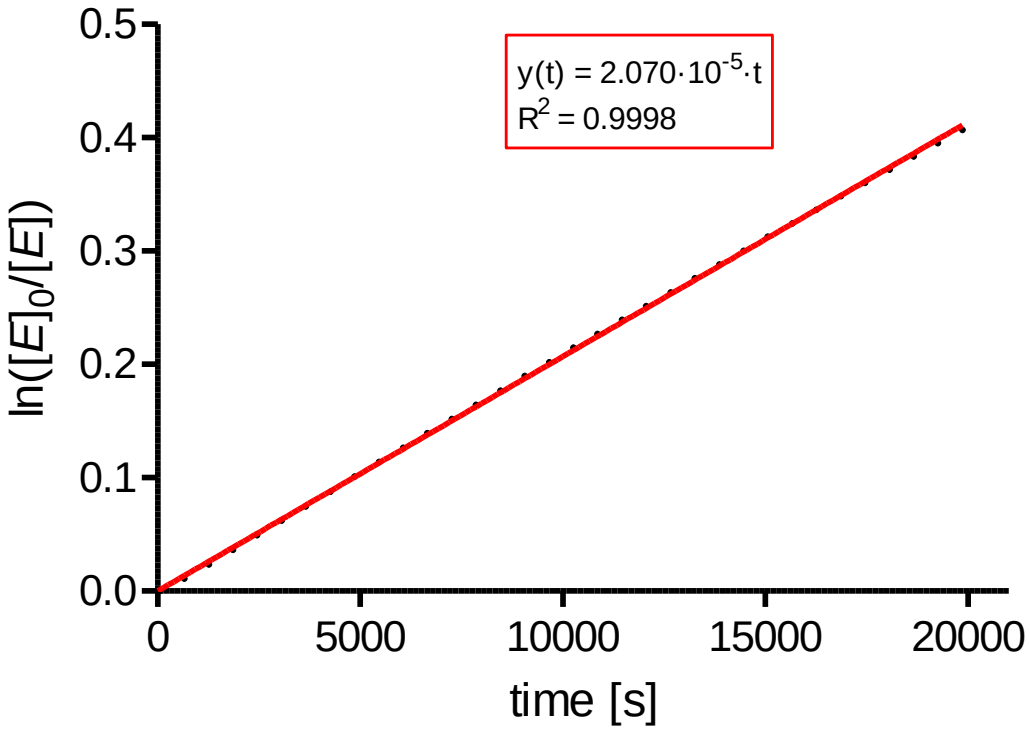

The linear fit gives the first order rate constant $k = 2.07 \cdot 10^{-5}$ s^{-1}. This corresponds to a Gibbs energy of activation of **$\Delta G^{\ddagger}$ = 97.4 kJ·mol^{-1} = 23.3 kcal·mol^{-1}**.

HPLC conditions

Column:	ChiralPak AD-H column (5 µm, 250 x 4.6 mm)
Mobile Phase	90:10 *n*-hexane/iPrOH (isocratic, 1 mL/min)
Isosbestic Point	502 nm (in HPLC mobile Phase)
t_R(E)	7.63 min
t_R(Z)	11.52 min

Solution composition (%*E*-isomer)

Initial solution composition before irradiation: *E*-isomer (0.48%) / *Z*-isomer (99.52%)

Time	**470 nm**	**Time**	**530 nm**
10 min	86.86	**10 min**	60.03
20 min	87.61	**30 min**	27.92
-	-	**50 min**	26.10

Note: The sample (1 mg/mL) was irradiated in DCM following a direct injection.

Representative HPLC traces

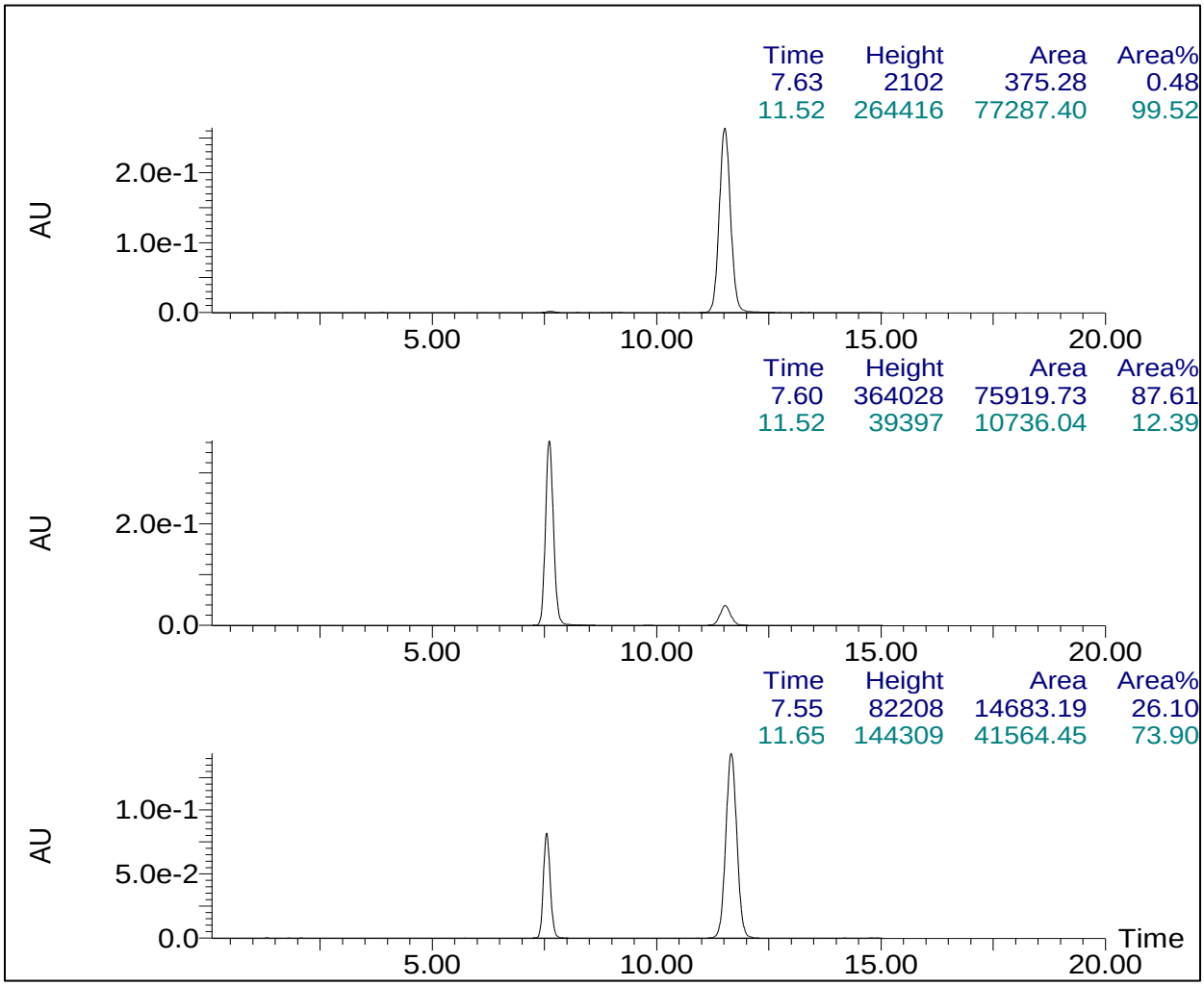

(*Z*)-2-((1H-Indol-2-yl)methylene)naphtho[2,1-b]thiophen-1(2H)-one (9)

Prepared according to general procedure B.

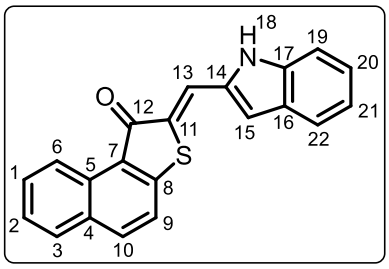

Hemithioindigo derivative **SI 5** (101 mg, 0.505 mmol, 1.0 eq.), PhMe (2.0 mL, 0.253 M) and indole-2-carbaldehyde (66.6 mg, 0.468 mmol, 0.93 eq.). Stirred for 3 h under Ar at 40°C. Afforded the title compound (*Z*)-**9** (86.6 mg, 0.265 mmol, 57%) as a red solid.

TLC: R_f = 0.78 (1:1 EtOAc/*n*-heptane + 1% TEA)

LCMS (ESI) $[M+H]^+$ *m/z* calcd for $C_{21}H_{14}NOS^+$: 328.0791, *m/z* found: 328.01 $[M+H]^+$

R_t: 3.41-4.28 min broad peak (total run time: 5.2 min), purity >N/A

^{1}H NMR (800 MHz, DMSO-d_6): δ 11.81 (s, 1H, **H-18**), 9.26 (d, *J* = 8.3 Hz, 1H, **H-6**), 8.30 (d, *J* = 8.5 Hz, 1H, **H-10**), 8.08 (d, *J* = 8.0 Hz, 1H, **H-3**), 8.03 (s, 1H, **H-13**), 7.92 (d, *J* = 8.5 Hz, 1H, **H-9**), 7.78 (ddd, *J* = 8.3, 6.8, 1.3 Hz, 1H, **H-1**), 7.72 (d, *J* = 7.9 Hz, 1H, **H-22**), 7.63 (ddd, *J* = 8.0, 6.8, 1.2 Hz, 1H, **H-2**), 7.48 (d, *J* = 8.1 Hz, 1H, **H-19**), 7.26 (ddd, *J* = 8.0, 6.7, 1.1 Hz, 1H, **H-20**), 7.14 (s, 1H, **H-15**), 7.10 (t, *J* = 7.4 Hz, 1H, **H-21**)

^{13}C NMR (151 MHz, DMSO-d_6): δ 187.5 (**C-12**), 148.6 (**C-8**), 137.9 (**C-16**), 136.6 (**C-10**), 133.0 (**C-14**), 131.5 (**C-4**/**5**), 130.5 (**C-4**/**5**), 129.8 (**C-1**), 129.1 (**C-11**), 129.0 (**C-3**), 128.6 (**C-17**), 126.5 (**C-2**), 124.6 (**C-20**), 123.7 (**C-13**), 122.9 (**C-7**), 122.3 (**C-9**), 122.1 (**C-6**), 121.6 (**C-22**), 120.5 (**C-21**), 111.9 (**C-19**), 107.4 (**C-15**)

^{1}H NMR (800 MHz, C_4H_8O): 11.03 (s, 1H, **H-18**), 9.66 (d, *J* = 8.4 Hz, 1H, **H-6**), 8.40 (d, *J* = 8.5 Hz, 1H), 8.26 (s, 1H, **H-13**), 8.21 (d, *J* = 8.0 Hz, 1H), 7.97 (d, *J* = 8.5 Hz, 1H), 7.94 (t, *J* = 7.6 Hz, 1H), 7.92 (d, *J* = 8.0 Hz, 1H), 7.80 (t, *J* = 7.4 Hz, 1H), 7.67 (d, *J* = 8.1 Hz, 1H), 7.47 (t, *J* = 7.5 Hz, 1H), 7.40 (d, *J* = 2.1 Hz, 1H), 7.33 (t, *J* = 7.4 Hz, 1H)

HRMS-ESI $[M+H]^+$ *m/z* calcd for $C_{21}H_{14}NOS^+$: 328.0791, *m/z* found: 328.0789 $[M+H]^+$ (ppm error: -0.610)

Melting point: 287-289°C

(*E*)-**9**:

^{1}H NMR (800 MHz, DMSO-d_6): δ 12.84 (s, 1H, **H-18**), 9.48 (d, *J* = 7.8 Hz, 1H), 8.28 (d, *J* = 8.5 Hz, 1H), 8.10 – 8.07 (m, 1H), 7.94 (t, 1H), 7.88 (d, *J* = 8.5 Hz, 1H), 7.81 (ddd, *J* = 8.3, 6.8, 1.3 Hz, 1H), 7.79 – 7.75 (m, 1H), 7.74 – 7.71 (m, 1H), 7.66 – 7.61 (m, 1H), 7.36 (ddd, *J* = 8.1, 6.8, 1.1 Hz, 1H), 7.28 – 7.25 (m, 1H), 7.15 – 7.12 (m, 1H)

^{1}H NMR (800 MHz, C_4H_8O): δ 13.41 (s, 1H, **H-18**), 9.83 (d, *J* = 8.3 Hz, 1H, **H-6**), 8.37 (d, *J* = 8.5 Hz, 1H), 8.21 (d, *J* = 8.0 Hz, 1H), 7.99 (t, *J* = 7.7 Hz, 1H), 7.92 – 7.87 (m, 4H), 7.82 (t, *J* = 7.4 Hz, 1H), 7.58 (t, *J* = 7.6 Hz, 1H), 7.34 (t, *J* = 7.4 Hz, 1H), 7.32 – 7.29 (m, 1H)

Note: A 1.5:1 (*Z*/*E*)-ratio was observed for (*E*)-**9** in DMSO, whereas THF afforded clean (*E*)-**9** by ^{1}H NMR.

UV-Vis spectroscopy

2-Indole HTI derivative (**9**) (33 µM in DCM)

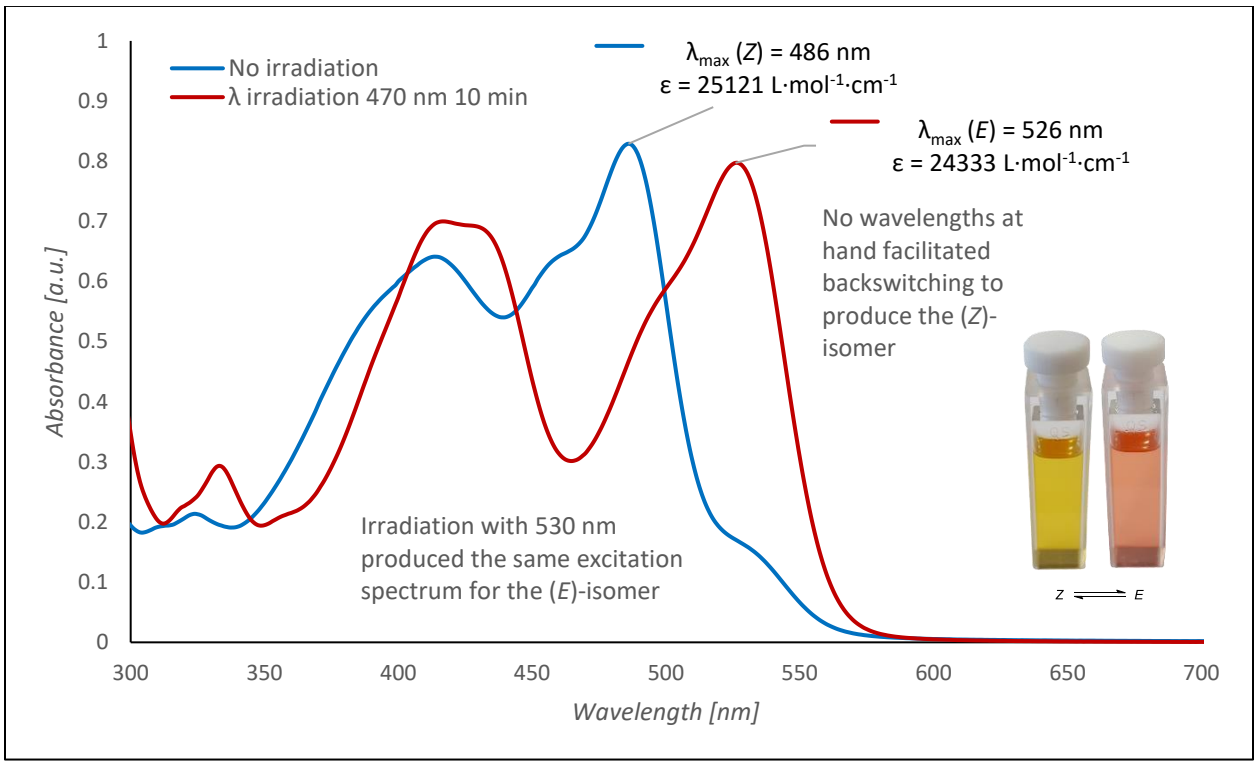

2-Indole HTI derivative (**9**) (33 µM in *n*-hexane/iPrOH 9:1)

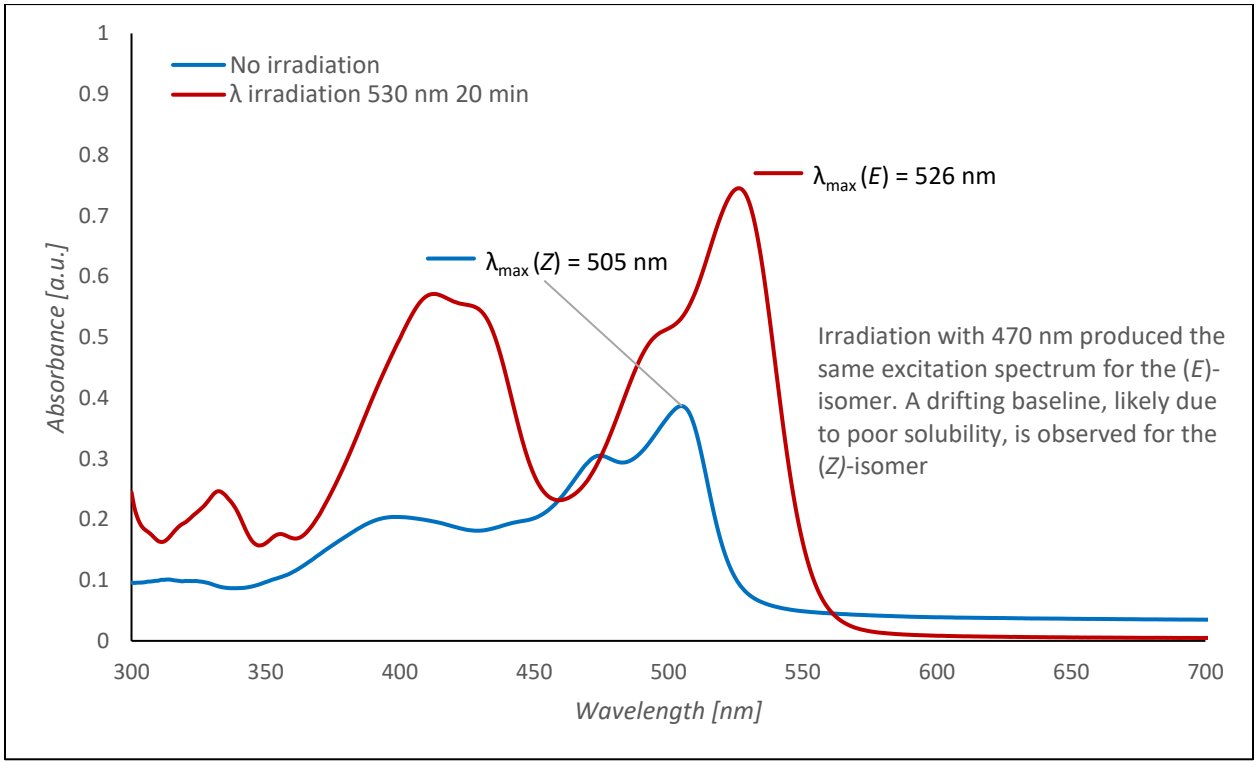

2-Indole HTI derivative (**9**) (33 µM in iPrOH)

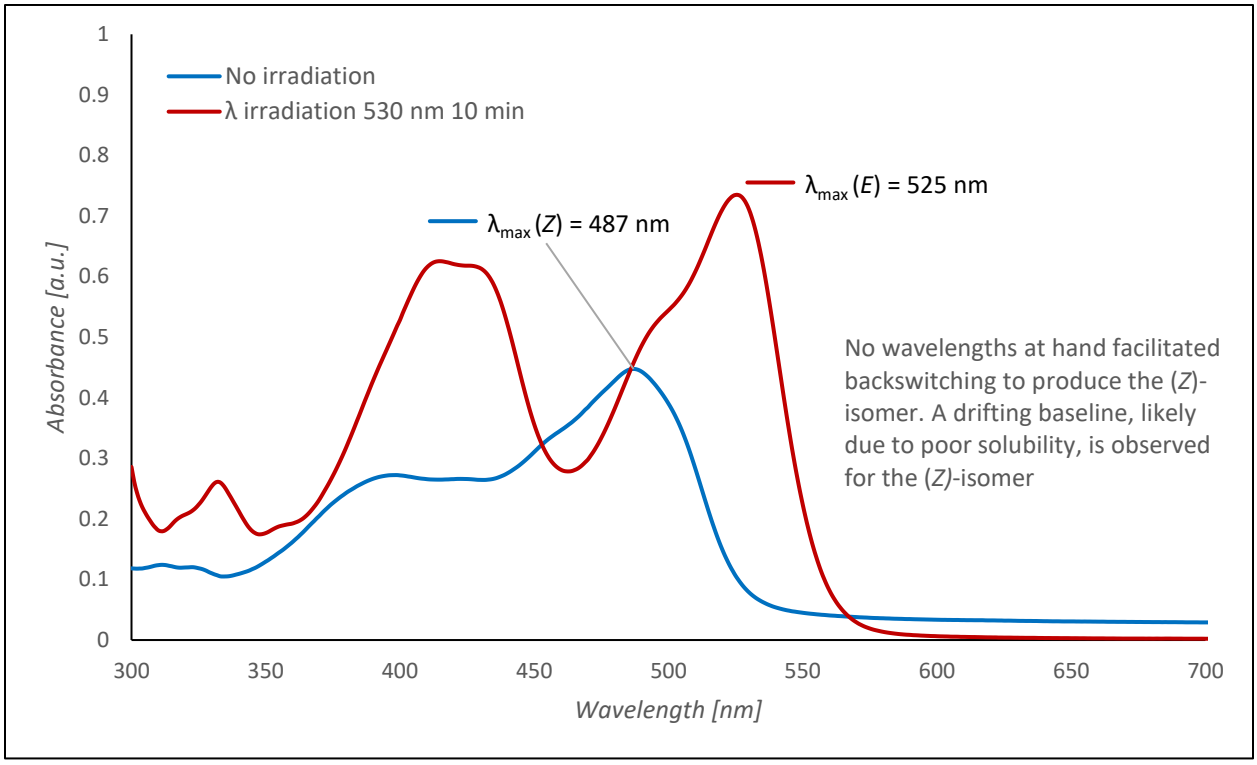

2-Indole HTI derivative (**9**) (33 µM in THF)

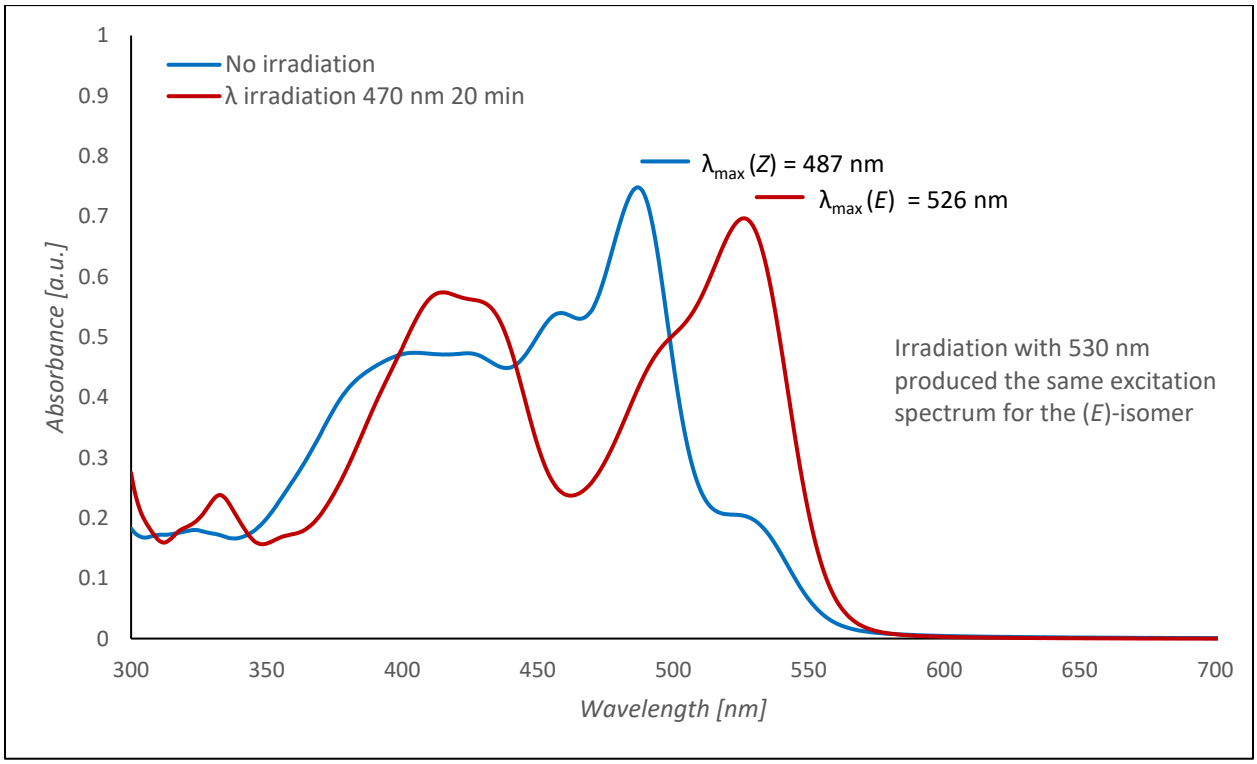

2-Indole HTI derivative (**9**) (33 μM in PhMe)

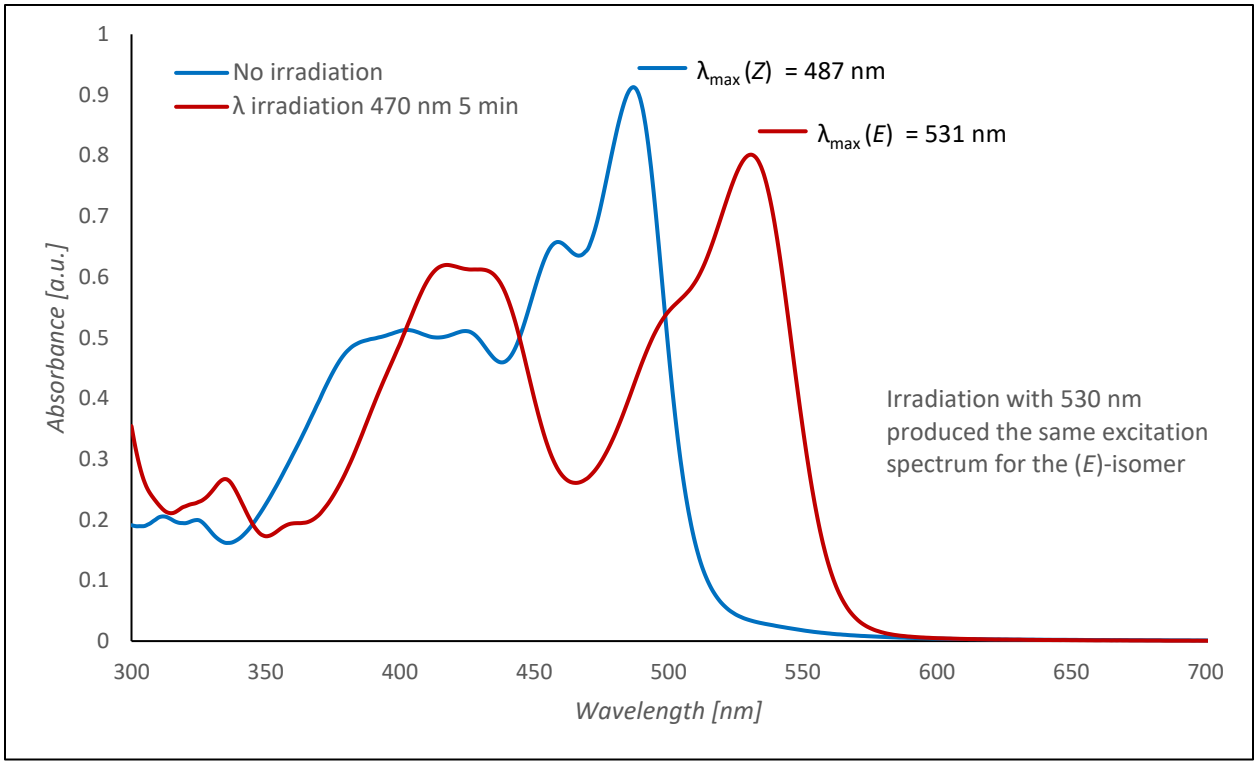

2-Indole HTI derivative (**9**) (33 μM in DMSO)

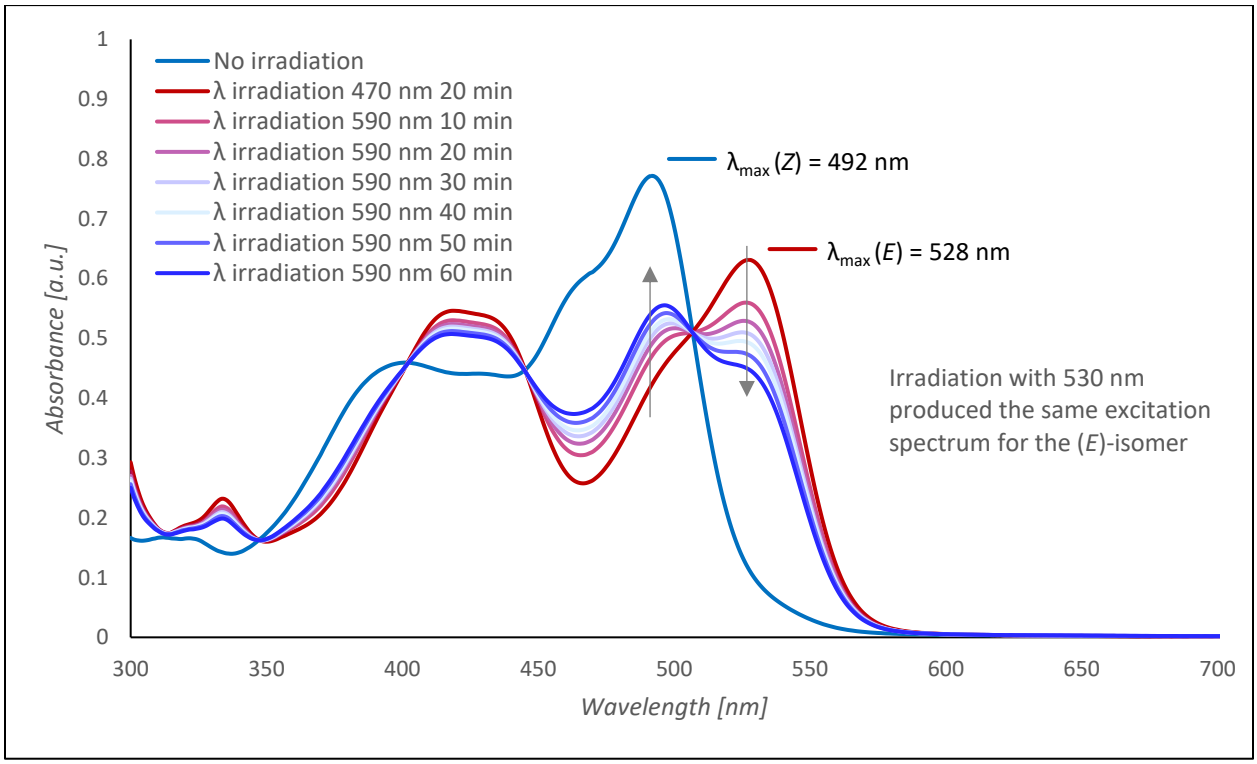

Fluorescence spectroscopy

2-Indole HTI derivative (**9**) (33 μM in DCM)

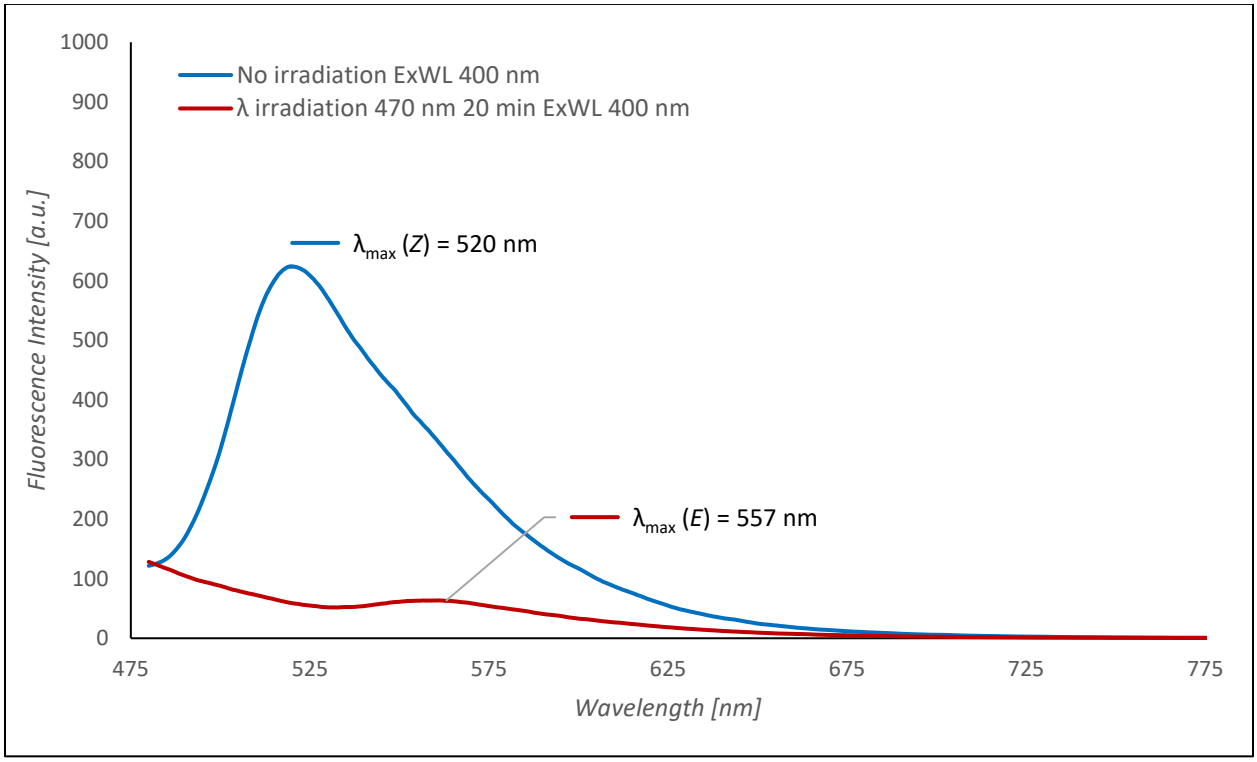

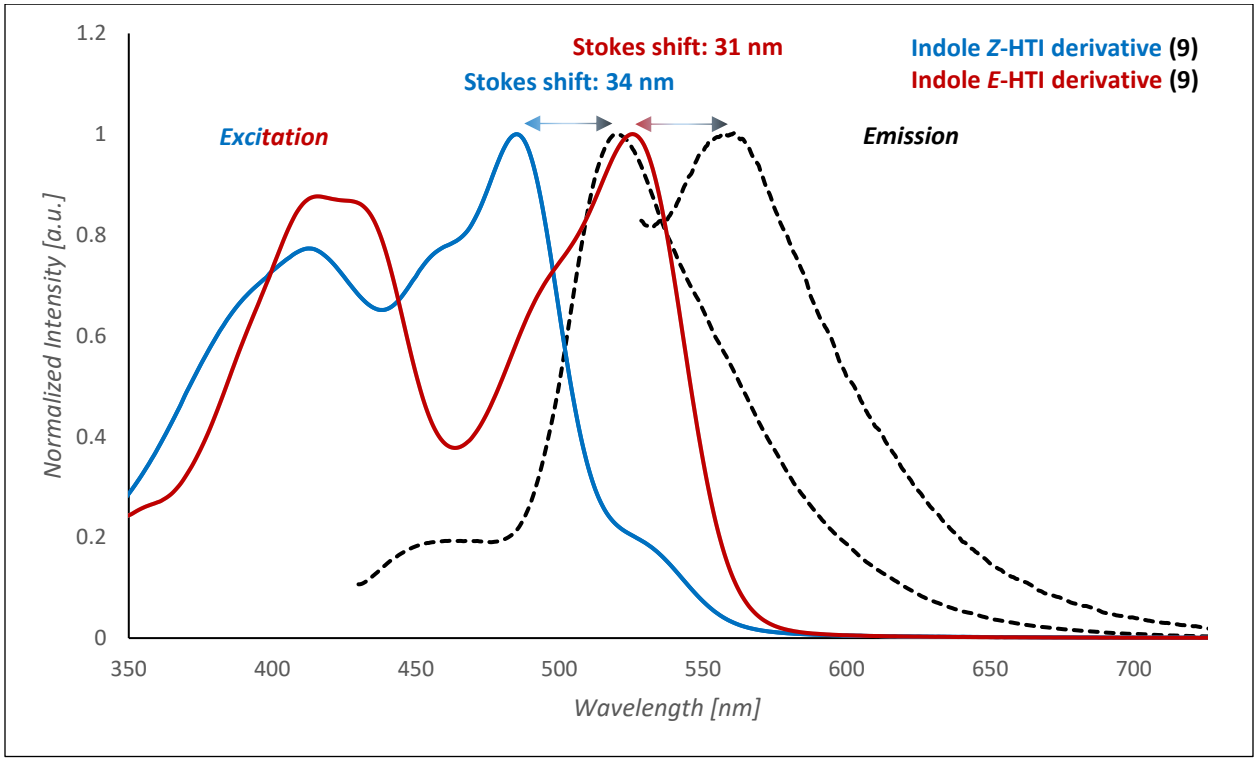

UV-Vis thermal relaxation spectroscopy

2-Indole HTI derivative (**9**) (33 µM in DMSO)

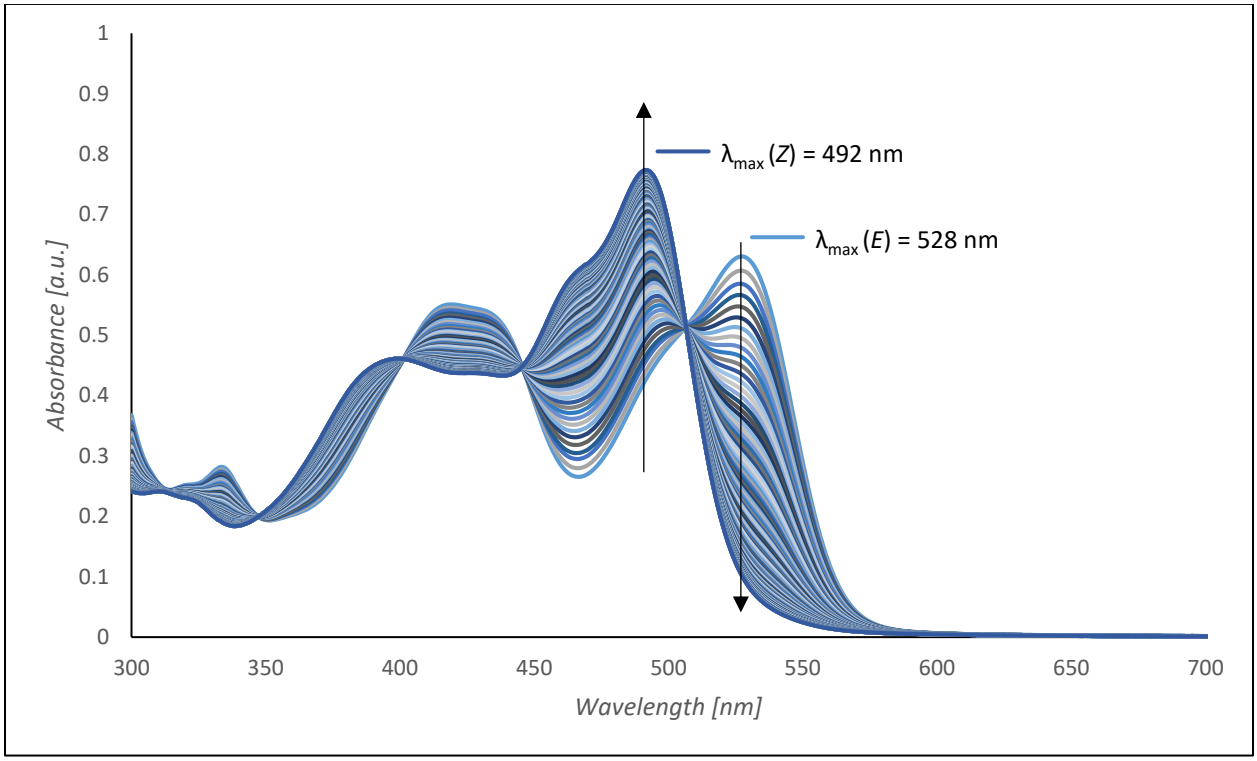

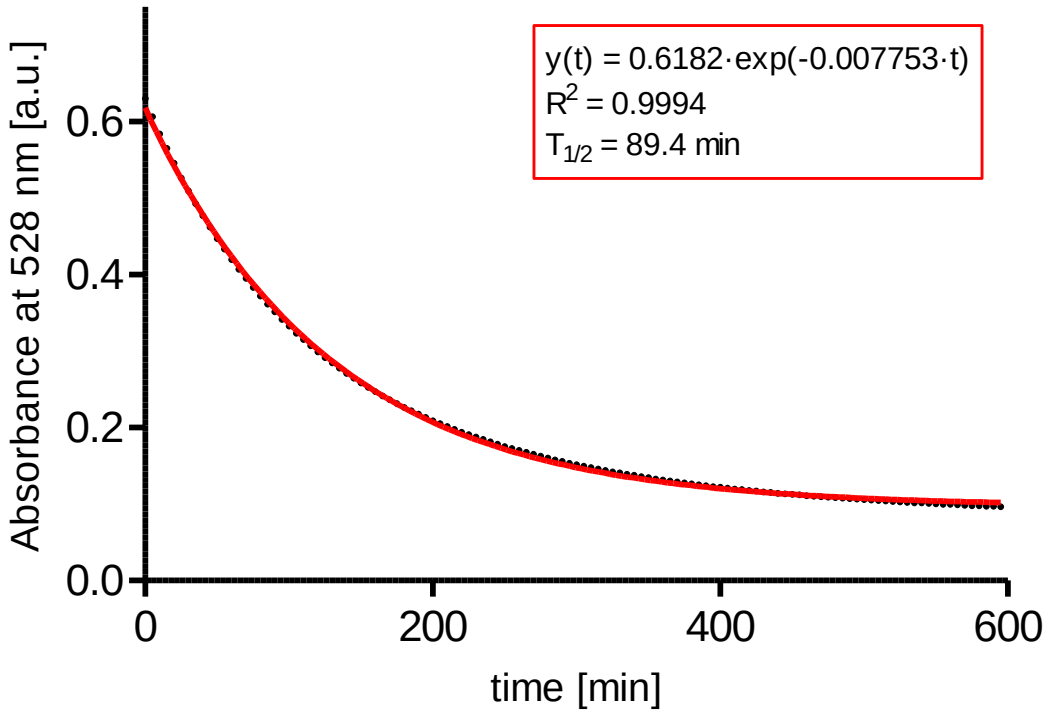

Kinetic analysis of thermal *E*-to-*Z* isomerisation

2-Indole HTI derivative (**9**) (33 µM in DMSO, T = 28 °C, first 80 minutes)

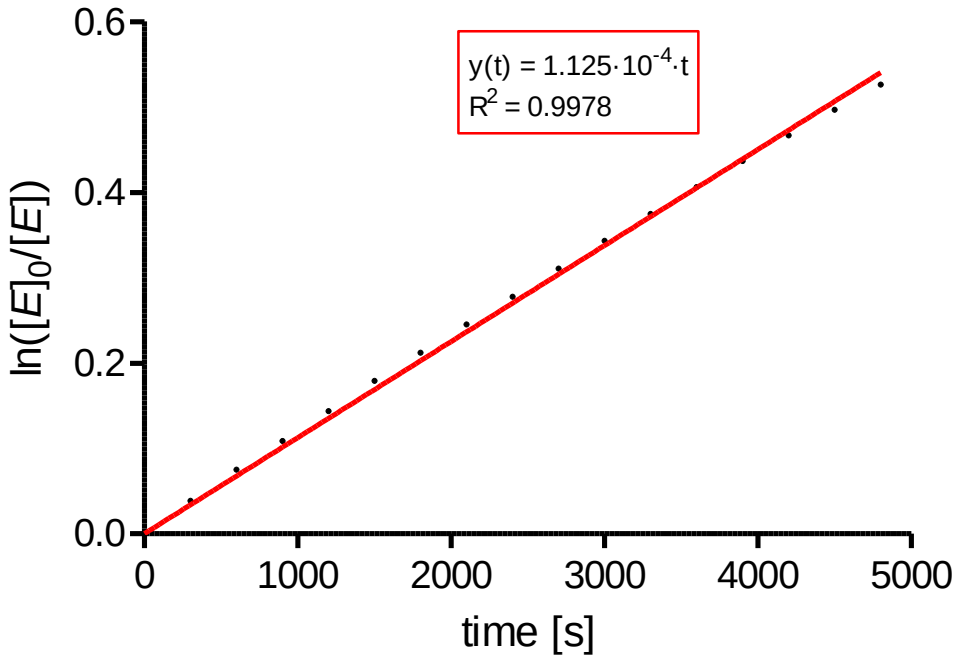

The linear fit gives the first order rate constant $k = 1.13 \cdot 10^{-4}$ s^{-1}. This corresponds to a Gibbs energy of activation of **$\Delta G^{\ddagger}$ = 96.6 kJ·mol^{-1} = 23.1 kcal·mol^{-1}**.

2-Indole HTI derivative (**9**) (33 μM in PhMe)

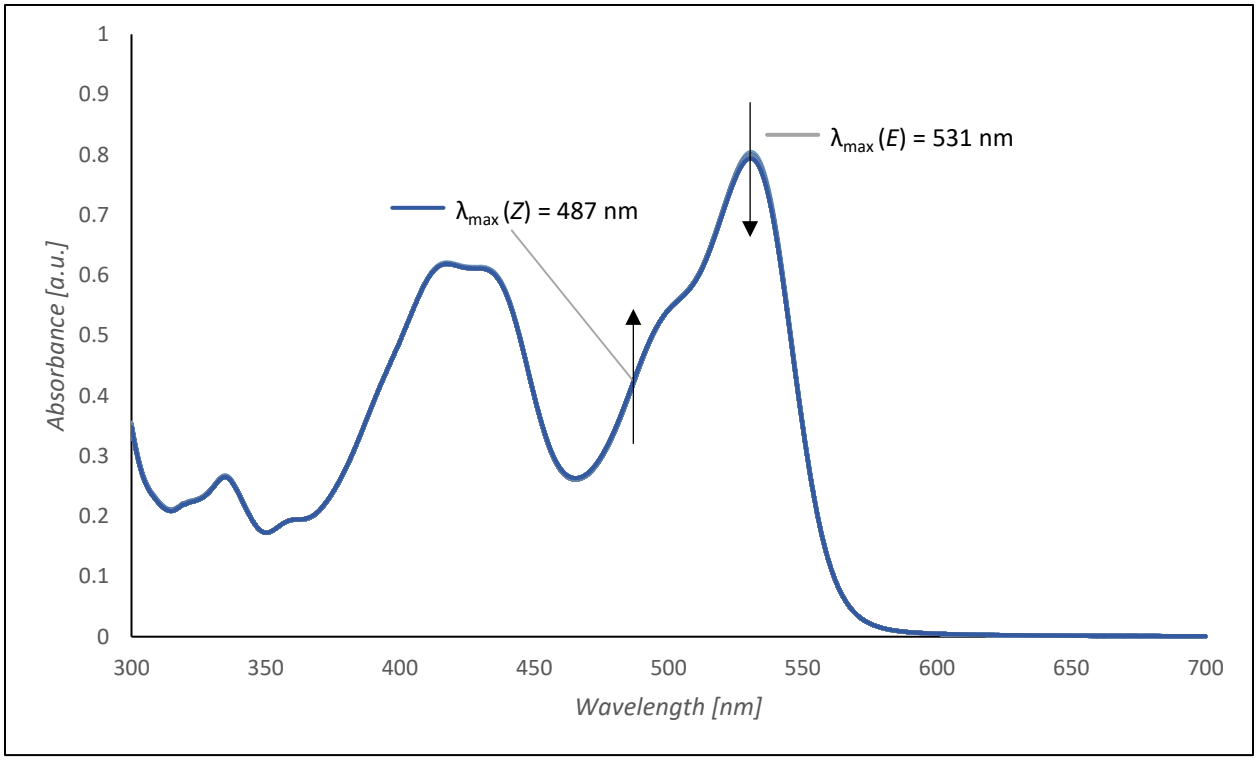

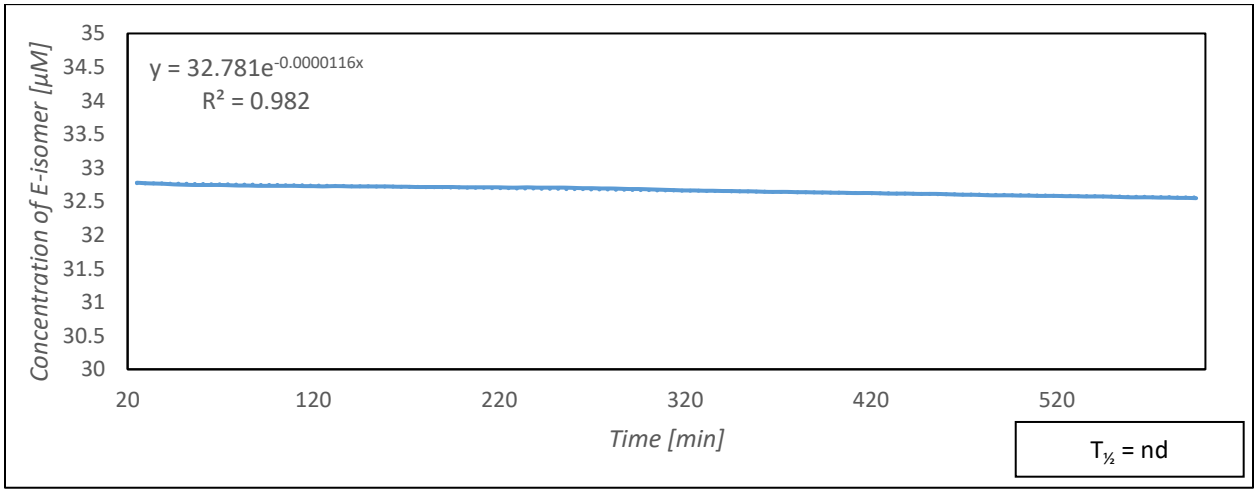

(*Z*)-2-(1H,1'H-[2,2'-Bipyrrol]-5-ylmethylene)benzo[b]thiophen-3(2H)-one (10)

Prepared according to general procedure B.

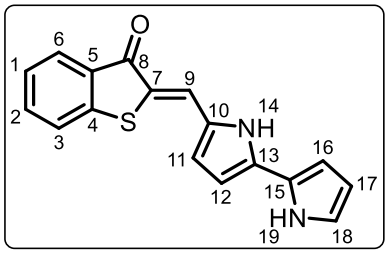

Hemithioindigo **SI 6** (53 mg, 0.353 mmol, 1.0 eq.), PhMe (2.0 mL, 0.176 M) and bipyrrole-5-carbaldehyde (46.0 mg, 0.287 mmol, 0.81 eq.). Stirred for 2.5 h under Ar at 100°C. Afforded the title compound (*Z*)-**10** (31.7 mg, 0.108 mmol, 38%) as a dark purple solid.

TLC: R_f = 0.52 (1:1 EtOAc/*n*-heptane + 1% TEA)

LCMS (ESI) $[M+H]^+$ *m/z* calcd for $C_{21}H_{14}NOS^+$: 328.0791, *m/z* found: 328.01 $[M+H]^+$

R_t: 3.41-4.28 min broad peak (total run time: 5.2 min)

^{1}H NMR (800 MHz, DMSO-d_6): δ 11.88 (s, 1H, **H-14/19**), 11.35 (s, 1H, **H-14/19**), 7.85 (s, 1H, **H-9**), 7.80 (d, *J* = 7.7 Hz, 1H, **H-6**), 7.76 (d, *J* = 7.9 Hz, 1H, **H-3**), 7.66 (t, *J* = 7.5 Hz, 1H, **H-2**), 7.37 (t, *J* = 7.4 Hz, 1H, **H-1**), 6.90 (d, *J* = 2.5 Hz, 1H, **H-18**), 6.84 (d, *J* = 4.2 Hz, 1H, **H-11**), 6.72 (d, *J* = 4.4 Hz, 1H, **H-12**), 6.53 (s, 1H, **H-16**), 6.15 (q, *J* = 2.8 Hz, 1H, **H-17**)

^{13}C NMR (201 MHz, DMSO-d_6): δ 185.8 (**C-8**), 143.8 (**C-5**), 134.5 (**C-2**), 133.3 (**C-13**), 131.4 (**C-4**), 127.9 (**C-10**), 125.7 (**C-6**), 125.6 (**C-1**), 124.4 (**C-3**), 123.8 (**C-15**), 122.7 (**C-9**), 121.4 (**C-7**), 119.9 (**C-16/18**), 117.4 (**C-11**), 109.3 (**C-17**), 108.8 (**C-12**), 106.1 (**C-16/18**)

HRMS-ESI $[M+H]^+$ *m/z* calcd for $C_{17}H_{13}N_2OS^+$: 293.0743, *m/z* found: 293.0744 $[M+H]^+$ (ppm error: 0.341)

Melting point: 273-275°C (decomposes)

UV-Vis spectroscopy

Bipyrrole HTI (**10**) (33 µM in DCM)

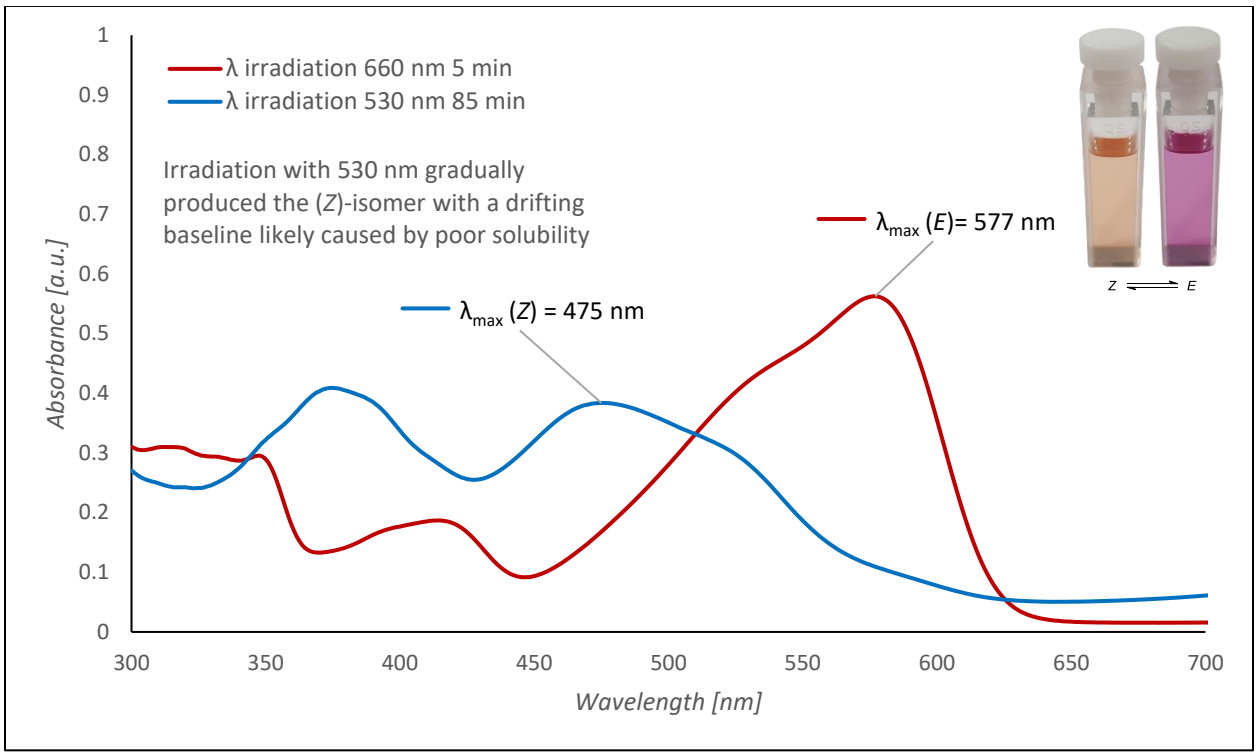

Bipyrrole HTI (**10**) (33 µM in *n*-hexane/iPrOH 9:1)

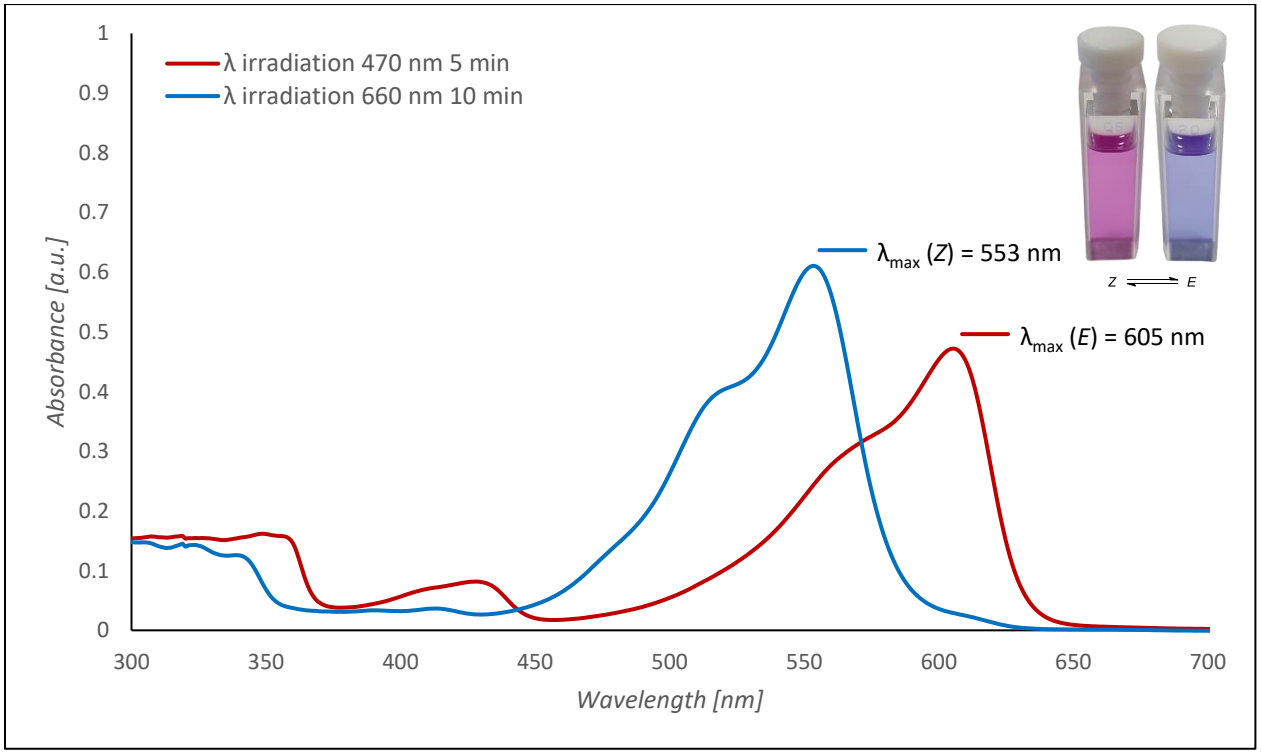

Bipyrrole HTI (**10**) (33 µM in iPrOH)

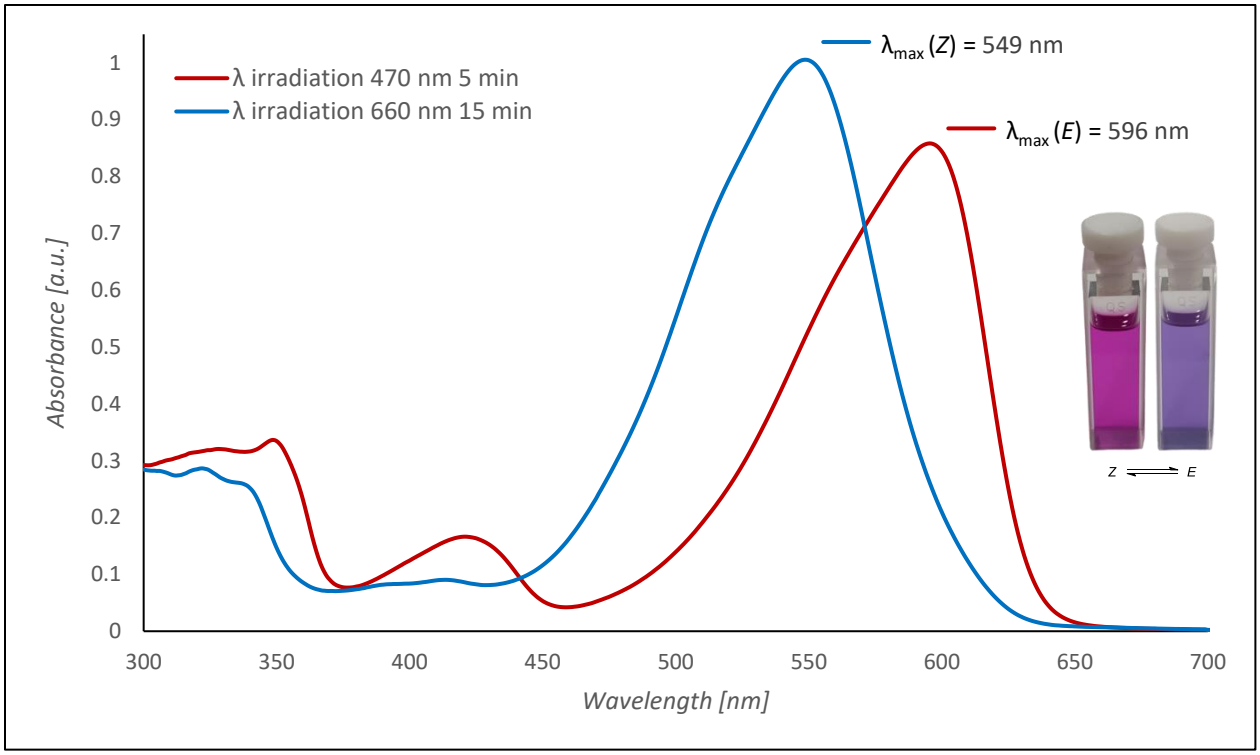

Bipyrrole HTI (**10**) (33 µM in THF)

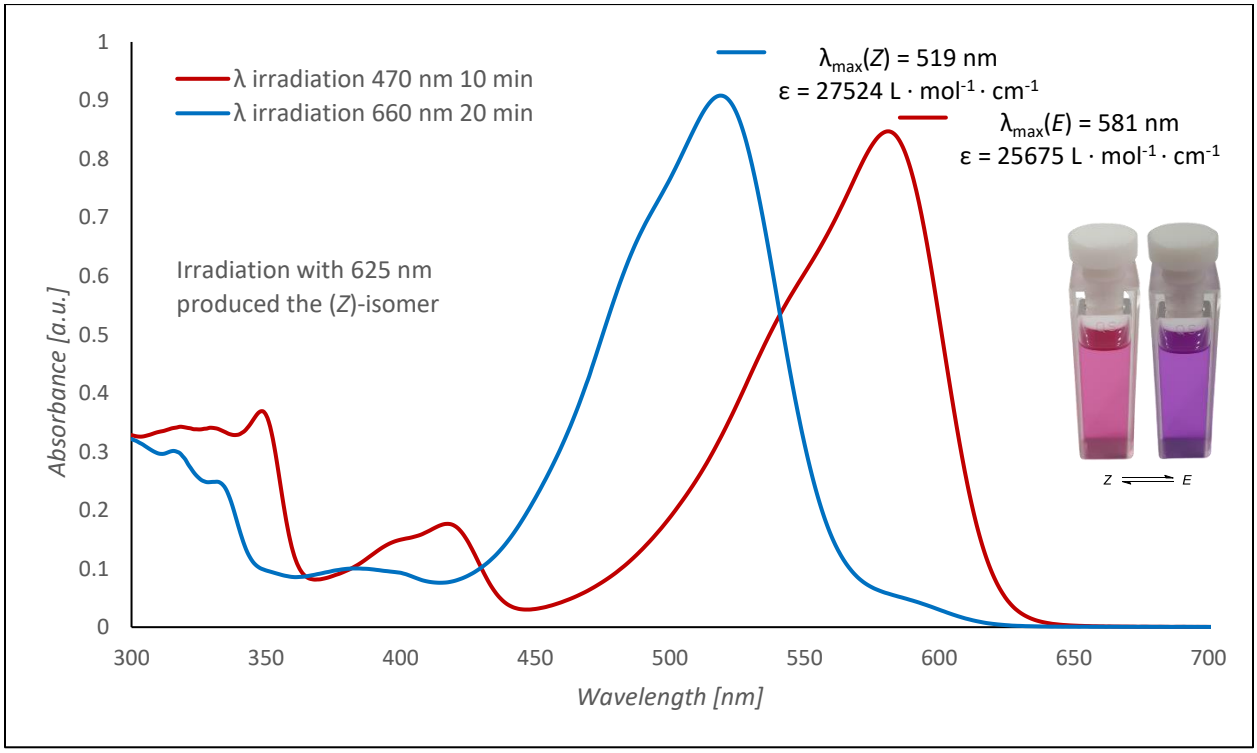

Bipyrrole HTI (**10**) (33 µM in PhMe)

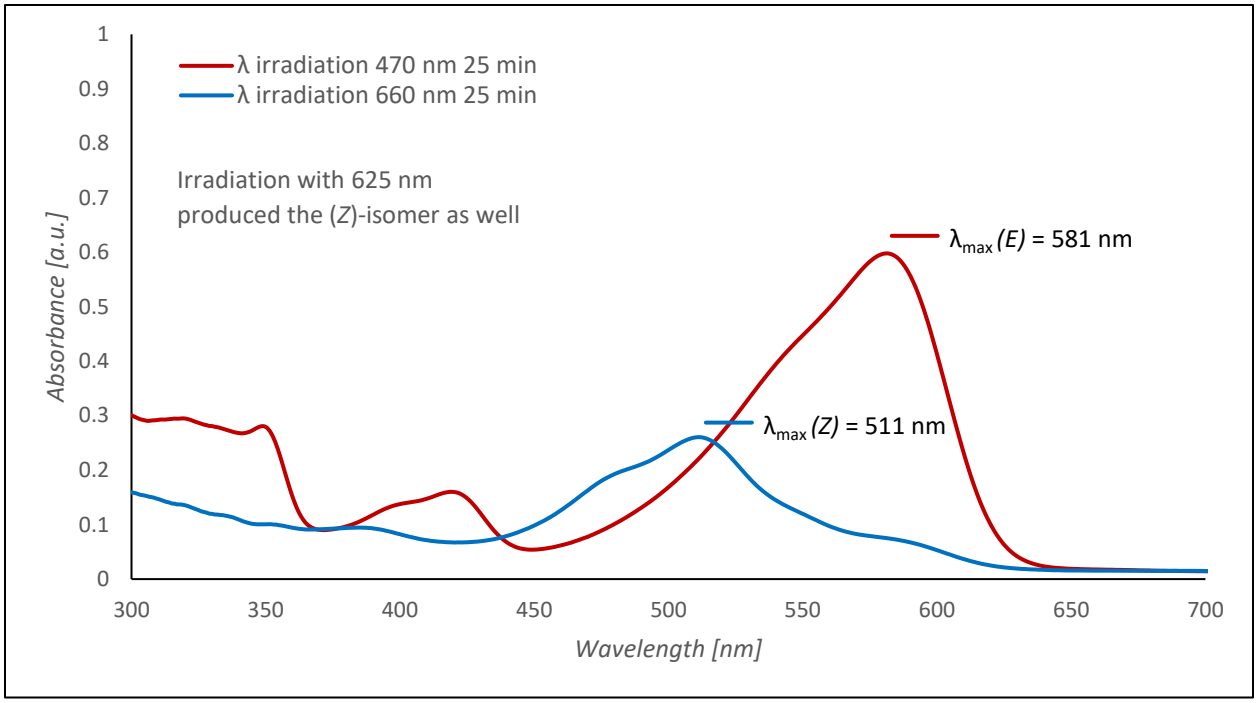

Bipyrrole HTI (**10**) (33 µM in DMSO)

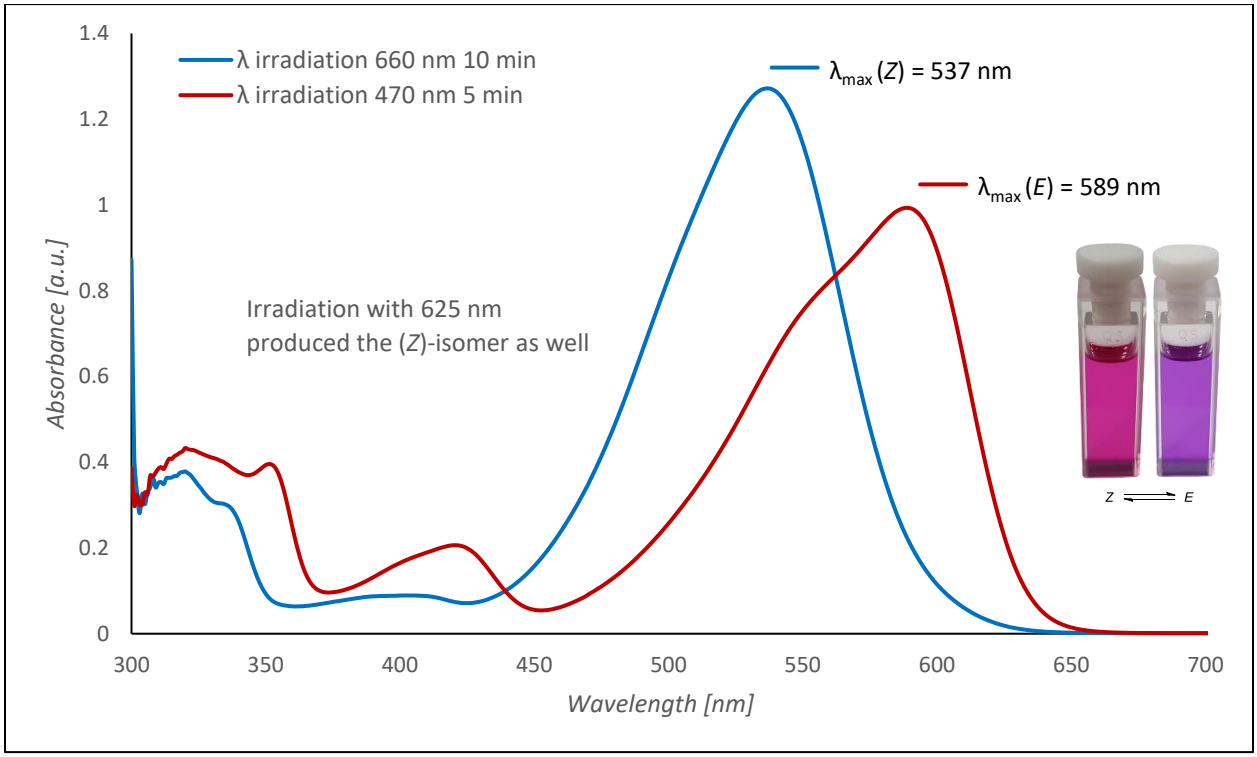

Bipyrrole HTI (**10**) (33 μM in acetone)

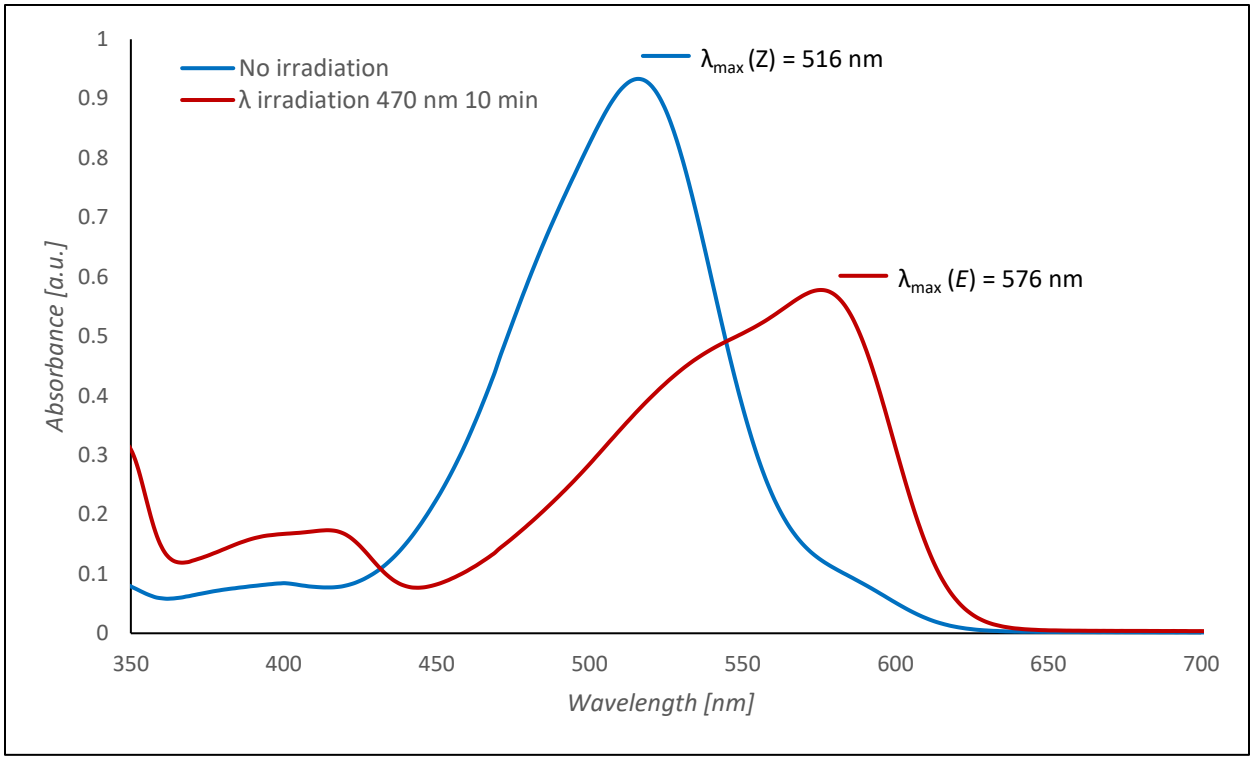

UV-Vis thermal relaxation spectroscopy

Bipyrrole HTI (**10**) (33 µM in THF)

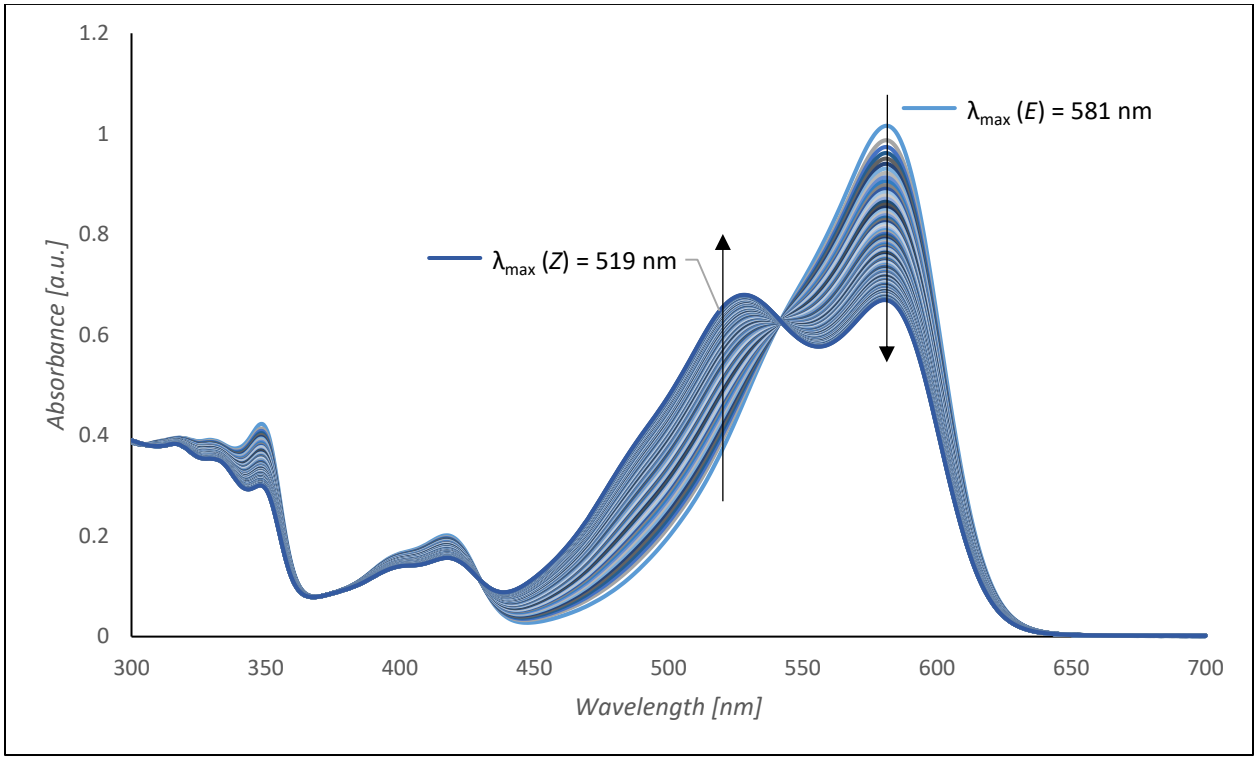

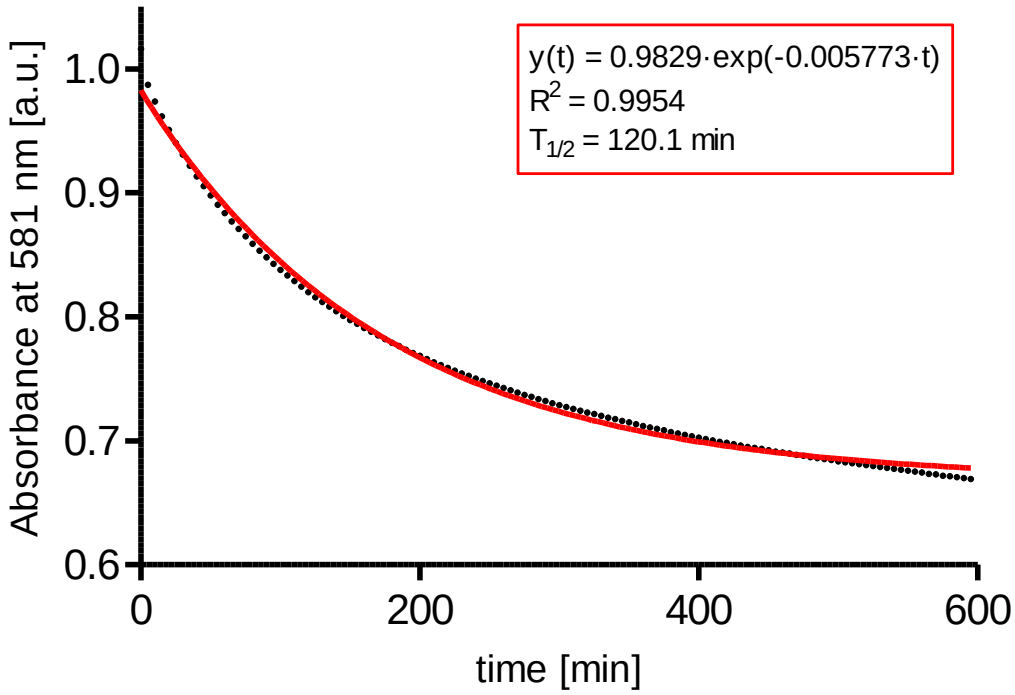

Kinetic analysis of thermal *E*-to-*Z* isomerisation

Bipyrrole HTI (**10**) (33 µM in THF, T = 28 °C, first 30 minutes)

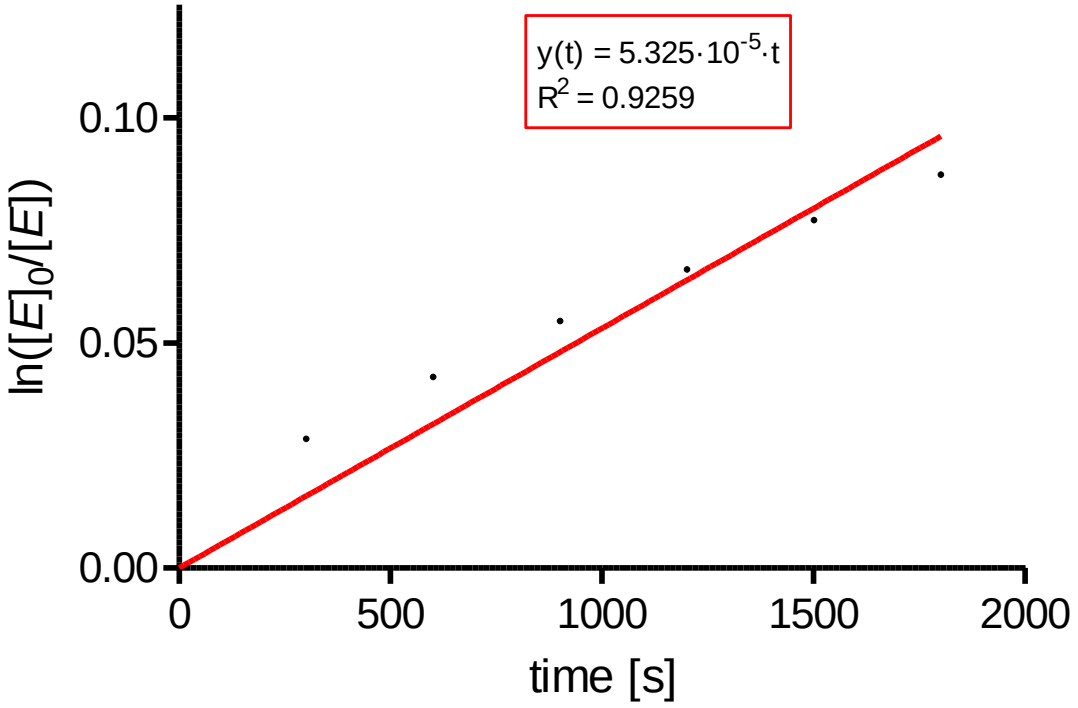

The linear fit gives the first order rate constant $k = 5.33 \cdot 10^{-5}$ s^{-1}. This corresponds to a Gibbs energy of activation of **$\Delta G^{\ddagger}$ = 98.4 kJ·mol^{-1} = 23.5 kcal·mol^{-1}**.

Bipyrrole HTI (**10**) (33 μM in PhMe)

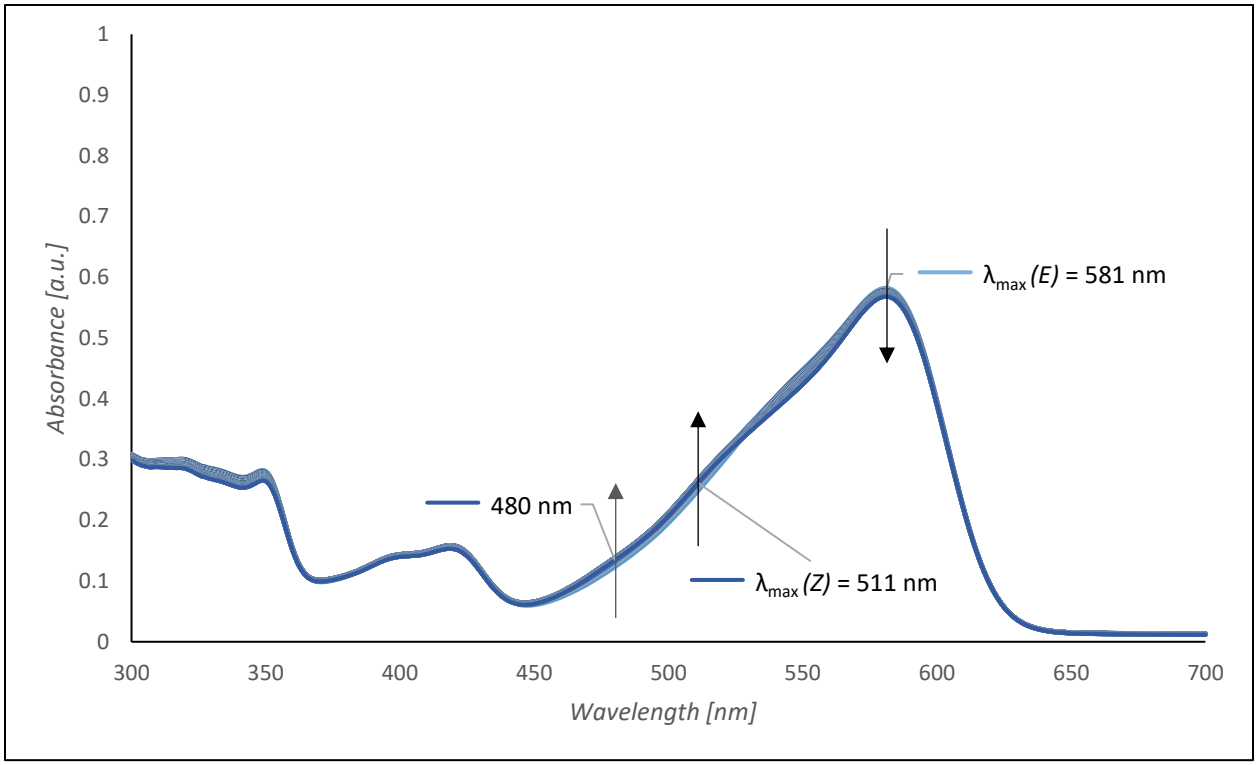

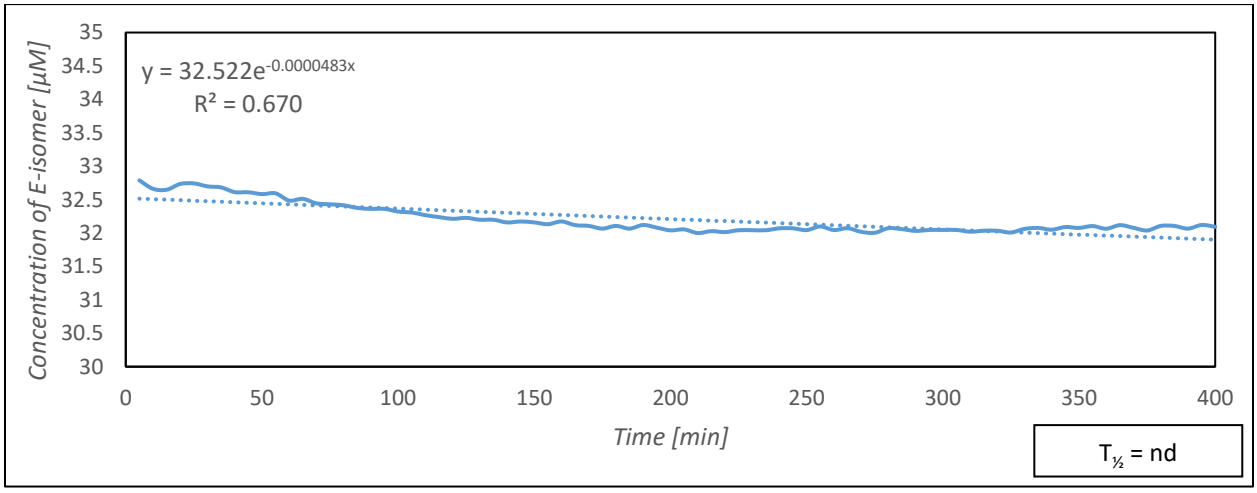

Note: Concentrations of isomers were calculated using 480 nm as representative for λ_{max} (*Z*) = 511 nm and λ_{max} (*E*) = 581 nm. An apparent lack of isosbestic points could be due to the difference in solubility between the two isomers, with the (E)-isomer being significantly more soluble in toluene.

Bipyrrole HTI (**10**) (33 µM in DMSO, T = 18 °C, measurement every 30 seconds for 30 minutes)

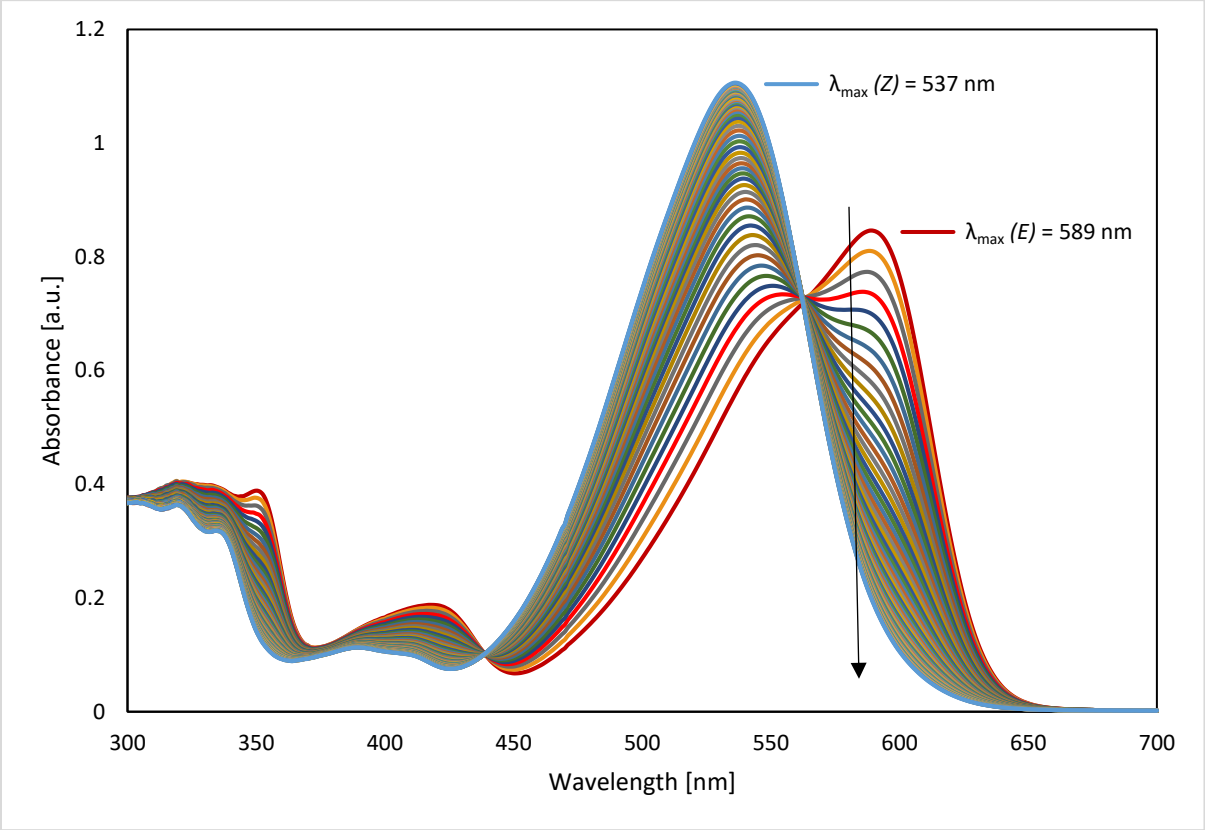

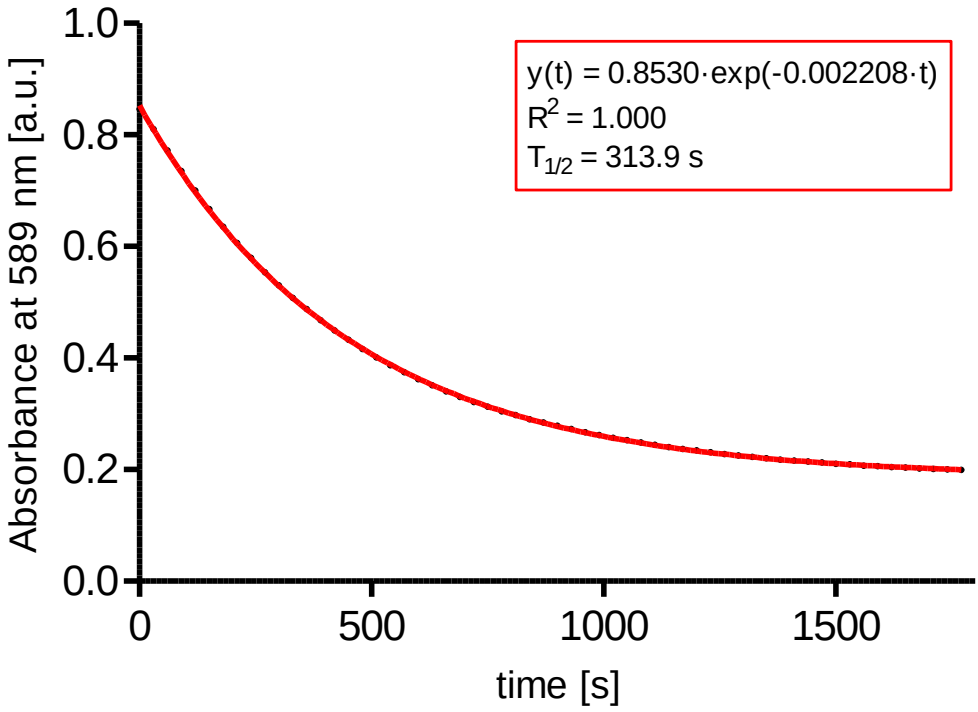

Kinetic analysis of thermal *E*-to-*Z* isomerisation

Bipyrrole HTI (**10**) (33 µM in DMSO, T = 18 °C, first 480 seconds)

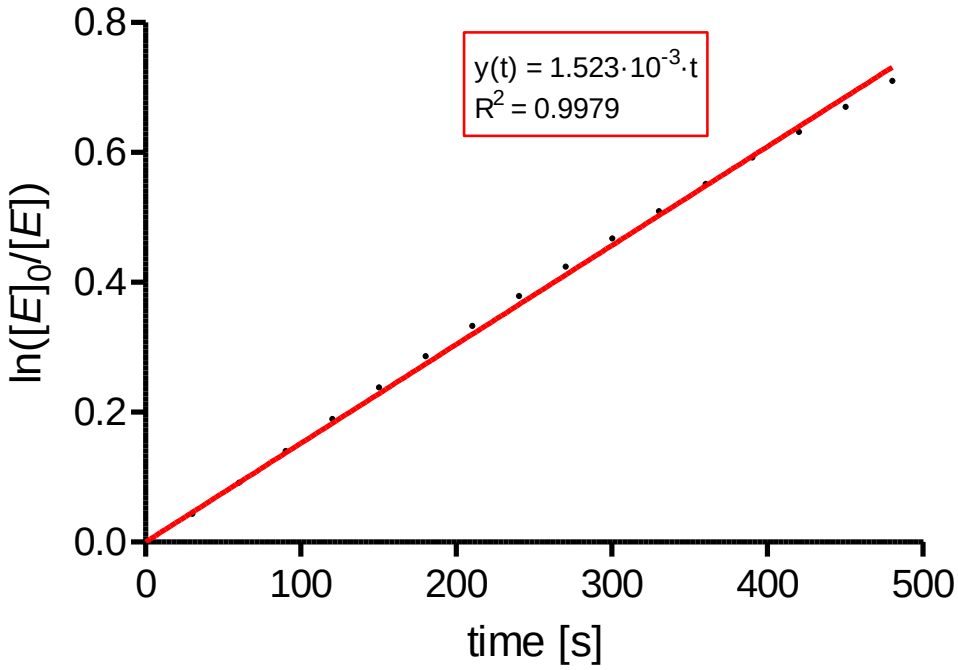

The linear fit gives the first order rate constant $k = 1.52 \cdot 10^{-3}$ s^{-1}. This corresponds to a Gibbs energy of activation of $\underline{\boldsymbol{\Delta G^{\ddagger} = 87.0\ kJ \cdot mol^{-1} = 20.8\ kcal \cdot mol^{-1}}}$.

UV-Vis photobleaching spectroscopy

Bipyrrole HTI (**10**) (33 μM in THF)

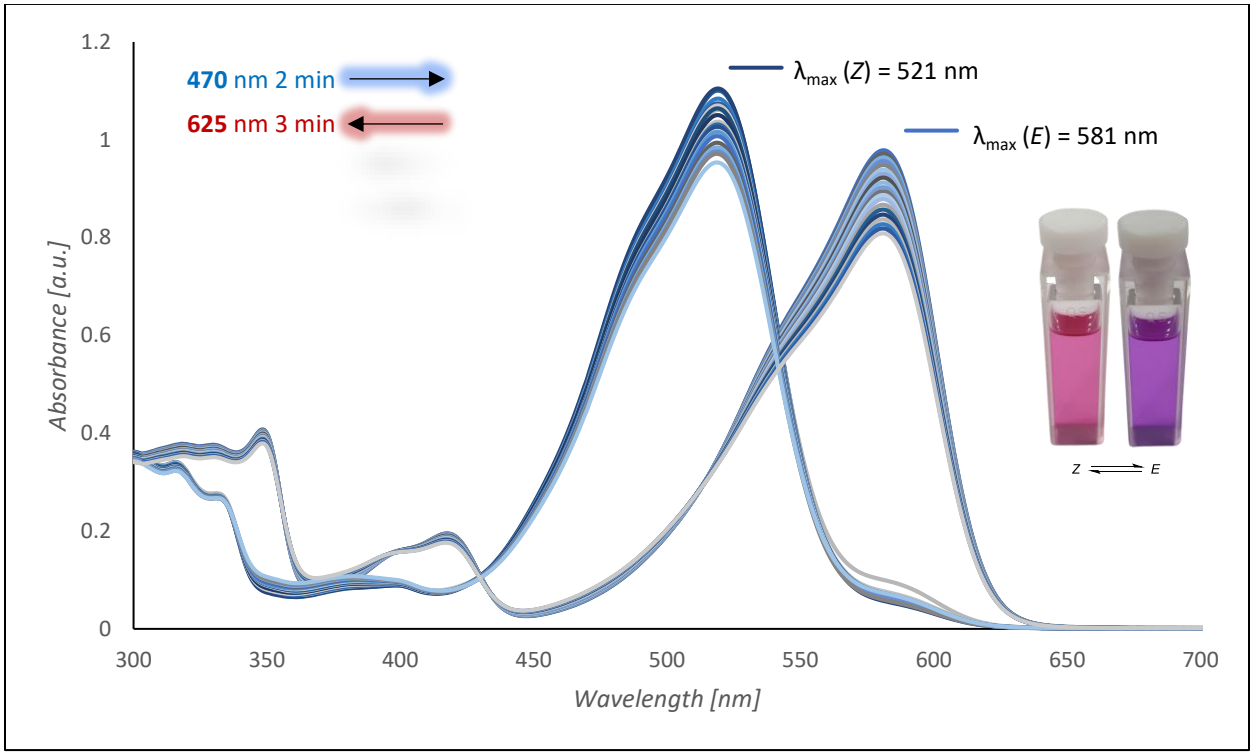

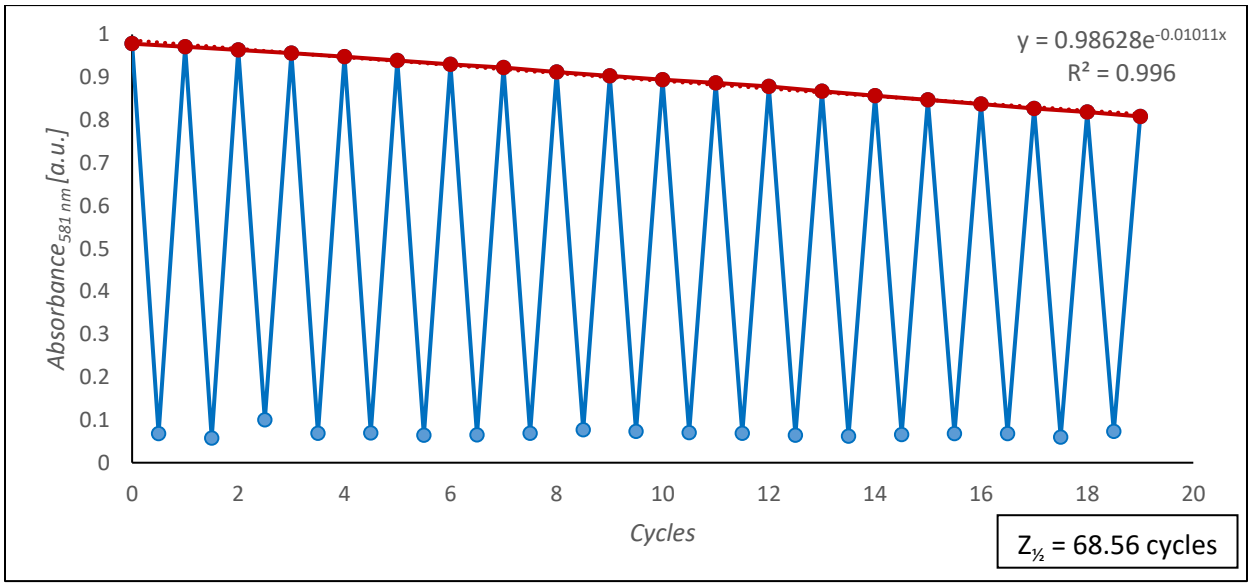

Note: Red marker is after irradiation with 625 nm (1 Amp) for 3 minutes, whereas blue marker is after irradiation with 470 nm (1 Amp) for 2 minutes, reaching the photostationary state in both cases.

6 Appendix

Nuclear magnetic resonance spectroscopy

^{1}H NMR, ^{13}C NMR

(2-Naphthylthio)acetic acid (SI 3)

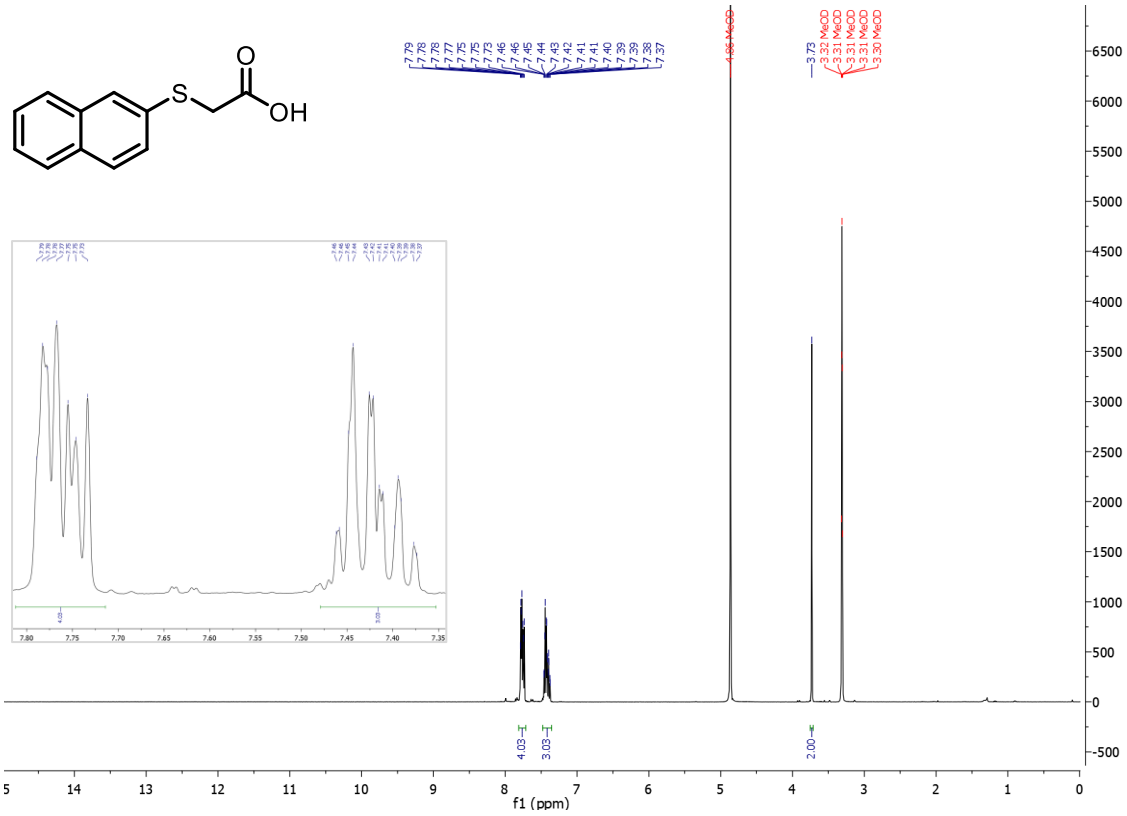

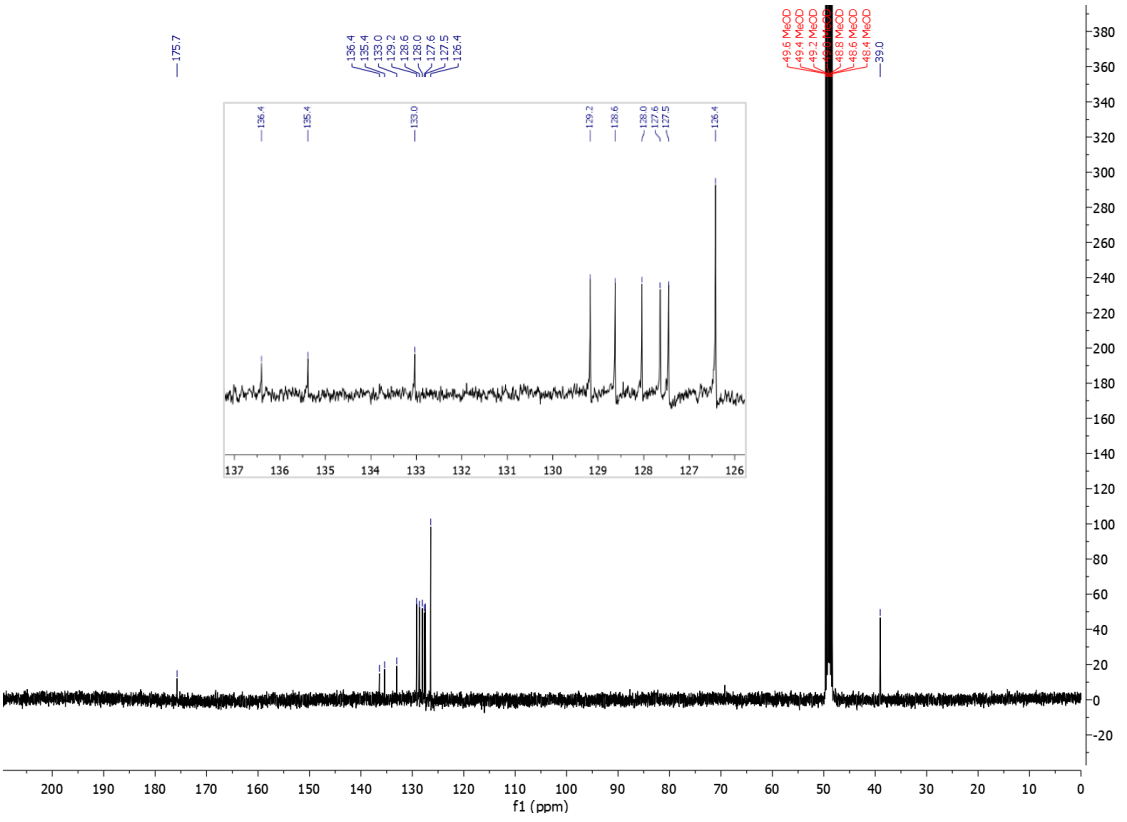

Naphtho[2,1-b]thiophen-1(2H)-one (SI 4)

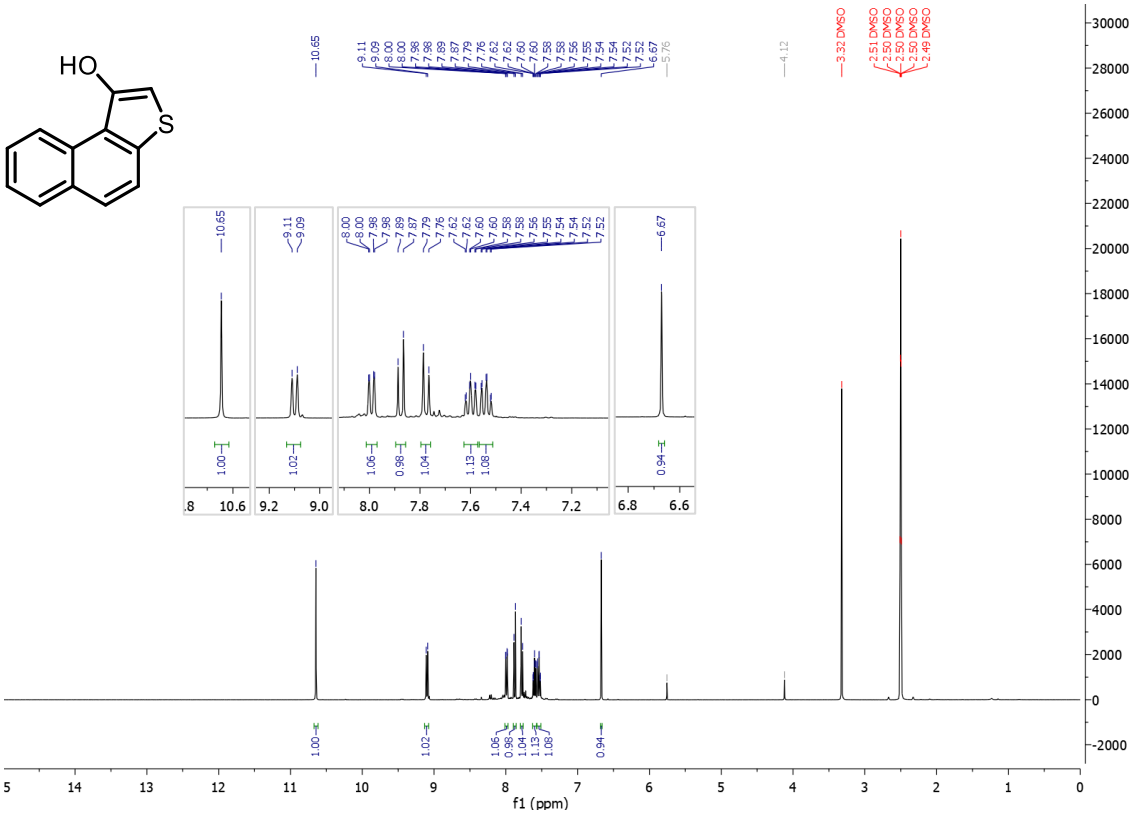

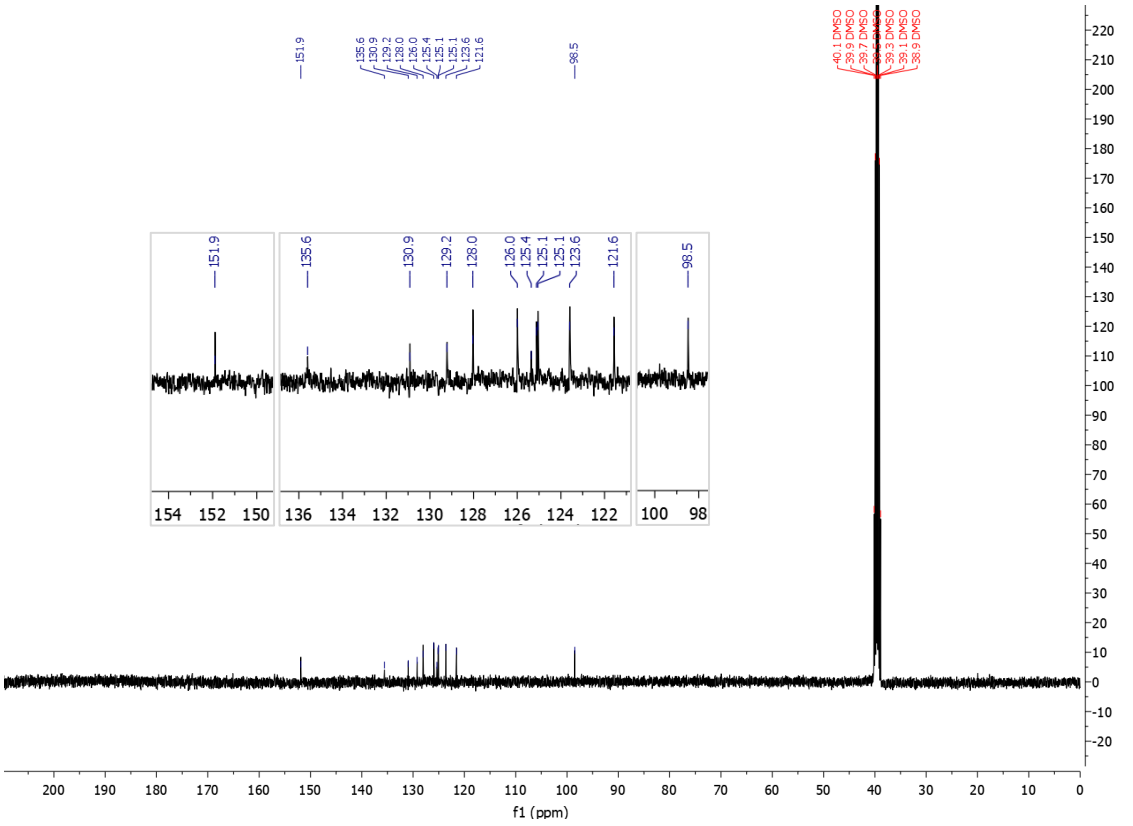

(*Z*)-2-(Naphthalen-1-ylmethylene)benzo[b]thiophen-3(2H)-one (2)

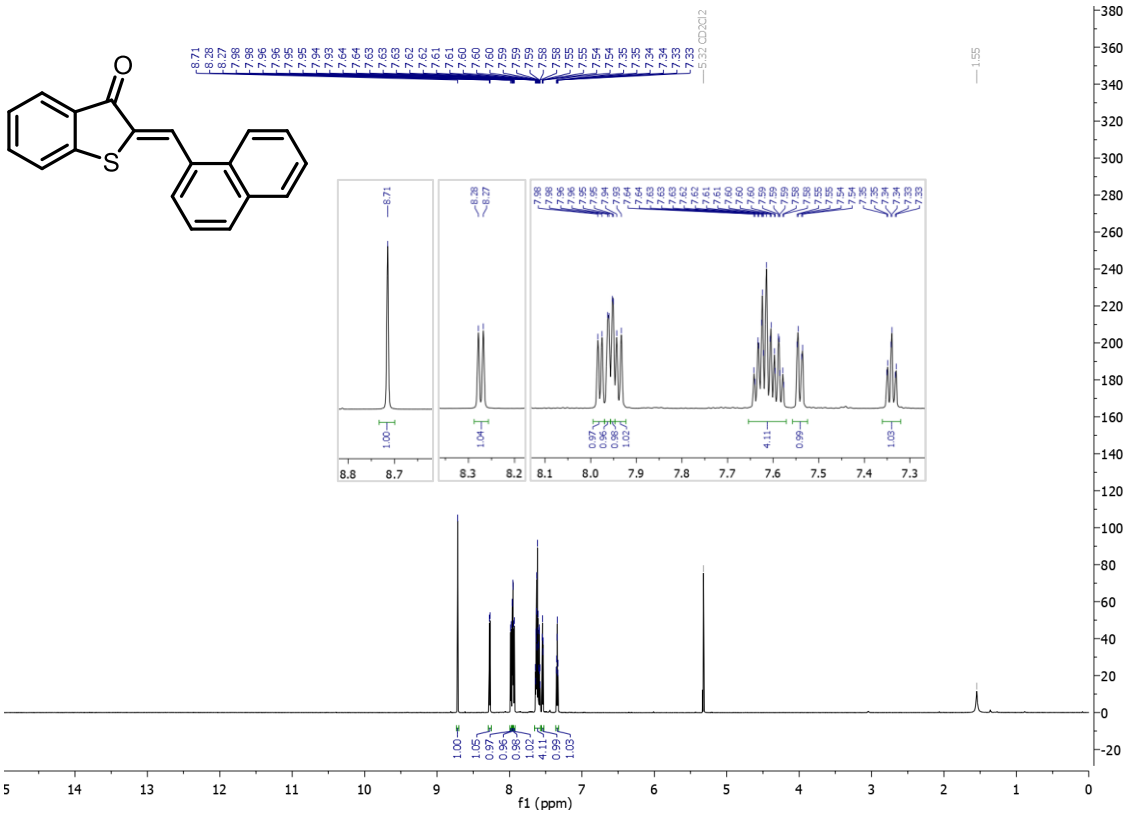

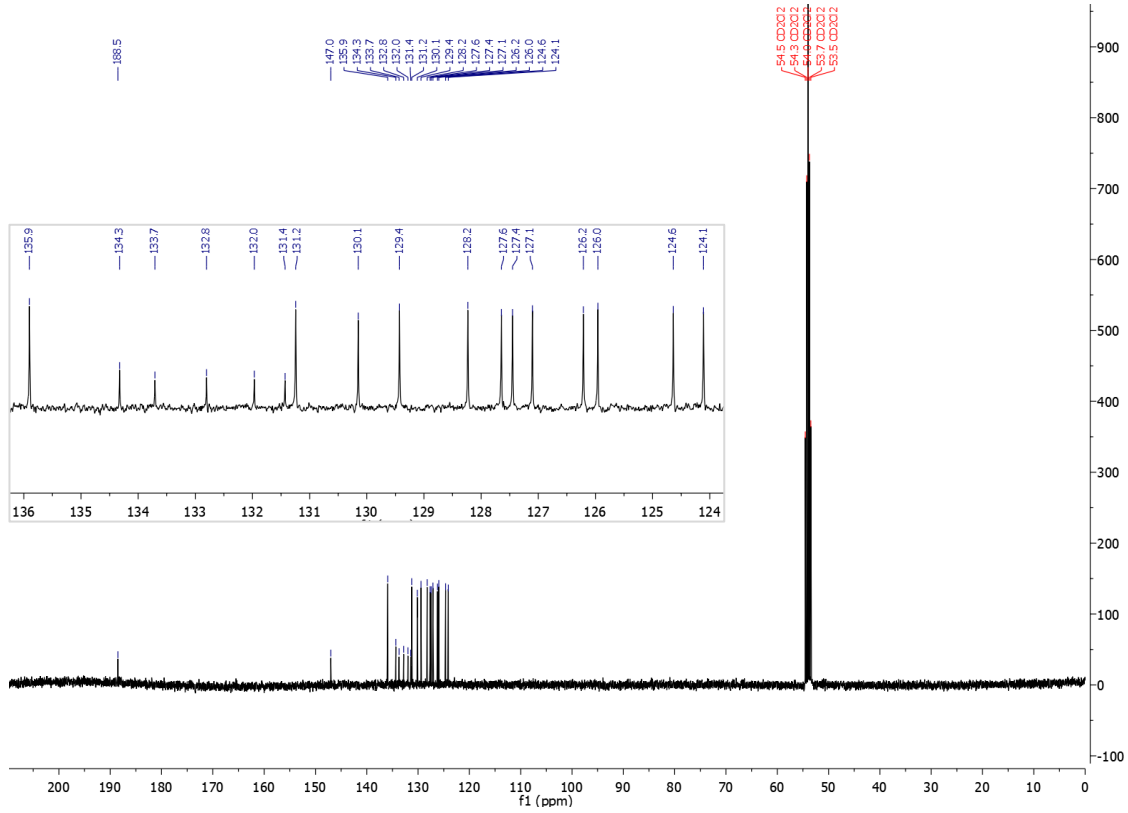

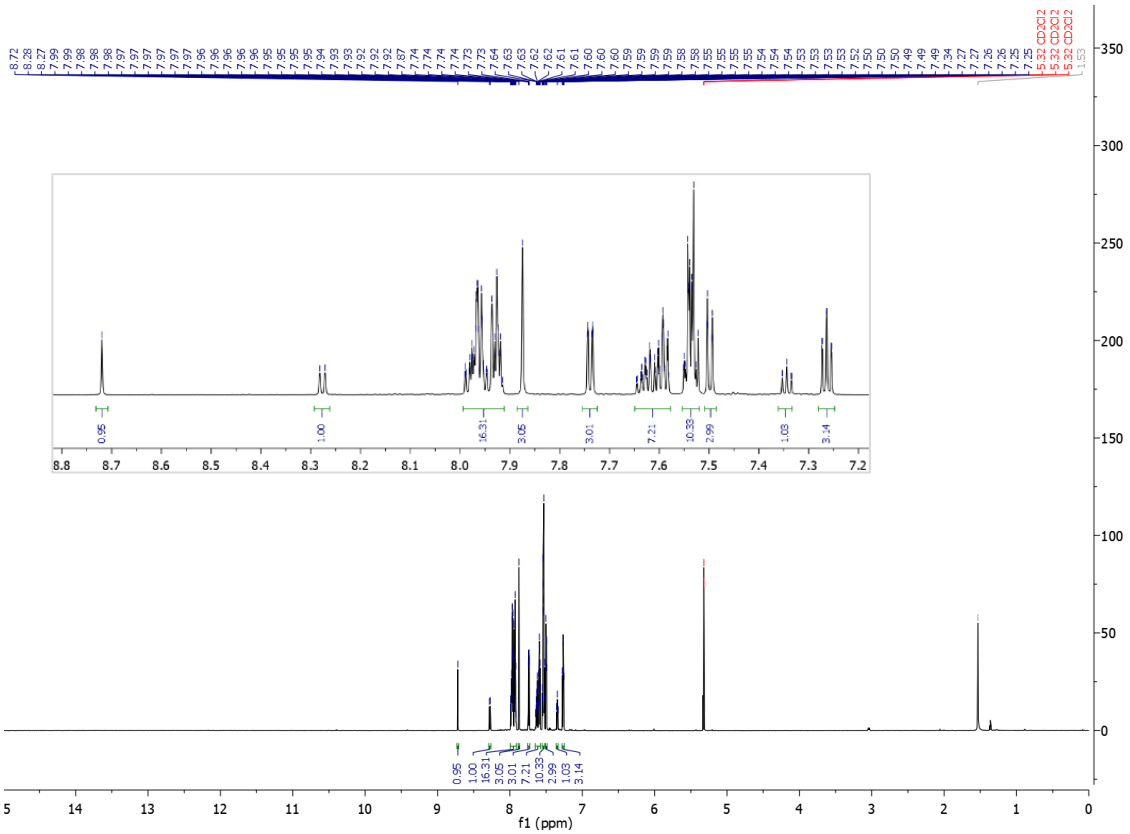

Note: Compound (**2**) in 1:3 (*Z*/*E*)

(*Z*)-2-(Naphthalen-2-ylmethylene)benzo[b]thiophen-3(2H)-one (3)

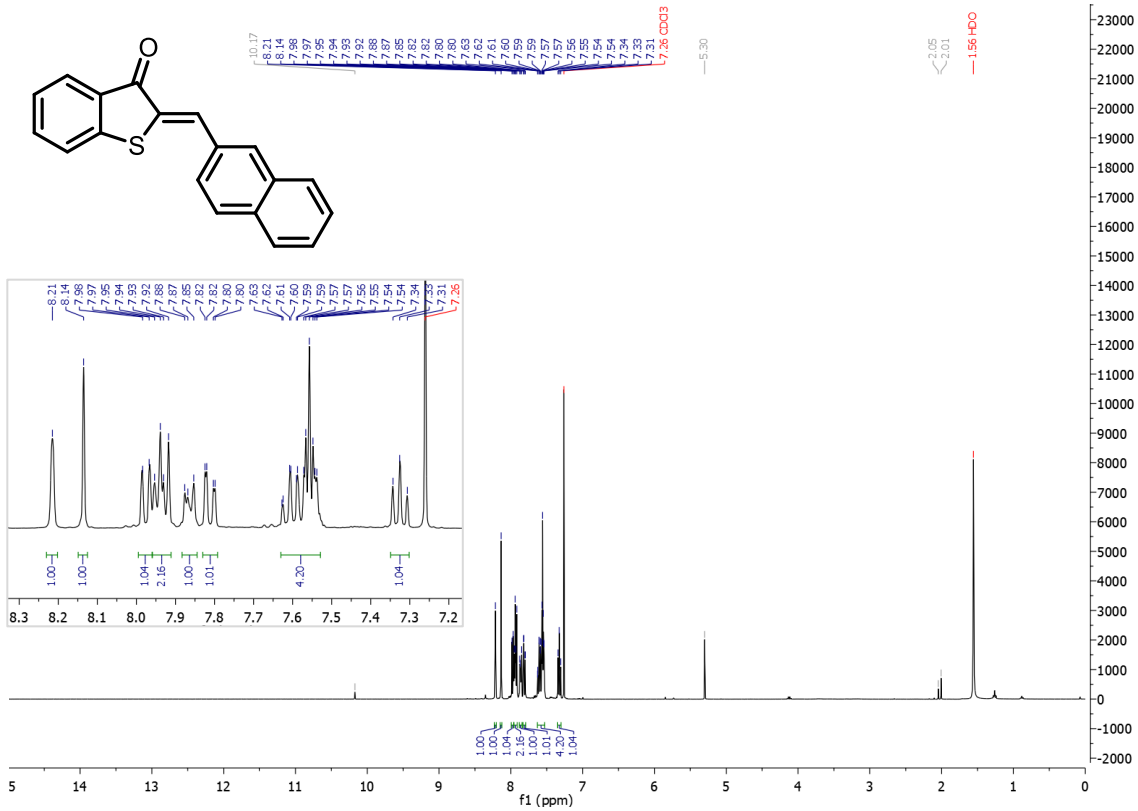

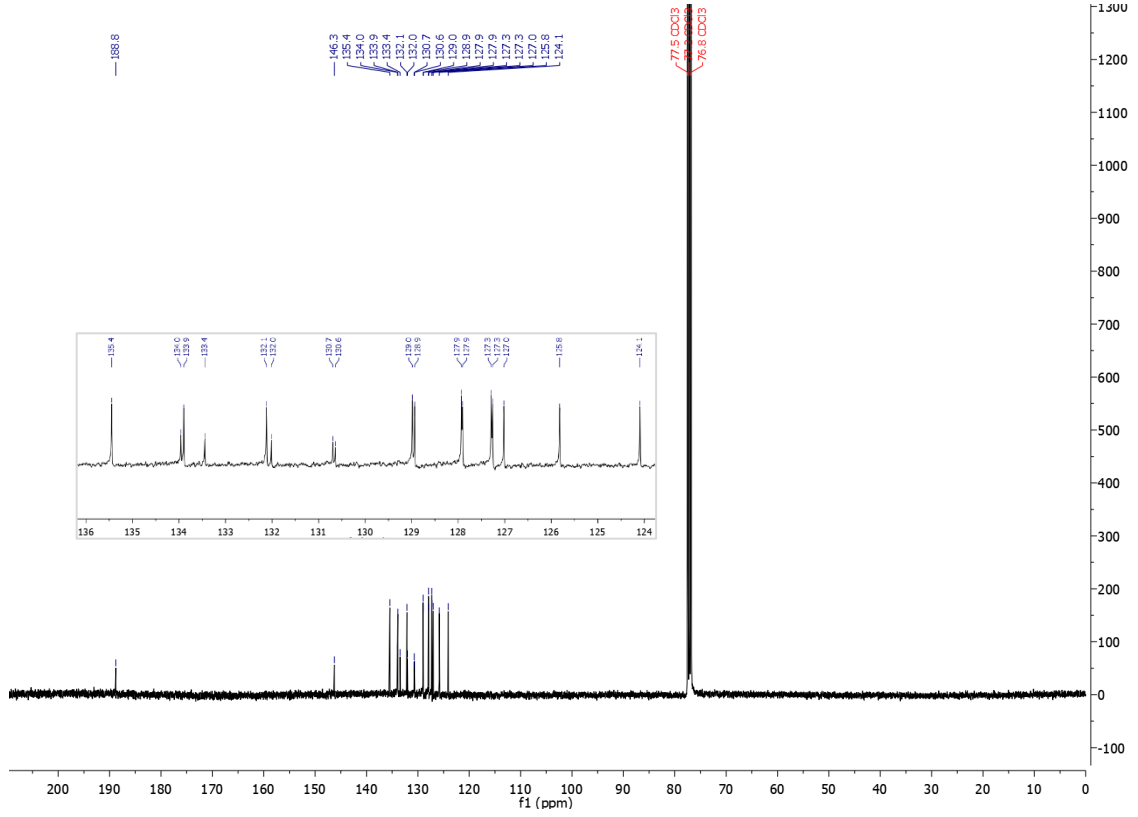

(*Z*)-2-benzylidenenaphtho[2,1-b]thiophen-1(2H)-one (4)

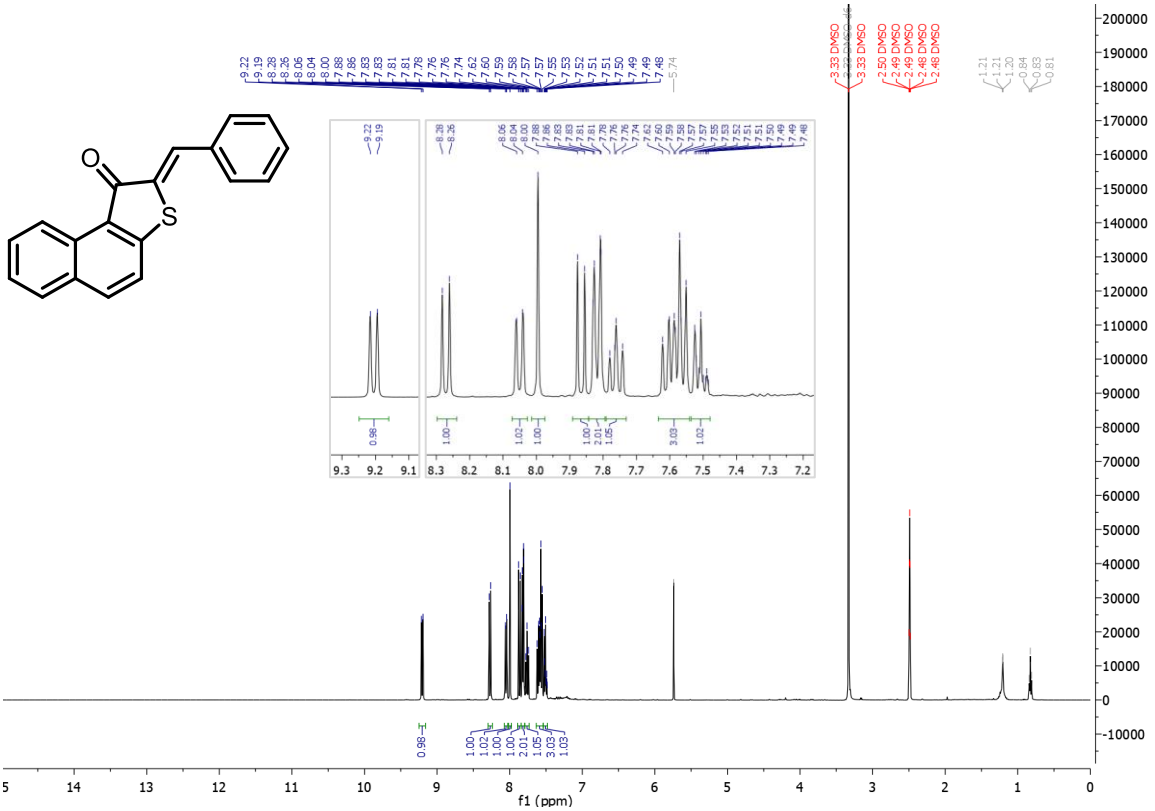

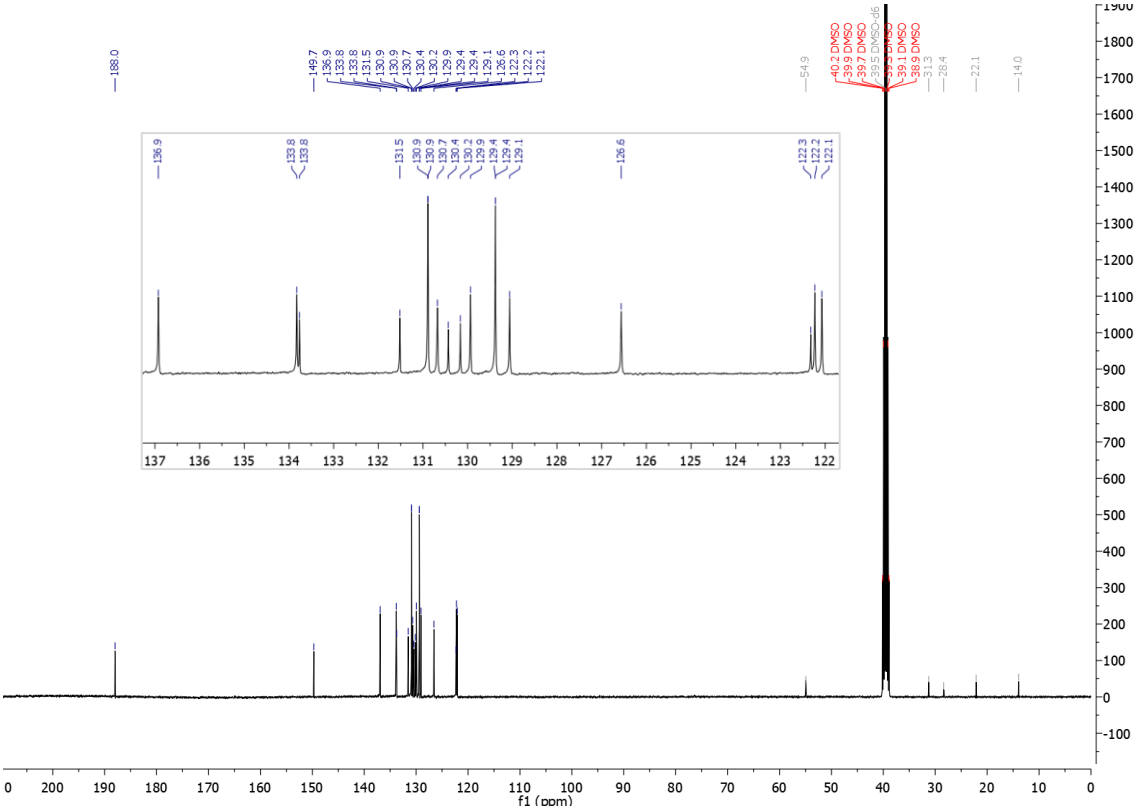

(*Z*)-2-(naphthalen-2-ylmethylene)naphtho[2,1-b]thiophen-1(2H)-one (5)

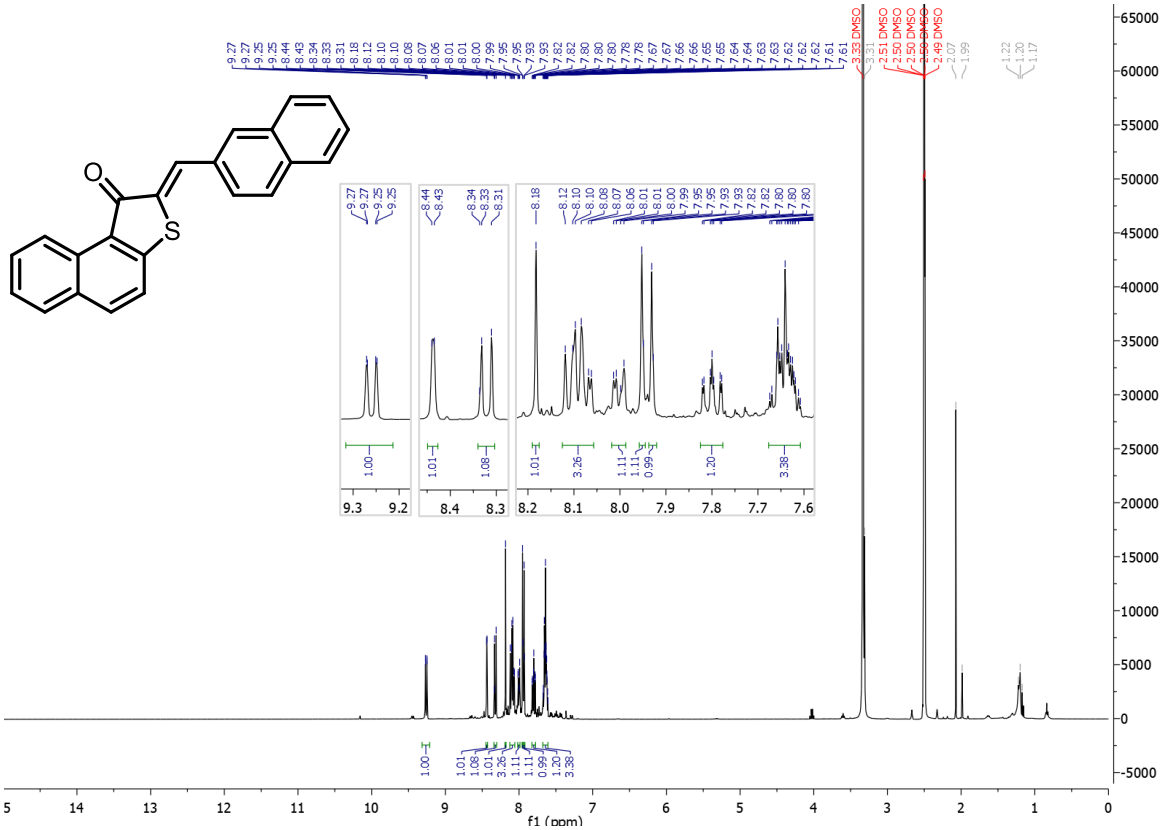

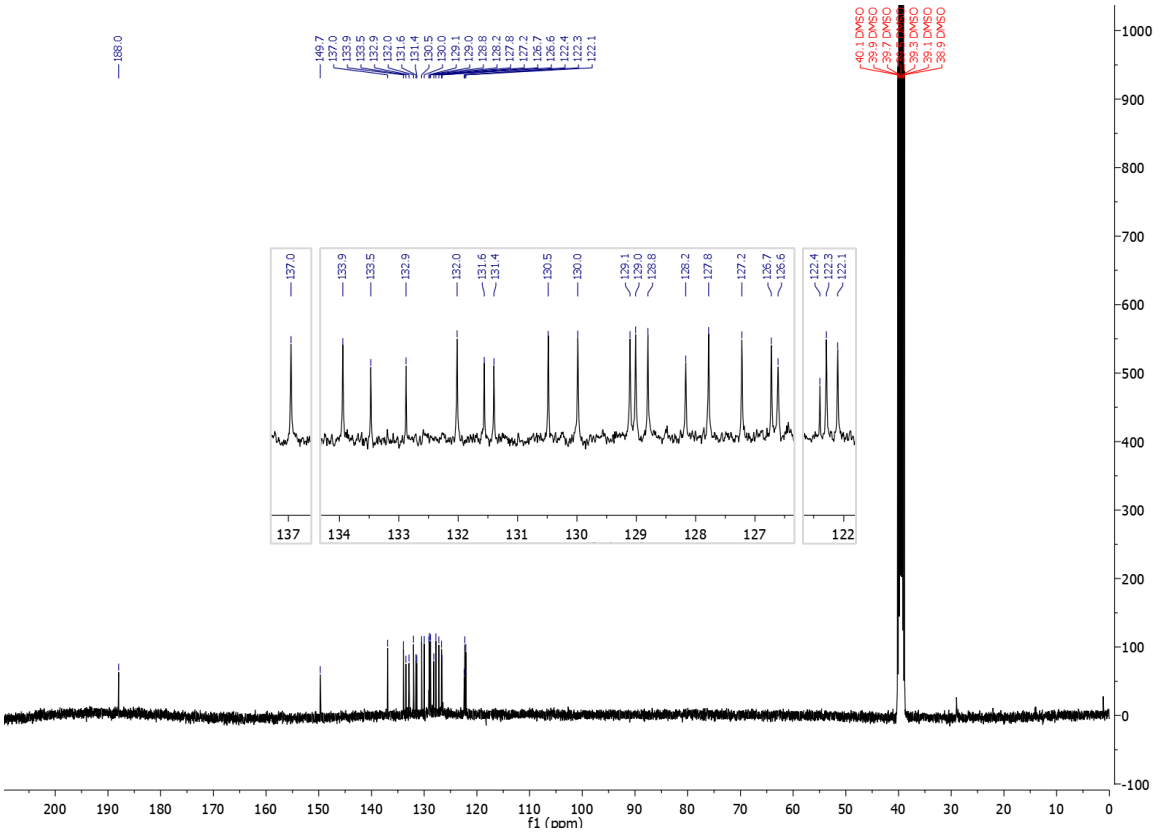

(*Z*)-2-((1H-Pyrrol-2-yl)methylene)benzo[b]thiophen-3(2H)-one (6)

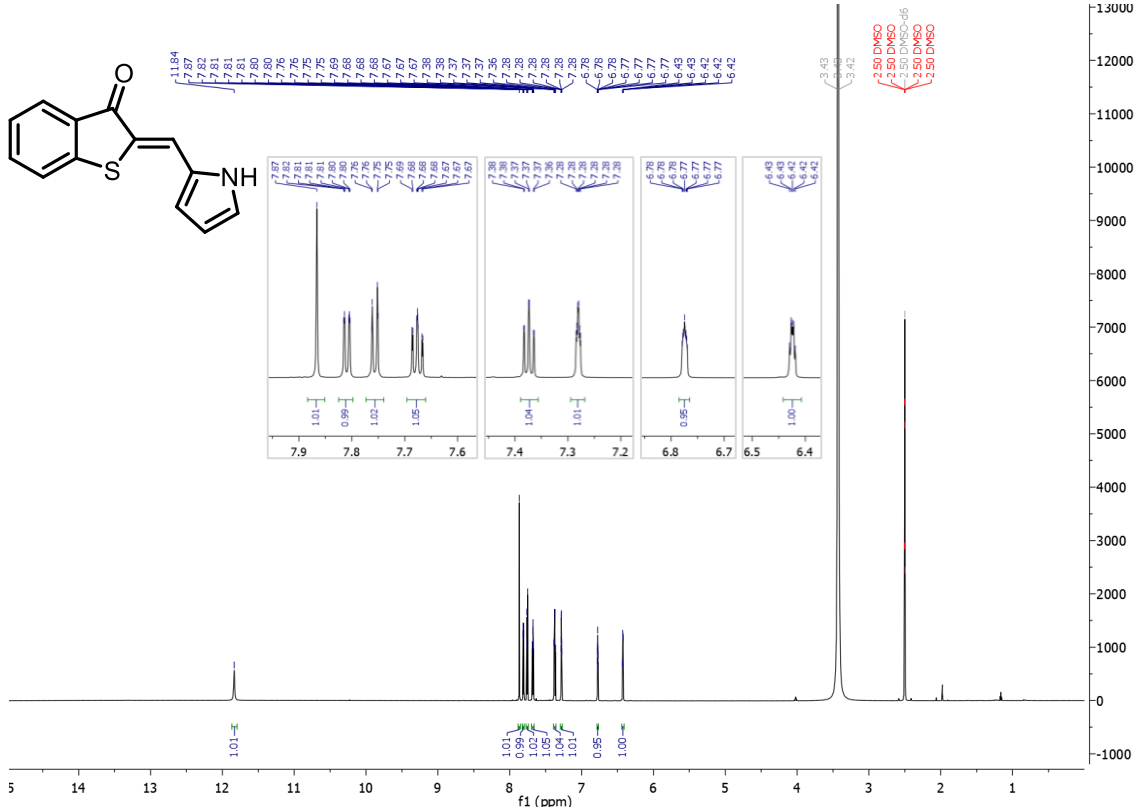

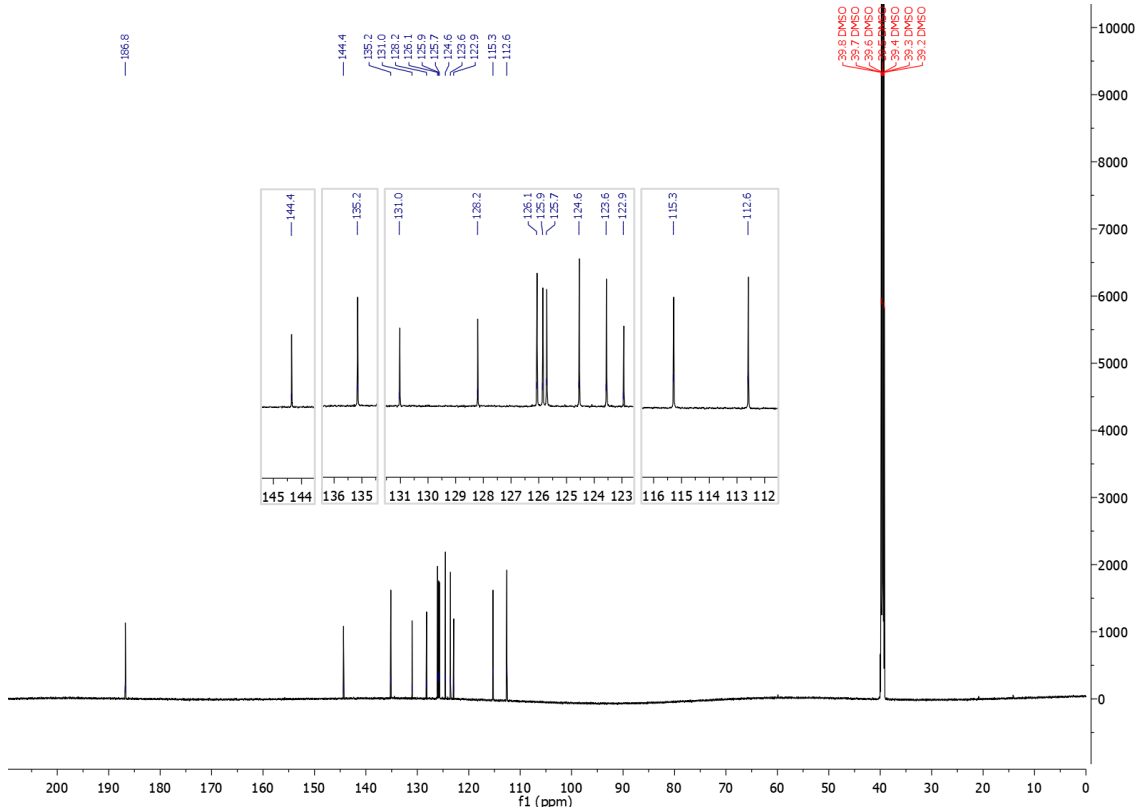

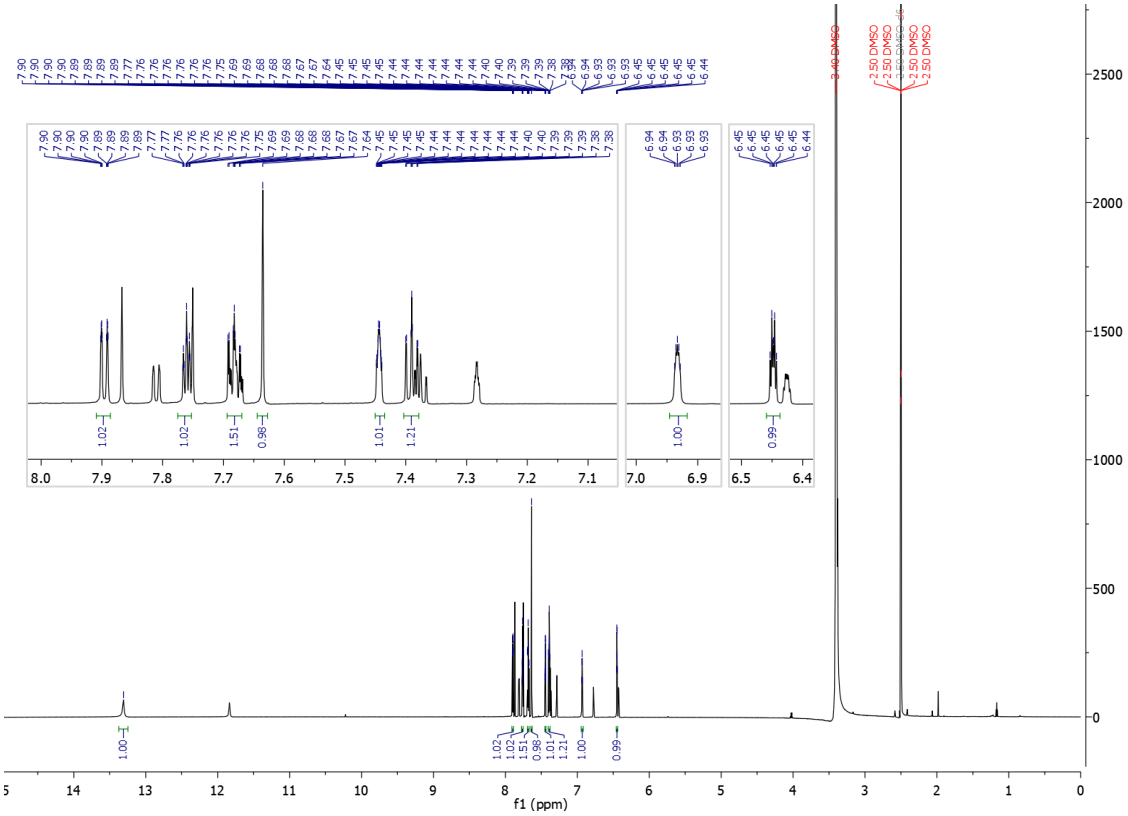

Note: Compound (**6**) in 1:2 (*Z*/*E*)

(*Z*)-2-((1H-Indol-2-yl)methylene)benzo[b]thiophen-3(2H)-one (7)

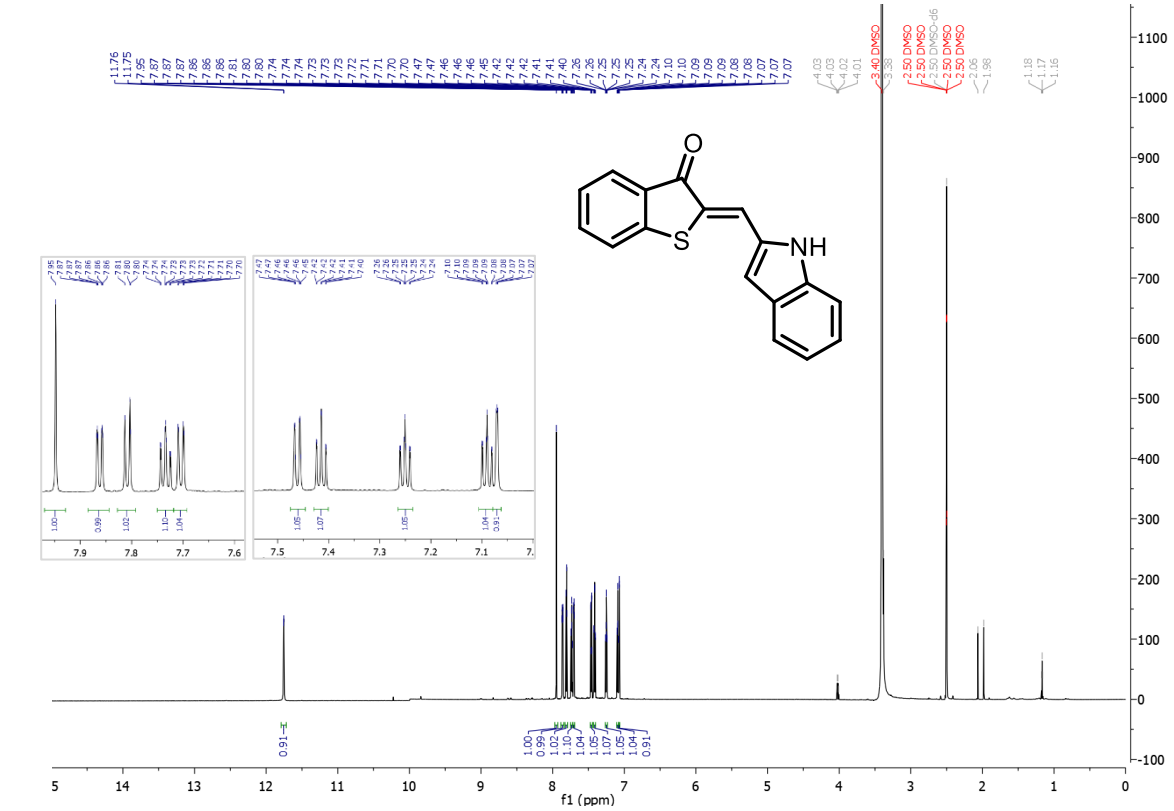

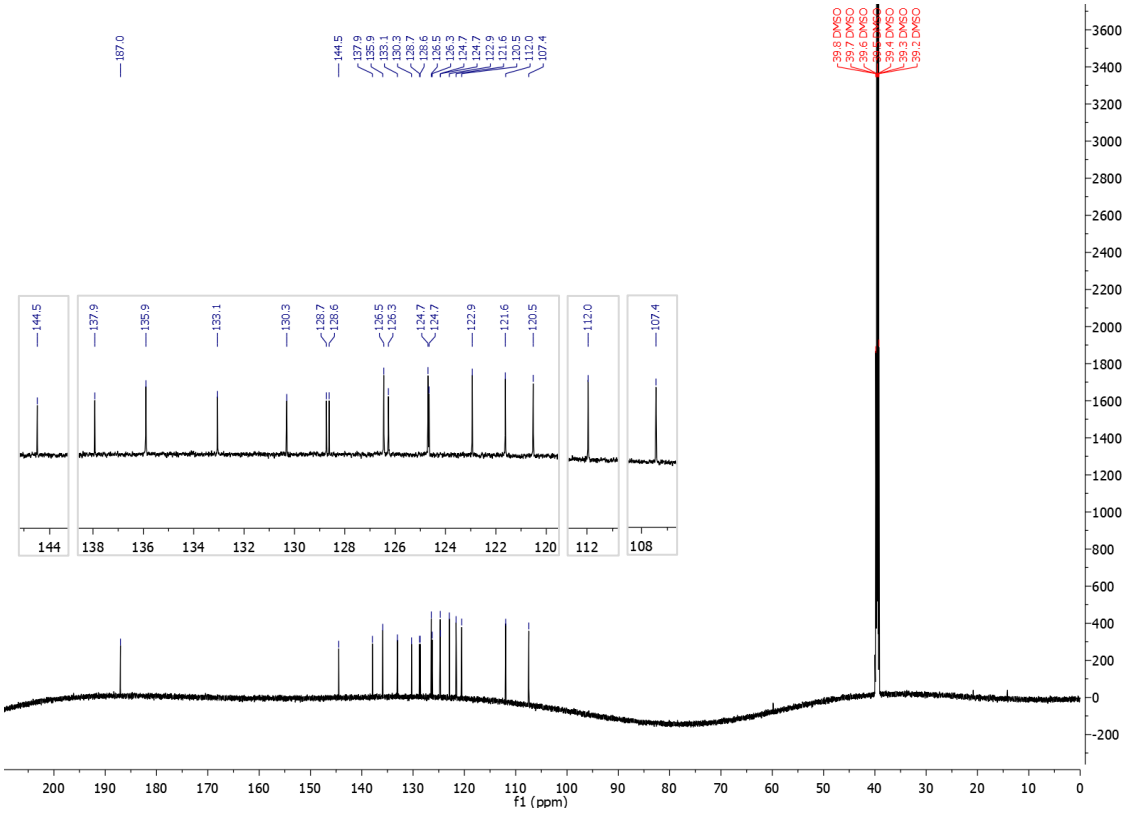

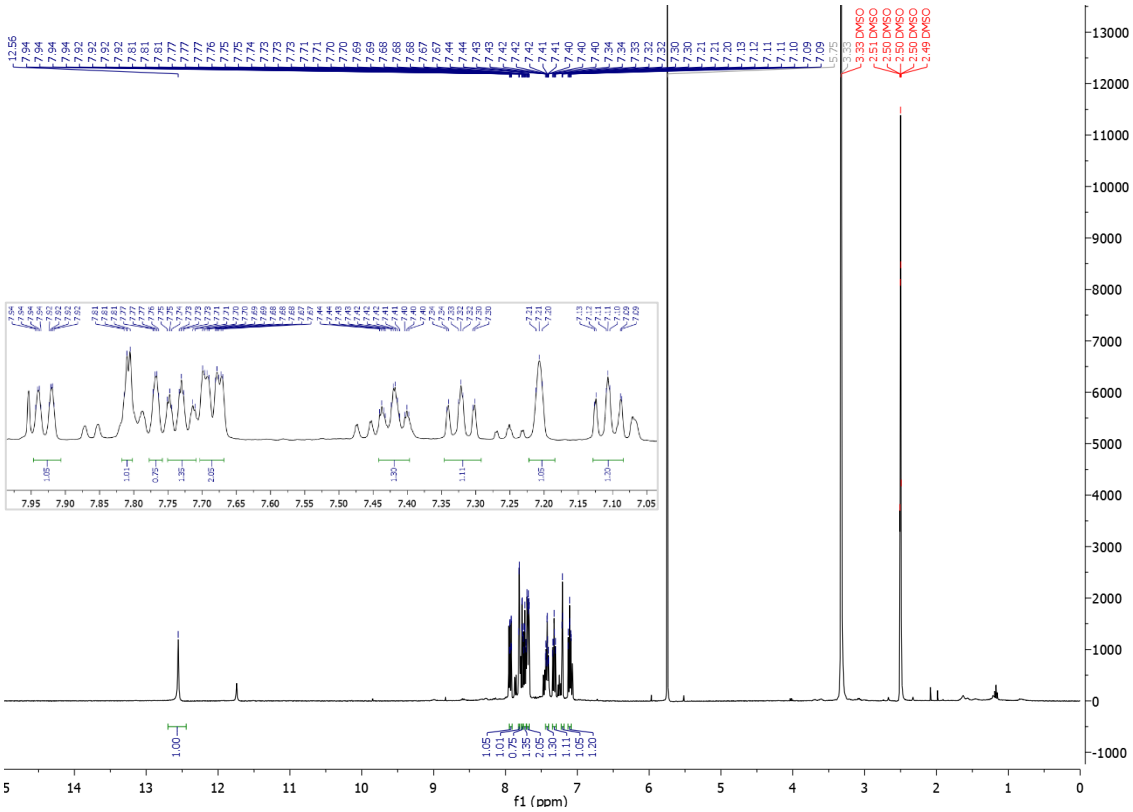

Note: Compound (**7**) in 1:4 (*Z*/*E*)

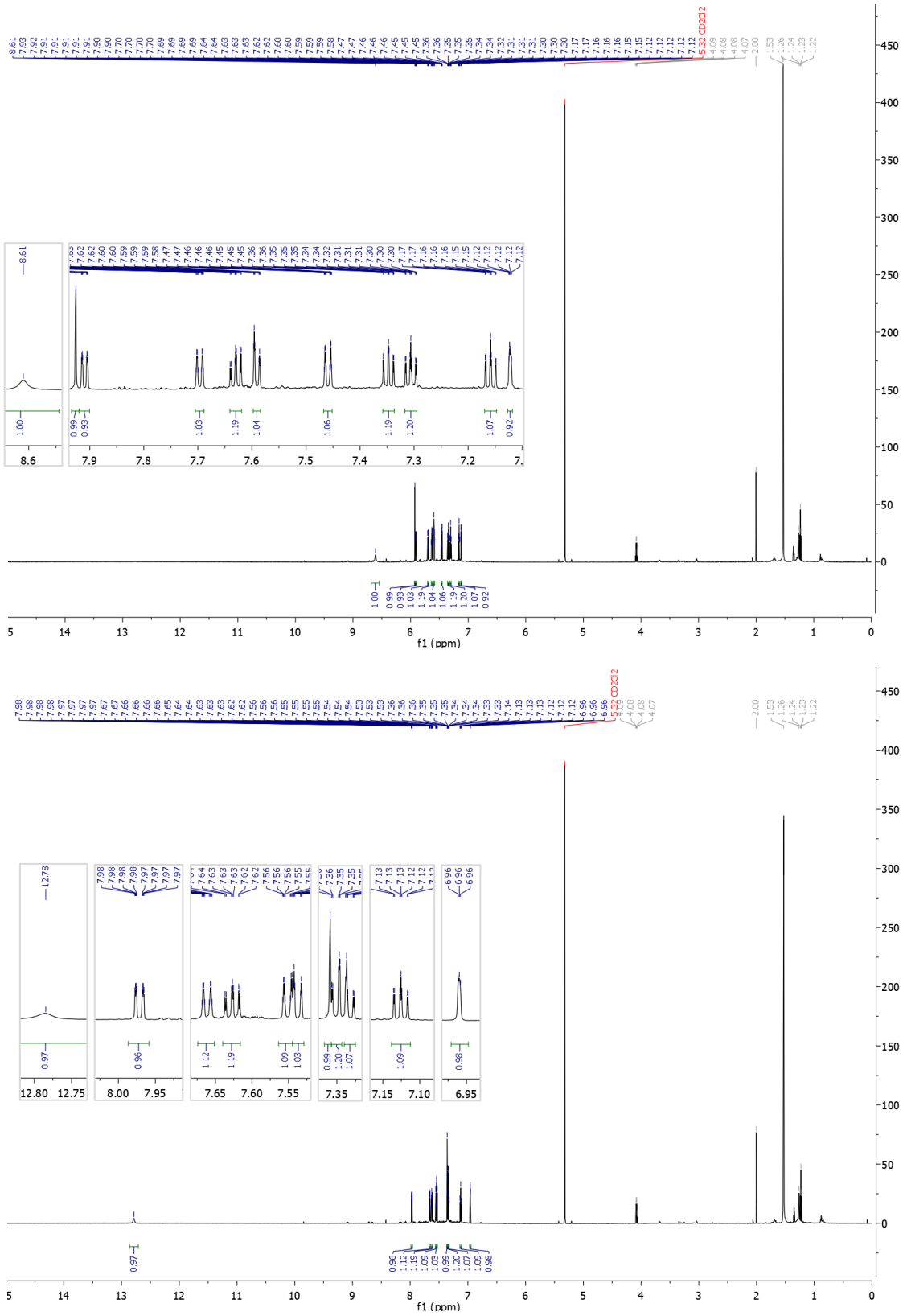

Note: Compound (**7**) in >99 (*E*)-isomer used for ^{1}H NMR thermal relaxation spectroscopy

(*Z*)-2-((1H-pyrrol-2-yl)methylene)naphtho[2,1-b]thiophen-1(2H)-one (8)

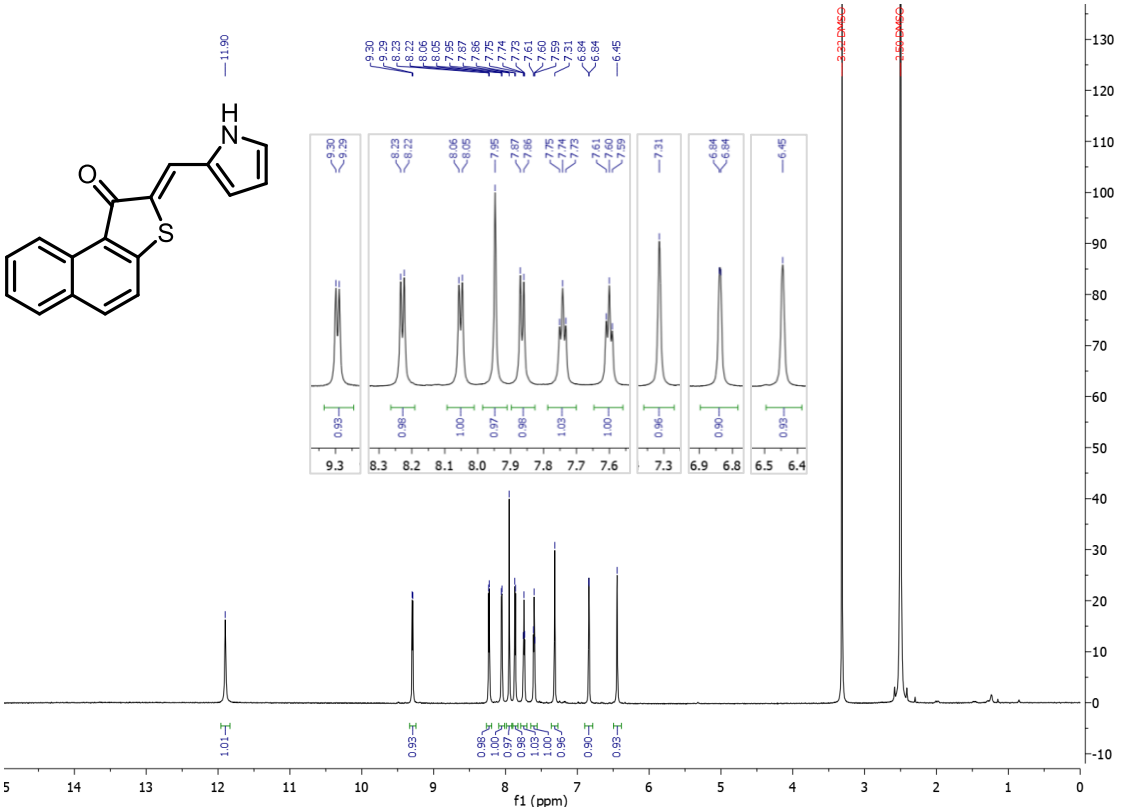

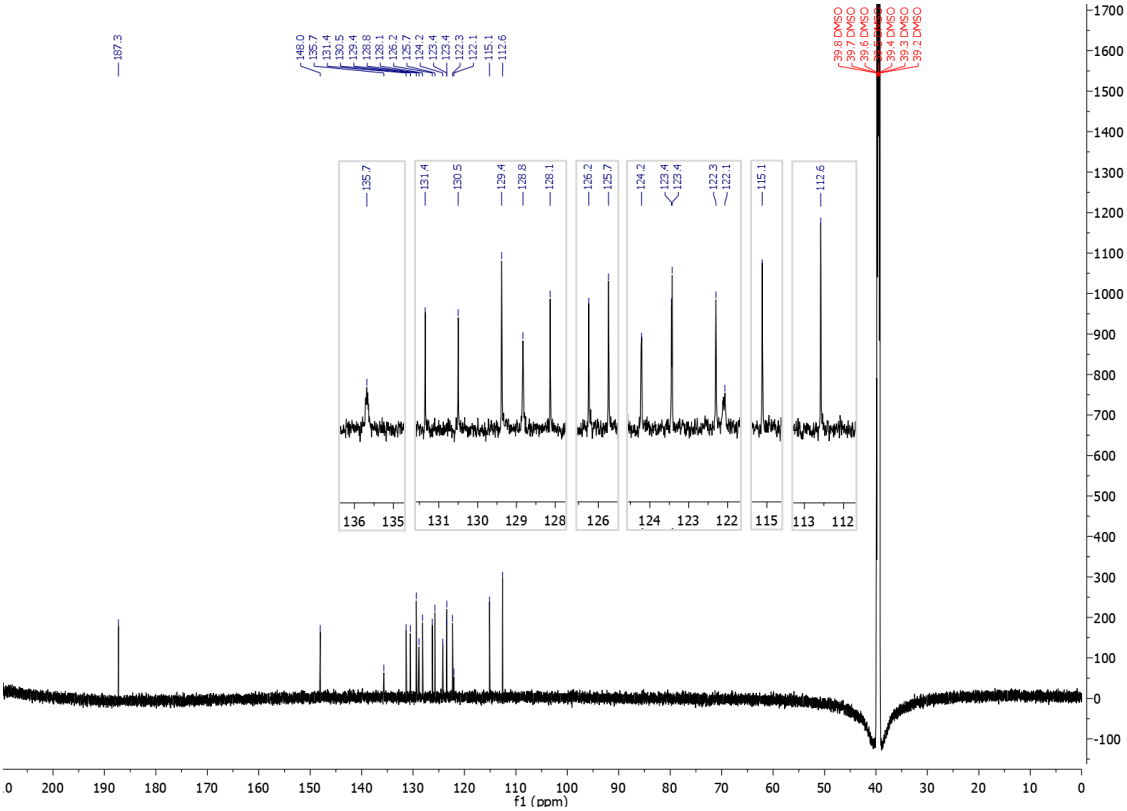

(*Z*)-2-((1H-indol-2-yl)methylene)naphtho[2,1-b]thiophen-1(2H)-one (9)

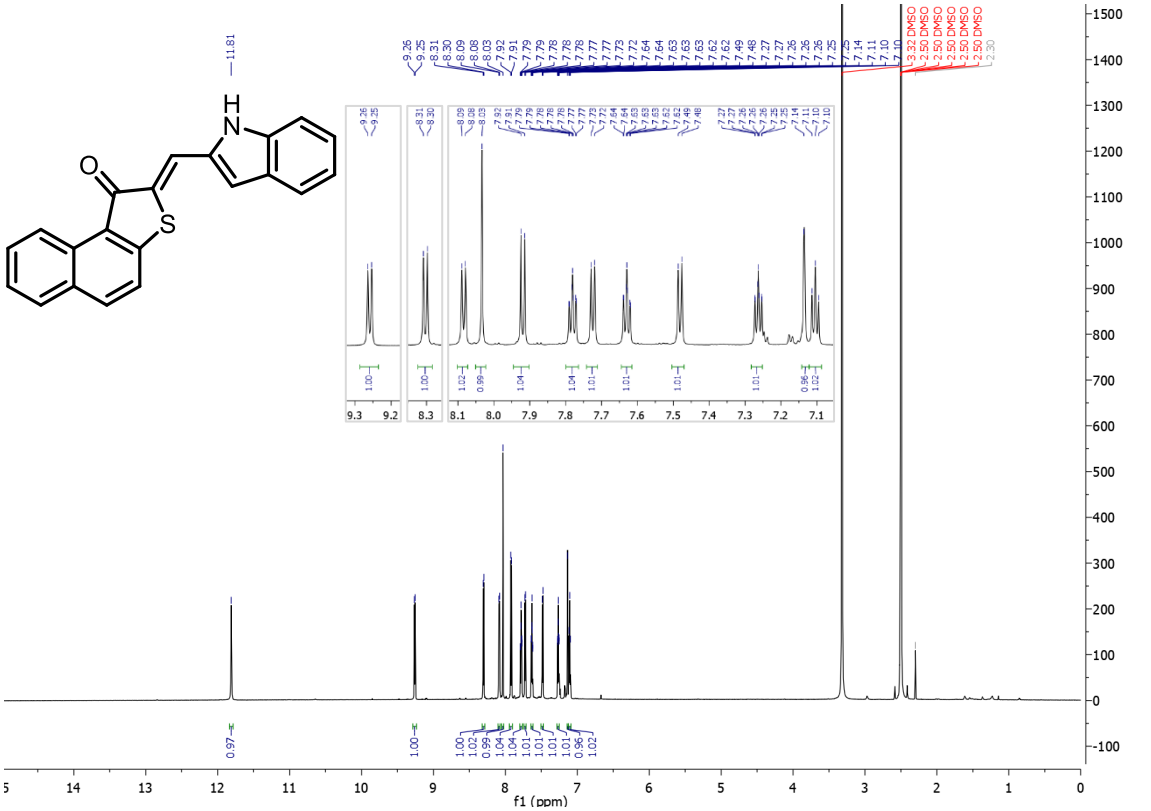

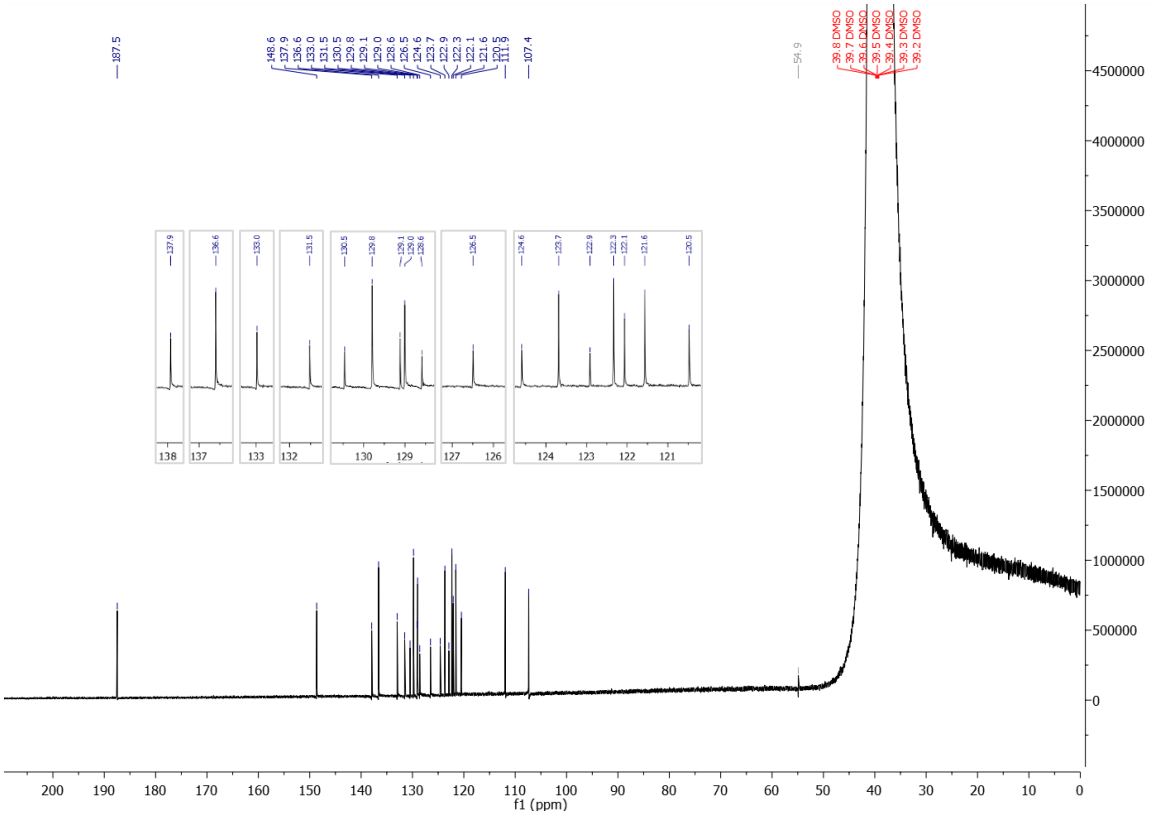

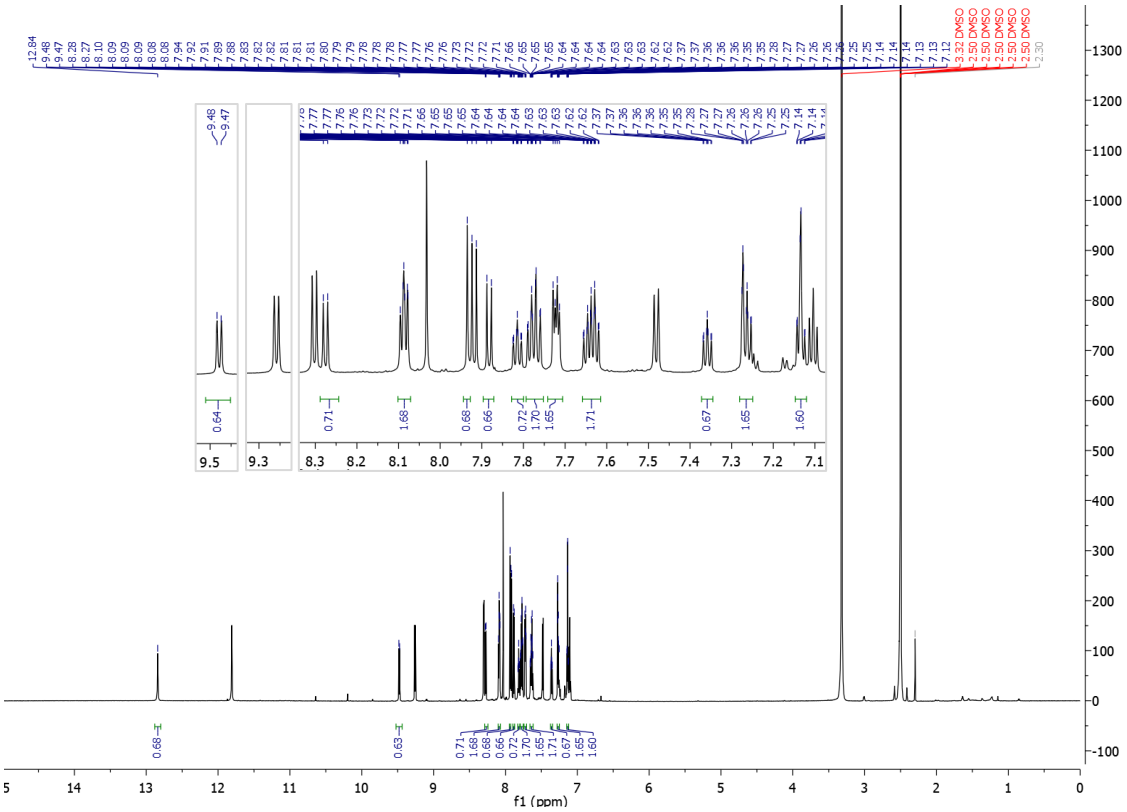

Note: Compound (**9**) in 1.5:1 (*Z*/*E*)

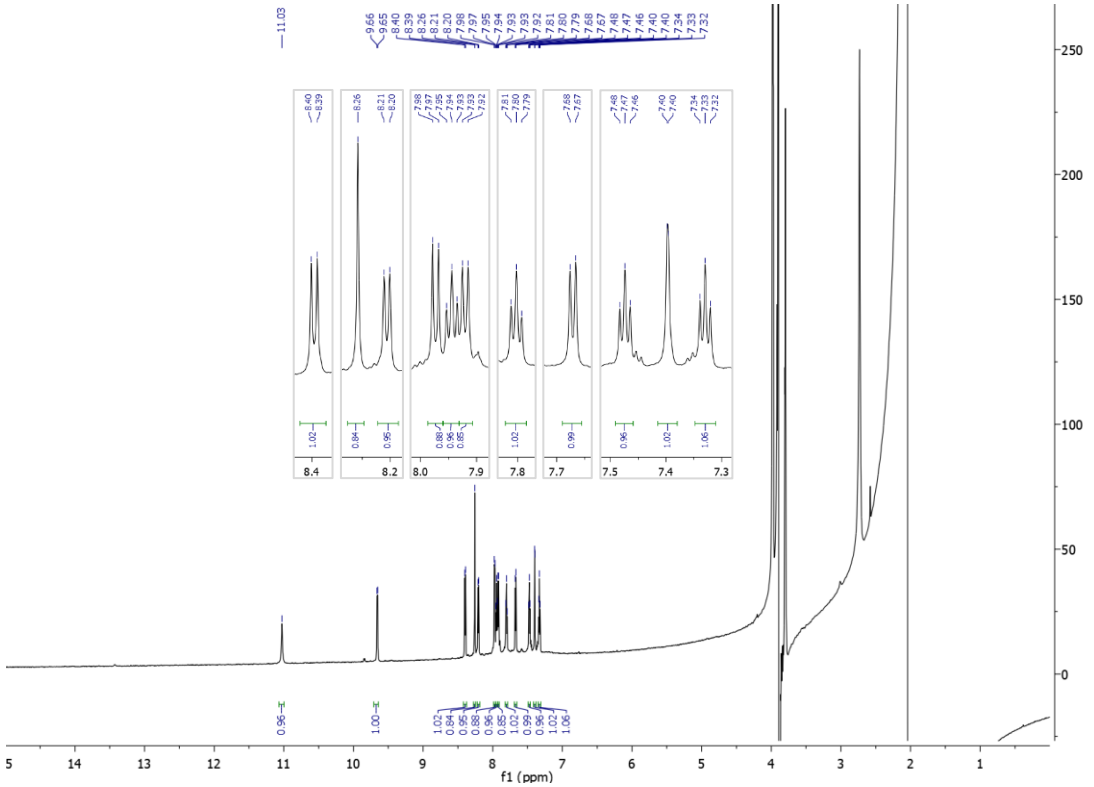

Note: Compound (***Z*-9**) with double solvent suppression of the THF proton signals

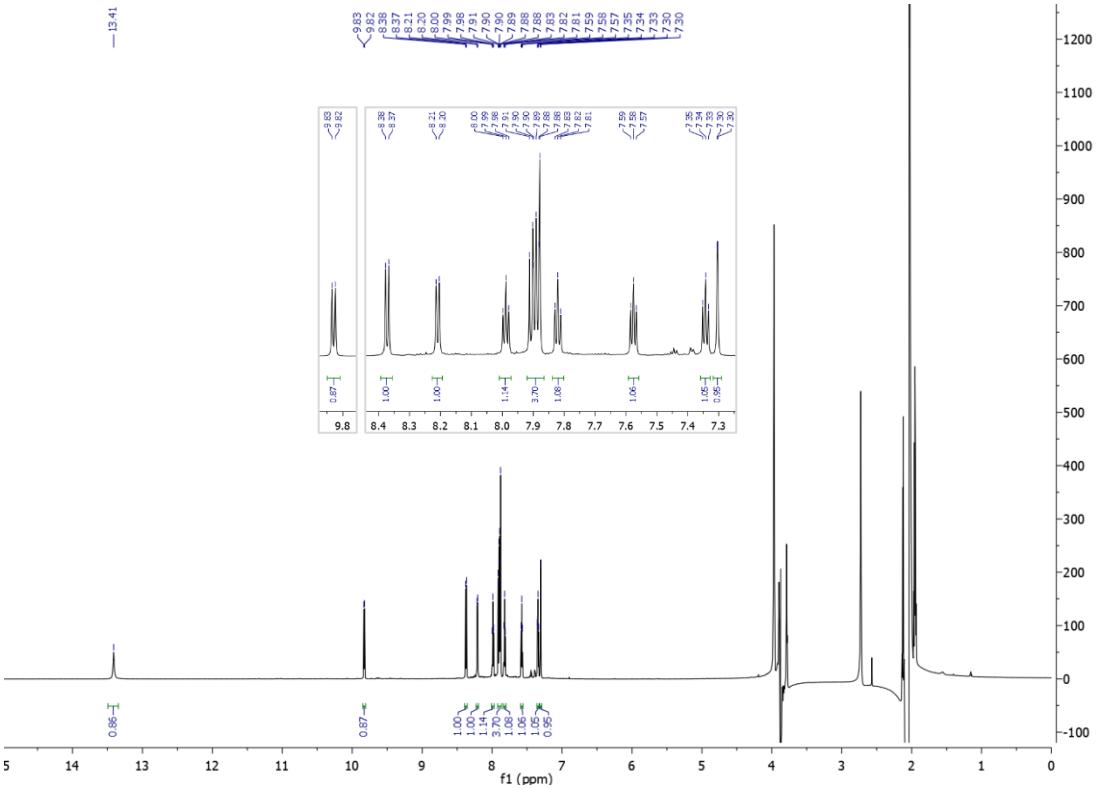

Note: Compound (***E*-9**) with double solvent suppression of the THF proton signals

(*Z*)-2-(1H,1'H-[2,2'-bipyrrol]-5-ylmethylene)benzo[b]thiophen-3(2H)-one (10)

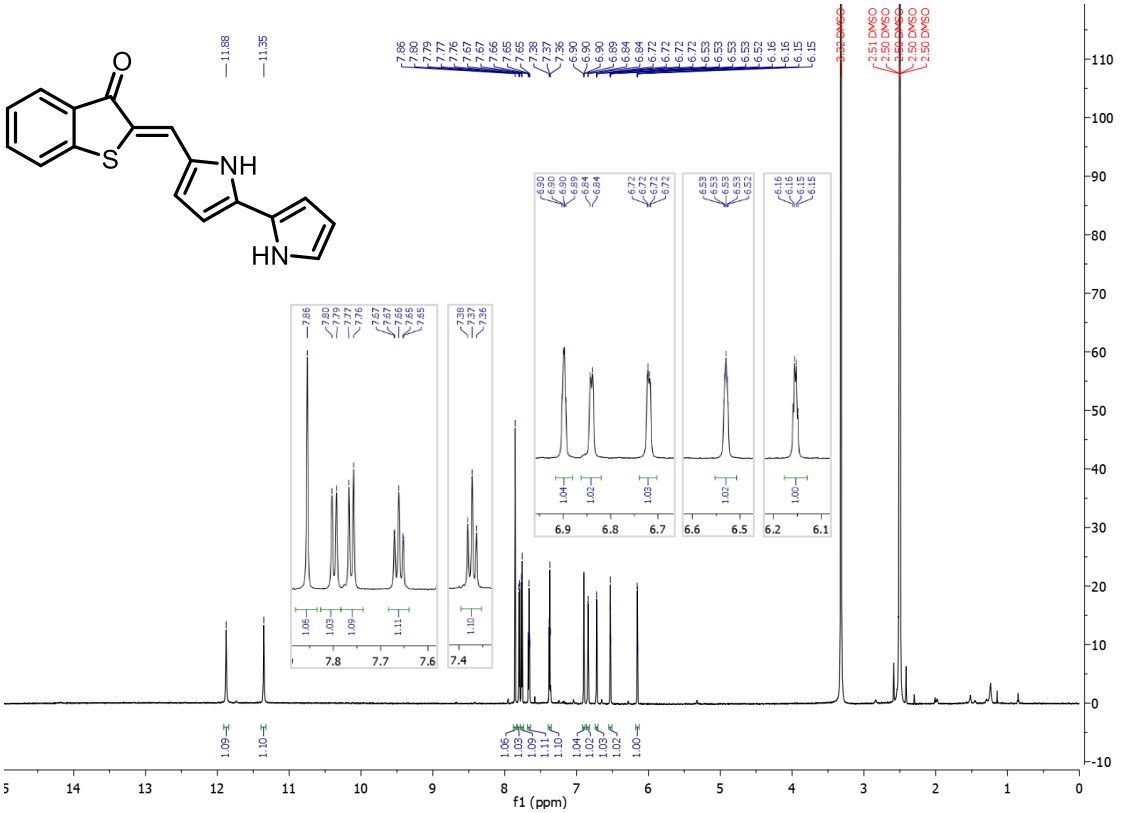

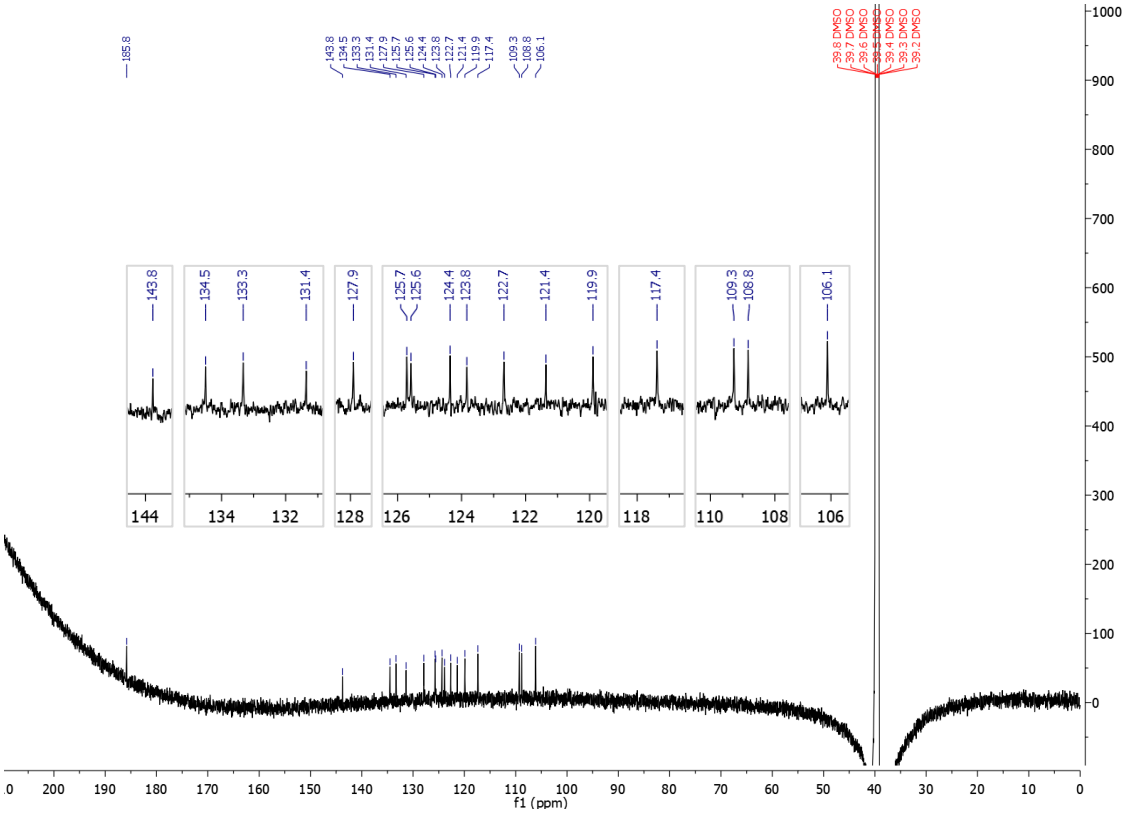

7 References

1 A. D. Becke, *Phys. Rev. A*, 1988, **38**, 3098.

2 C. Lee, W. Yang and R. G. Parr, *Phys. Rev. B*, 1988, **37**, 785.

3 A. D. Becke, *J. Chem. Phys.*, 1993, **98**, 5648–5652.

4 A. D. Laurent, J. M. André, E. A. Perpète and D. Jacquemin, *Chem. Phys. Lett.*, 2007, **436**, 84–88.

5 T. H. Dunning Jr, *J. Chem. Phys.*, 1989, **90**, 1007–1023.

6 A. V Marenich, C. J. Cramer and D. G. Truhlar, *J. Phys. Chem. B*, 2009, **113**, 6378–6396.

7 E. Papajak, J. Zheng, X. Xu, H. R. Leverentz and D. G. Truhlar, *J. Chem. Theory Comput.*, 2011, **7**, 3027–3034.

8 F. Neese, *Wiley Interdiscip. Rev. Comput. Mol. Sci.*, 2012, **2**, 73–78.

9 F. Neese, *Wiley Interdiscip. Rev. Comput. Mol. Sci.*, 2018, **8**, e1327.

10 H. Zulfikri, M. A. J. Koenis, M. M. Lerch, M. Di Donato, W. Szymański, C. Filippi, B. L. Feringa and W. J. Buma, *J. Am. Chem. Soc.*, 2019, **141**, 7376–7384.

11 J. Tomasi, B. Mennucci and R. Cammi, *Chem. Rev.*, 2005, **105**, 2999–3094.

12 B. O. Roos, P. R. Taylor and P. E. M. Sigbahn, *Chem. Phys.*, 1980, **48**, 157–173.

13 K. Andersson, P. A. Malmqvist, B. O. Roos, A. J. Sadlej and K. Wolinski, *J. Phys. Chem.*, 1990, **94**, 5483–5488.

14 K. Andersson, P. Malmqvist and B. O. Roos, *J. Chem. Phys.*, 1992, **96**, 1218–1226.

15 J. Finley, P.-Å. Malmqvist, B. O. Roos and L. Serrano-Andrés, *Chem. Phys. Lett.*, 1998, **288**, 299–306.

16 J. Stålring, A. Bernhardsson and R. Lindh, *Mol. Phys.*, 2001, **99**, 103–114.

17 G. Ghigo, B. O. Roos and P.-Å. Malmqvist, *Chem. Phys. Lett.*, 2004, **396**, 142–149.

18 N. Forsberg and P.-Å. Malmqvist, *Chem. Phys. Lett.*, 1997, **274**, 196–204.

19 F. Aquilante, P.-Å. Malmqvist, T. B. Pedersen, A. Ghosh and B. O. Roos, *J. Chem. Theory Comput.*, 2008, **4**, 694–702.

20 I. Fdez. Galván, M. Vacher, A. Alavi, C. Angeli, F. Aquilante, J. Autschbach, J. J. Bao, S. I. Bokarev, N. A. Bogdanov, R. K. Carlson, L. F. Chibotaru, J. Creutzberg, N. Dattani, M. G. Delcey, S. S. Dong, A. Dreuw, L. Freitag, L. M. Frutos, L. Gagliardi, F. Gendron, A. Giussani, L. González, G. Grell, M. Guo, C. E. Hoyer, M. Johansson, S. Keller, S. Knecht, G. Kovačević, E. Källman, G. Li Manni, M. Lundberg, Y. Ma, S. Mai, J. P. Malhado, P. Å. Malmqvist, P. Marquetand, S. A. Mewes, J. Norell, M. Olivucci, M. Oppel, Q. M. Phung, K. Pierloot, F. Plasser, M. Reiher, A. M. Sand, I. Schapiro, P. Sharma, C. J. Stein, L. K. Sørensen, D. G. Truhlar, M. Ugandi, L. Ungur, A. Valentini, S. Vancoillie, V. Veryazov, O. Weser, T. A. Wesołowski, P.-O. Widmark, S. Wouters, A. Zech, J. P. Zobel and R. Lindh, *J. Chem. Theory Comput.*, 2019, **15**, 5925–5964.

21 Z.-L. Cai, M. J. Crossley, J. R. Reimers, R. Kobayashi and R. D. Amos, *J. Phys. Chem. B*, 2006, **110**,

15624–15632.

22 R. Kobayashi and R. D. Amos, *Chem. Phys. Lett.*, 2006, **420**, 106–109.

23 R. Li, J. Zheng and D. G. Truhlar, *Phys. Chem. Chem. Phys.*, 2010, **12**, 12697–12701.

24 V. Josef, F. Hampel and H. Dube, *Angew. Chemie Int. Ed.*, 2022, e202210855.

25 M. Jevric, A. U. Petersen, M. Mansø, S. Kumar Singh, Z. Wang, A. Dreos, C. Sumby, M. B. Nielsen, K. Börjesson and P. Erhart, *Chem. Eur. J.*, 2018, **24**, 12767–12772.

26 A. Ranzenigo, F. M. Cordero, M. Cacciarini and M. B. Nielsen, *Molecules*, 2021, **26**, 6462.

27 J. K. Johnson, E. M. Skoda, J. Zhou, E. Parrinello, D. Wang, K. O'Malley, B. R. Eyer, M. Kazancioglu, K. Eisermann, P. A. Johnston, J. B. Nelson, Z. Wang and P. Wipf, *ACS Med. Chem. Lett.*, 2016, **7**, 785–790.

28 J. E. Zweig and T. R. Newhouse, *J. Am. Chem. Soc.*, 2017, **139**, 10956–10959.

29 T. Dohi, K. Morimoto, A. Maruyama and Y. Kita, *Org. Lett.*, 2006, **8**, 2007–2010.

30 J. Ostapko, K. Nawara, M. Kijak, J. Buczyńska, B. Leśniewska, M. Pietrzak, G. Orzanowska and J. Waluk, *Chem. - A Eur. J.*, 2016, **22**, 17311–17320.

31 T. B. Nguyen and P. Retailleau, *Org. Lett.*, 2018, **20**, 186–189.